REPORT NO. FR-79-27-1014
HAC REF. NO. E2852

FINAL TECHNICAL REPORT

X-BAND SLOTTED ARRAY TEST PANEL AND TEST FIXTURE

AUGUST 1979

RADAR SYSTEMS GROUP
HUGHES
HUGHES AIRCRAFT COMPANY
CULVER CITY, CALIFORNIA

Report No. FR-79-27-1014
HAC Ref. No. E2852
Dept. Ref. No. 2753.20/1692

X-BAND SLOTTED ARRAY TEST PANEL AND TEST FIXTURE

FINAL TECHNICAL REPORT

Contract No. NAS 9-15611

August 1979

Prepared by:

Antenna Department
Radar Microwave Laboratory
Radar Systems Group

CONTENTS

LIST OF ILLUSTRATIONS

1.0 INTRODUCTION

The purpose of this report is to document the data from the development of the X-band Slotted Array Test Panel, X-band Array Test Fixture, and the X/L-band Test Fixture for the SIR program. This contract, NAS 9-15611, was completed for National Aeronautics and Space Administration at the Lyndon B. Johnson Space Center, Houston, Texas.

The objective of the program was to build an X-band array and install with an existing L-band module in such a way as to permit antenna pattern measurements in a series of nonplanar configurations that might simulate the thermal effects of nonuniform solar illumination on the array in a space environment. This was accomplished with eight X-band subpanels mounted adjacently on individually adjusted supports which were then co-mounted to a larger frame which served to mount and physically distort the existing L-band module.

The L-band module is an array section that was fabricated on a Hughes IR&D program to demonstrate the performance capabilities of a slotted waveguide array at L-band frequencies. It is being loaned to NASA to be used on the distortion fixture. The L-band module was built to demonstrate high RF efficiency and not the mechanical fabrication techniques applicable to space application. Therefore, it is a heavy electrical breadboard unit.

This report contains descriptions of test configurations and test data collected. The appendices to the report contain additional test data, drawings, and mechanical analysis.

2.0 UNIT DESCRIPTIONS

2.1 BACKGROUND AND GENERAL DESIGN

The planar array antenna configuration offers many advantages compared to reflector antennas when microwave efficiency, precise control of the beam shape, and stowed and deployed volumes are important considerations. Of the potential planar array configurations available, those with waveguide-excited slots provide better performance than arrays of printed-circuit radiators or dipole radiators because the dissipative losses associated with the waveguide feed system can be made to be very small. The basic design considerations for waveguide slotted arrays are reviewed in this section, with emphasis on those design requirements that are most significant in both airborne and spaceborne synthetic array radar (SAR) systems. As an illustration of both design procedures and performance capability of slotted waveguide planar arrays, an L-band planar array was designed, fabricated, and tested. This array has an aperture approximately one meter wide by two meters high and was designed to be a typical submodule of a larger antenna. Measurements of radiation patterns, gain, and VSWR were recorded and are presented in Appendix E, together with the performance characteristics predicted on the basis of theoretical analysis.

2.1.1 Planar Array Advantages

The use of planar array antennas for large spaceborne SAR systems has many advantages compared with reflector types of antennas. These advantages include high aperture efficiency, precise control of the aperture distribution function, excellent packaging and stowage characteristics,

freedom from nonuniform solar illumination caused by feed shadowing, and reduced surface tolerances. The last are permissible because the aperture acts as a generator or source of the microwave energy rather than as a reflector. The use of slotted waveguide and waveguide feed structures has the further advantage of extremely low dissipative loss. In addition, there is a wealth of design data, computer programs, and experience available for slotted array design that generally assures achievement of predicted performance levels.

An example of an X-band array that was designed, fabricated, and space-qualified for a SAR application at the Hughes Aircraft Company some years ago is shown in Figure 2-1. This antenna, which was roughly 7.27 meters (24 feet) long by 1.2 meters (4 feet) high, was found to have outstanding microwave performance characteristics, most of which were directly attributable to the use of a waveguide feed and slotted waveguide radiating sections. A portion of this report is a feasibility demonstration model of a planar array with a similar design configuration but developed at L-band. It is shown that, at L-band as at X-band, the slotted waveguide type of planar array can provide superior performance.

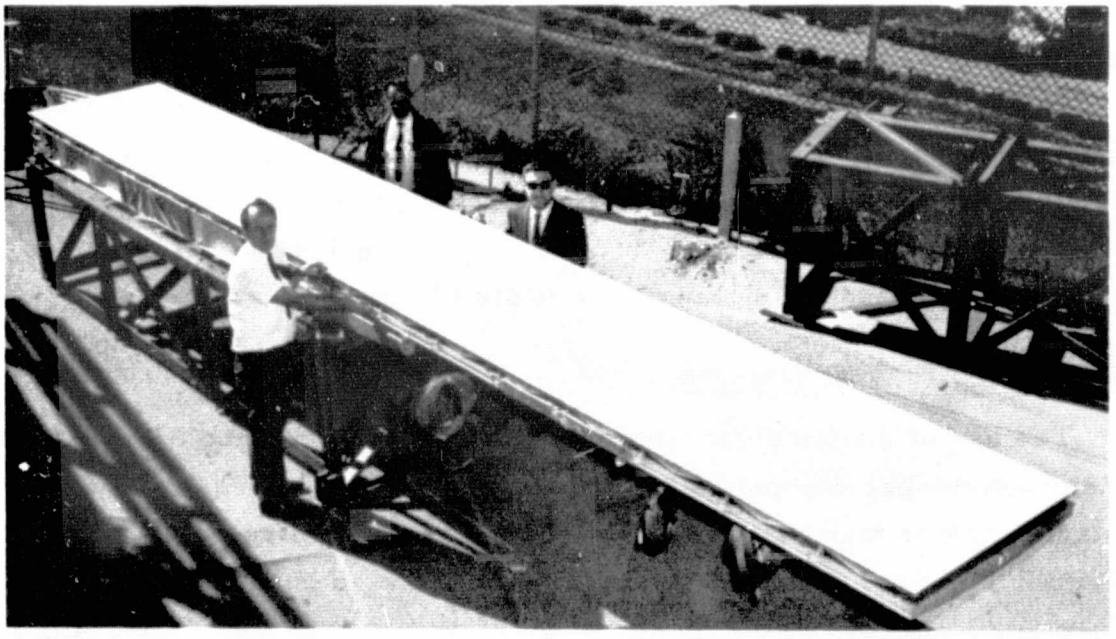

4R-13532

Figure 2-1. Space-qualified X-band array for SAR applications.

2.1.2 General Design Considerations

Typical SAR system requirements call for a radiation pattern with a fan beam shape, with the antenna oriented so that the broad section of the beam provides the desired swath coverage. The fan beam pattern requirement naturally leads to the use of a long narrow aperture of the type shown in Figure 2-1. Typically in a planar array, the aperture is divided both electrically and mechanically into a number of modules or subarrays, as shown in Figure 2-2. The modules are electrically combined with a corporate feed structure as indicated. The subdivision of the aperture provides a useful frequency bandwidth, allows for thermal expansion joints to prevent aperture bowing, simplifies fabrication of the antenna, and facilitates folding if required for stowage during launch and retrieval.

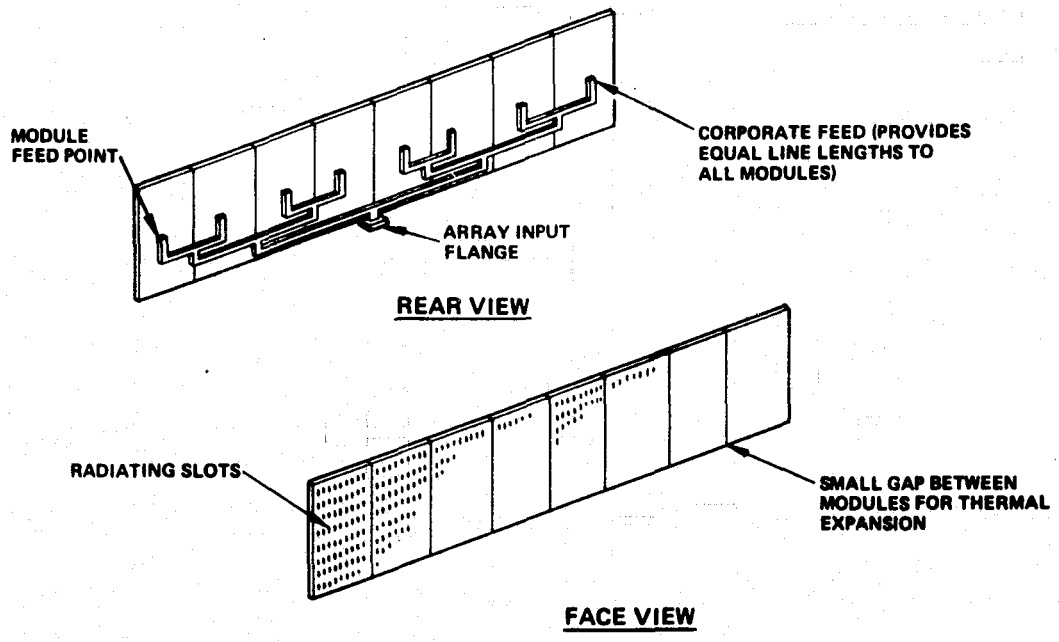

Figure 2-2. Subdivided aperture.

In Figure 2-3, it is possible to see most of the essential details of the construction of a single module of an array. In practice, the modules in a given array are usually identical, so that Figure 2-3 actually characterizes a complete antenna system. As shown, the radiating elements of the module

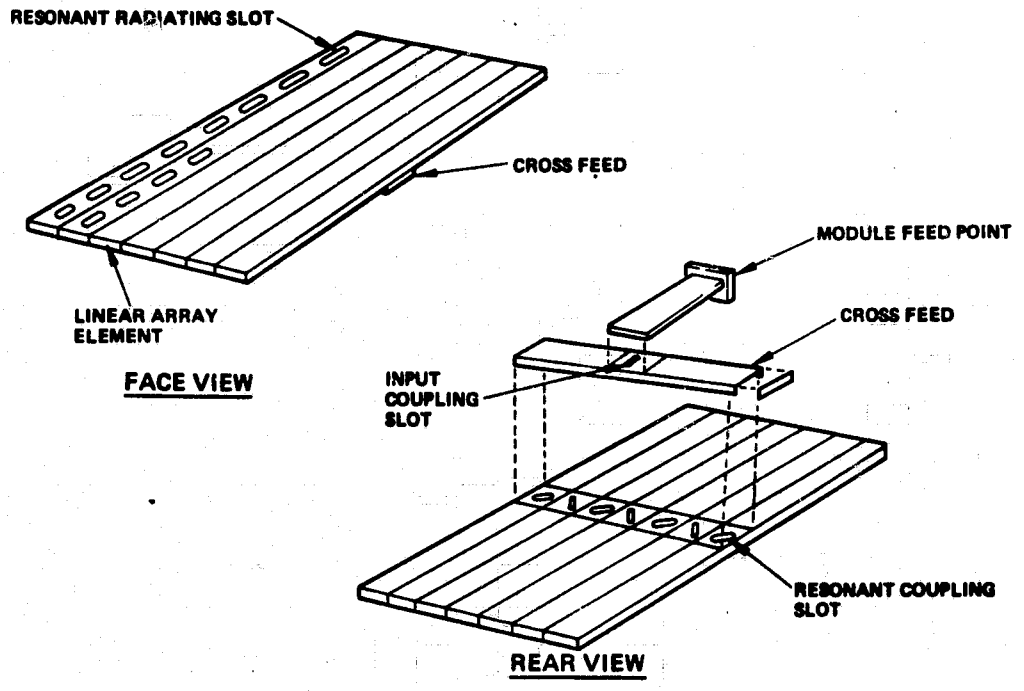

Figure 2-3. Typical module construction.

are formed from resonant slots cut in the broadwalls of a number of sections of waveguide. Each section of waveguide thus becomes an individual linear array. The module aperture is formed by joining these waveguide sections together in the manner illustrated. The individual linear array elements are slot coupled to a cross feed guide that runs across the back of the module. The cross feed is in turn slot coupled to a flanged module feed guide section. This feed guide is the common feed point for all the slots in a given module.

In the module configuration of Figure 2-3, it is generally most convenient to employ a resonant, or standing-wave design, for both the cross feed and the linear array element guide sections. For good pattern characteristics to be obtained over a wide frequency range with this type of design, the number of elements that appear in series in any given element must be limited. Typically, for example, it has been found that square arrays of 16 slots can provide useful bandwidths of about 13 percent.

The aperture distribution in the slot array can be tailored to provide precise control of the antenna beam shape. The mechanisms for such control are simple: the amount of power radiated by any individual slot is

controlled by the amount the slot is offset from the centerline of the waveguide in which it appears, the power coupled from the cross feed to any individual linear array element is controlled by the angle at which the coupling slot is cut with respect to the guide axis, and the resonant frequencies of the slots are determined by the slot lengths. In the interest of mechanical simplicity, it is common to use separable aperture distribution functions in the E- and H-planes; this approach leads to a design in which all waveguide array elements have identical radiating slot patterns.

An indication of the degree of flexibility possible in the design of the module is provided by the equivalent circuit representation of Figure 2-4. Each of the slot susceptances is individually controllable, as is the impedance transformation ratio of each of the coupling slots. Thus, various design configurations involving both different aperture distributions and different internal impedance levels can be easily realized. Because both radiating and coupling slot characteristics are well documented on both theoretical and experimental levels, design of a module for any desired set of pattern, bandwidth, gain, and impedance characteristics is a straightfoward process. In general, the effects of such factors as mutual coupling between slots are accounted for during the design process by the use of the appropriate slot data.

The design procedure for most cases can be summarized neatly:

- The antenna gain and pattern requirements determine the aperture size and shape.
- The radar signal bandwidth requirements then established the maximum module size.
- The radiating and coupling slots are then selected to generate the aperture distribution corresponding to the beamshape requirements.
- The impedance levels and resonant frequencies of the slots are designed to provide a good input impedance match.

2.1.3 Multipactor and Ionization Breakdown

A common problem with waveguide antennas for space applications is the multipactor and ionization breakdown. The multipactor problem occurs when near vacuum conditions of space allows the mean free path to

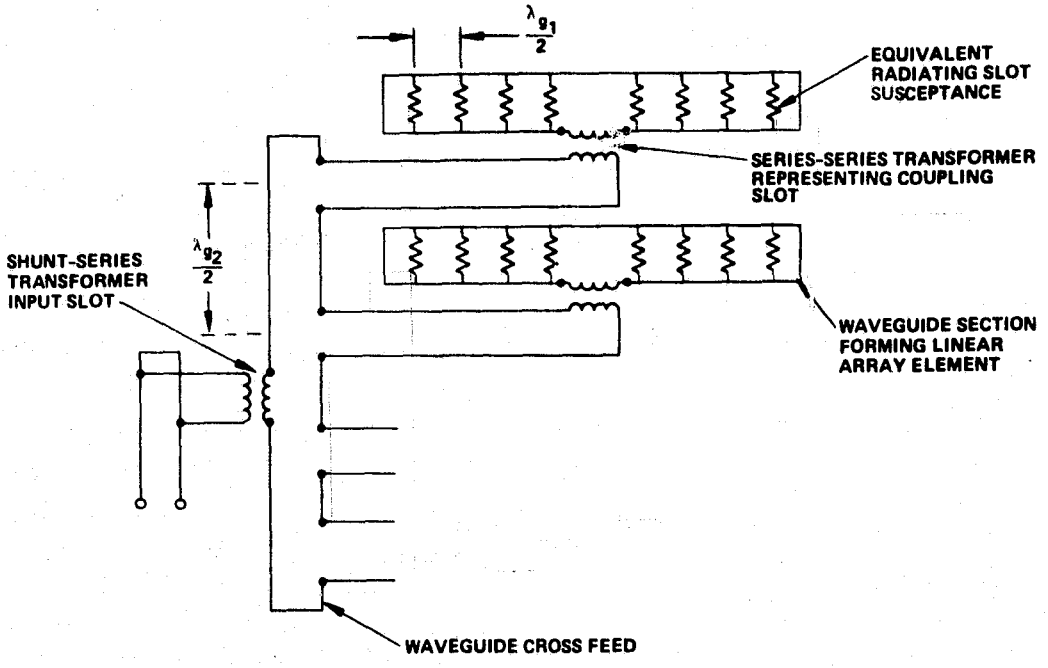

Figure 2-4. Equivalent circuit of module.

approach waveguide dimensions. Ionization breakdown can occur as a result of localized atmosphere around the vehicle. Each of these subjects were considered at the beginning of the contract and are summarized in Appendix F.

2.2 X-BAND SLOTTED ARRAY TEST PANEL

The X-band Slotted Array consists of eight subpanels and a three piece eight-way waveguide power divider which all mount to a flat plate surface. Eight flex waveguides are used between the feed and subpanels to allow subpanel movement. This assembly can be seen in Figure 2-5. Detail drawings for the assembly are found in Appendix A.

2.3 X/L-BAND TEST FIXTURE

The X/L-band Test Fixture is a large frame that will hold the X-band Assembly and also function to hold and deform the L-band panel. The L-band panel is a scaled version of the X-band panel. This assembly can be seen in Figures 2-6 and 2-7 with the X-band Slotted Array mounted above the L-band panel. Detail drawings for the assembly are found in Appendix A.

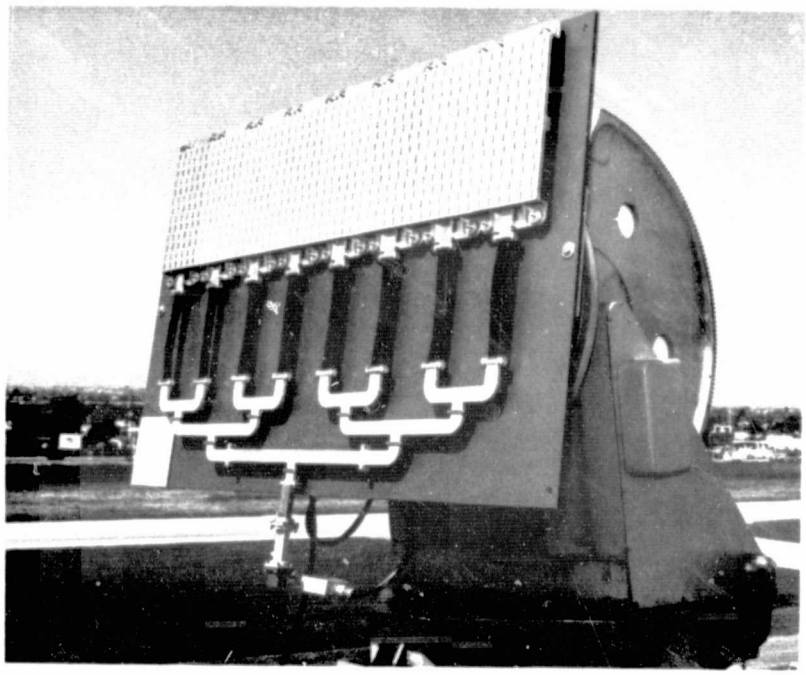

4R-54270

Figure 2-5. X-band slotted array assembly.

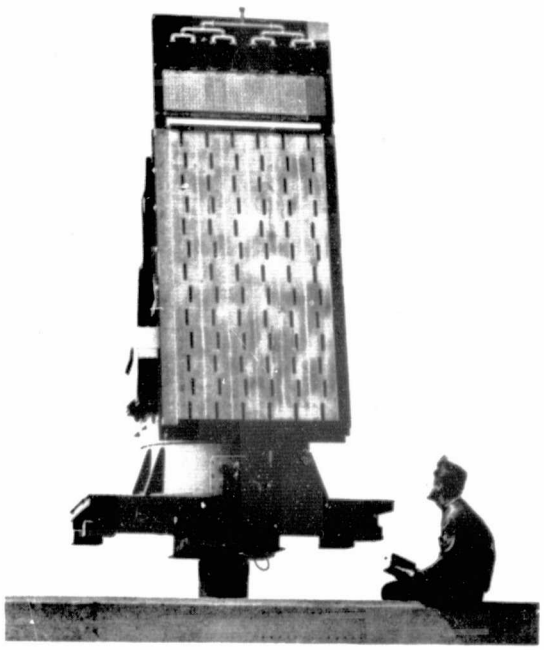

4R-54321

Figure 2-6. X/L-band test fixture — front view on range mount.

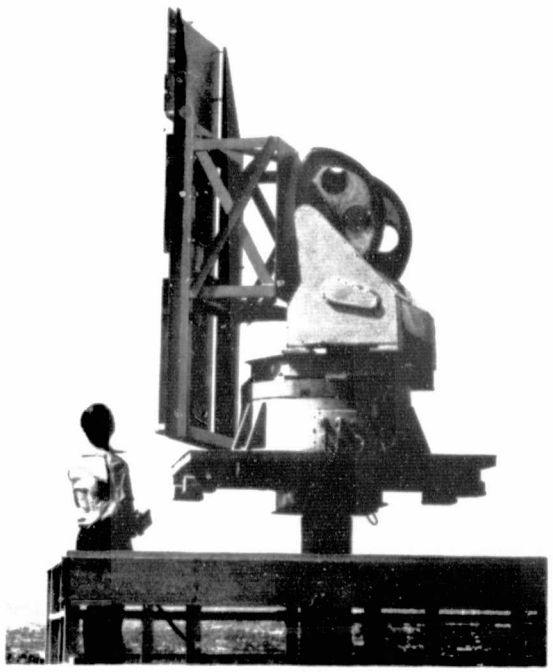

4R-54322

Figure 2-7. X/L-band test fixture — side view on range mount.

3.0 ELECTRICAL TEST CONDITIONS – X-BAND PANEL

3.1 INPUT VSWR

The input VSWR of the X-band Panel Assembly was measured at the waveguide step transition flange using a slotted line. This flange can be identified in Figure 3-1 between the step transition and attenuator (see arrow).

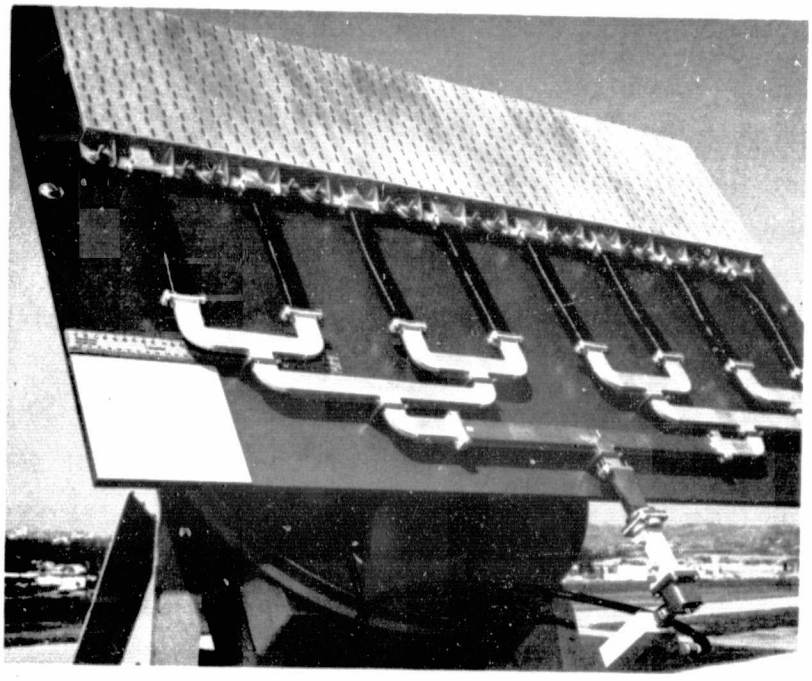

4R-54271

Figure 3-1. X-band panel assembly. (Input VSWR measured at the waveguide step transition input)

3.2 GAIN

The gain of the X-band Panel Assembly was measured at the waveguide step transition and referenced to an isotropic source by using a Scientific Atlanta standard gain horn. This flange can be identified in Figure 3-1 between the step transition and attenuator.

3.3 PATTERNS

E-plane and H-plane patterns were measured and recorded with the eight sub-arrays adjusted to a flat configuration. E-plane patterns were recorded ±90 and ±30 degrees. All patterns were taken from 9.3 to 9.8 GHz in 0.1 GHz increments. Appendix B contains the recorded patterns.

3.4 CROSS POLARIZATION

The available sources for cross polarization measurements included only dish radiators. The cross polarization measurements were not made because the dish radiators were known to produce significantly poorer polarization purity than that expected from the array. In the experience of Hughes Aircraft Company, such planar arrays easily exhibit cross polarization better than -30 dB with typical figures being -40 dB.

3.5 BORESIGHT

Cadmium-plated steel mounting were provided on the X-band Panel Assembly (see Figure 3-1 lower left hand corner of mounting structure) and X/L-band fixture (see Figure 2-6 lower left hand side of fixture). Both plates were finished with a 0.002 inch flatness. These plates were chosen to accommodate NMSU's magnetically mounted boresight mirror. Hughes does not use this type of boresight instrument and a boresight measurement was not made. Also, the intended use at NMSU was believed to be for establishing a repeatable reference at the time of deformation measurements.

4.0 TEST RESULTS

4.1 X-BAND SLOTTED ARRAY TEST PANEL

The panel input VSWR and gain are shown in Figures 4-1 and 4-2. Additional patterns, feed data and subpanel data are contained in Appendices B and C.

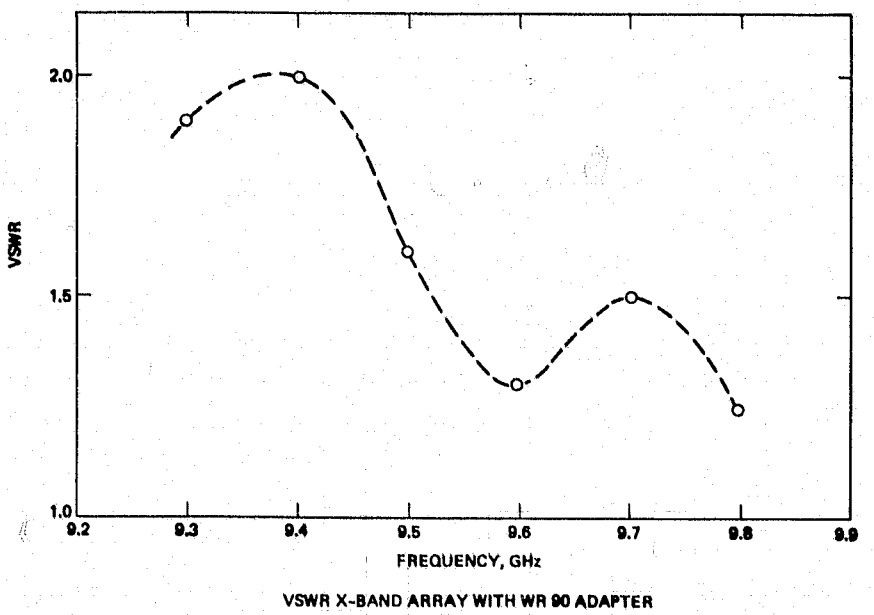

Figure 4-1. X-band panel assembly input. (VSWR measured with the full height to half height step transition)

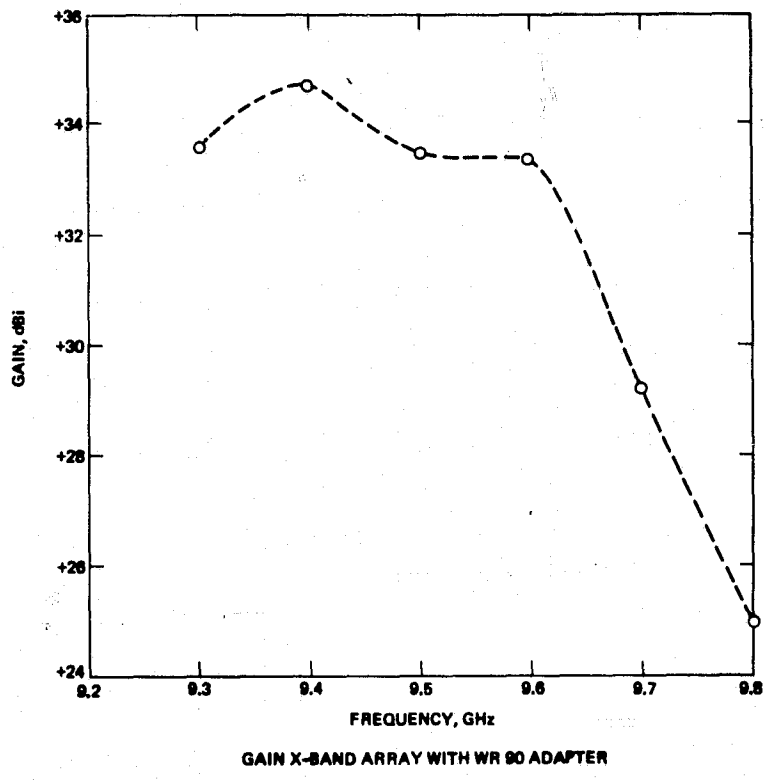

Figure 4-2. X-band panel assembly.
(Gain measured with the step transition)

4.2 L-BAND ANTENNA SUBPANEL

Appendix E contains the L-band module performance.

5.0 CONCLUSIONS

The X-band Array Antenna Test Panel is a good working tool for investigating the aperture distortion versus performance degradation relationship. The panel performance is optimum over approximately 300 MHz from 9.4 to 9.7 GHz. This is concurrent with the original breadboard module performance and does not represent any design iteration to improve the module over a wider bandwidth. All X-band modules were constructed from the breadboard dimensions and the L-band module is a scaling of the X-band dimensions.

APPENDIX A

DRAWINGS

NOTES: UNLESS OTHERWISE SPECIFIED

1. ASSEMBLY SEQUENCE VENDOR'S OPTION.
2. BRAZE PER MIL-B-7883, TYPE V, GRADE A.
3. REMOVE TAPE WELDS AND BRAZE FOIL FROM PASSAGE ITEM 5.
4. INSIDE OF ASSEMBLY TO BE FREE OF BURRS AND BRAZING MATERIAL.
5. CHEMICAL CONVERSION COAT PER MIL-C-5541, CLASS 1A.

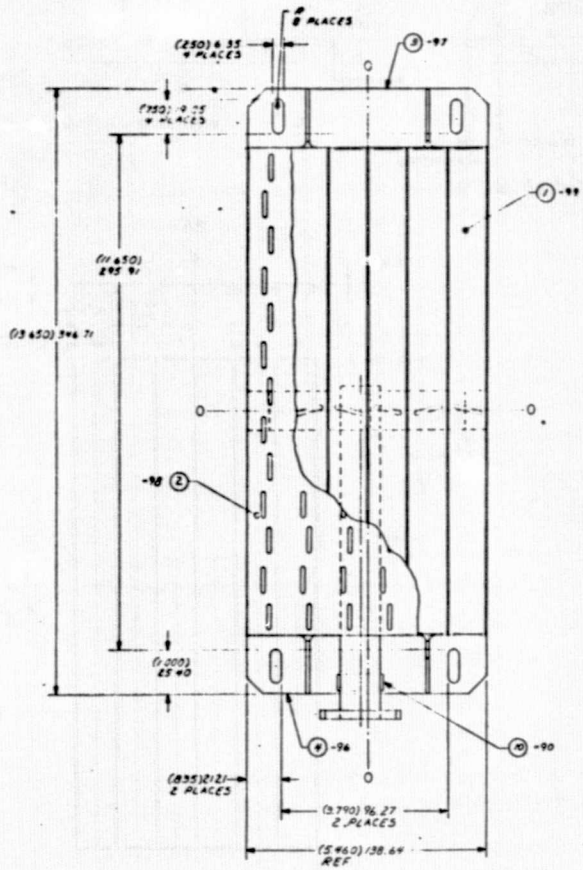

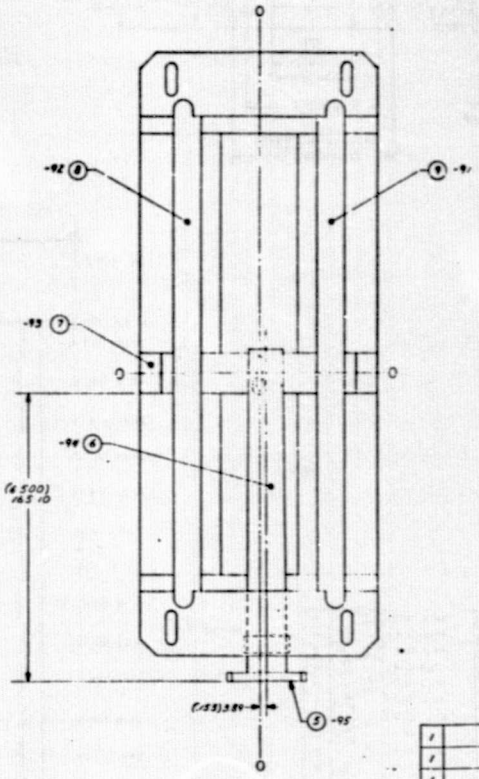

A-1

1		-90	SUPPORT-FEED	AL ALLOY 6061-T4, QQ-A-250/11, TEM T4	10
1		-91	STIFFENER, LEFT HAND		9
1		-92	STIFFENER RIGHT HAND		8
1		-93	FEED, CROSS		7
1		-94	FEED, MAIN		6
1		-95	FLANGE		5
1		-96	BRACKET, END		4
1		-97	BRACKET, END		3
1		-98	PLATE-FACE		2
1		-99	PLATE-BASE	AL ALLOY 6061-T4, QQ-A-225/11, TEM T4	1

QTY REQD	CODE IDENT	PART OR IDENTIFYING NO.	NOMENCLATURE OR DESCRIPTION	DASH NO.	ITEM NO.

UNLESS OTHERWISE SPECIFIED DIMENSIONS ARE IN INCHES AND PER ANSI Y14.5
XXX ± .010 XX ± .03 ANGLES ± 0° 30'
MATERIAL

HUGHES AIRCRAFT COMPANY CULVER CITY, CALIFORNIA

SIR X-BAND SUBSYSTEM

SIZE E | CAGE NO. 82577 | DRAWING NO. 3499210

NEXT ASSY | USED ON | APPLICATION

DO NOT SCALE DRAWING | SHEET

3499210

3499210

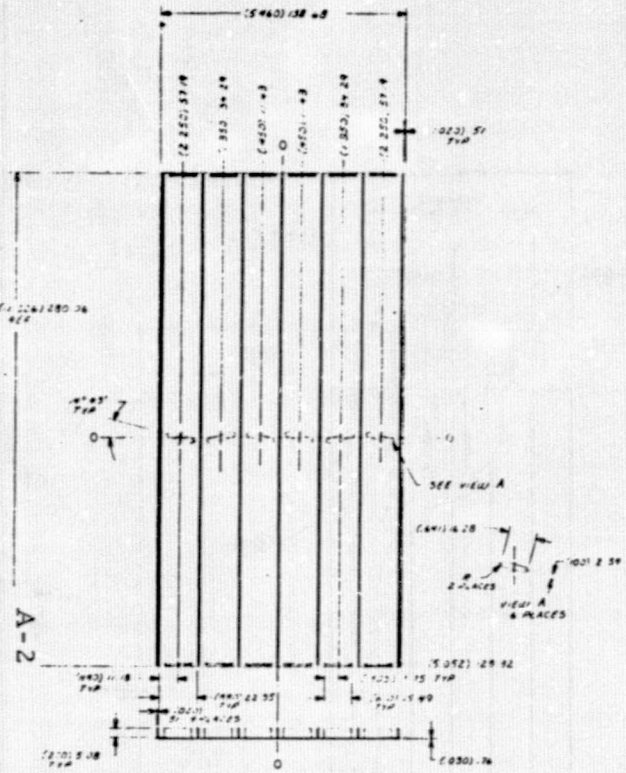

A-2

-99

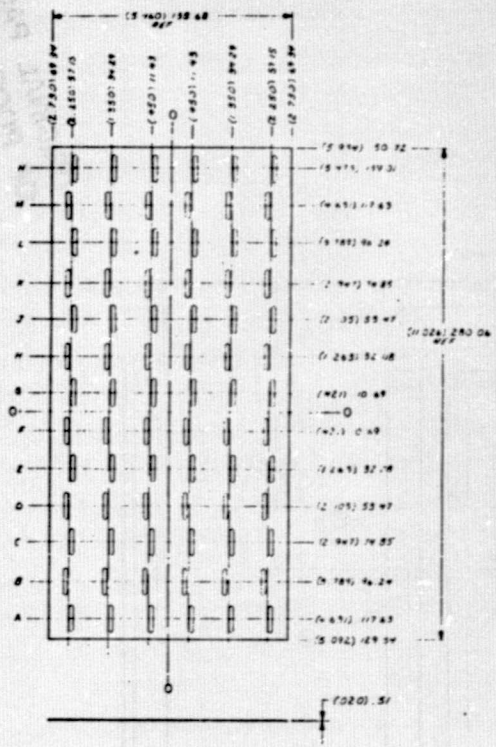

-98

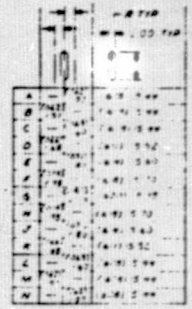

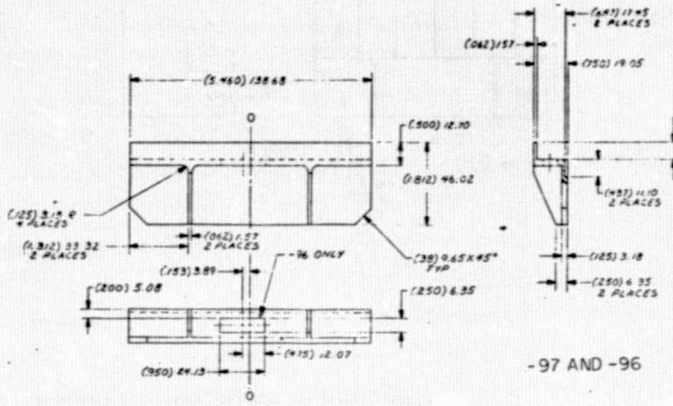

-97 AND -96

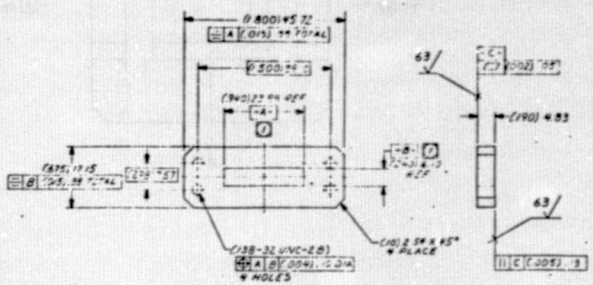

-95 SCALE 2/1

[0] DIMENSION TO MATCH -94

HUGHES AIRCRAFT COMPANY CULVER CITY, CALIFORNIA	CONTRACT		
	SCALE	FSCM NO. 82577	DWG NO. 77210
			SHEET

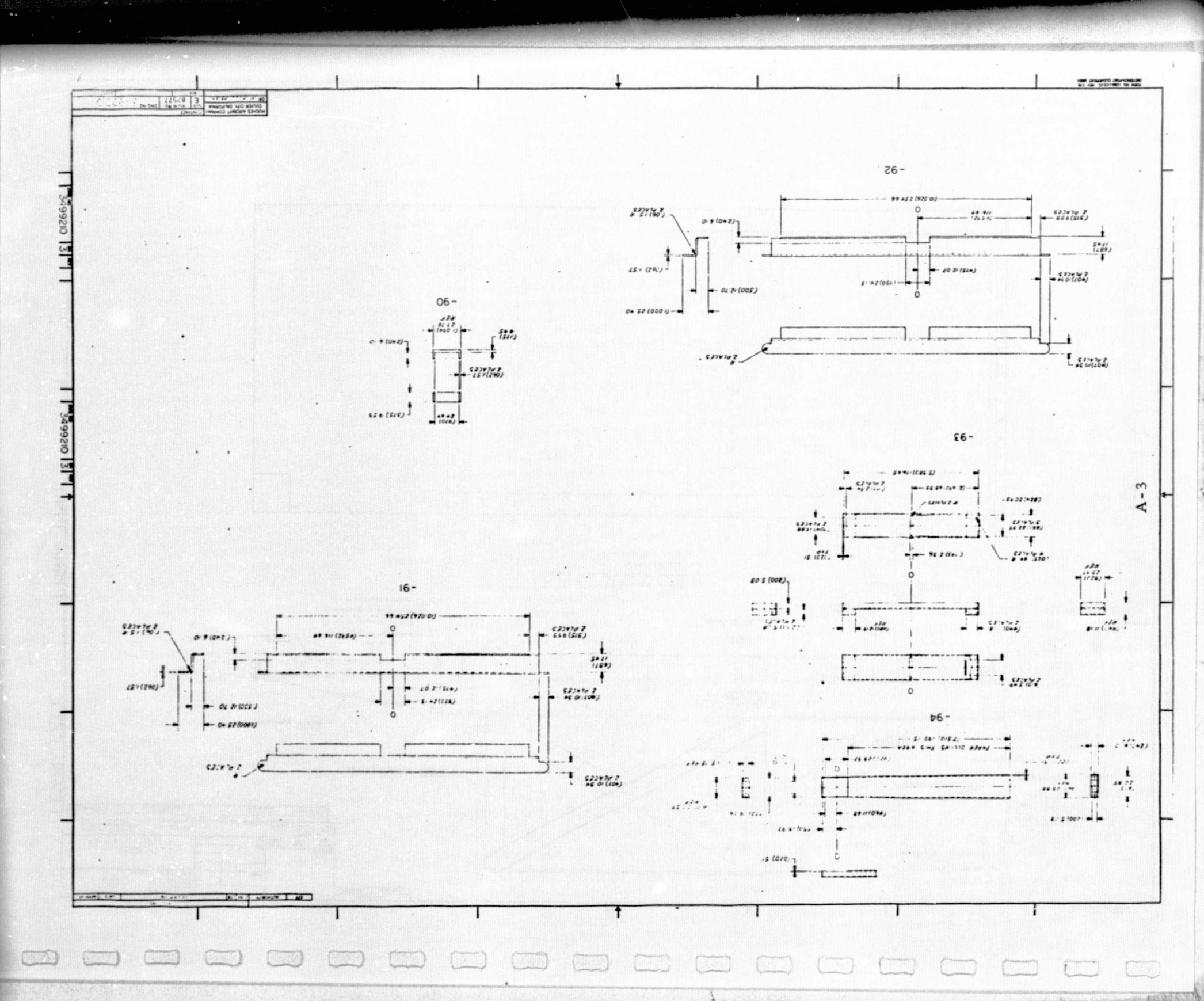

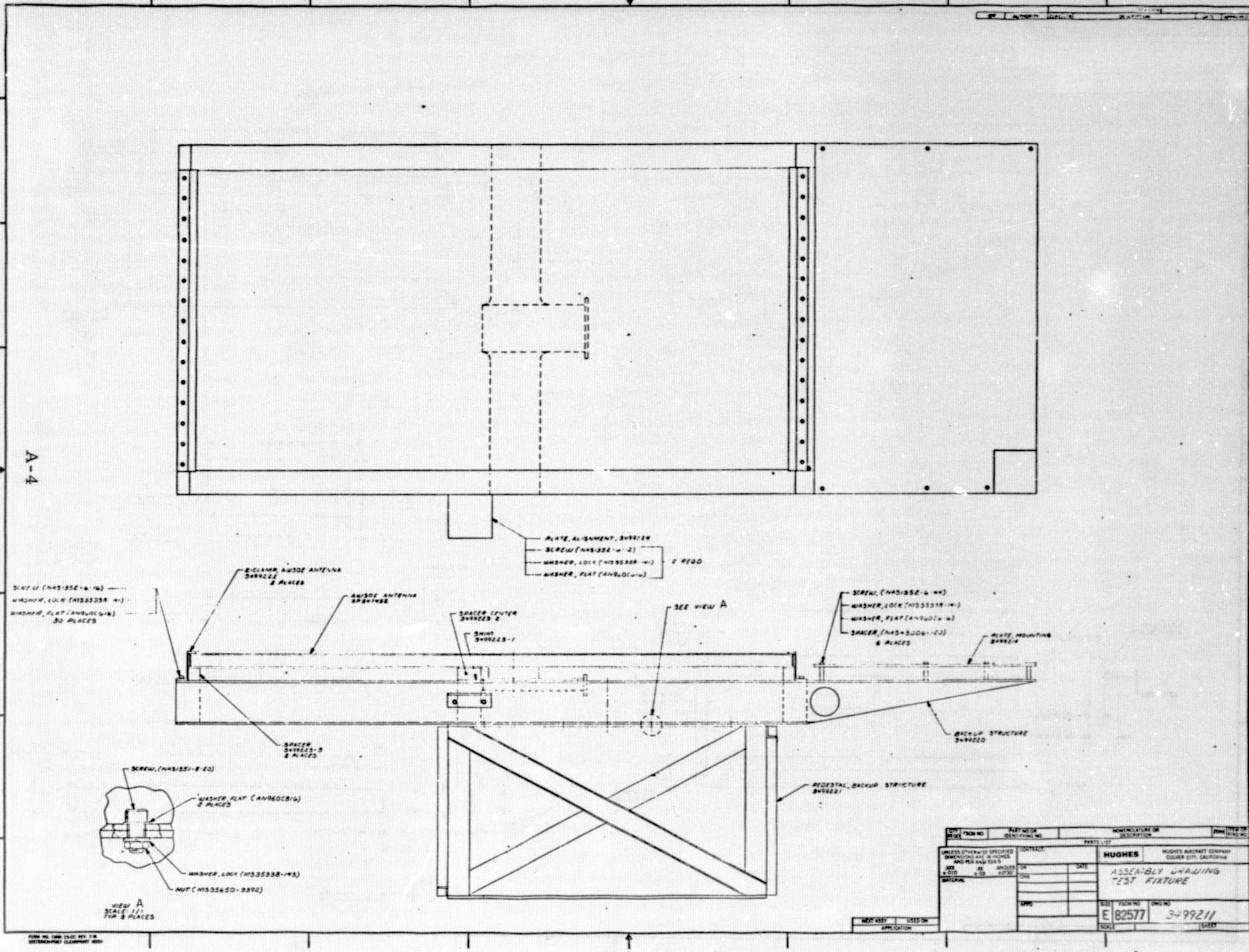
PLATE, ALIGNMENT, 3499224
SCREW (NAS1352-4-2)
WASHER, LOCK (MS35338-41)
WASHER, FLAT (AN960C4)
2 REQD
E-CLAMP, AWSOE ANTENNA
3499222
2 PLACES
SCREW (NAS1352-6-16)
WASHER, LOCK (MS35338-41)
WASHER, FLAT (AN960C616)
30 PLACES
AWSOE ANTENNA
SPACER CENTER
3499223-2
SHIM
3499223-1
SEE VIEW A
SCREW, (NAS1352-6-44)
WASHER, LOCK (MS35338-141)
WASHER, FLAT (AN960C6-6)
SPACER, (NAS43DD6-120)
6 PLACES
PLATE, MOUNTING
3499214
BACKUP STRUCTURE
3499220
SPACER
3499223-3
2 PLACES
PEDESTAL, BACKUP STRUCTURE
3499221
SCREW, (NAS1351-8-20)
WASHER FLAT (AN960C816)
2 PLACES
WASHER, LOCK (MS35338-145)
NUT (MS35650-3392)
VIEW A
SCALE: 1/1
TYP 8 PLACES
PARTS LIST
UNLESS OTHERWISE SPECIFIED DIMENSIONS ARE IN INCHES
HUGHES
HUGHES AIRCRAFT COMPANY
CULVER CITY, CALIFORNIA
ASSEMBLY DRAWING
TEST FIXTURE
E
82577
3499211

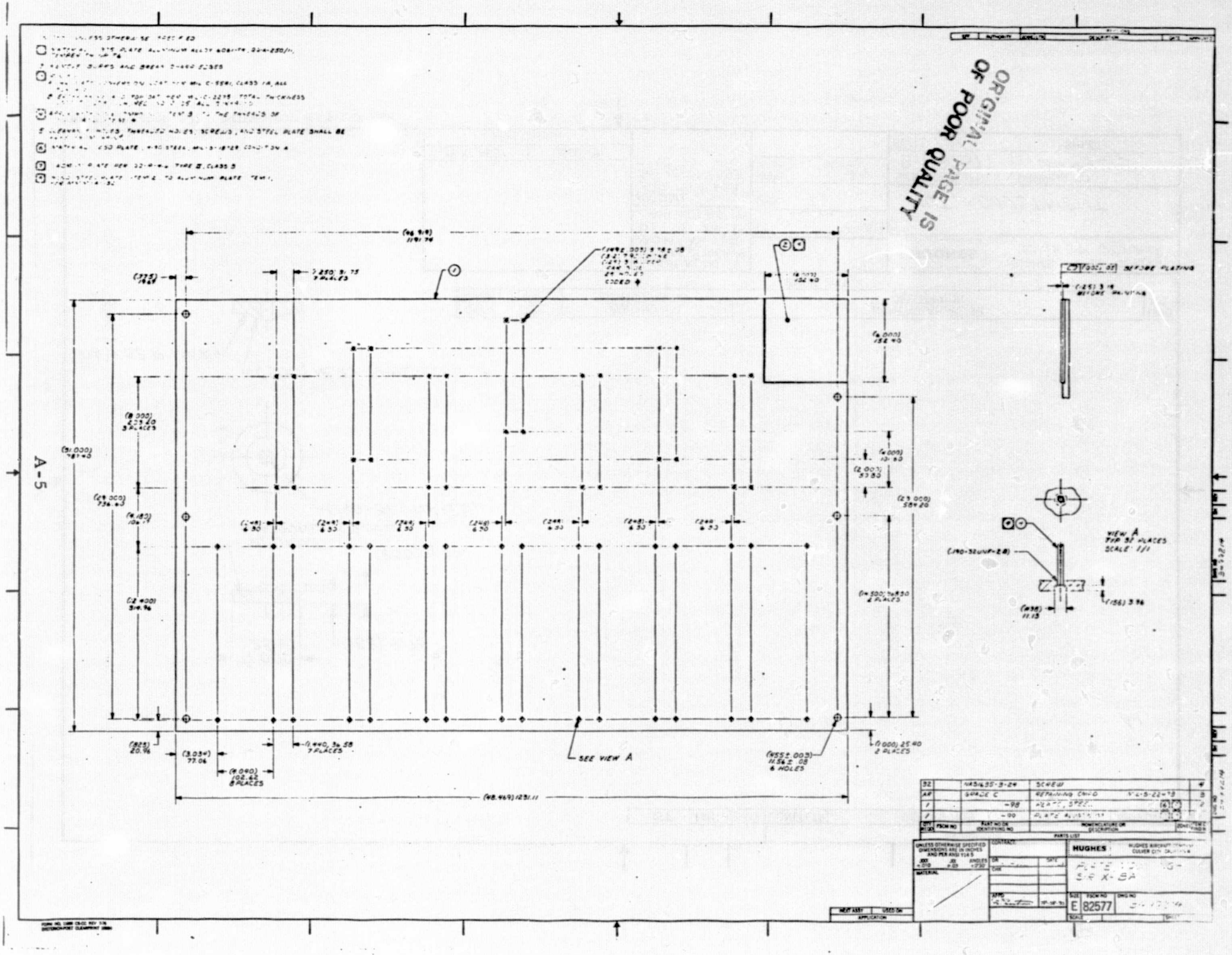
A-5
ORIGINAL PAGE IS
OF POOR QUALITY
SEE VIEW A
VIEW A
SCALE: 1/1
BEFORE PLATING
(46.969) 1193.01
(48.469) 1231.11
(31.000) 787.40
(29.000) 736.60
(23.000) 584.20
(12.400) 314.96
(6.000) 152.40
(3.034) 77.06
(.825) 20.96
(.156) 3.96
(1.000) 25.40
2 PLACES
(4.040) 102.62
8 PLACES
(1.440) 36.58
7 PLACES
(.455±.003) 11.56±.08
6 HOLES
32 | NAS1635-3-24 | SCREW | 4
AR | GRADE C | RETAINING COMPOUND | 3
1 | -98 | PLATE, STEEL | 2
1 | -99 | PLATE ALUMINUM | 1
QTY REQD | FSCM NO | PART NO OR IDENTIFYING NO | NOMENCLATURE OR DESCRIPTION | ZONE | ITEM FIND NO
PARTS LIST
UNLESS OTHERWISE SPECIFIED DIMENSIONS ARE IN INCHES AND PER ANSI Y14.5
.XXX ±.010
.XX ±.03
ANGLES ±0°30'
MATERIAL
CONTRACT
DR
DATE
CHK
APPD
HUGHES
HUGHES AIRCRAFT COMPANY
CULVER CITY, CALIFORNIA
SIR X-BA
SIZE
E
FSCM NO
82577
DWG NO
SCALE
SHEET
NEXT ASSY
USED ON
APPLICATION

REVISIONS						
EFF	AUTHORITY	ZONE	LTR	DESCRIPTION	DATE	APPROVED

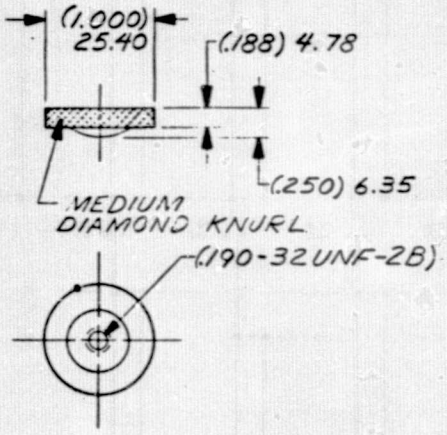

A-6

QTY REQD	CODE IDENT	PART NO. OR IDENTIFYING NO.	NOMENCLATURE OR DESCRIPTION	FIND NO.

PARTS LIST

EXCEPT AS NOTED
DIM. ARE IN INCHES
AND PER ANS Y14.5
.XXX .XX ANGLES
±.010 ±.03 ±0°30'

MATERIAL
BAR, TYPE 303
Se, ASTM A582
CONDITION A

DR R Eisen 78-08-29
CHK
APPD 78-8-31

NEXT ASSY | USED ON
APPLICATION

HUGHES HUGHES AIRCRAFT COMPANY
CULVER CITY, CALIFORNIA

NUT, ADJUSTMENT

SIZE	CODE IDENT NO.	DRAWING NO.
B	82577	3499215

SCALE 1/1 SHEET

FORM NO. 11063-CS-CC 3/72 DIETERICH-POST CLEARPRINT 1000H

A-7

REVISIONS						
EFF	AUTHORITY	ZONE	LTR	DESCRIPTION	DATE	APPROVED

NOTES:
1. MATERIAL: ALUMINUM ALLOY, 6061-T4, QQ-A-250/11, TEM T4.
2. REMOVE BURRS AND BREAK SHARP EDGES.
3. FINISH:
   A. CHROMATE CONVERSION COAT PER MIL-C-5541, CL IA.
   B. EPOXY PRIME AND TOPCOAT PER MIL-C-22751, TOTAL THICKNESS .002 TO .003 INCH, RED NO. 21105.
4. THREADED HOLES TO BE FREE OF PAINT.

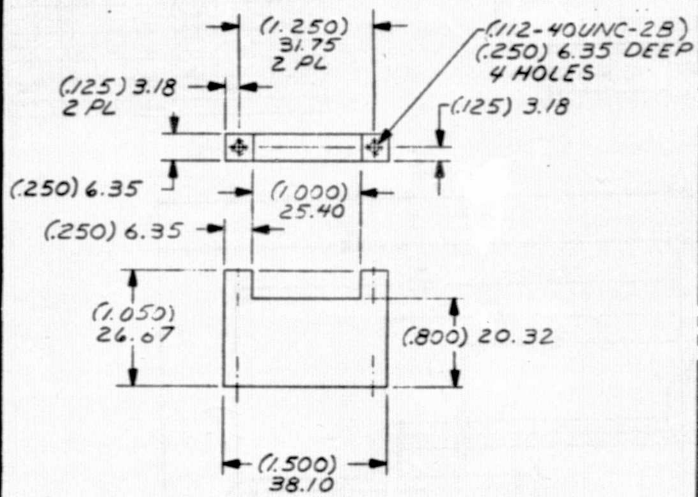

NOTES:
1. MATERIAL: .040 SHEET, ALUMINUM ALLOY, 6061-T4, QQ-A-250/11, TEM T4.
2. REMOVE BURRS AND BREAK SHARP EDGES.

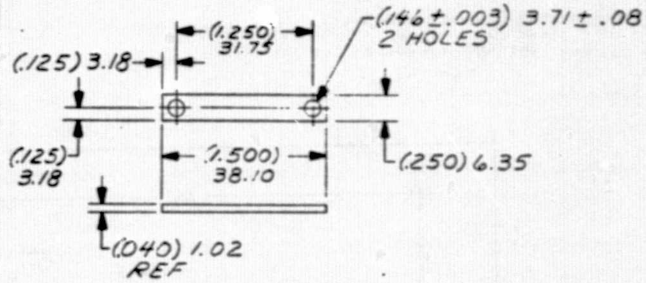

3. FINISH:
   A. CHROMATE CONVERSION COAT PER MIL-C-5541, CL IA
   B. EXPOXY PRIME AND TOPCOAT PER MIL-C-22751, TOTAL THICKNESS .002 TO .003 INCH, RED NO. 21105.

QTY REQD	CODE IDENT	PART NO. OR IDENTIFYING NO.	NOMENCLATURE OR DESCRIPTION	FIND NO.

PARTS LIST

NEXT ASSY	USED ON

APPLICATION

EXCEPT AS NOTED DIM. ARE IN INCHES AND PER ANS Y14.5
.XXX ±.010 .XX ±.03 ANGLES ±0°30'

MATERIAL

DR R. [illegible] 76-23-[illegible]
CHK
APPD [illegible]

HUGHES — HUGHES AIRCRAFT COMPANY, CULVER CITY, CALIFORNIA

BRACKET, WAVEGUIDE

SIZE	CODE IDENT NO.	DRAWING NO.
B	82577	3499216

SCALE 1/1 SHEET

FORM NO. 11063-CS-CC 3/72 DIETERICH-POST CLEARPRINT 1000H

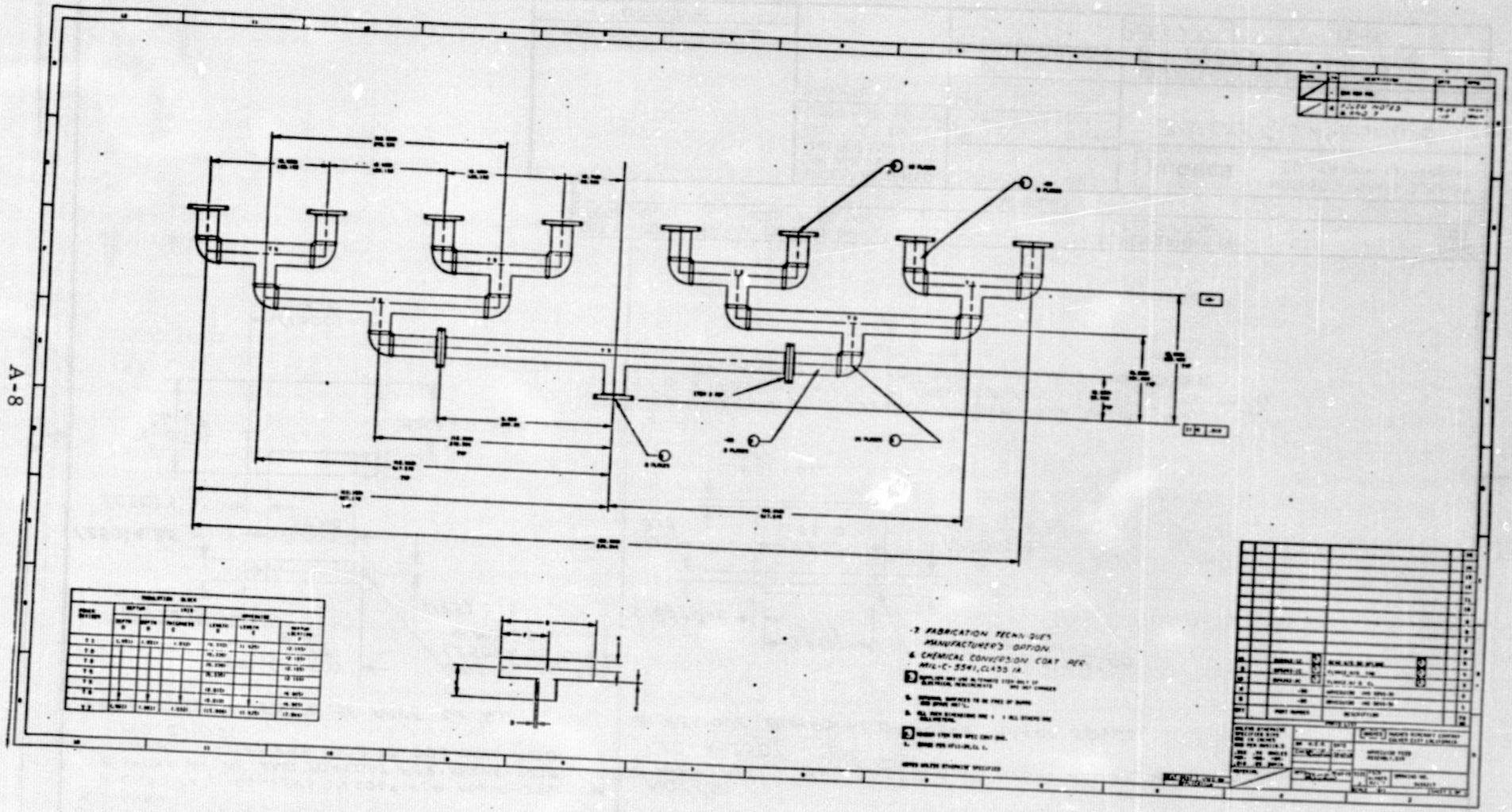

3499218

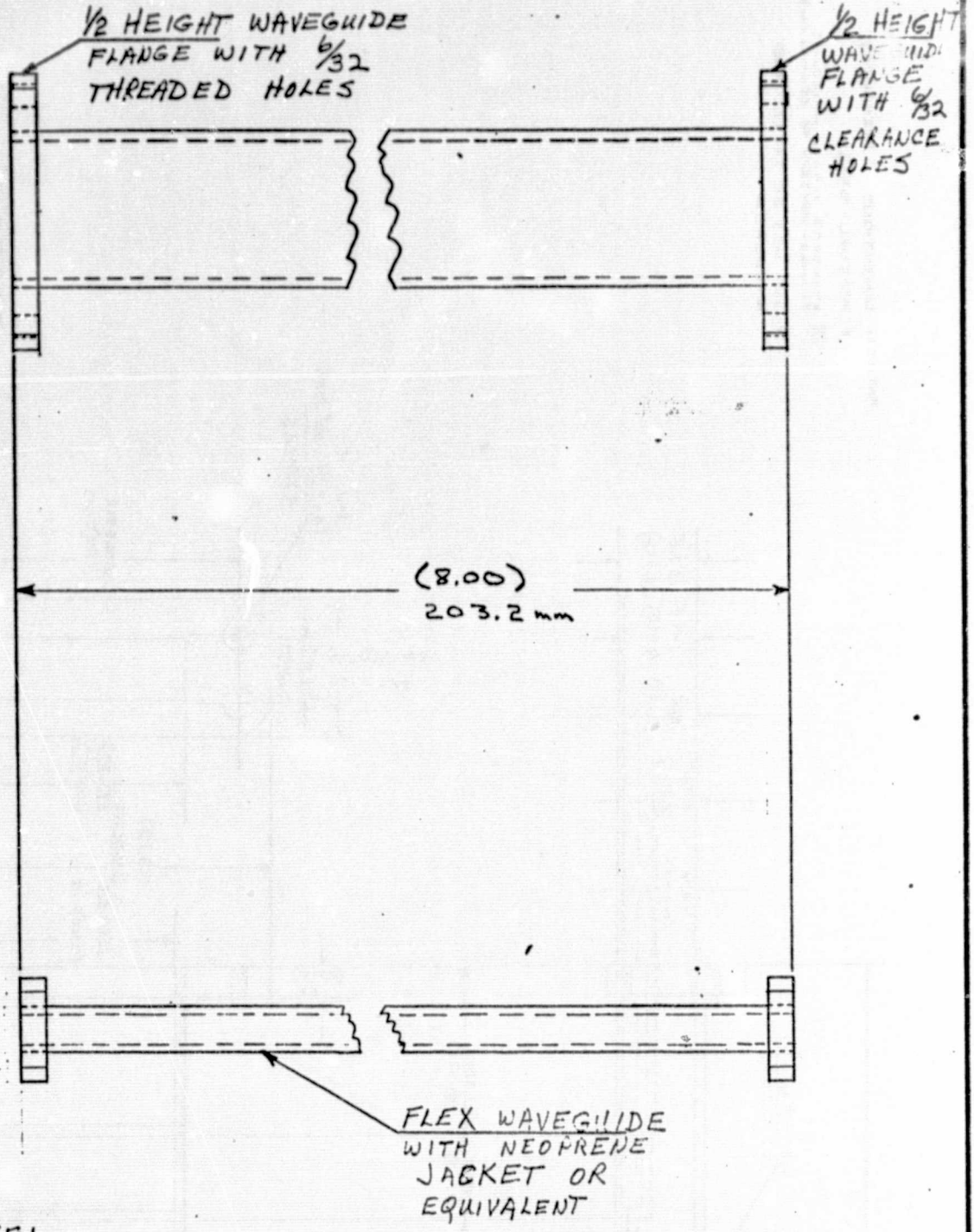

NOTE:

① USE 929203 INTERFACE DIMENSION FOR FLANG DETAIL

② BRASS FLANGES

PURPOSE: SIR					TITLE: FLEX WAVEGUIDE - SIR		
MATL. & SPEC.: BRASS ½ HEIGHT FLEXGUIDE					SCALE: —	TOLERANCES: ANGULAR ± / LINEAR ±	
ORIGINATOR: W. Schneider	APPR.	DATE: 7-17-78	BLDG.: 20	ROOM (STA.): 1453	PHONE: 3343	HUGHES AIRCRAFT CO. CULVER CITY, CALIF.	3499218

FORM 437 - REV. 3-65

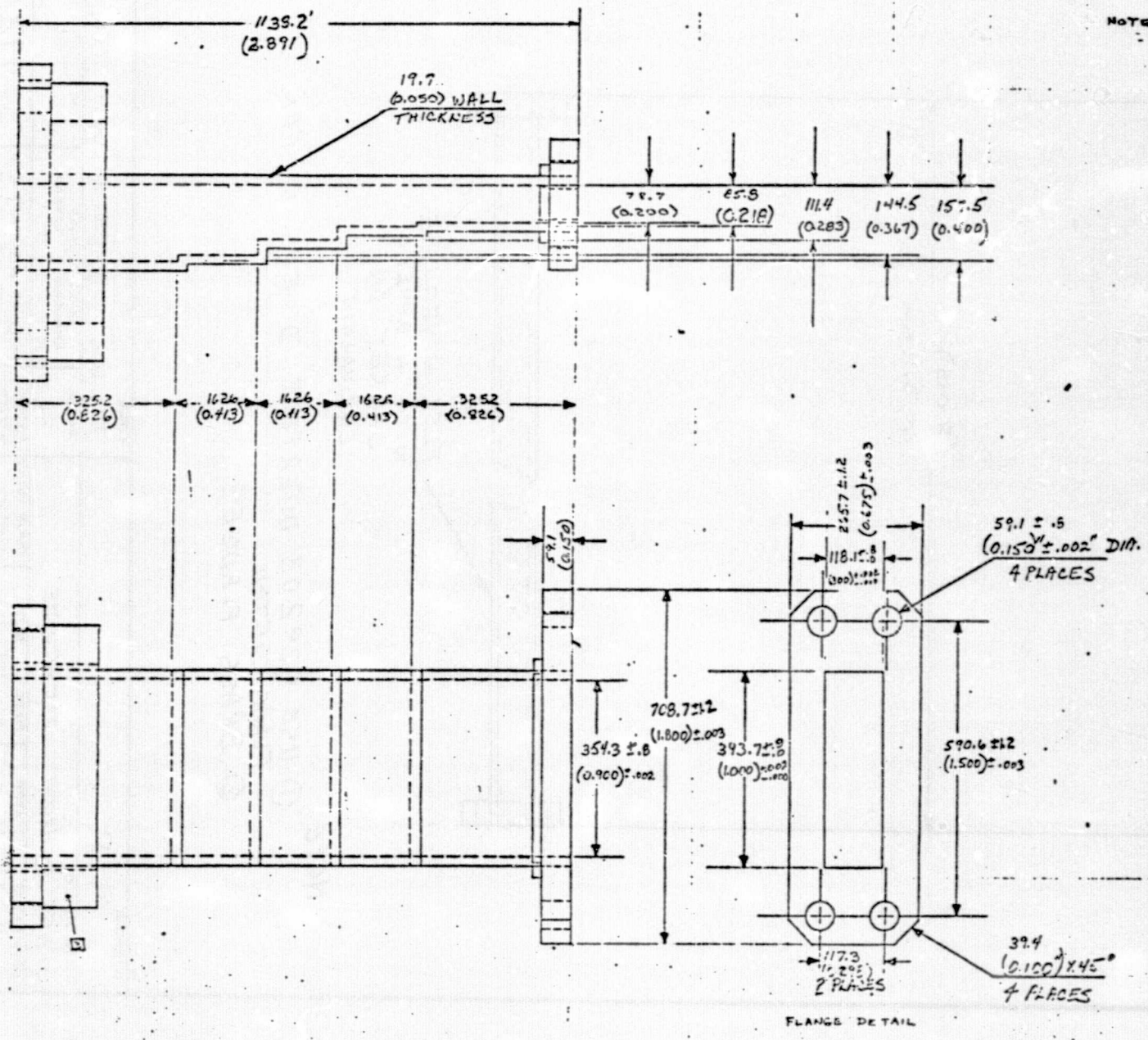

FLANGE DETAIL

NOTES: 1. DIMENSIONS SI (ENGLISH)
2. MATERIAL - BRASS
3. STANDARD X-BAND WAVEGUIDE FLANGE - UG135/U OR EQUIVALENT
4. UNIT MAY BE TACKED AND SOLDERED

ORIGINAL PAGE IS OF POOR QUALITY

3499219
SIR
X-BAND TRANSITION
JULY 7, 1978
DRG B/: W. SCHNEIDER
RTR 7-19-78

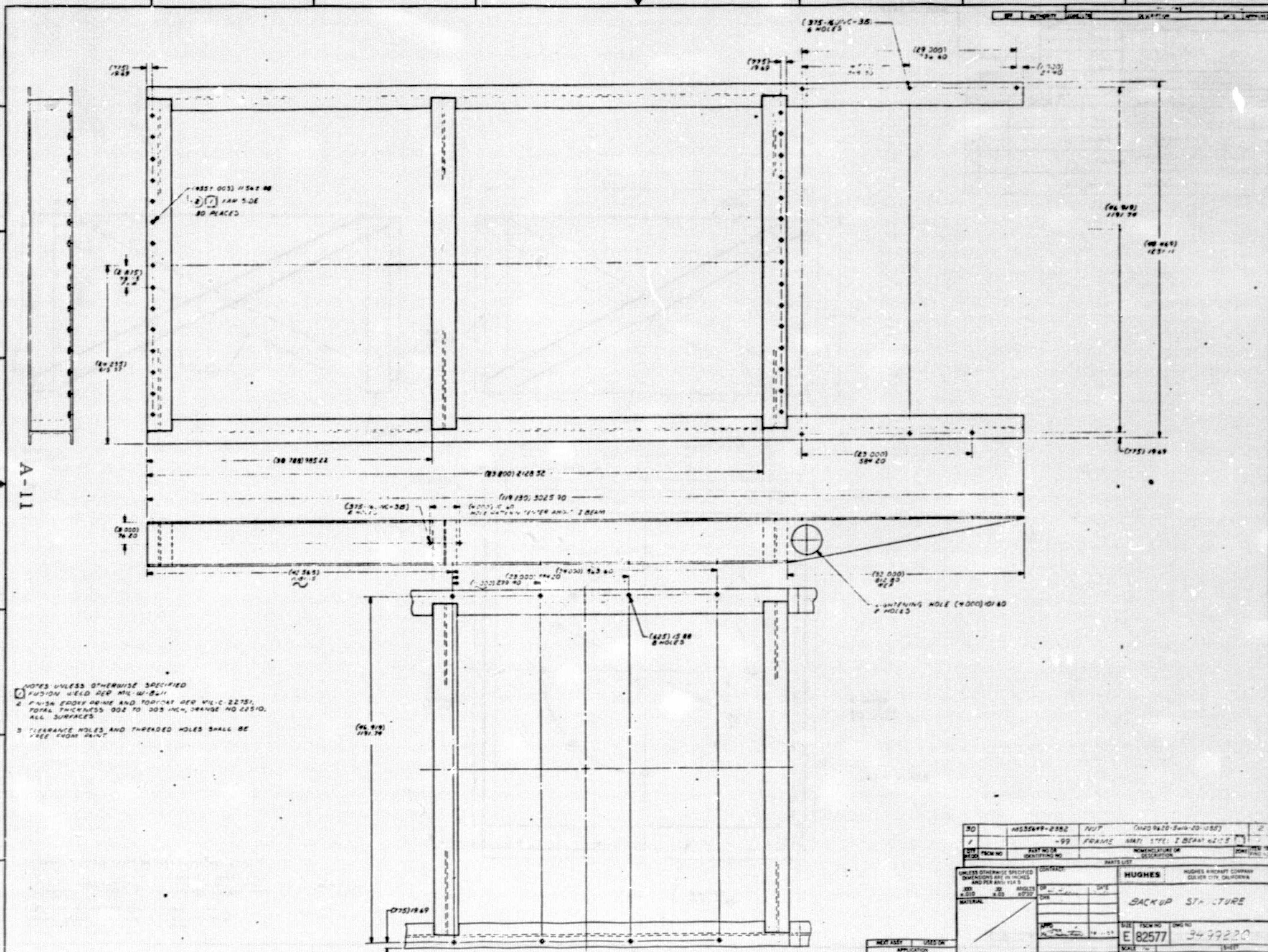
NOTES UNLESS OTHERWISE SPECIFIED
1 FUSION WELD PER MIL-W-8611
2 FINISH EPOXY PRIME AND TOPCOAT PER MIL-C-22751, TOTAL THICKNESS .002 TO .003 INCH, ORANGE NO 22510, ALL SURFACES
3 CLEARANCE HOLES AND THREADED HOLES SHALL BE FREE FROM PAINT
30 MS35649-2382 NUT 2
1 -99 FRAME
QTY REQD
FSCM NO
PART NO OR IDENTIFYING NO
NOMENCLATURE OR DESCRIPTION
ZONE
PARTS LIST
UNLESS OTHERWISE SPECIFIED DIMENSIONS ARE IN INCHES
.XXX ±.010
.XX ±.03
ANGLES ±0°30'
MATERIAL
CONTRACT
DR
DATE
CHK
APPD
HUGHES
HUGHES AIRCRAFT COMPANY
CULVER CITY, CALIFORNIA
BACK UP STRUCTURE
SIZE E
FSCM NO 82577
DWG NO 3499220
SCALE
SHEET
NEXT ASSY
USED ON
APPLICATION
(4.000) 101.60
LIGHTENING HOLE
(.625) 15.88
8 HOLES
(.775) 19.69
30 PLACES
(96.919)
1191.74
(119.130) 3025.90
(83.800) 2128.52
(38.785) 985.22
(23.000) 584.20
(29.300)
(3.000) 76.20
(32.000) 812.80

NOTES: UNLESS OTHERWISE SPECIFIED
1 [illegible] PER MIL-[illegible]
2 HEAT TREAT [illegible] TEMPER T6 PER MIL-H-6088
3 REMOVE BURRS AND BREAK SHARP EDGES
4 FINISH
A [illegible] CONVERSION [illegible] PER MIL-C-5541, CL 1A
B [illegible] PER MIL-[illegible] [illegible] ORANGE NO 22510 ALL SURFACES
5 CLEARANCE HOLES SHALL BE FREE FROM PAINT

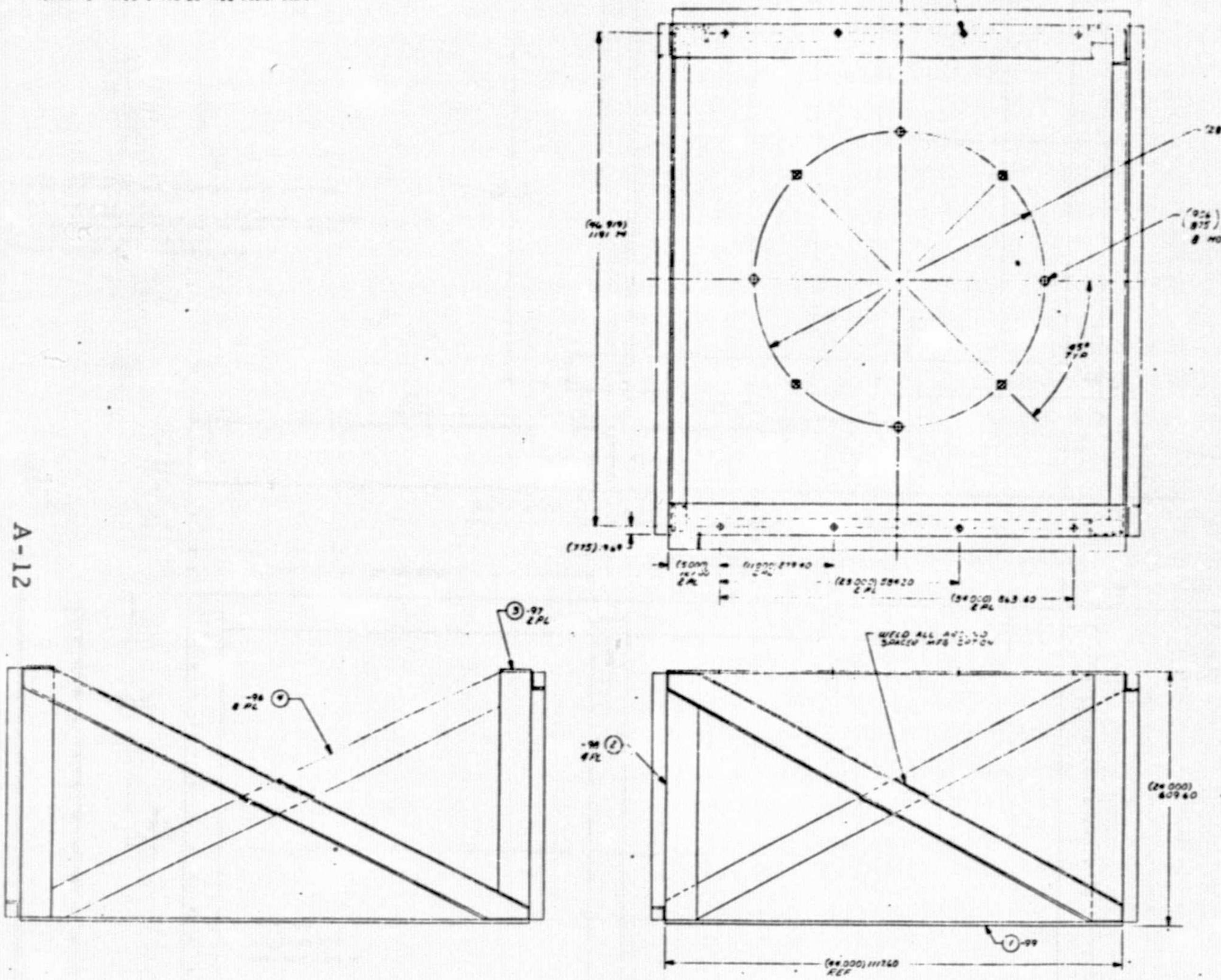

QTY REQD	FSCM NO	PART NO OR IDENTIFYING NO	NOMENCLATURE OR DESCRIPTION		ZONE	ITEM OR FIND NO
8		-96	CHANNEL	MS1007-9-6061-T6		4
2		-97	PLATE, TOP	.250 PLATE, AL ALLOY [illegible] QQ-A-250/[illegible], TEMPER T6 (3.00) 76.20 W X (44.000) 1117.6 L		3
4		-98	ANGLE	[illegible] MS[illegible]-35 (23.500) 596.90 LONG		2
1		-99	PLATE	.500 PLATE, AL ALLOY [illegible] QQ-A-250/[illegible], TEMPER T6 [illegible] X (45.469) [illegible]		1

PARTS LIST

UNLESS OTHERWISE SPECIFIED DIMENSIONS ARE IN INCHES AND PER ANSI Y14.5
.XXX ±.010 .XX ±.03 ANGLES ±0°30'

MATERIAL

CONTRACT | DR | CHK | APPD | DATE

HUGHES HUGHES AIRCRAFT COMPANY CULVER CITY, CALIFORNIA

PEDESTAL - BACK UP STRUCTURE

SIZE E | FSCM NO 82577 | DWG NO 3479221
SCALE | SHEET

NEXT ASSY | USED ON
APPLICATION

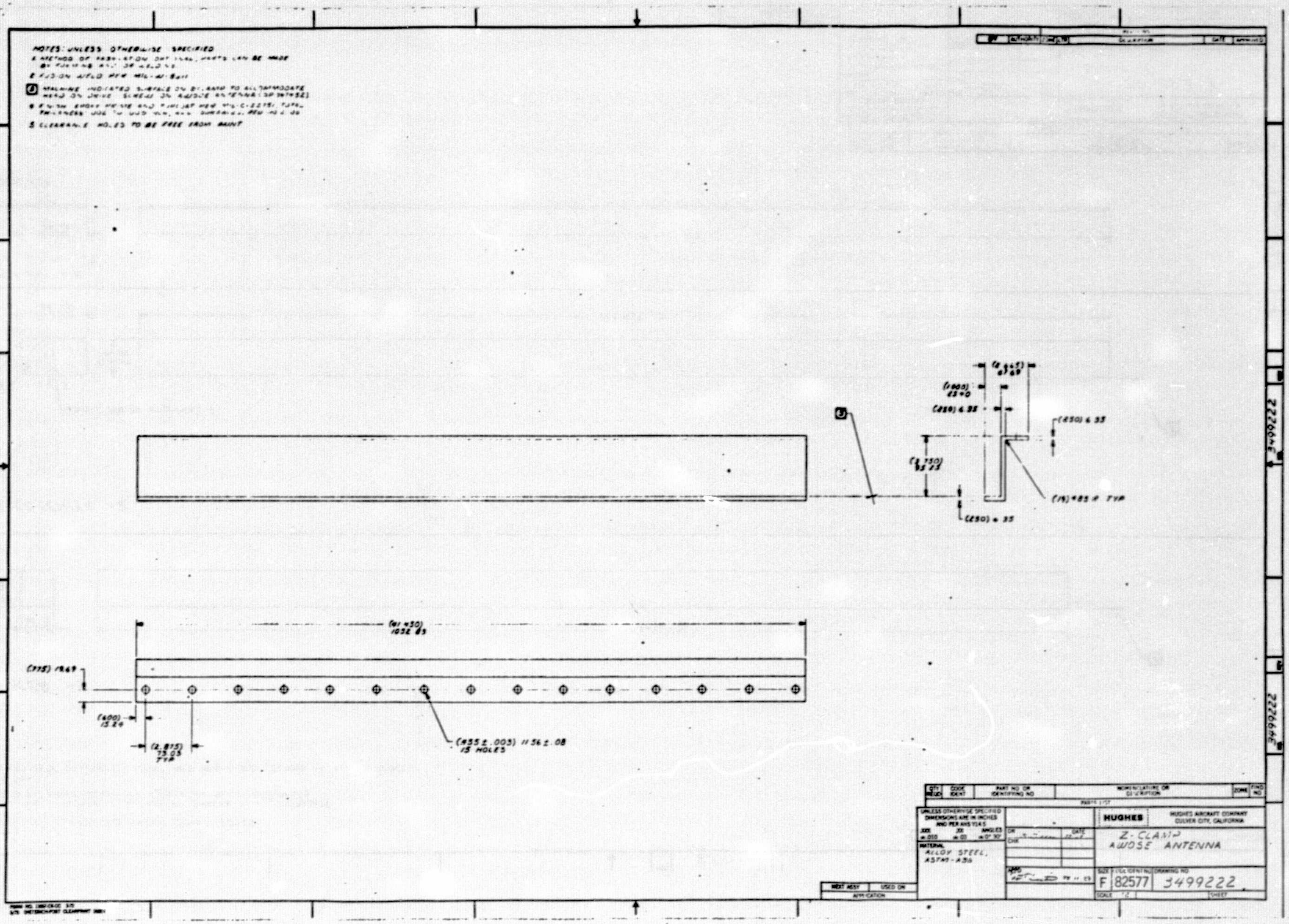
NOTES: UNLESS OTHERWISE SPECIFIED
5 CLEARANCE HOLES TO BE FREE FROM PAINT
(.775) 19.69
(.600) 15.24
(2.875) 73.03 TYP
(.455 ± .003) 11.56 ± .08 15 HOLES
(2.750)
(.250) 6.35
(19) 483 R TYP
(.250) 6.35
UNLESS OTHERWISE SPECIFIED DIMENSIONS ARE IN INCHES AND PER ANS Y14.5
MATERIAL ALLOY STEEL, ASTM-A36
HUGHES
HUGHES AIRCRAFT COMPANY CULVER CITY, CALIFORNIA
Z-CLAMP
AWOSE ANTENNA
SIZE F
82577
DRAWING NO 3499222
PARTS LIST
NEXT ASSY
USED ON
APPLICATION
3499222

E2266-F

NOTES: -1, -2, -3

1. REMOVE BURRS AND BREAK SHARP EDGES

2. (boxed) MACHINE INDICATED SURFACE ON SPACER TO ACCOMMODATE HEAD ON DRIVE SCREW ON ALSOE ANTENNA (SP347432).

3. FINISH:
A CHROMATE CONVERSION COAT PER MIL-C-5541, CLASS 1A, ALL SURFACES.

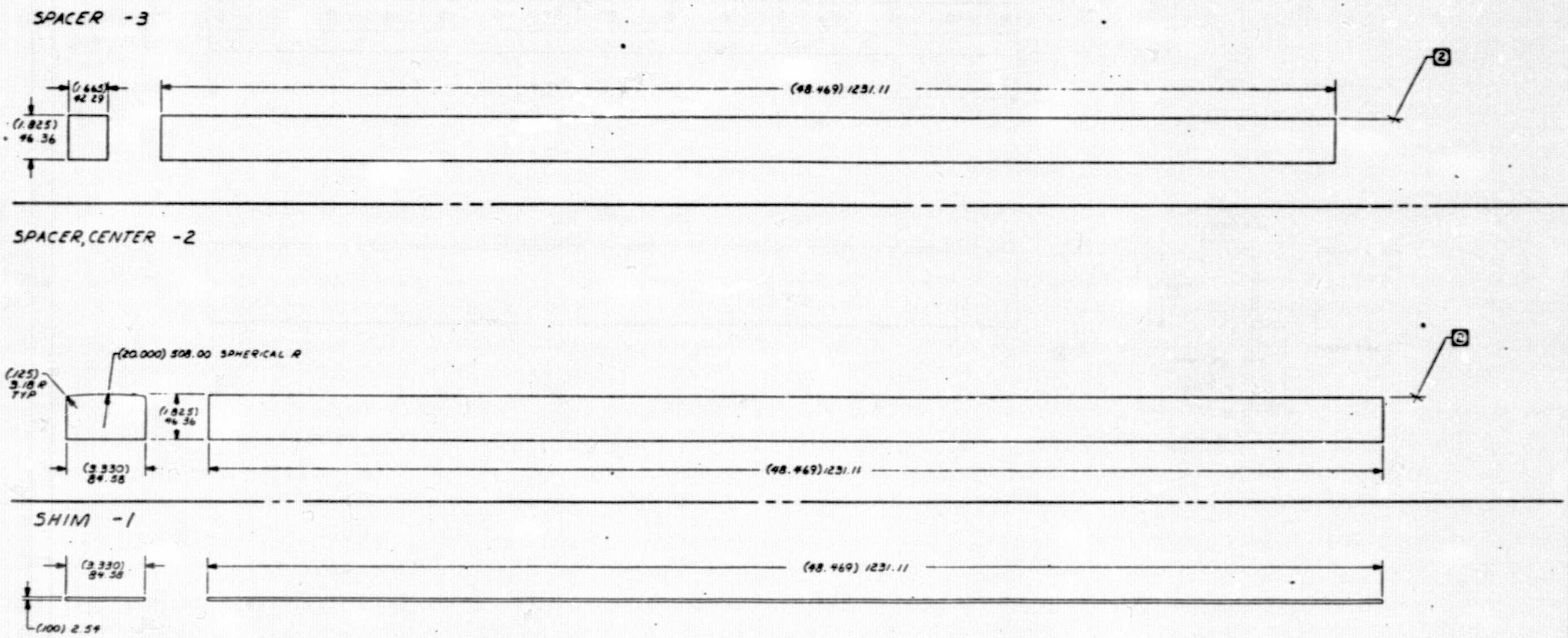

QTY REQD	CODE IDENT	PART NO OR IDENTIFYING NO	NOMENCLATURE OR DESCRIPTION	ZONE	FIND NO

PARTS LIST

UNLESS OTHERWISE SPECIFIED DIMENSIONS ARE IN INCHES AND PER ANS Y14.5
XXX ±.010 XX ±.03 ANGLES ±0° 30'

MATERIAL: ALUMINUM ALLOY 6061-T6, QQ-A-250/11 TEMPER T6

DR / DATE / CHK / APPD

HUGHES — HUGHES AIRCRAFT COMPANY, CULVER CITY, CALIFORNIA

SPACER -2, -3 & SHIM -1

SIZE D | CODE IDENT NO 82577 | DRAWING NO 3499223

SCALE 1/1 | SHEET

NEXT ASSY | USED ON | APPLICATION

3499223

NOTES: UNLESS OTHERWISE SPECIFIED
1. REMOVE BURRS AND BREAK SHARP EDGES.
2. CADMIUM PLATE PER QQ-P-416, TYPE II, CLASS 3.

EFF	AUTHORITY	LTR	DESCRIPTION	DATE	APPROVED

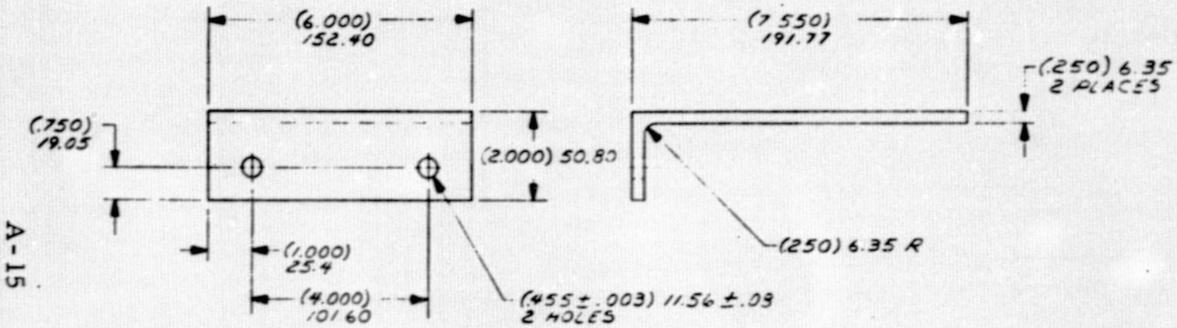

ORIGINAL PAGE IS OF POOR QUALITY

DWG NO 3499224

QTY REQD	FSCM NO	PART NO OR IDENTIFYING NO	NOMENCLATURE OR DESCRIPTION	ITEM OR FIND NO

PARTS LIST

EXCEPT AS NOTED DIM ARE IN INCHES AND PER ANSI Y14.5 .XXX .XX ANGLES ±.010 ±.03 ±0°30'	CONTRACT:	HUGHES — HUGHES AIRCRAFT COMPANY CULVER CITY, CALIFORNIA
MATERIAL ALLOY STEEL ASTM-A36	DR R. Bive / CHK / APPD	PLATE, ALIGNMENT
NEXT ASSY / USED ON / APPLICATION		SIZE C / FSCM NO 82577 / DWG NO 3499224 / SCALE 1/2 / SHEET

FORM NO. 11064-CS-CC REV. 7-76
DIETERICH-POST CLEARPRINT 1000H

APPENDIX B
PATTERNS OF X-BAND ARRAY AND FEED DATA

B.1 X-BAND ARRAY MEASURED RADIATION PATTERNS

The following sequence of 24 radiation pattern plots describes the behavior of the array of eight modules over the frequency range from 9.3 GHz to 9.8 GHz in the two principal planes.

LIST OF RADIATION PATTERNS

Sequence Number	Pattern Number	Frequency	Plane	Comment	Page Number
1	1	9.7	Horiz.	±90 degrees	B-2
2	2	9.7	Horiz.	±30 degrees	B-3
3	4	9.7	Vert.	±90 degrees	B-4
4	3	9.7	Vert.	±30 degrees	B-5
5	6	9.6	Horiz.	±90 degrees	B-6
6	5	9.6	Horiz.	±30 degrees	B-7
7	7	9.6	Vert.	±90 degrees	B-8
8	8	9.6	Vert.	±30 degrees	B-9
9	12	9.8	Horiz.	±90 degrees	B-10
10	11	9.8	Horiz.	±30 degrees	B-11
11	10	9.8	Vert.	±90 degrees	B-12
12	9	9.8	Vert.	±30 degrees	B-13
13	13	9.5	Horiz.	±90 degrees	B-14
14	16	9.5	Horiz.	±30 degrees	B-15
15	15	9.5	Vert.	±90 degrees	B-16
16	14	9.5	Vert.	±30 degrees	B-17
17	18	9.4	Horiz.	±90 degrees	B-18
18	17	9.4	Horiz.	±30 degrees	B-19
19	19	9.4	Vert.	±90 degrees	B-20
20	20	9.4	Vert.	±30 degrees	B-21
21	23	9.3	Horiz.	±90 degrees	B-22
22	24	9.3	Horiz.	±30 degrees	B-23
23	22	9.3	Horiz.	±90 degrees	B-24
24	21	9.3	Horiz.	±30 degrees	B-25

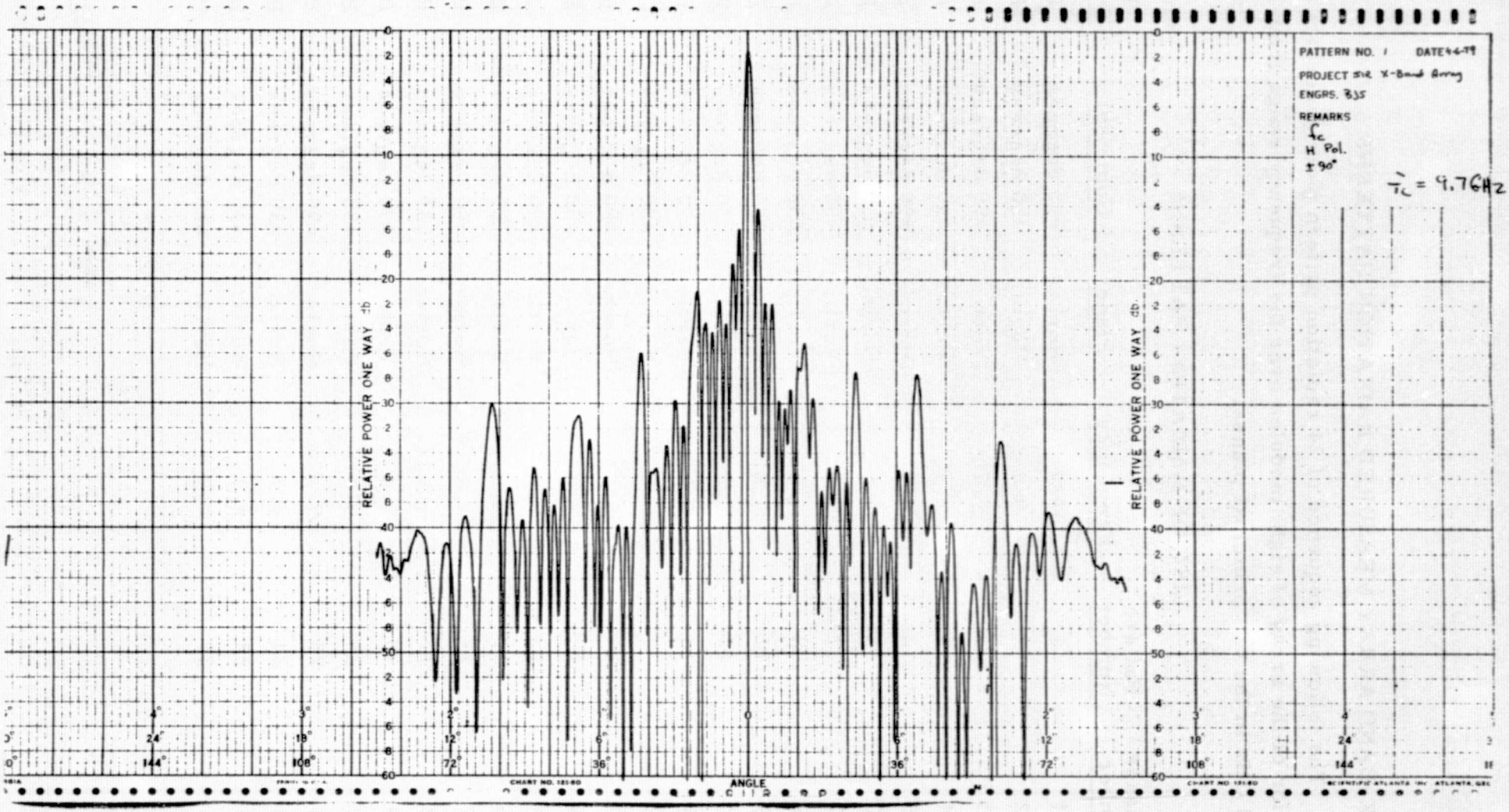
PATTERN NO. 1 DATE 4-6-79
PROJECT SIR X-Band Array
ENGRS. BJS
REMARKS
f_c
H Pol.
±90°
f_c = 9.76GHz
RELATIVE POWER ONE WAY dB
ANGLE
CHART NO. 121-60
SCIENTIFIC ATLANTA INC ATLANTA, GEO

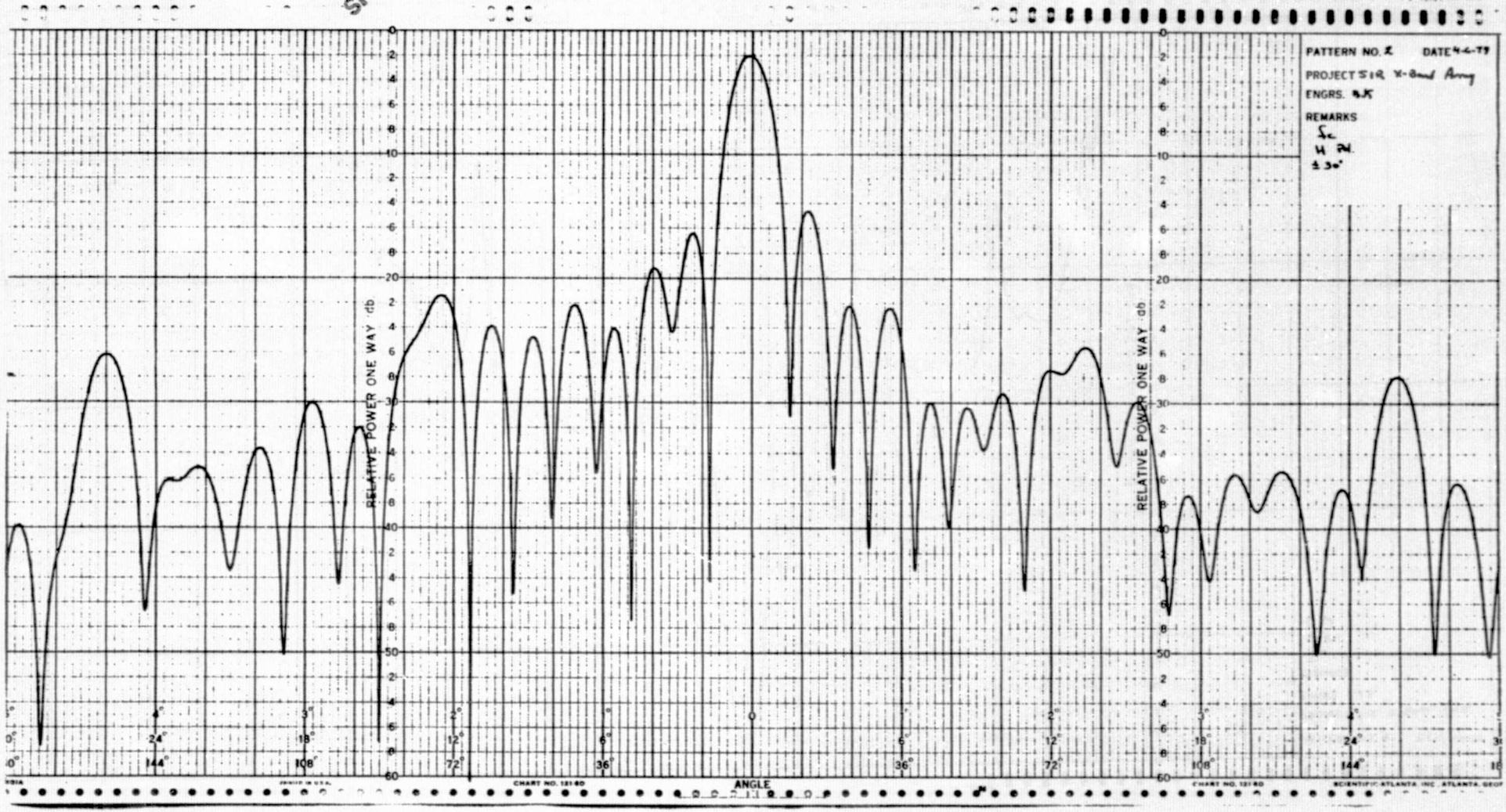

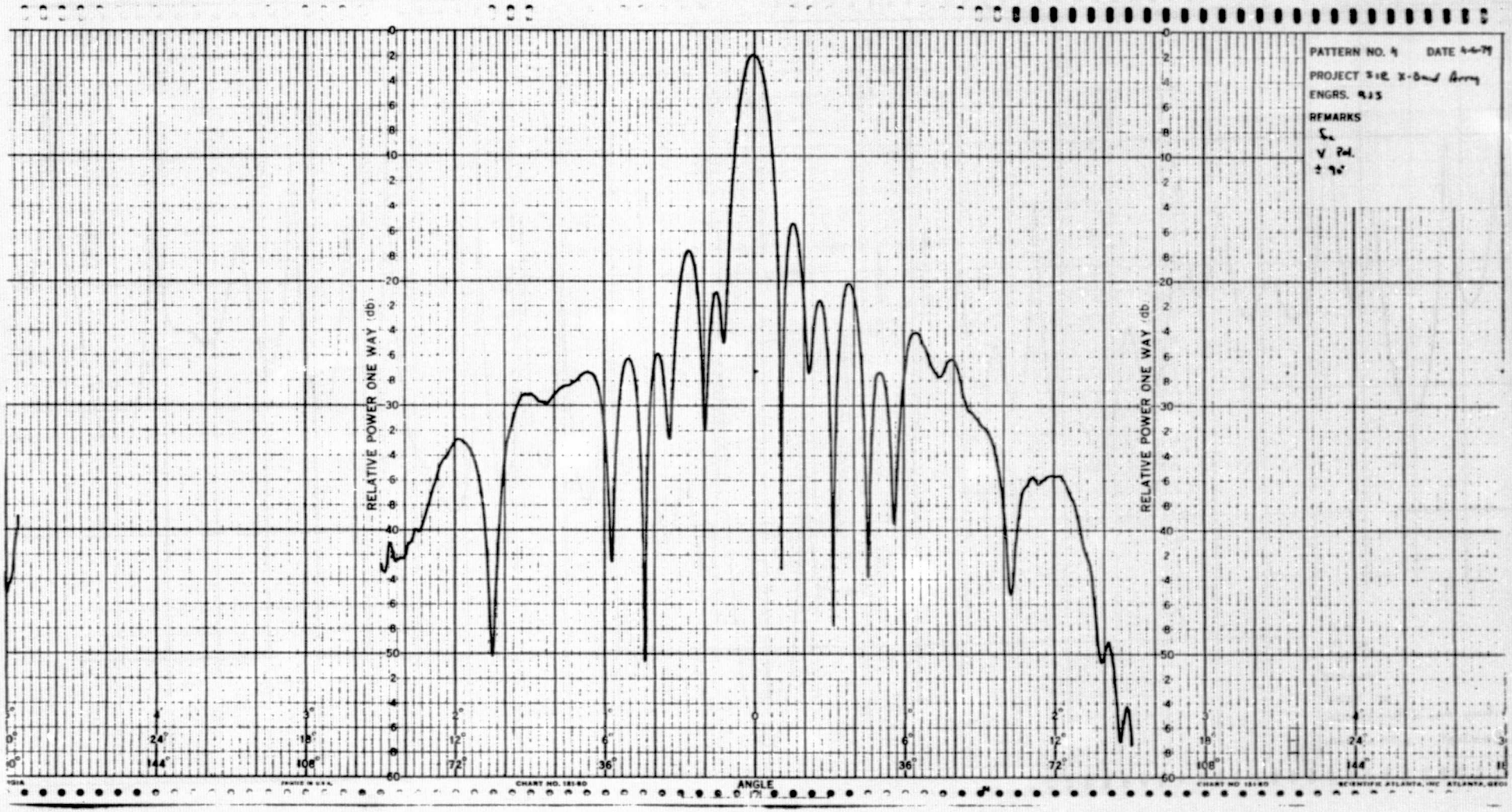
PATTERN NO. 4 DATE 4-6-79
PROJECT 3:1 X-Band Array
ENGRS. RJS
REMARKS
E-
V Pol.
± 90°
RELATIVE POWER ONE WAY (db)
ANGLE
0
2
4
6
8
10
20
30
40
50
60
144°
108°
72°
36°
24°
18°
12°
6°

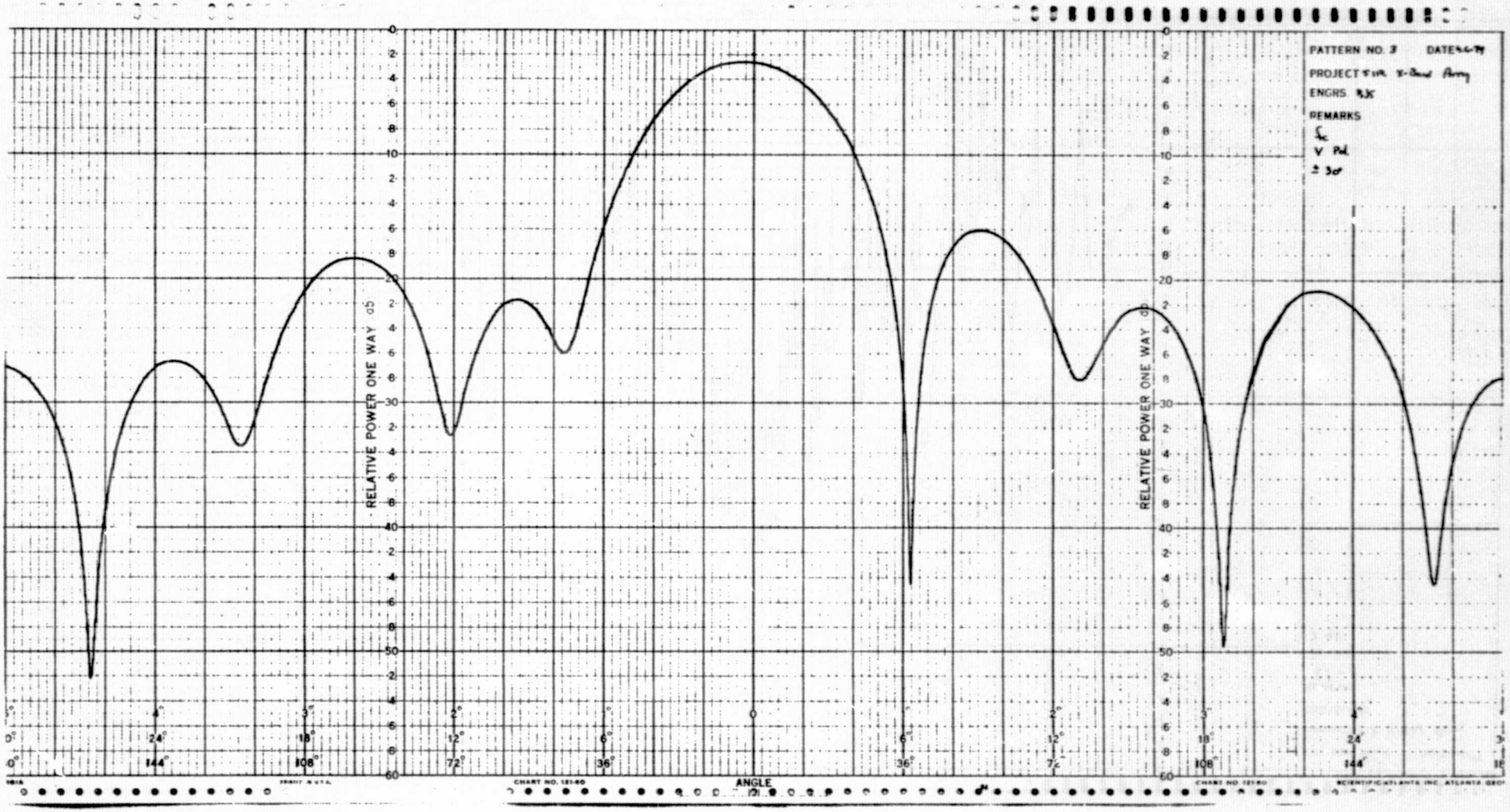
PATTERN NO. 3
PROJECT S-Band Array
ENGRS.
REMARKS
E
V Pol
± 30°
RELATIVE POWER ONE WAY dB
ANGLE
0
2
4
6
8
10
20
30
40
50
60
144°
108°
72°
36°
0°
24°
18°
12°
6°
3°
2°
1°

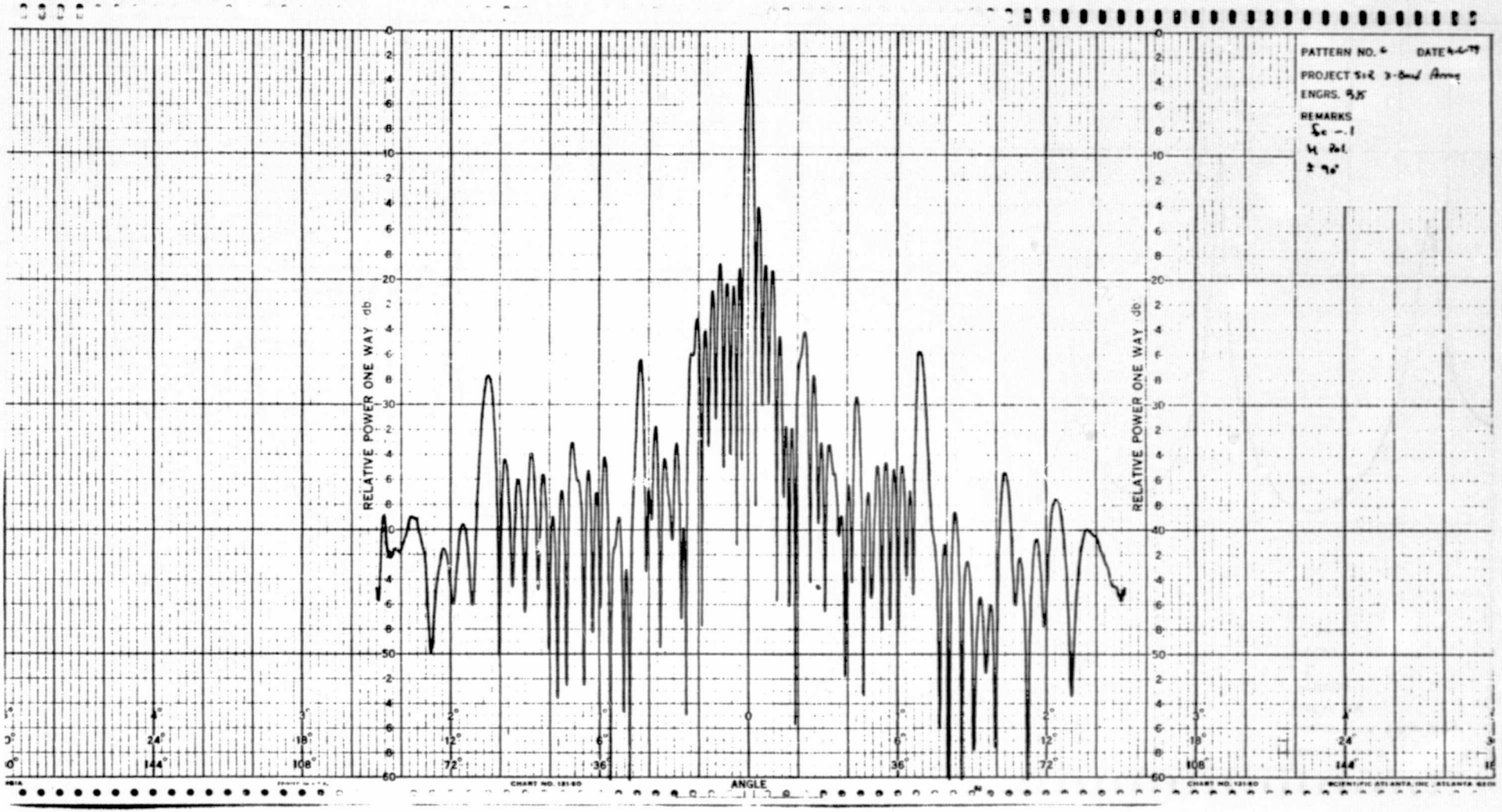
PATTERN NO. 4 DATE 4-6-79
PROJECT S-2 3-Band Array
ENGRS. RJS
REMARKS
Sc -.1
H 201
± 90°
RELATIVE POWER ONE WAY db
RELATIVE POWER ONE WAY db
ANGLE
CHART NO. 121-60
CHART NO. 121-60

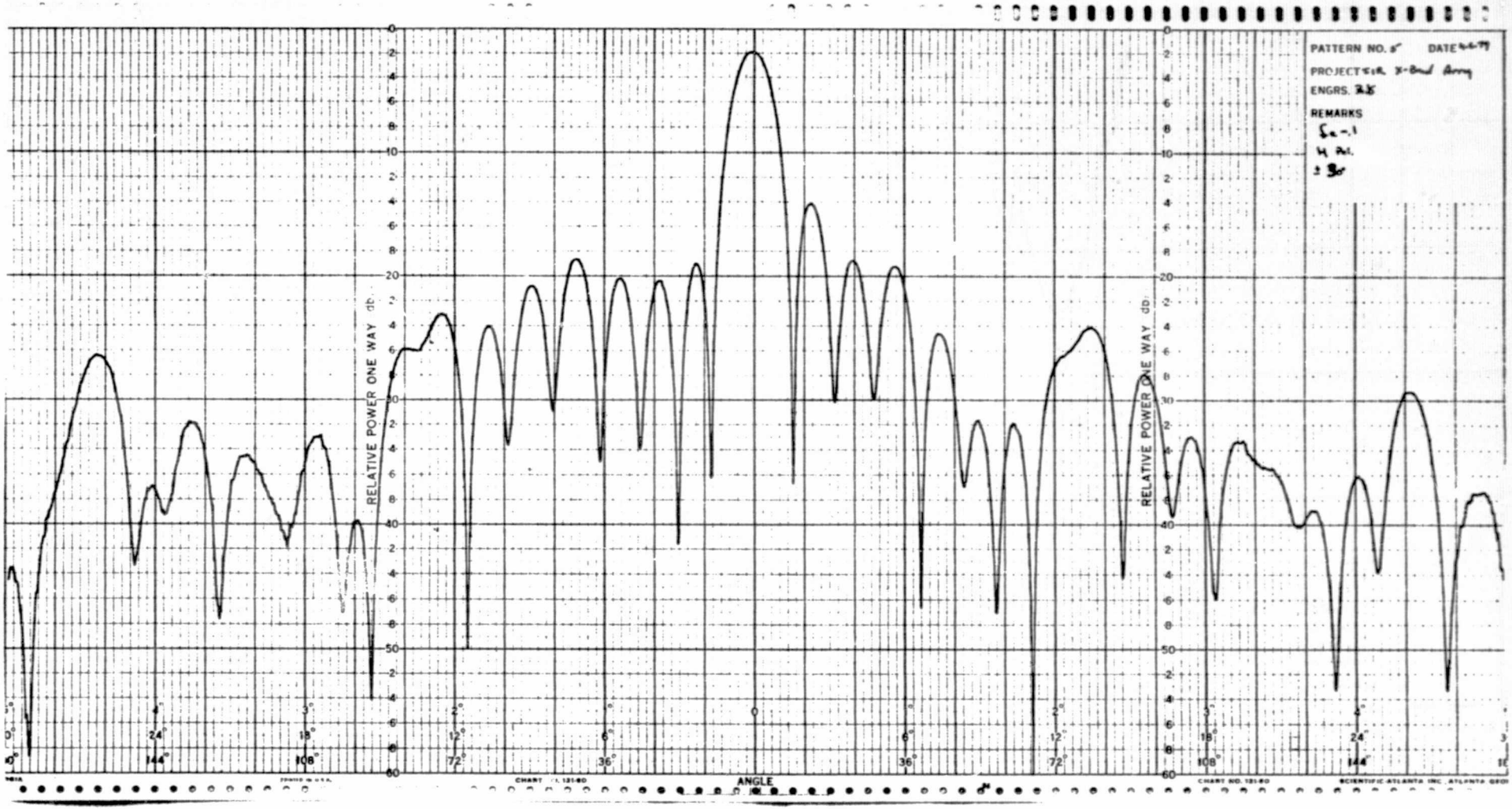
PATTERN NO. 5
DATE 4-6-79
PROJECT S-B X-Band Array
ENGRS. RB
REMARKS
Sa -.1
4 Pol.
± 3°
RELATIVE POWER ONE WAY dB
ANGLE
144°
108°
72°
36°
24°
18°
12°
6°
4°
3°
2°
0°

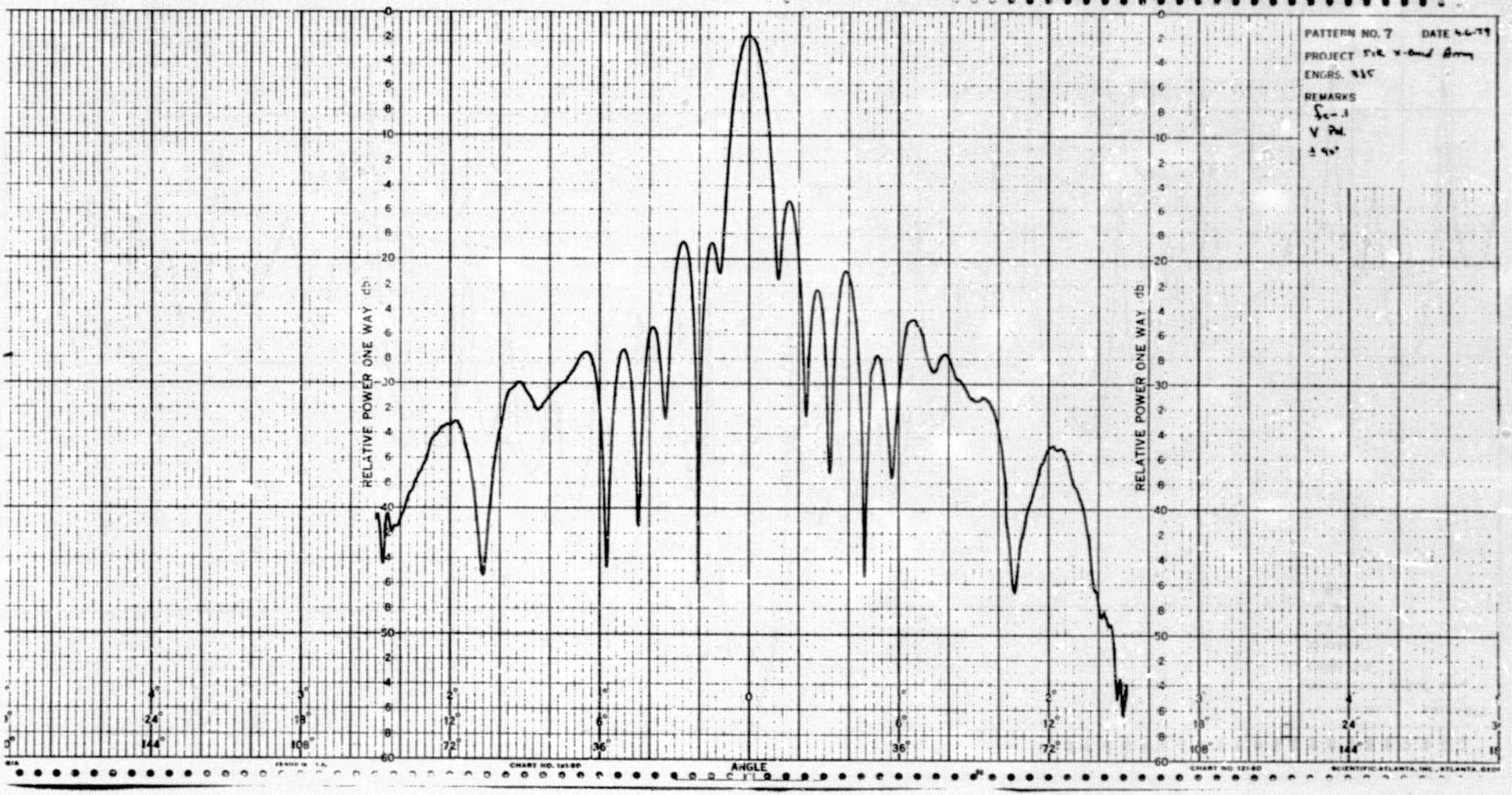
PATTERN NO. 7
DATE 4-6-79
PROJECT 5'x8' X-band Array
ENGRS. RLS
REMARKS
Sec. 3
V Pol.
± 90°
RELATIVE POWER ONE WAY db
ANGLE
CHART NO. 121-80
SCIENTIFIC ATLANTA, INC., ATLANTA, GEOR

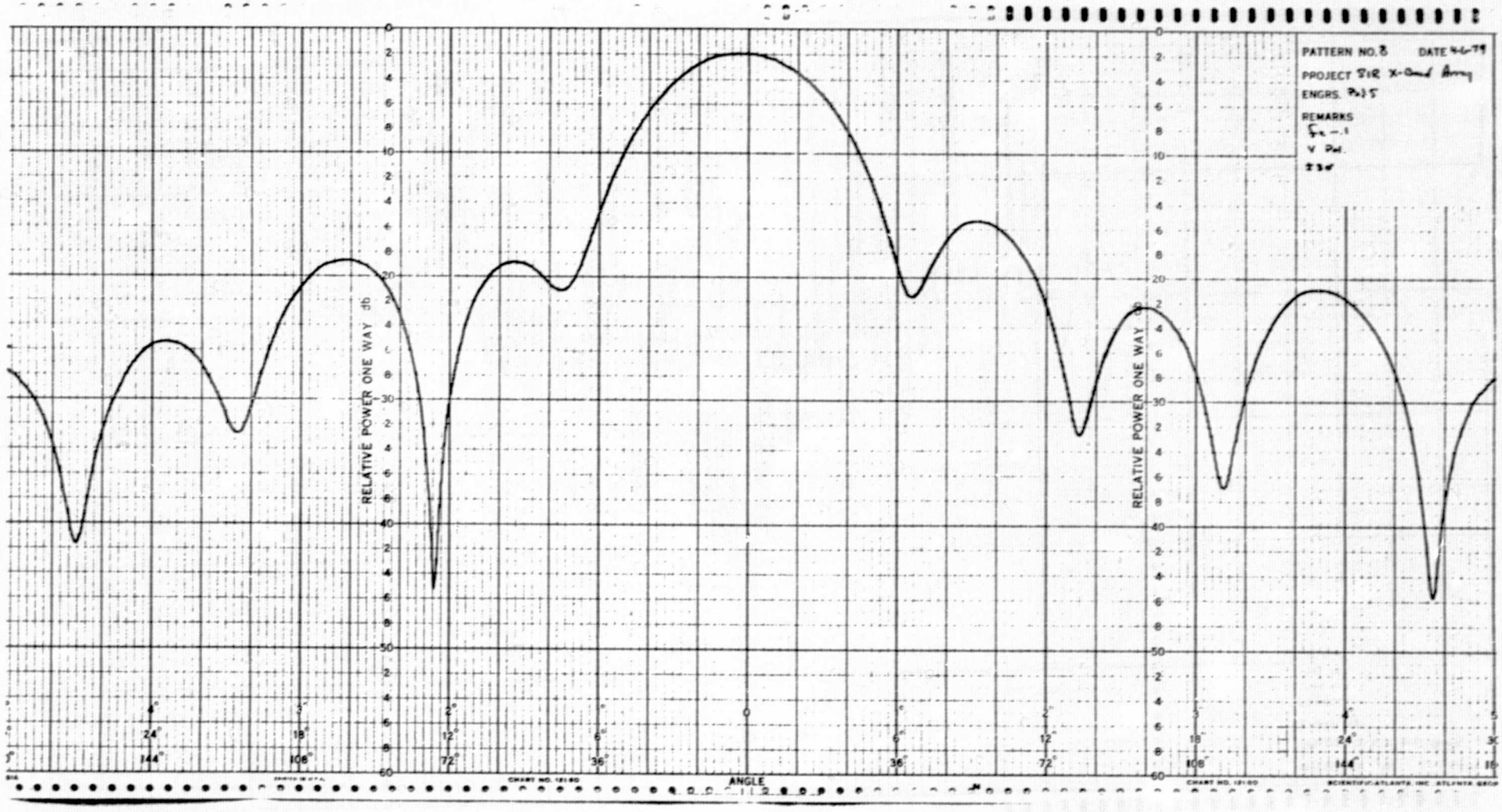
PATTERN NO. 8 DATE 4-6-79
PROJECT TIR X-Band Array
ENGRS. PJS
REMARKS
Fo -.1
V Pol.
230
RELATIVE POWER ONE WAY db
ANGLE
0
2°
4°
6°
12°
18°
24°
36°
72°
108°
144°

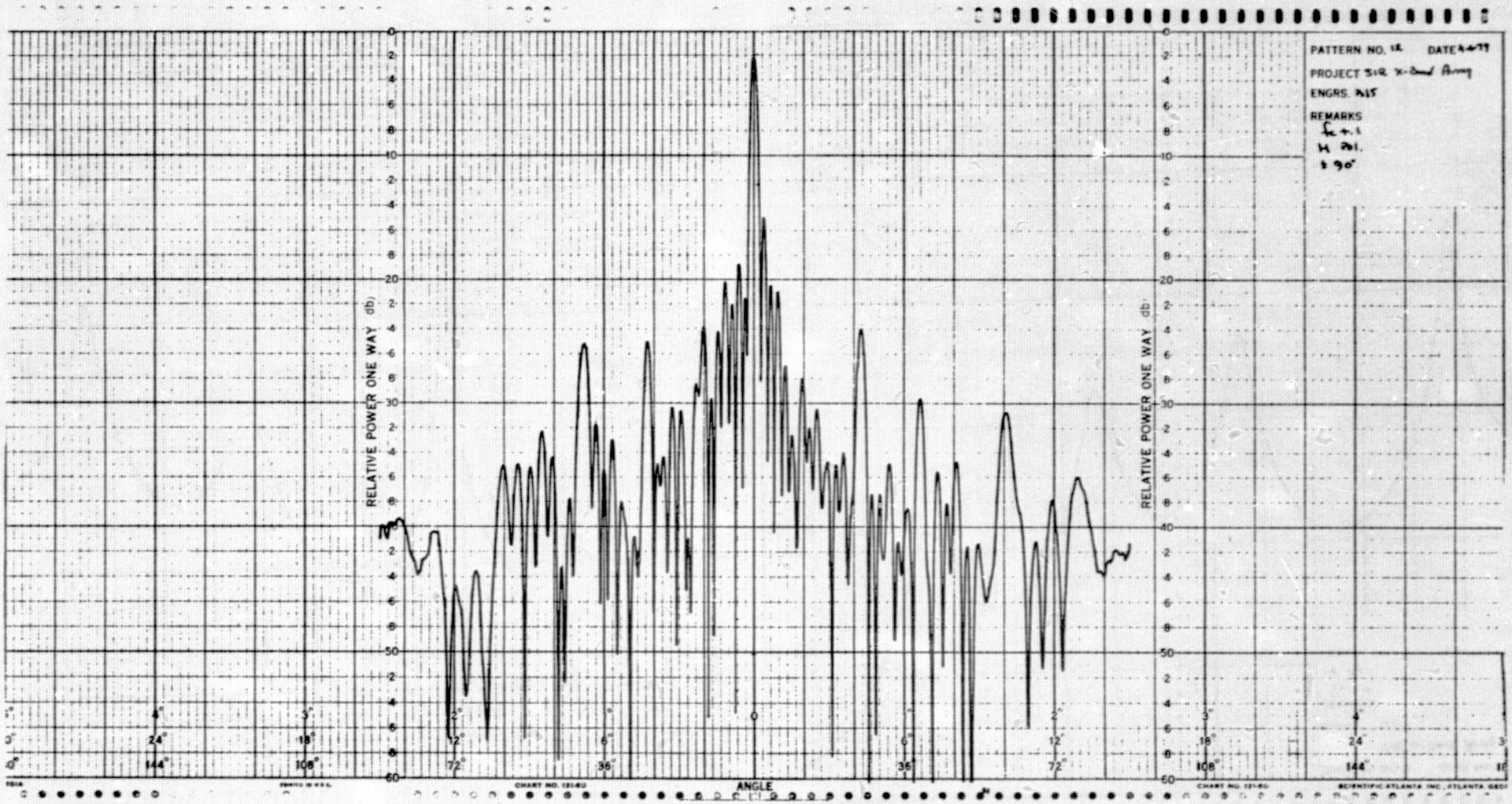
PATTERN NO. 12 DATE 4-79
PROJECT 512 X-Band Array
ENGRS. RJS
REMARKS
f = 9.1
H 20.
ϕ 90°
RELATIVE POWER ONE WAY db
ANGLE
CHART NO. 121-6U
SCIENTIFIC ATLANTA INC., ATLANTA GEO

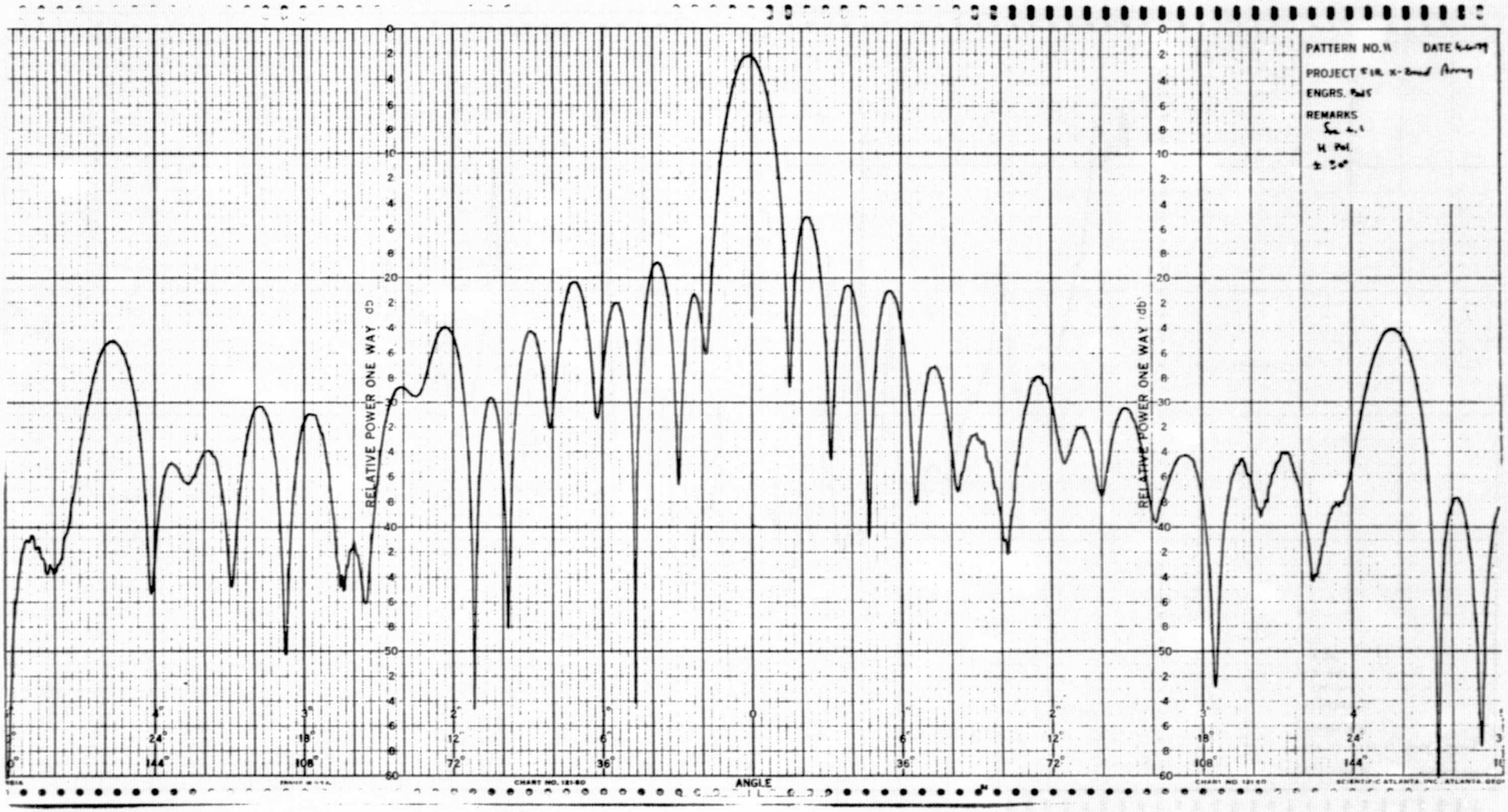
PATTERN NO. 11
DATE
PROJECT
ENGRS.
REMARKS
H Pol
RELATIVE POWER ONE WAY db
ANGLE
CHART NO. 121-60
SCIENTIFIC ATLANTA INC. ATLANTA GEO

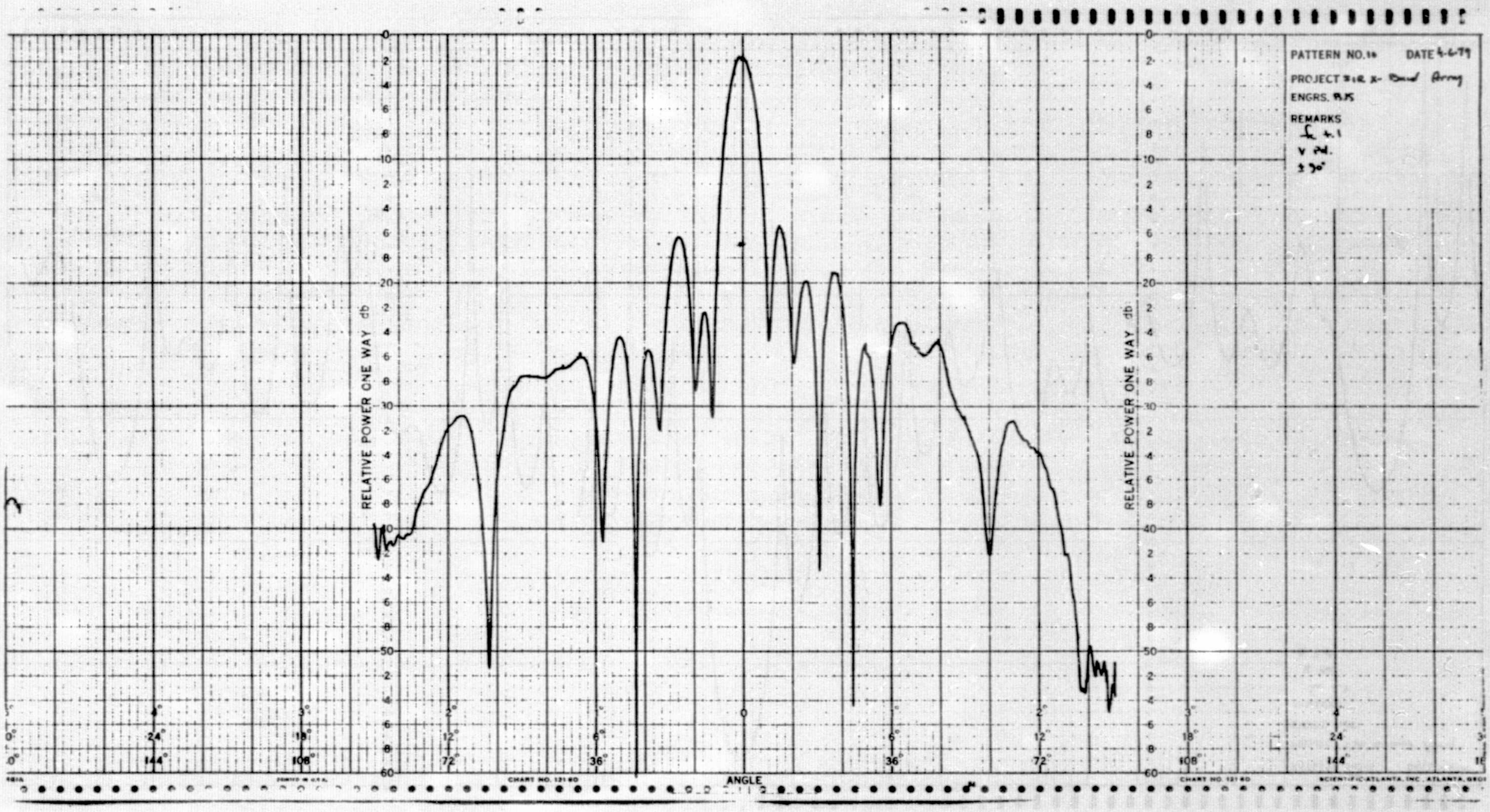
PATTERN NO.
DATE 4-6-79
PROJECT
ENGRS.
REMARKS
RELATIVE POWER ONE WAY db
ANGLE
CHART NO. 121 60
SCIENTIFIC-ATLANTA, INC., ATLANTA, GEO

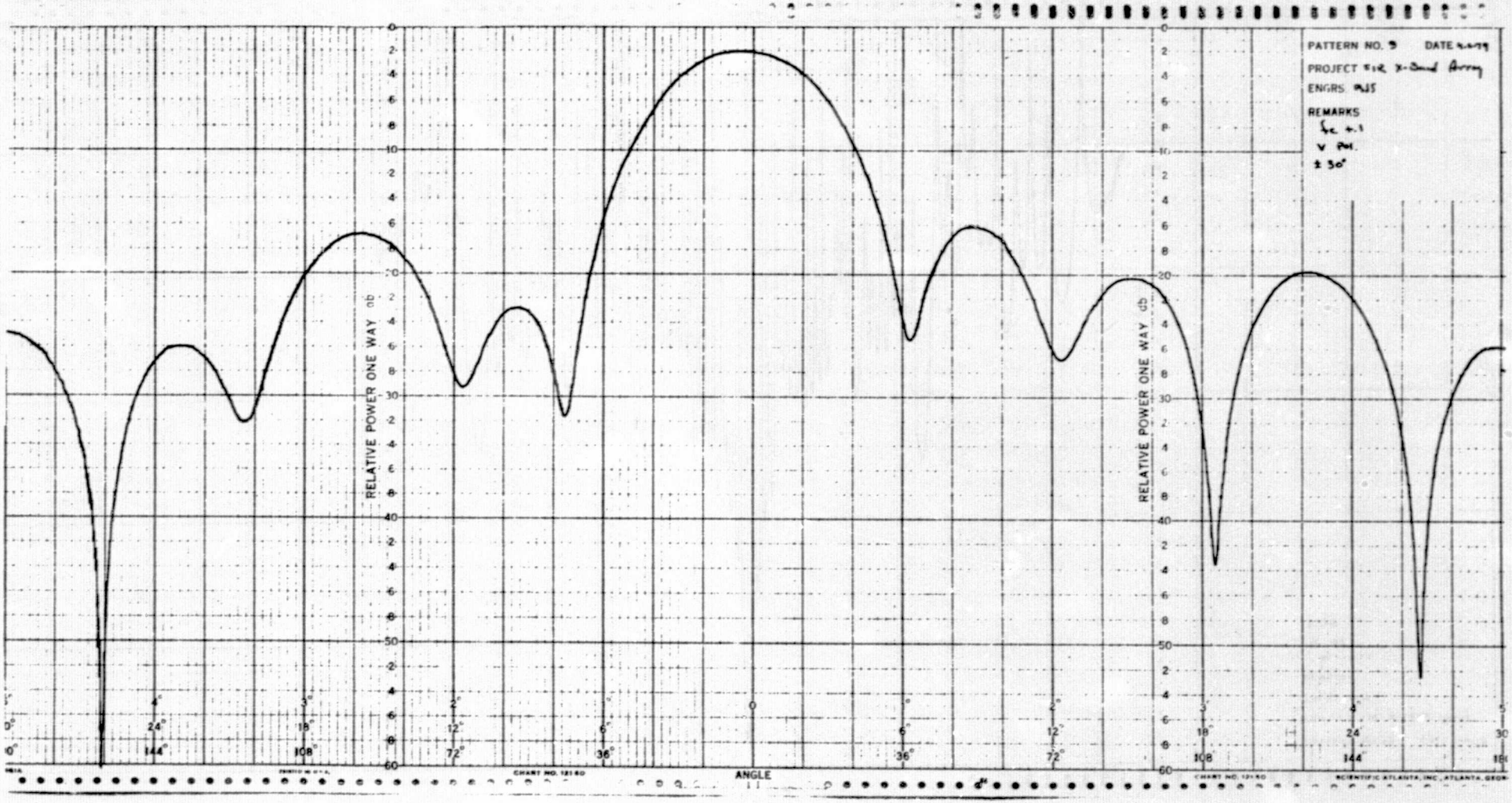
PATTERN NO. 3 DATE 4-27-79
PROJECT T-R X-Band Array
ENGRS RJS
REMARKS
Sec 4.1
V Pol.
± 30°
RELATIVE POWER ONE WAY db
ANGLE
CHART NO. 121-60
SCIENTIFIC ATLANTA, INC., ATLANTA, GEOR

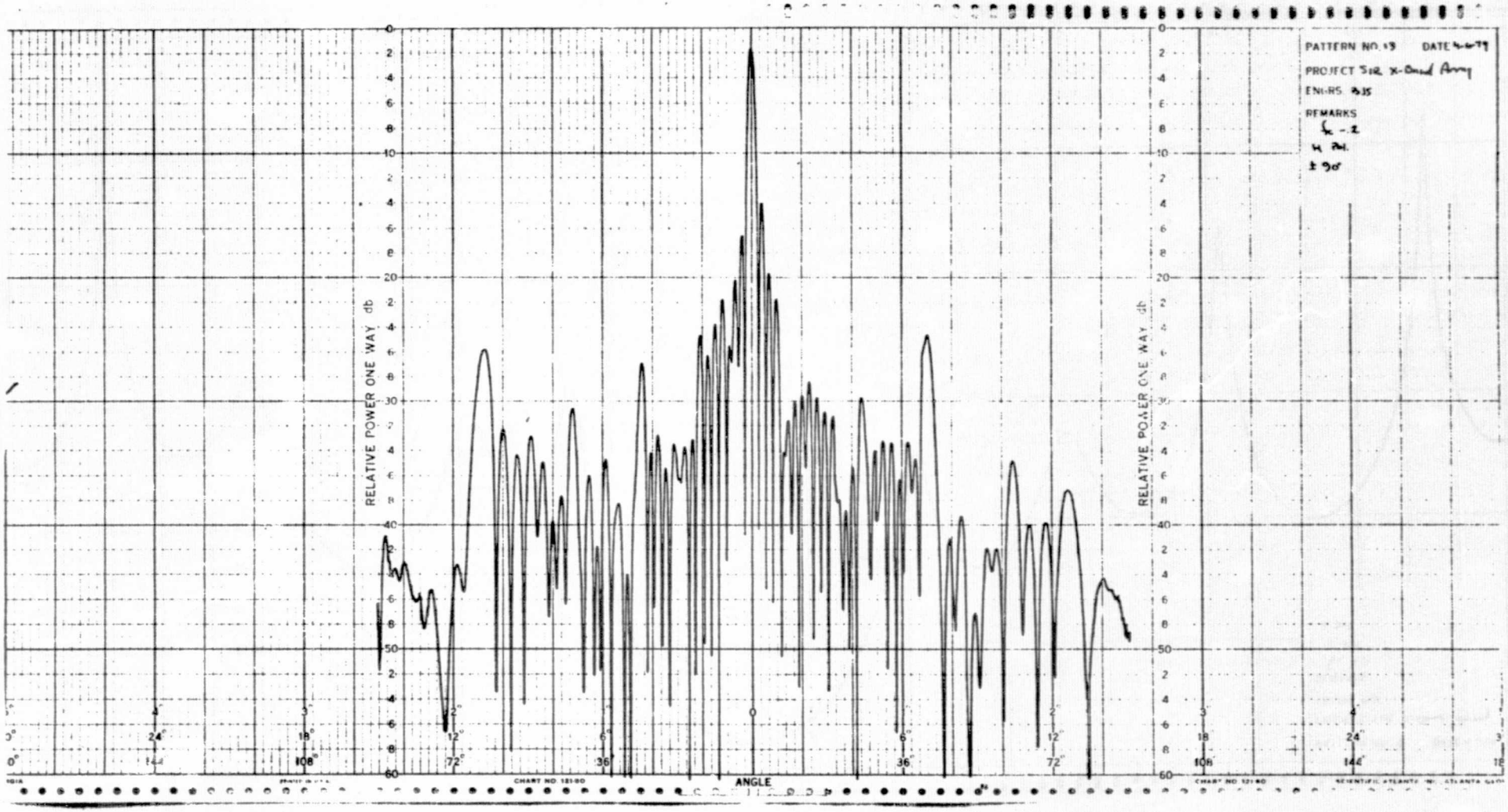

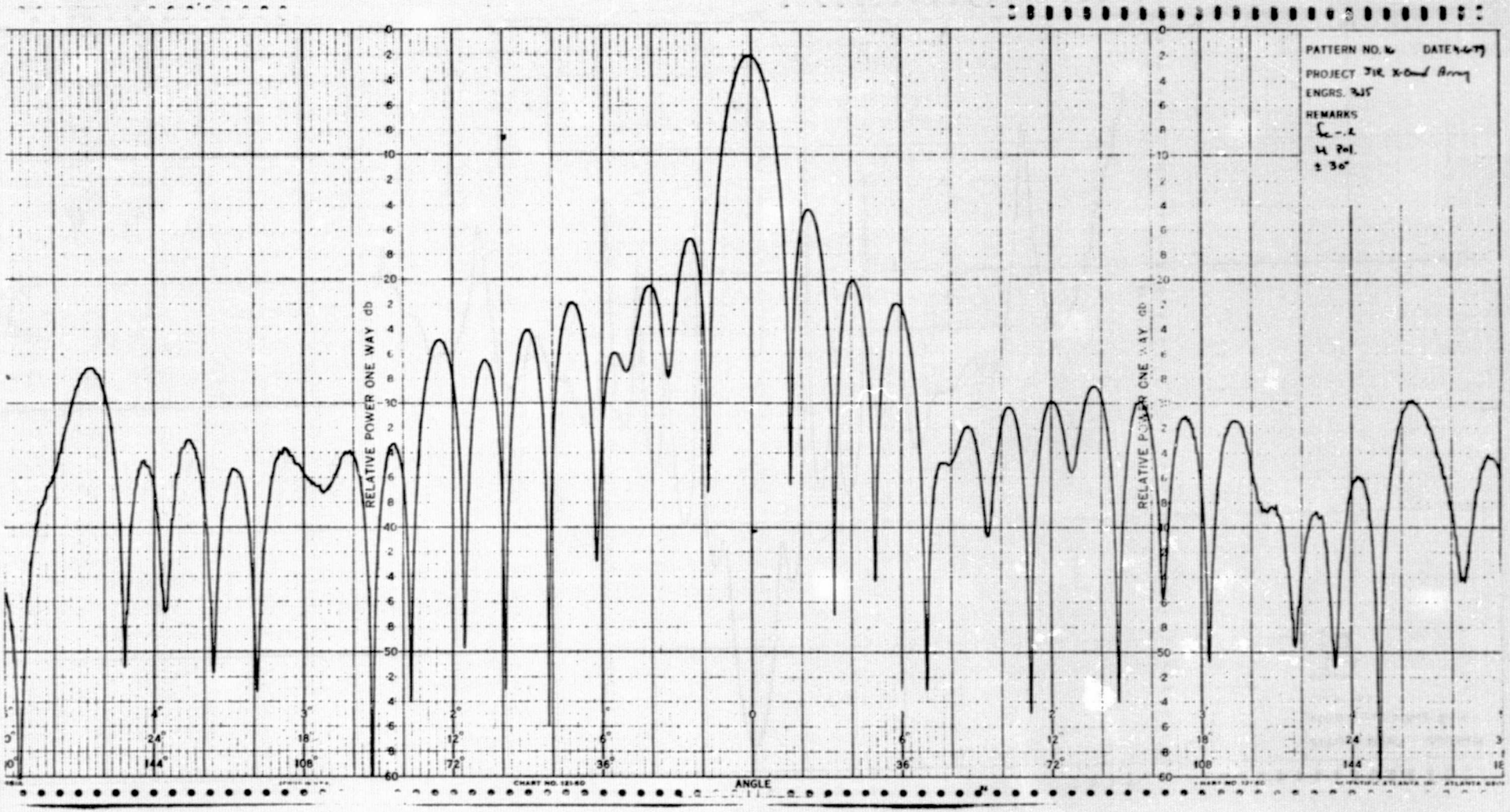
PATTERN NO. 6
PROJECT
ENGRS.
REMARKS
RELATIVE POWER ONE WAY db
ANGLE

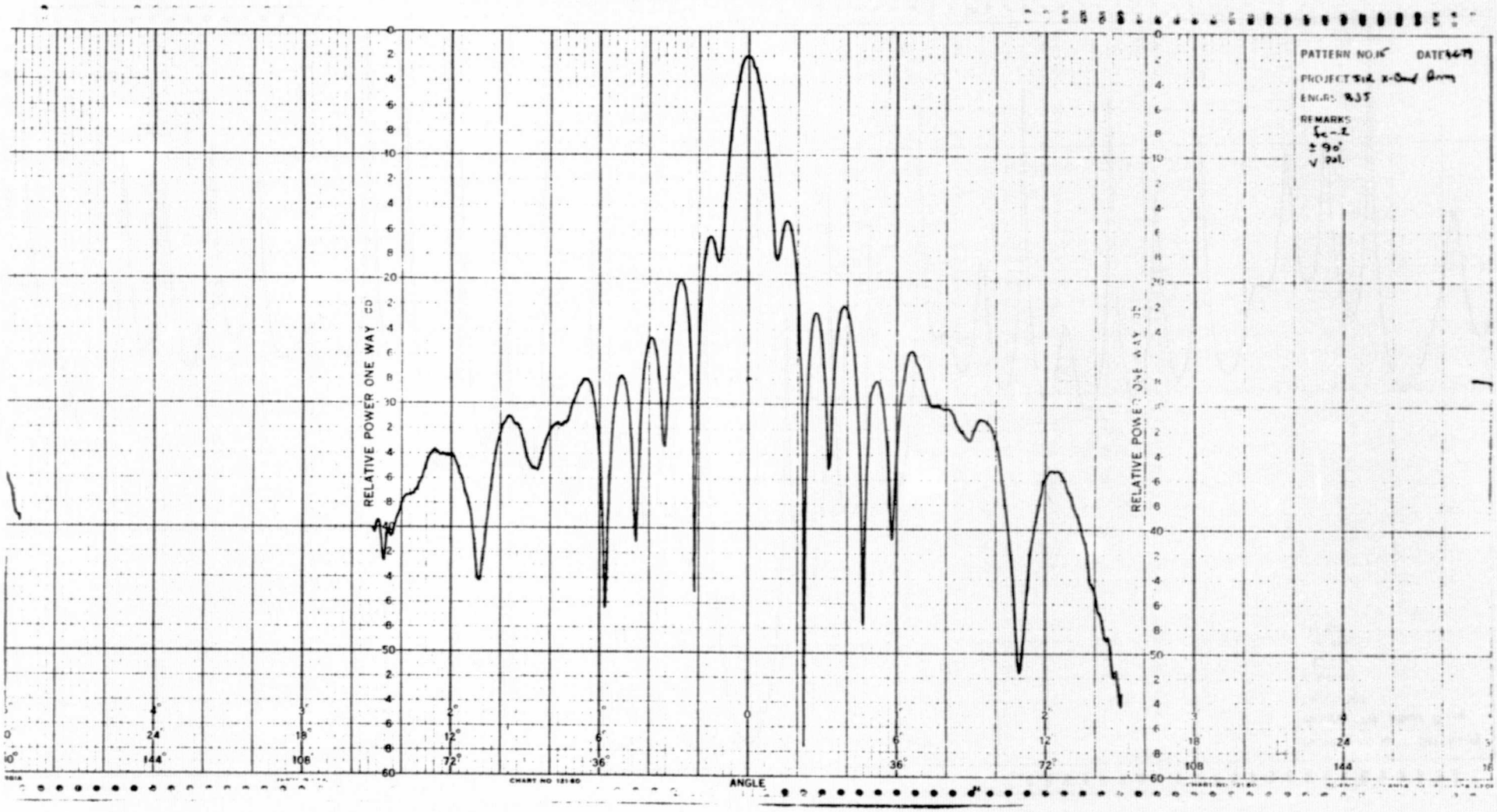
PATTERN NO.
DATE
PROJECT
ENGR.
REMARKS
RELATIVE POWER ONE WAY DB
ANGLE
CHART NO 12140

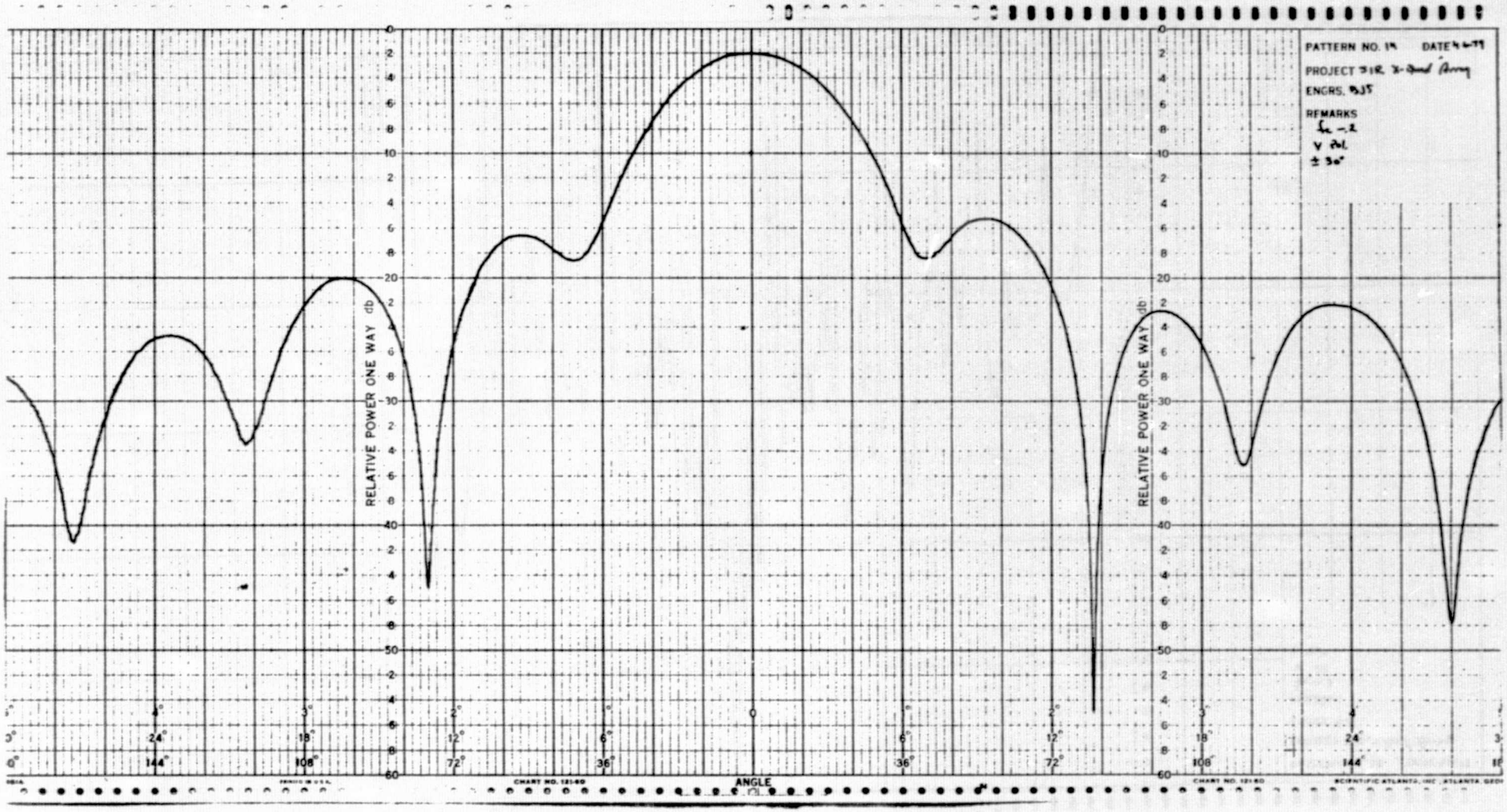
PATTERN NO. 1A
PROJECT
ENGRS.
REMARKS
RELATIVE POWER ONE WAY db
ANGLE

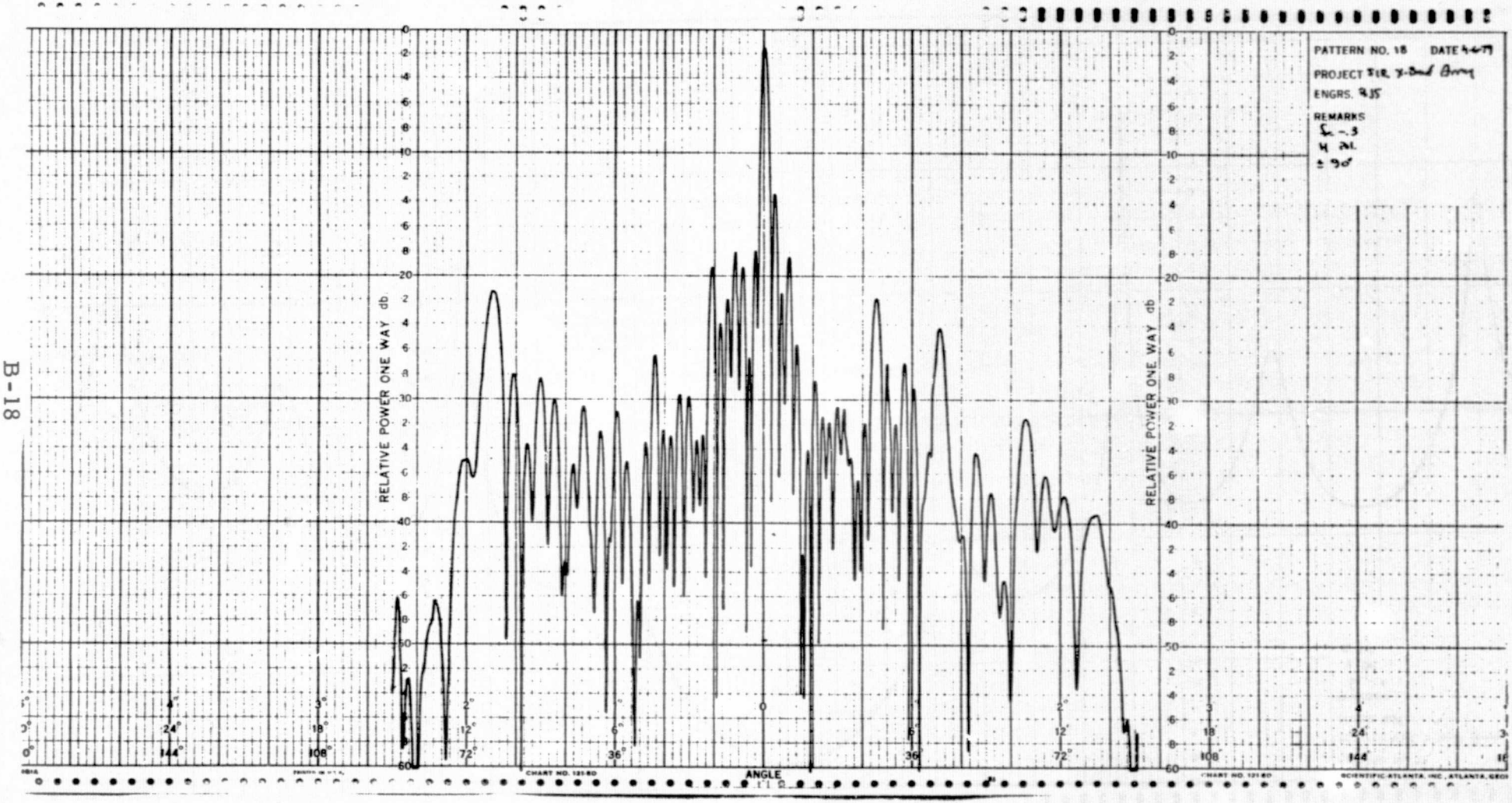
PATTERN NO. 18 DATE 4-67
PROJECT TIR, X-Band Array
ENGRS. RJS
REMARKS
Sc = .3
4 at
± 90°
RELATIVE POWER ONE WAY db
RELATIVE POWER ONE WAY db
ANGLE
CHART NO. 121-60
SCIENTIFIC-ATLANTA, INC., ATLANTA, GEOR

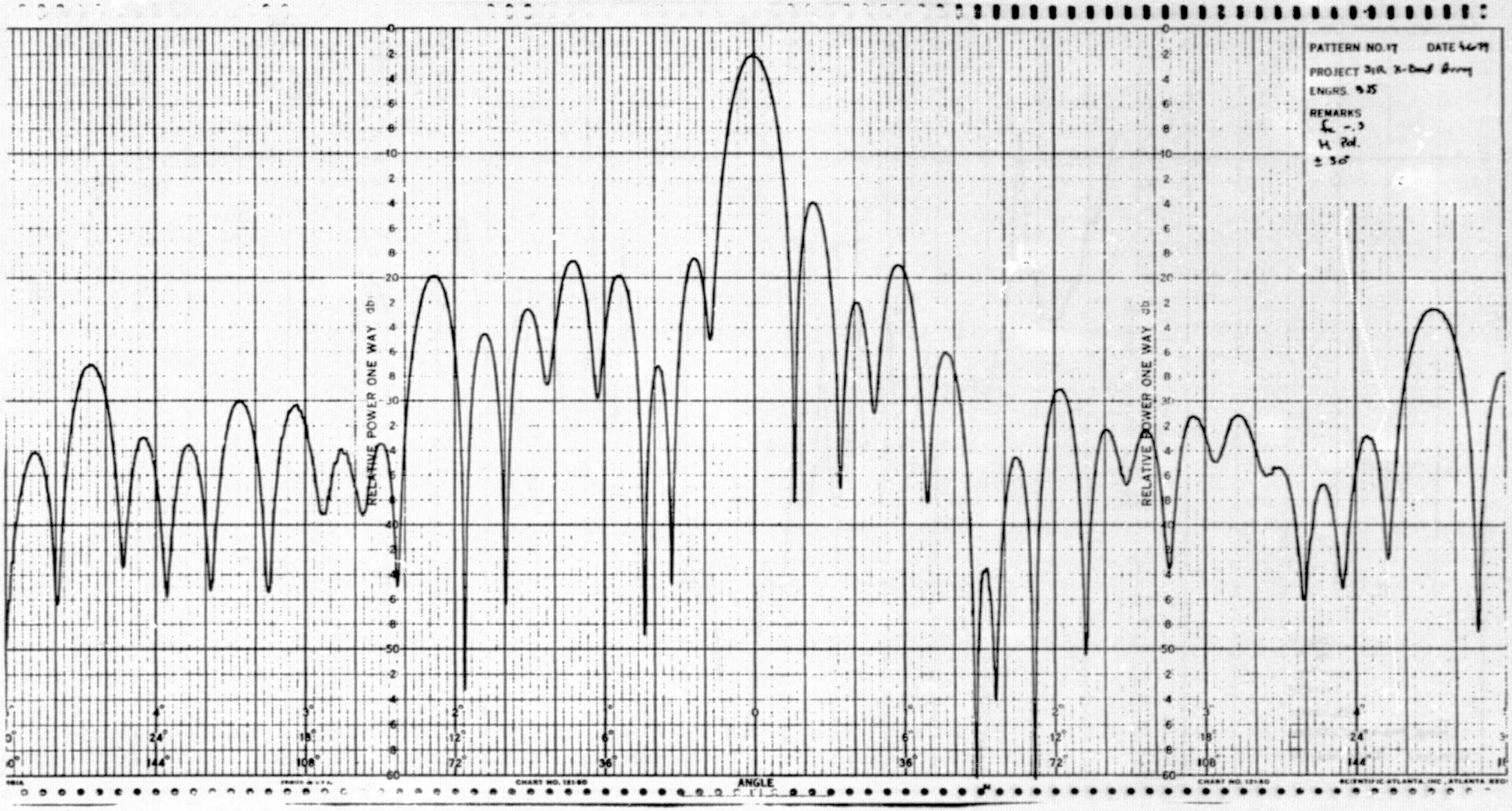
PATTERN NO. 17 DATE 4-6-79
PROJECT 31A X-Band Array
ENGRS. SS
REMARKS
f_c = -.3
H Pol.
± 30°
RELATIVE POWER ONE WAY db
ANGLE
CHART NO. 121-60
SCIENTIFIC ATLANTA, INC., ATLANTA, GEO.

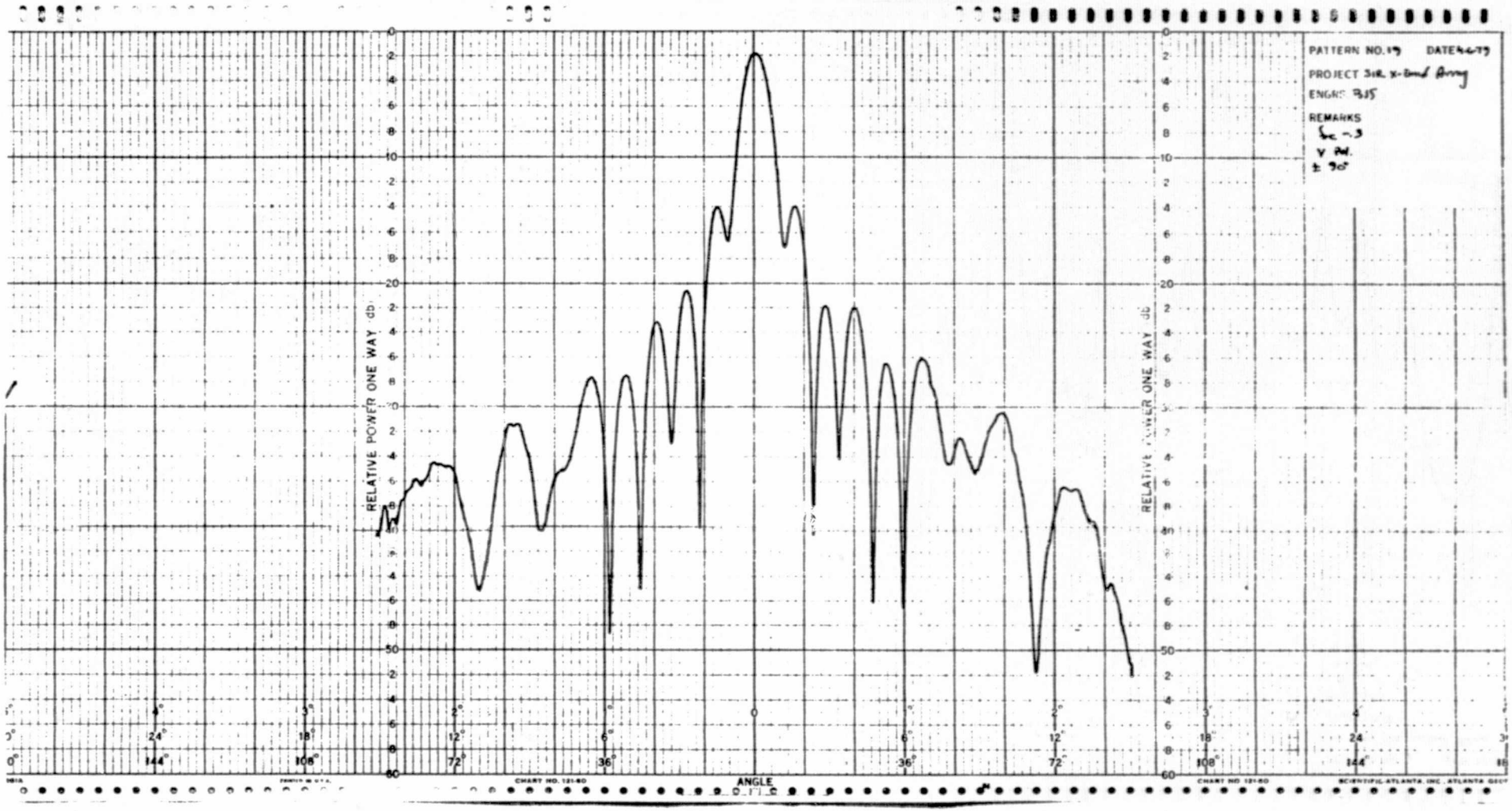
PATTERN NO. 19 DATE 4-79
PROJECT 3IR, X-band Array
ENGR: BJS
REMARKS
Sc -.3
V Pol.
± 90°
RELATIVE POWER ONE WAY dB
ANGLE
CHART NO. 121-60

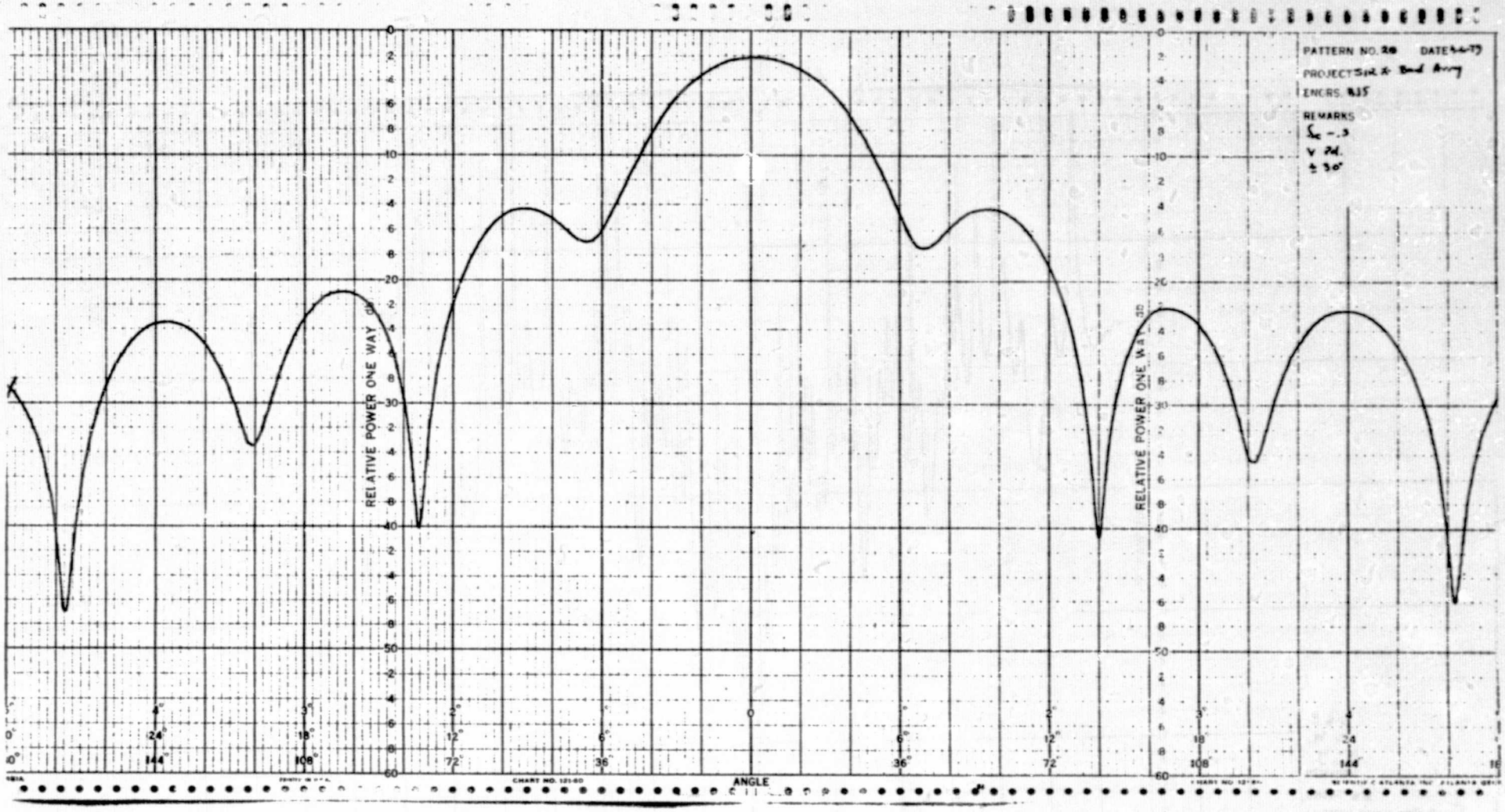
PATTERN NO. 20 DATE 5-6-77
PROJECT SIR X Band Array
ENGRS. RJS
REMARKS
S_{xc} -.3
V Pol.
± 30°
RELATIVE POWER ONE WAY dB
RELATIVE POWER ONE WAY dB
ANGLE
4° 3° 2° 0 2° 3° 4°
24° 18° 12° 6° 6° 12° 18° 24°
144° 108° 72° 36° 36° 72° 108° 144°

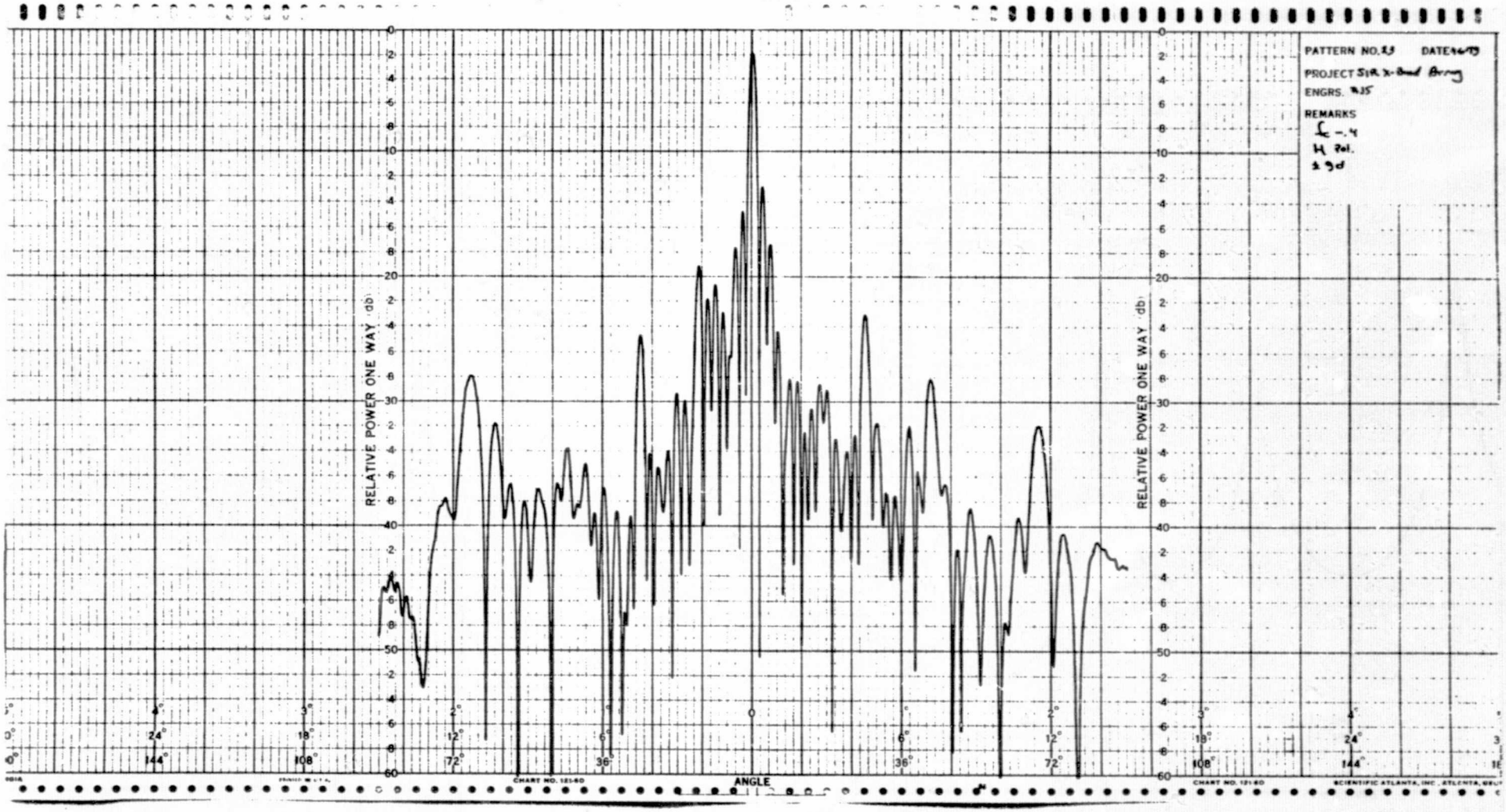
PATTERN NO. 23 DATE 4-10
PROJECT S-B X-Band Array
ENGRS. WJS
REMARKS
E -.4
H Pol.
±3d
RELATIVE POWER ONE WAY (db)
ANGLE
CHART NO. 12140
SCIENTIFIC ATLANTA, INC., ATLANTA, GA.

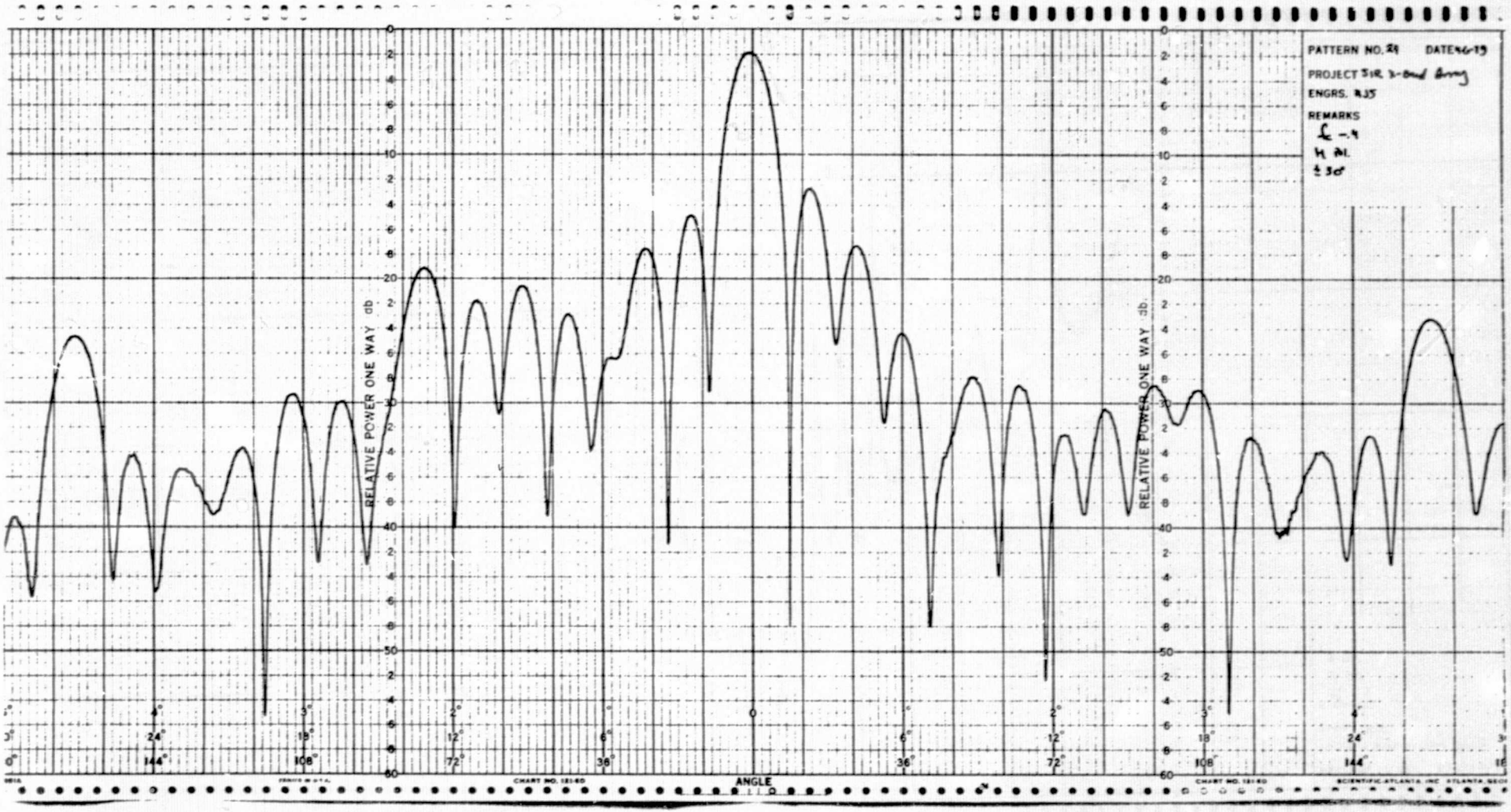
PATTERN NO. 29 DATE 4-69
PROJECT SIR X-Band Array
ENGRS. RJS
REMARKS
E -4
H 20
± 30°
RELATIVE POWER ONE WAY db
ANGLE
4°
24°
144°
3°
18°
108°
2°
12°
72°
6°
36°
0
6°
36°
2°
12°
72°
3°
18°
108°
4°
24°
144°
CHART NO. 121-60
SCIENTIFIC-ATLANTA, INC. ATLANTA, GEO

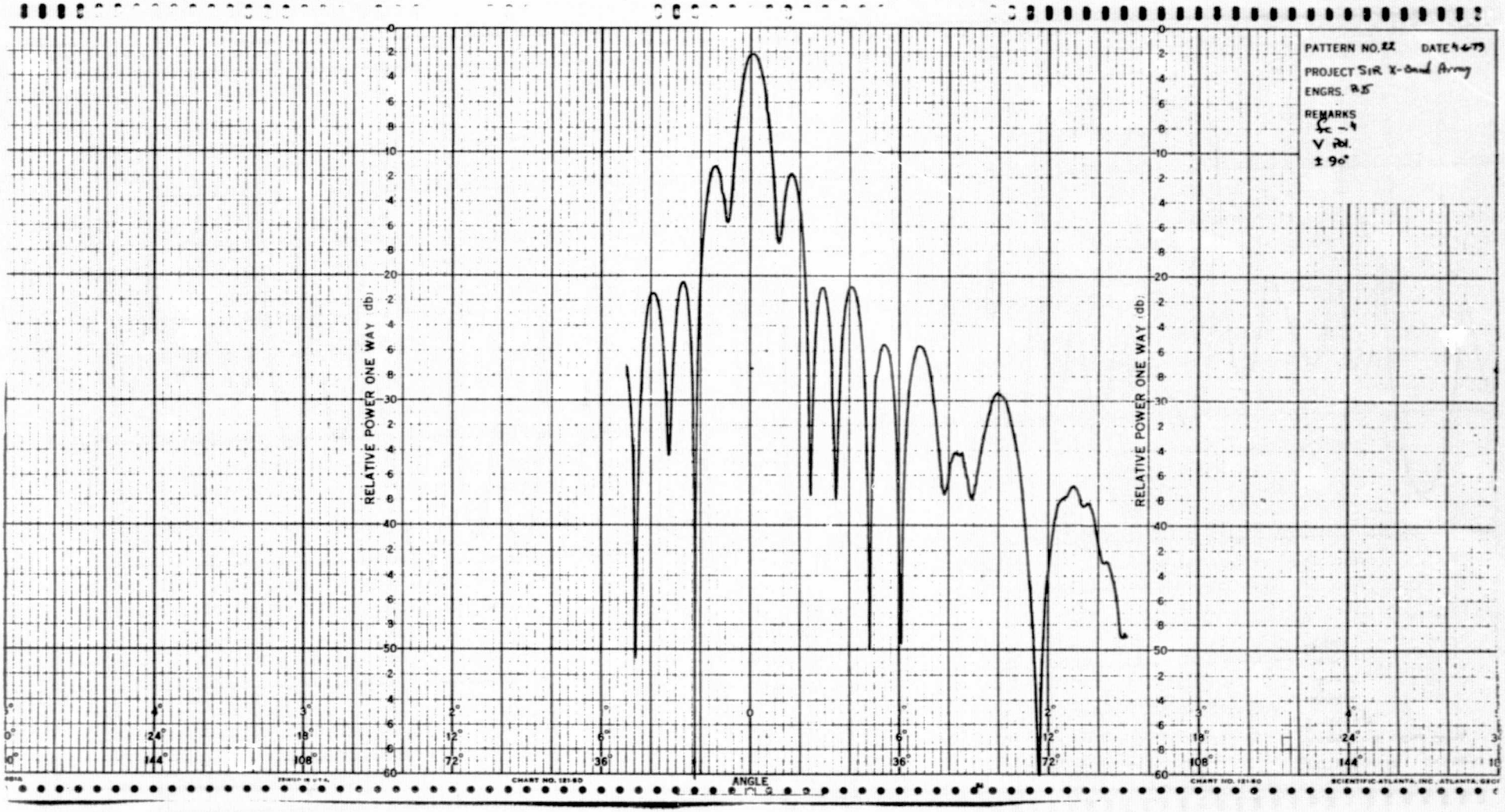
PATTERN NO. 22 DATE 4-6-73
PROJECT SIR X-Band Array
ENGRS. RS
REMARKS
Sec - 4
V Pol.
± 90°
RELATIVE POWER ONE WAY (db)
ANGLE
CHART NO. 121-60
SCIENTIFIC-ATLANTA, INC., ATLANTA, GEO

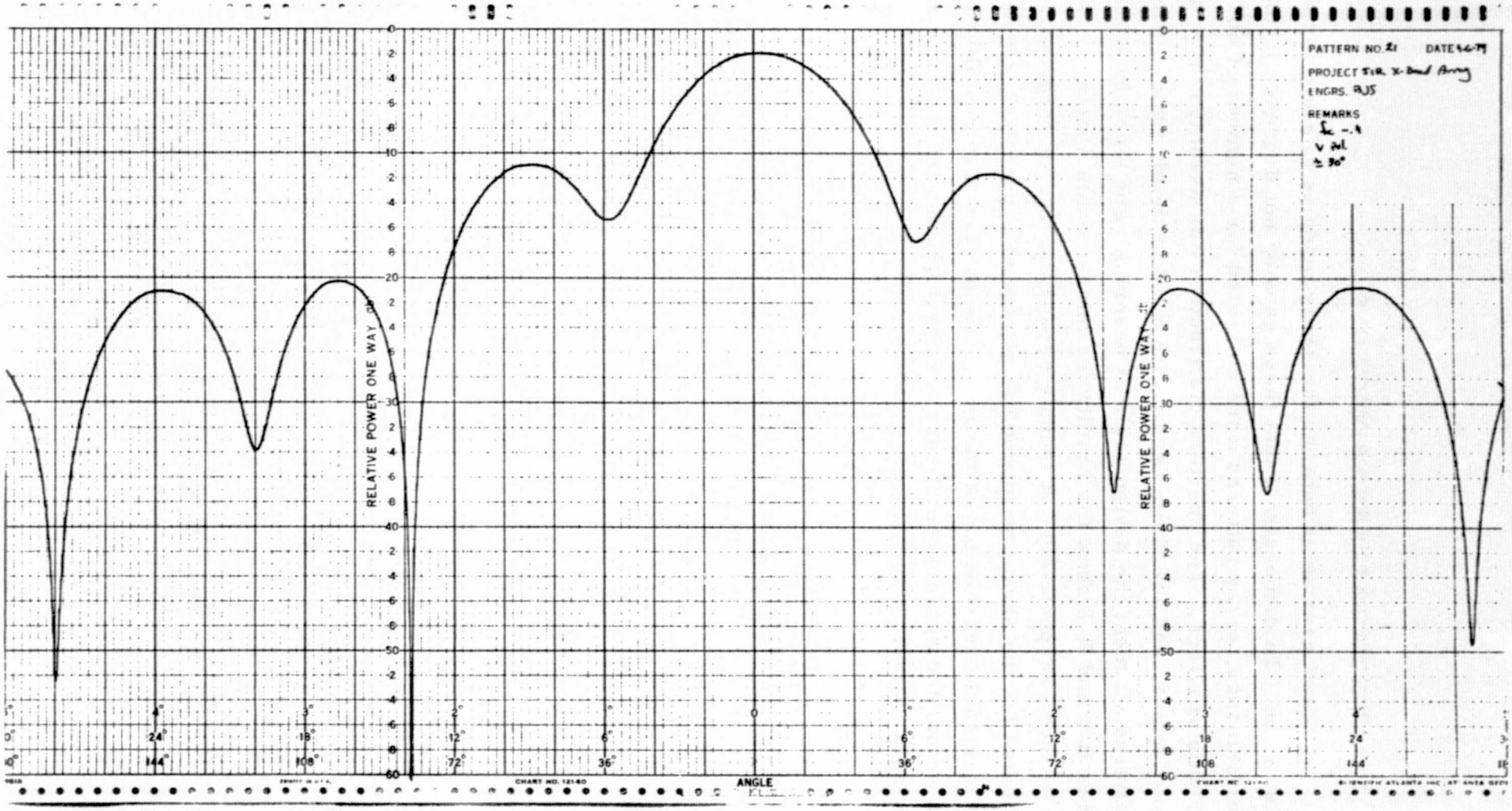
PATTERN NO. 21 DATE 4-6-79
PROJECT TIR X-Band Array
ENGRS. RJS
REMARKS
E_x -.9
V pol
± 30°
RELATIVE POWER ONE WAY dB
ANGLE
CHART NO. 121-60
144°
108°
72°
36°
0
24°
18°
12°
6°

B.2 ANTENNA PATTERN PREDICTIONS

Small gaps exist between the array modules to allow for thermal distortion. To demonstrate that these gaps do not degrade the microwave performance, array patterns were computed for a number of different inter-module spacings. The aperture distribution was assumed to be uniform in the E-plane, and -16.5 dB Taylor with $\bar{n} = 3$ in the H-plane. The computed patterns all meet the design goals of beamdidth and sidelobe levels. Figures B-1 and B-2 show the results for inter-module spacings of 0.0 and 0.02 inch, respectively. A module separation of 0.06 inch, such as is planned for the array, produced the pattern of Figure B-3. There is no unacceptable degradation of the important pattern features although, as expected, the appearance of very low level grating lobes is evident in the E-plane pattern of Figure B-3.

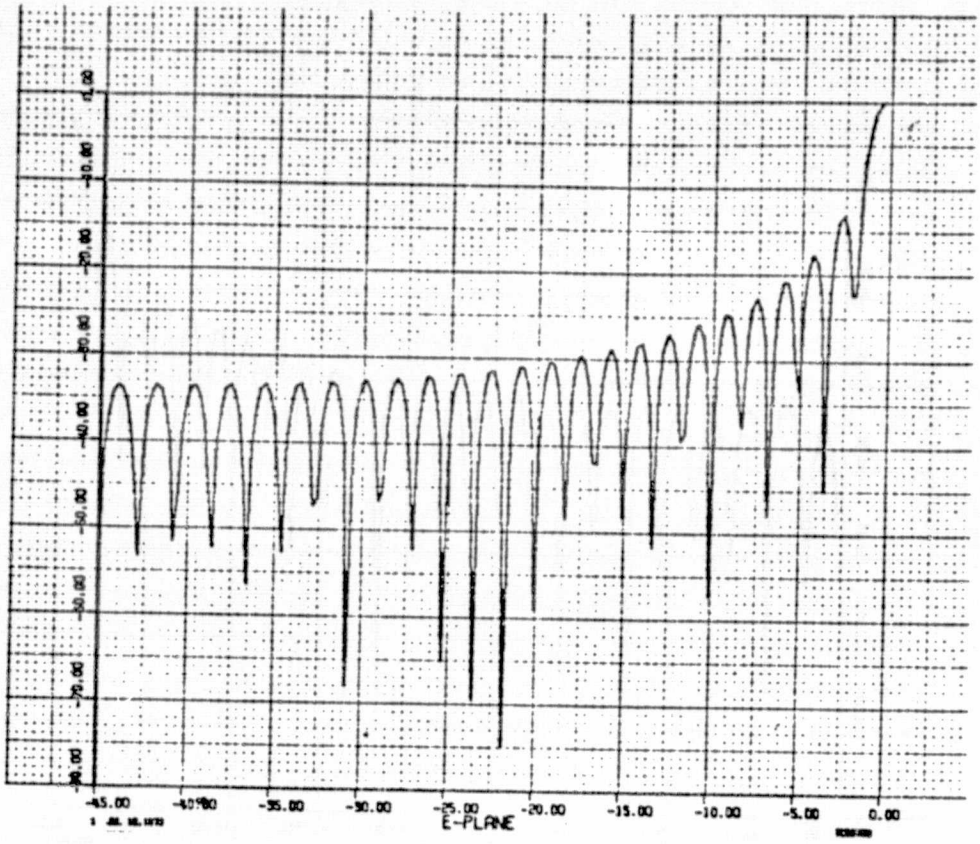

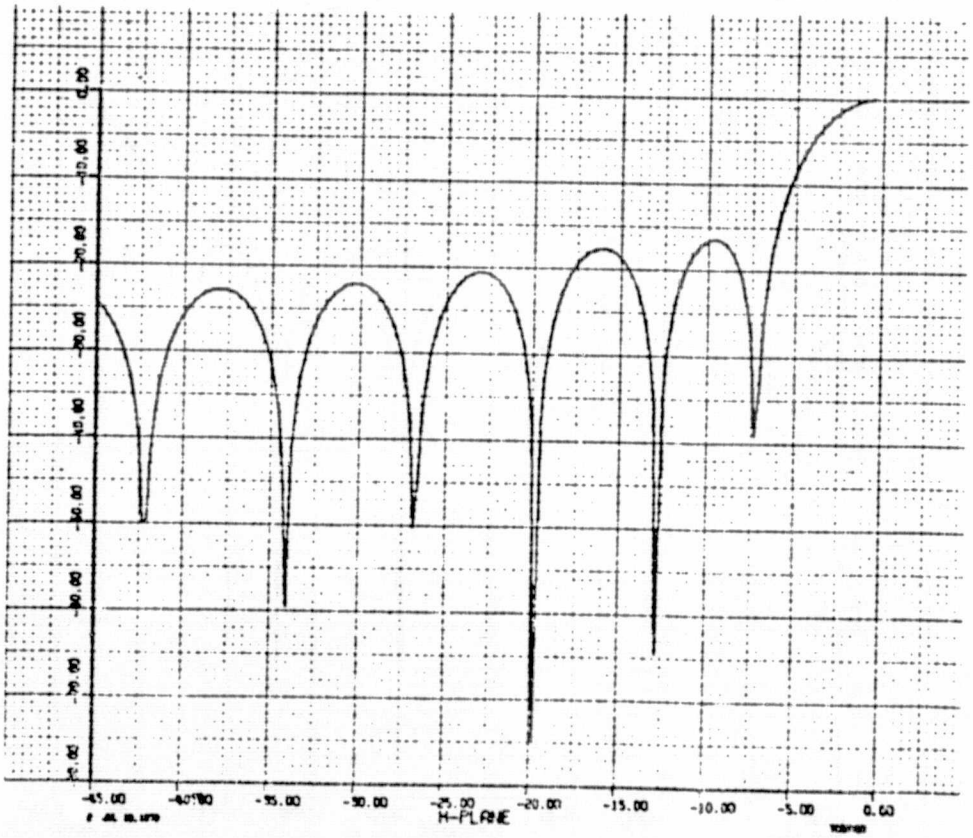

Figure B-1. 0.0 Inch subpanel separation.

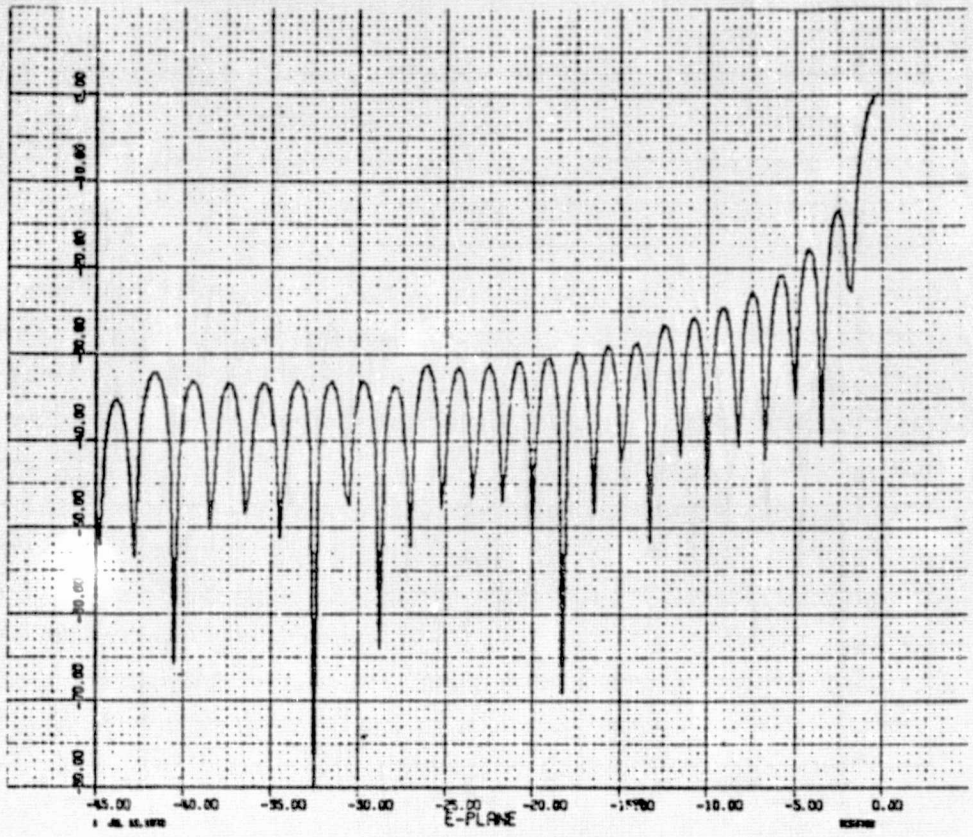

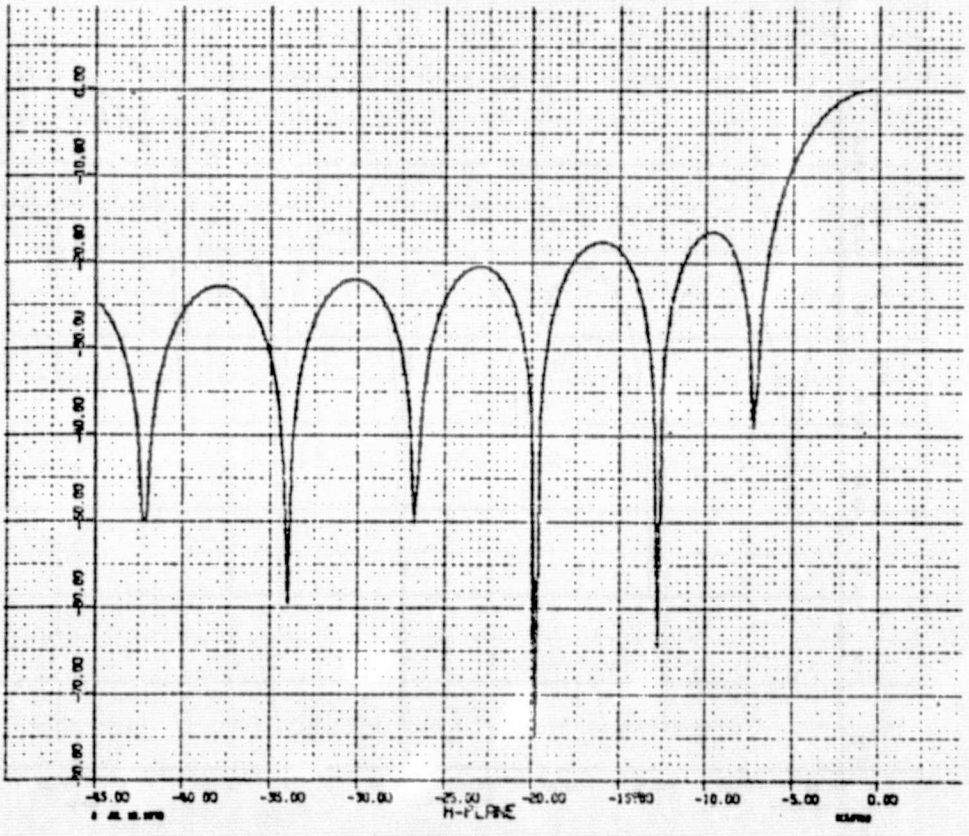

Figure B-2. 0.02 Inch subpanel separation.

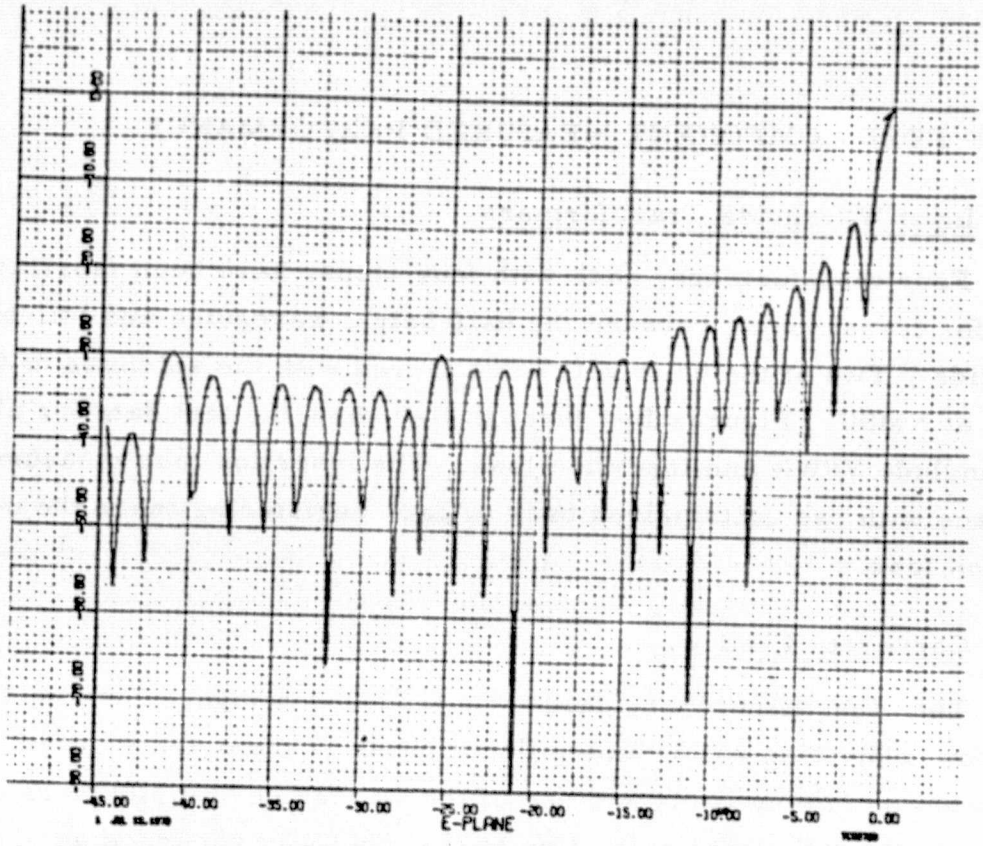

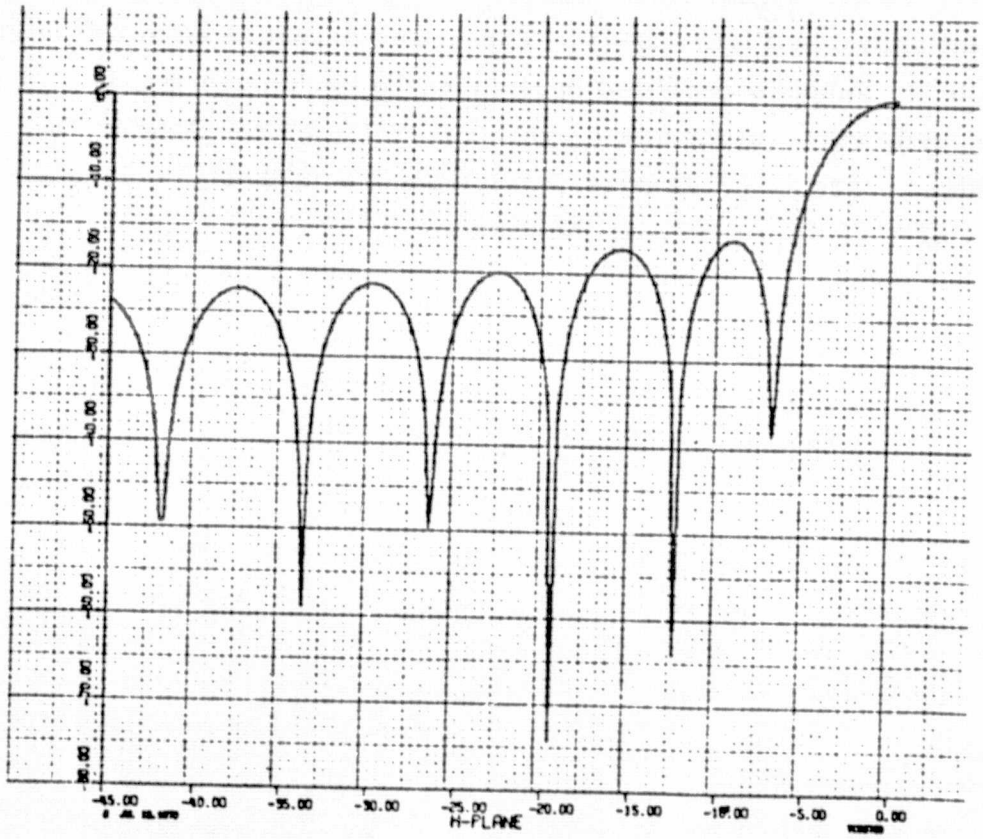

Figure B-3. 0.06 Inch subpanel separation.

B.3 RF FEED COMPONENT MEASURED PERFORMANCE

B.3.1 Input Waveguide Transformers

Four transformers, each with four steps, have been fabricated and tested for transitioning between the half-height waveguide and full-height waveguide. Two of the units will be delivered with the antennas to facilitate testing at NMSU. Figures B-4 through B-9 show the test date for all units which include VSWR and insertion loss. The insertion loss measurement was made with two units paired back to back registering twice the normal insertion loss.

B.3.2 Corporate Feed

The eight-port binary corporate feed was designed for low VSWR, equal power division ratio, and uniform phase at the outputs. With all outputs terminated in dummy loads and one of the waveguide transformers used at the input port, the RF signal reflection at the input was recorded as given in the VSWR plot shown in Figure B-10. The power output at each of the eight ports relative to the input is provided in Figures B-11 through B-13; in a perfect, lossless feed, each output would exhibit a -9.03 dB coupling ratio. The phase at the output ports at 9.7 GHz is provided in Table B-1, showing a maximum variation of ±3.5 degrees from the median.

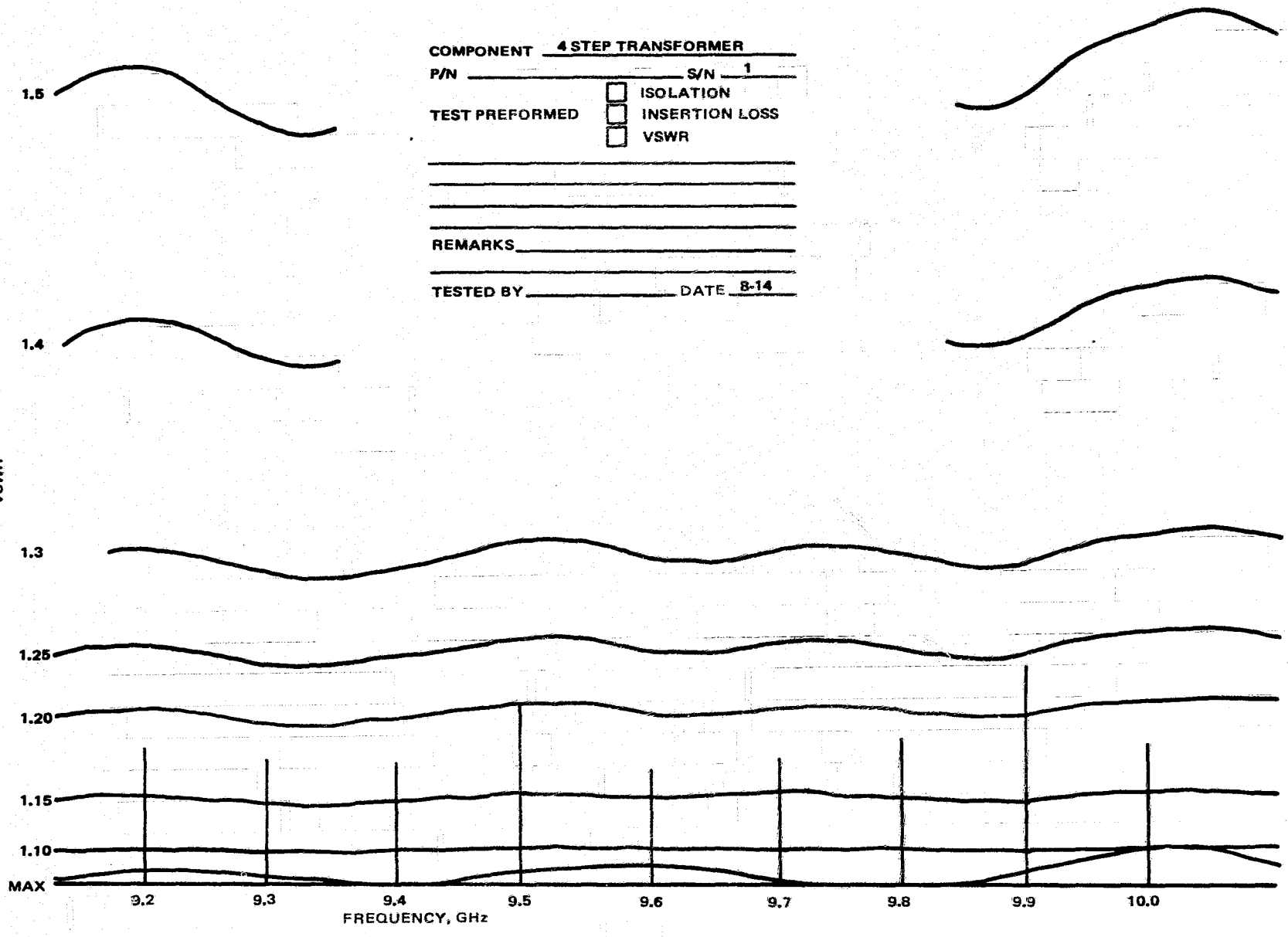

Figure B-4. Measured VSWR of 4-step transformer S/N 1.

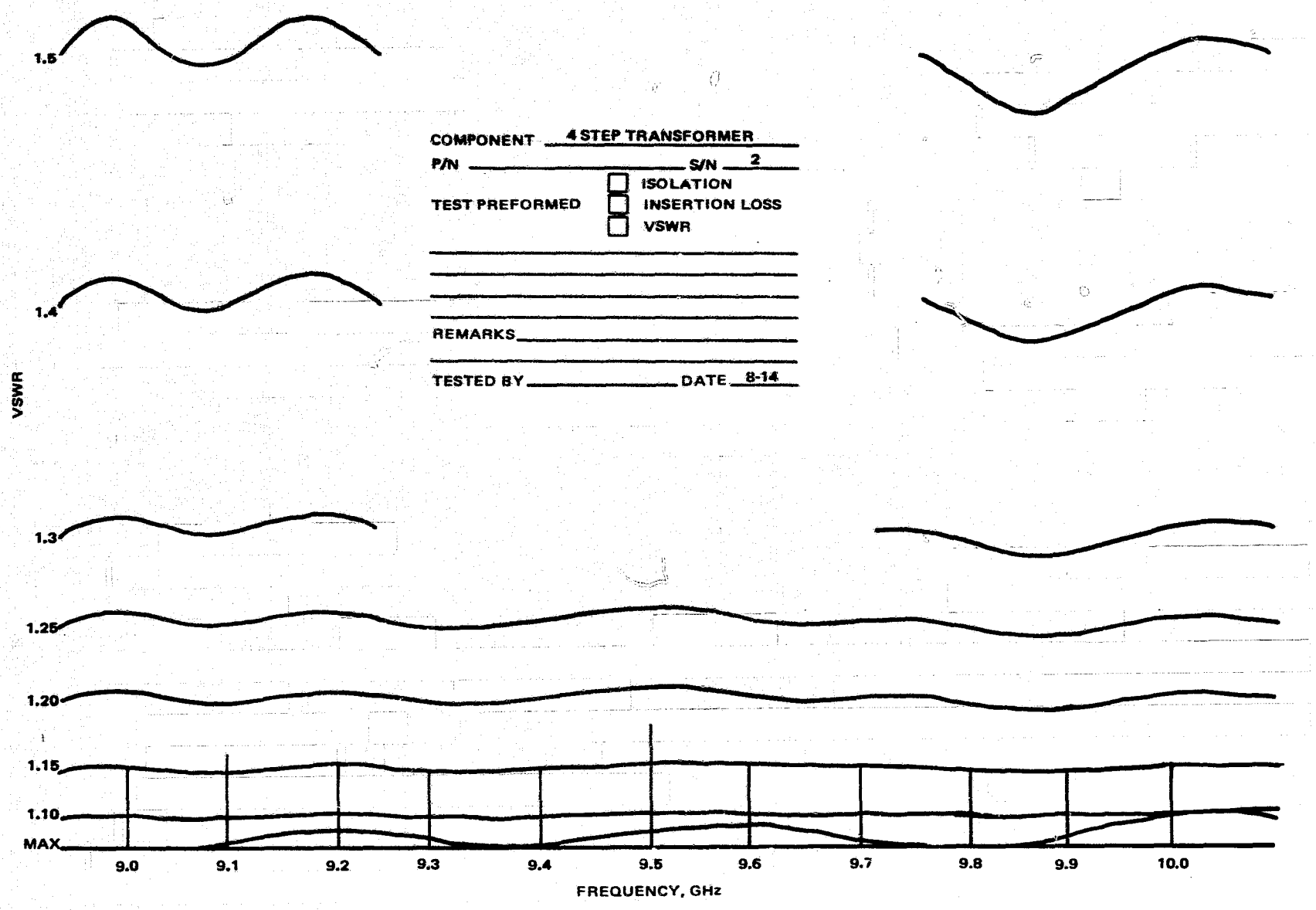

Figure B-5. Measured VSWR of 4-step transformer S/N 2.

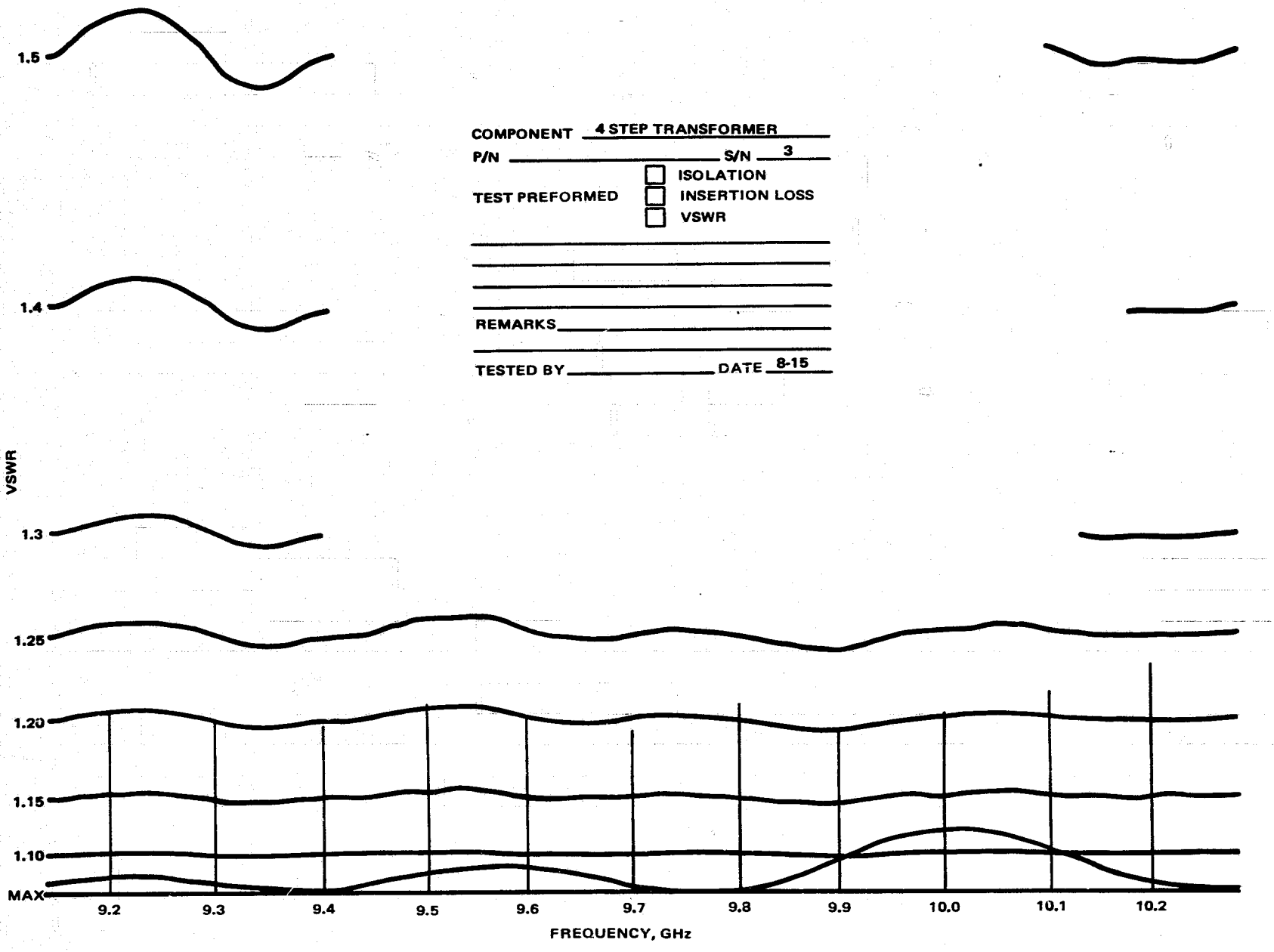

Figure B-6. Measured VSWR of 4-step transformer S/N 3.

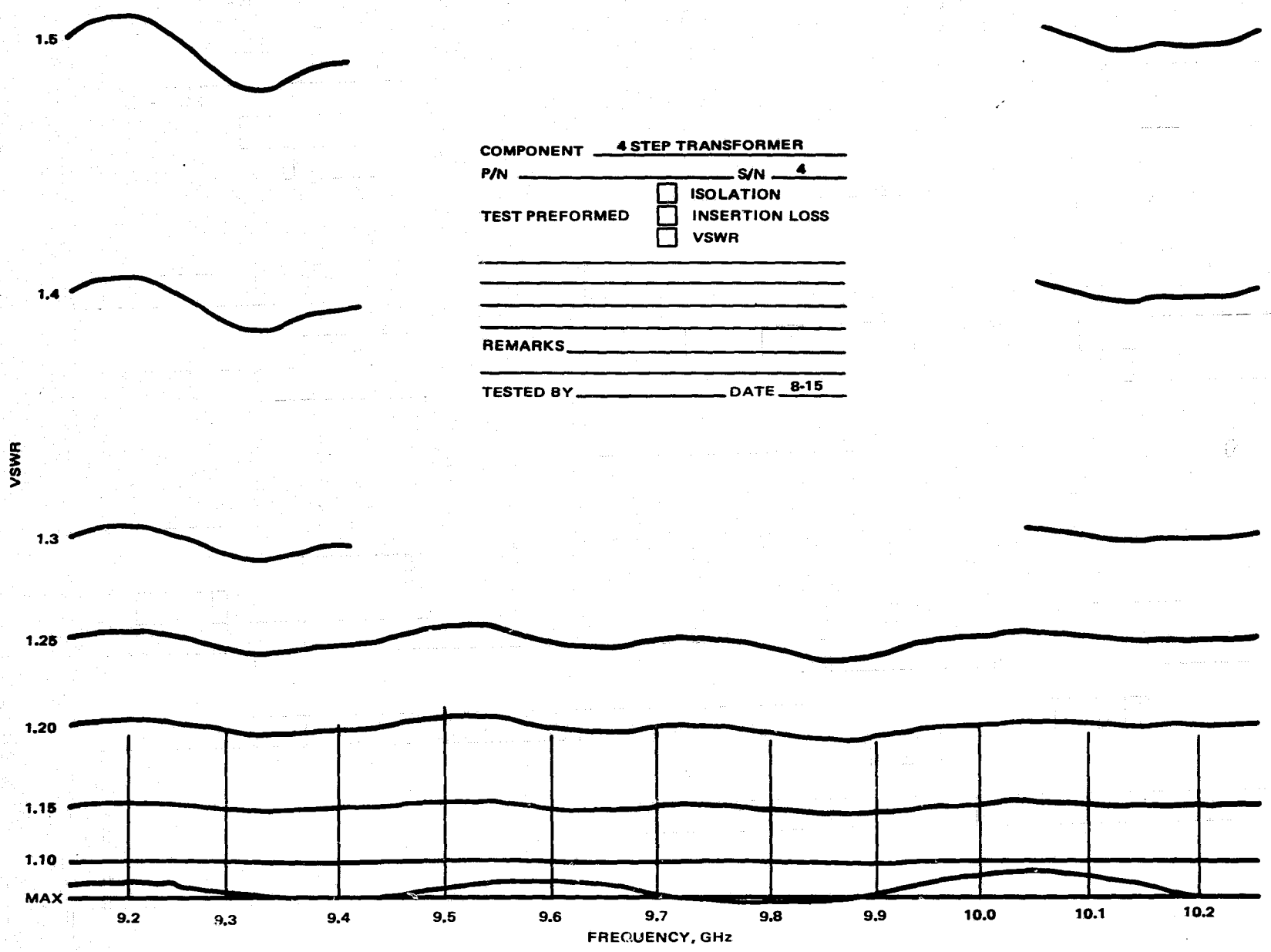

Figure B-7. Measured VSWR of 4-step transformer S/N 4.

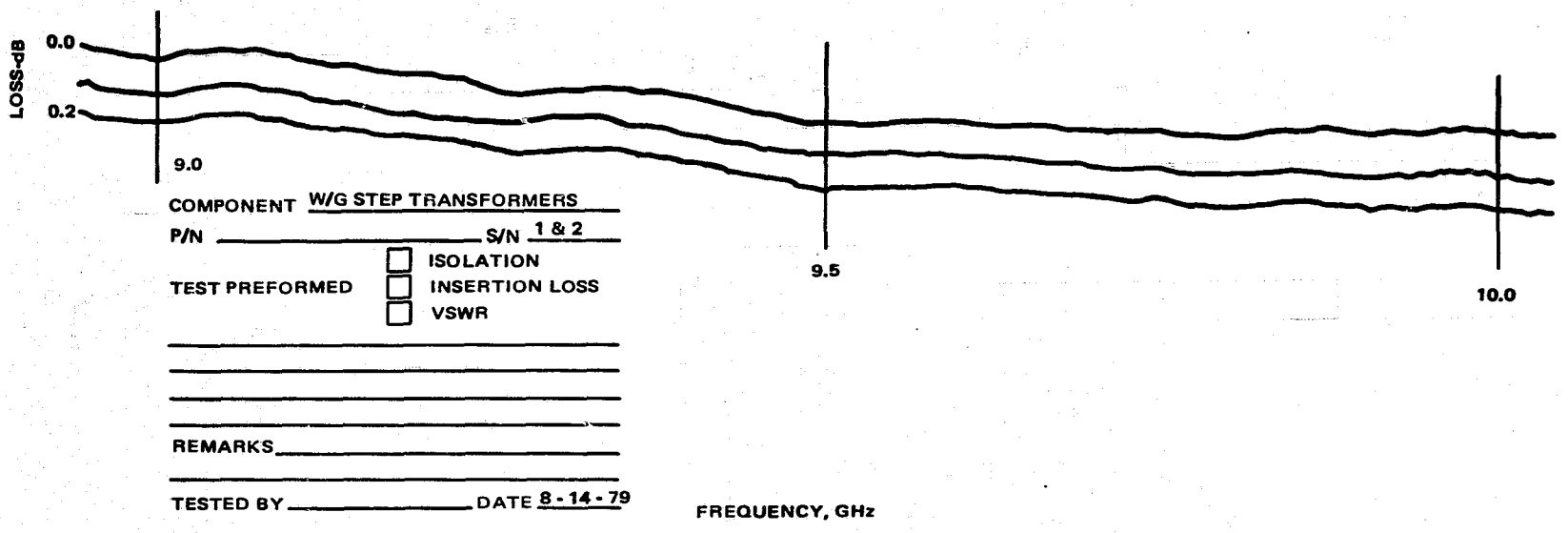

Figure B-8. Measured insertion loss of 4-step transformers S/N 1 and S/N 2.

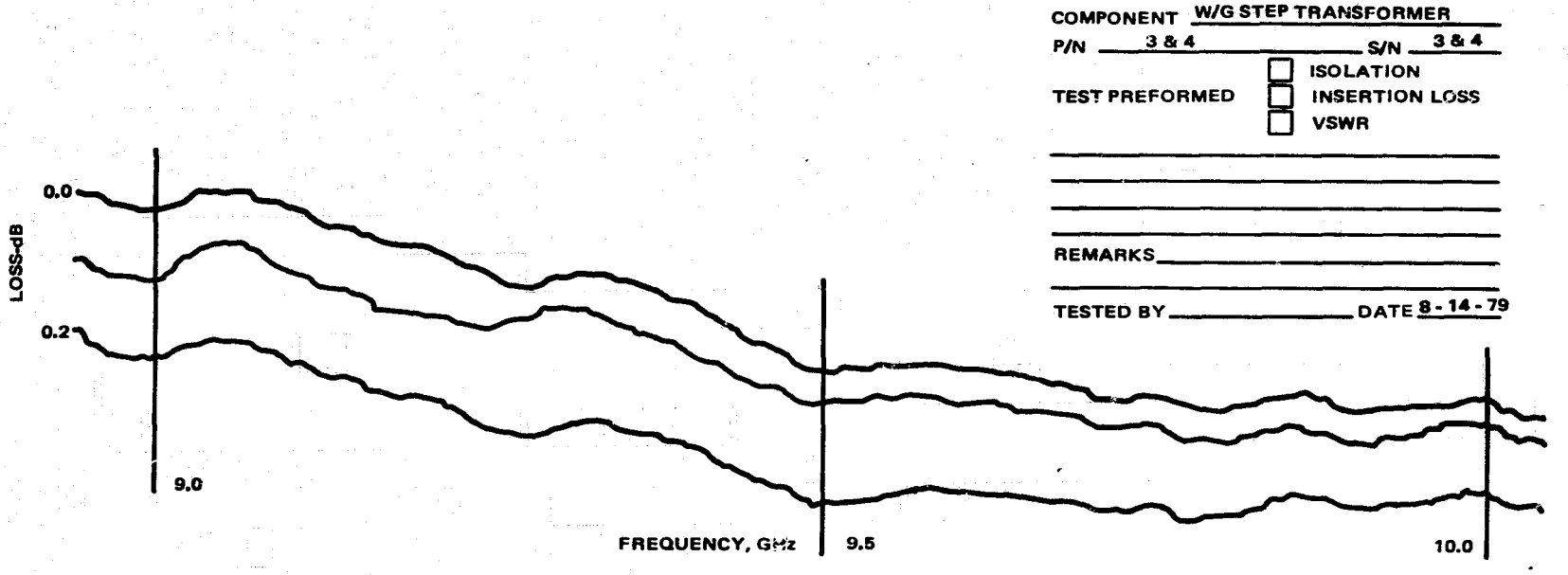

Figure B-9. Measured insertion loss of 4-step transformers S/N 3 and S/N 4.

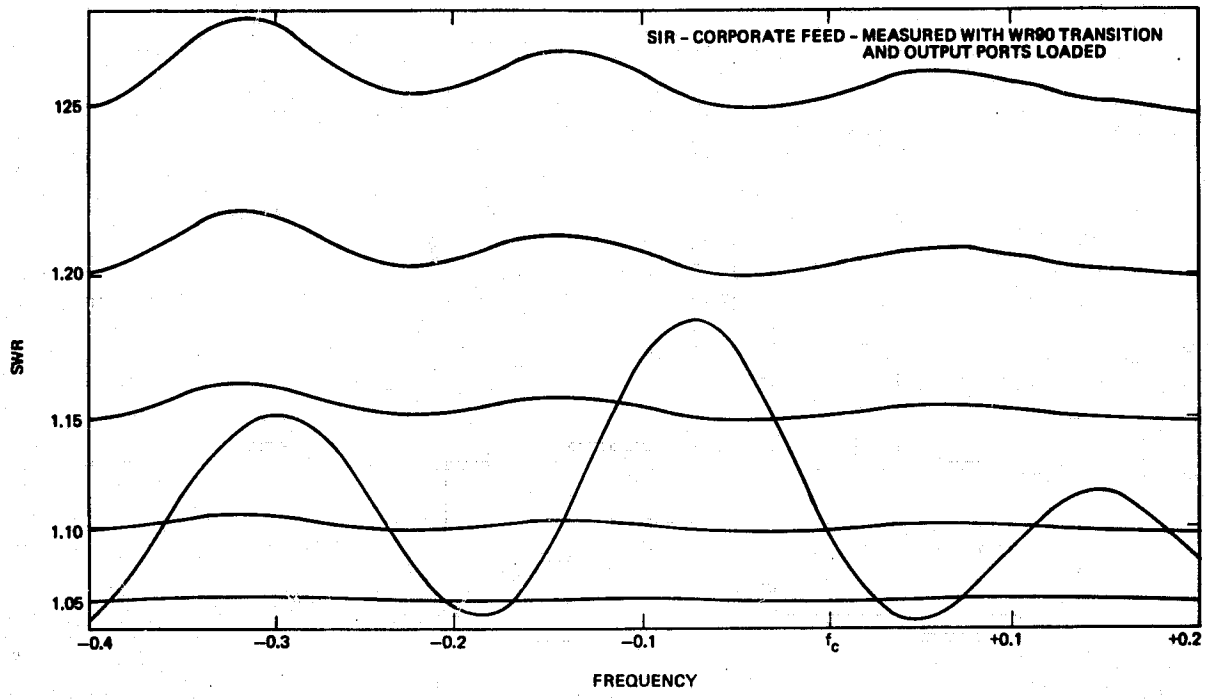

Figure B-10. RF signal reflection at the corporate feed input port.

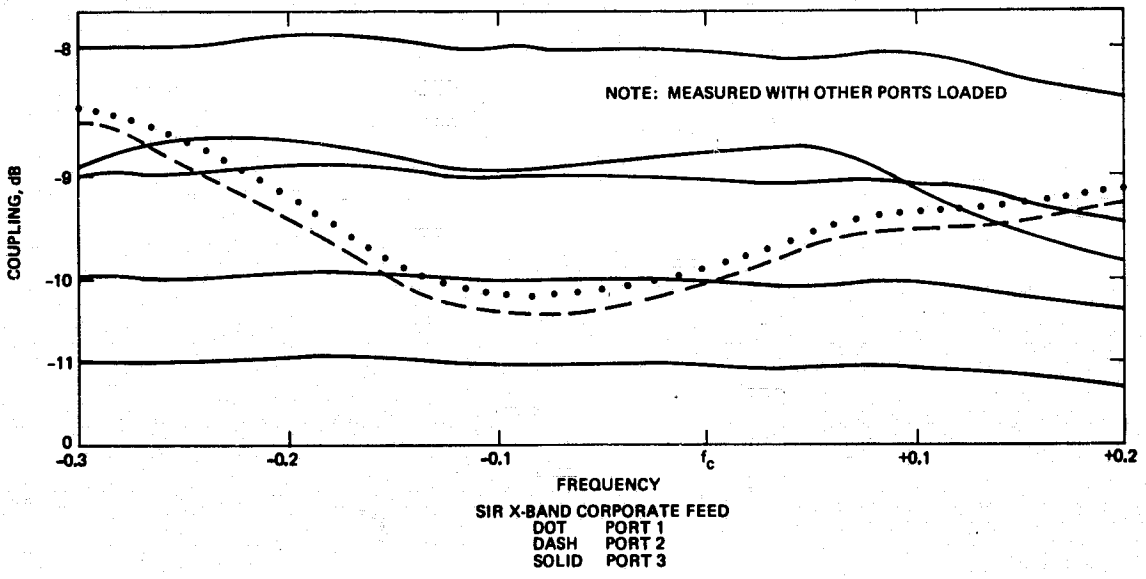

Figure B-11. Relative output power ratio of the corporate feed.

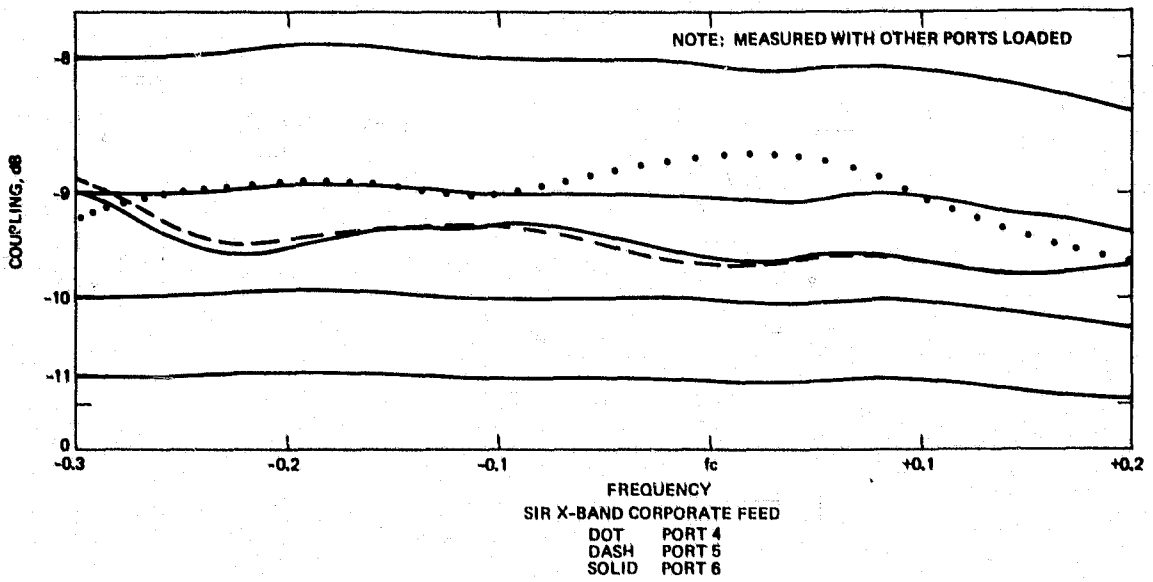

Figure B-12. Relative output power ratio of the corporate feed.

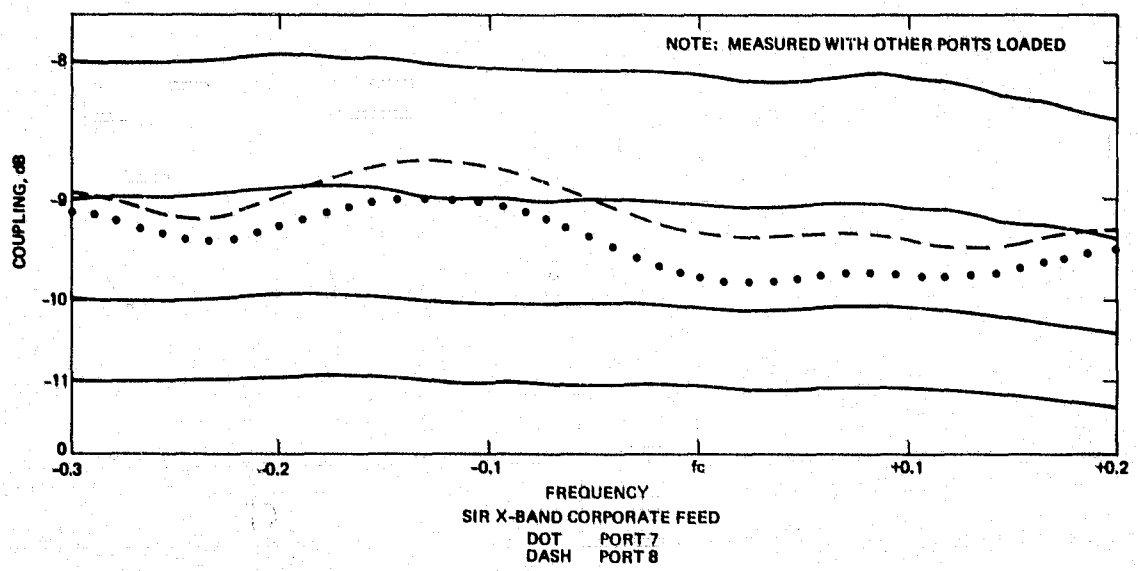

Figure B-13. Relative output power ratio of the corporate feed.

TABLE B-1. SIR X-BAND CORPORATE FEED – PHASE AT THE OUTPUT PORTS @ f_c RELATIVE TO PORT 1

Port	Phase Δ (degrees)
1	0 (reference)
2	-2.5
3	0
4	-4.8
5	-2.3
6	-2.8
7	-7.0
8	-6.5

4-5-79

APPENDIX C

INSTALLATION AND ASSEMBLY INSTRUCTIONS

APPENDIX C
INSTALLATION AND ASSEMBLY INSTRUCTIONS

C.1 X-BAND SLOTTED ARRAY TEST PANEL

The assembled array is shown in Figures 2-5 or 3-1. The mounting plate (3499214, Apperdix A) has been configured with a hole mounting pattern that allows the eight subpanels to be mounted adjacent to each other. Each subpanel is supported on four stainless steel 10-32 screws with eight large adjustment nuts (3499215, Appendix A) as seen in Figure C-1. The height of each subpanel can then be adjusted using a depth gauge or height gauge between the subpanel and mounting plate. This was designed to allow for ±0.25 inch of adjustment for each subpanel.

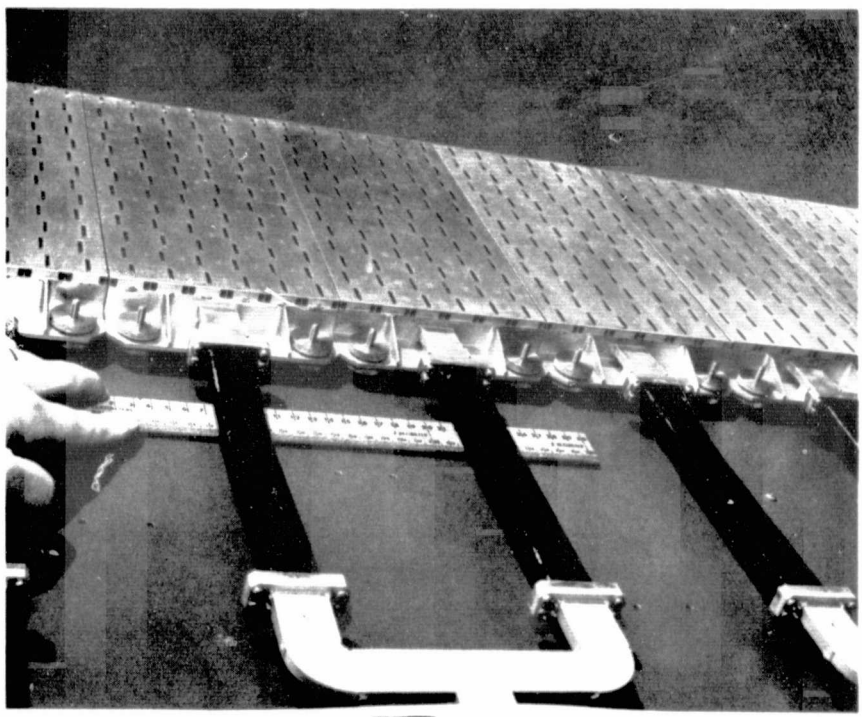

4R-54273

Figure C-1. X-band subpanel mounting.

The feed (3499215, Appendix A) is formed from three pieces that are screwed together at the flanges. Note that the feed flanges and subpanels have been numbered 1 to 8, reading from right to left, to duplicate the assembly as tested at Hughes Aircraft Company. No identification was assigned to the flex waveguide. The feed is supported above the mounting plate by seven brackets (3499216, Appendix A), which can be seen in Figure 3-1. Note that the mounting plate has been fabricated with two sets of mounting holes for the seven brackets, which allows the flex waveguides to be removed and the feed to be directly mounted to the subpanels.

A cadmium-steel plate has been bonded to the corner of the mounting plate with clearance from the feed to provide the mounting surface for a magnetically mounted boresight optics. This surface will provide the repeatable boresight for the subpanel adjustment.

C.2 X/L-BAND FIXTURE

The assembled X/L-band Fixture is shown in Figures 2-6, 2-7, C-2, C-3 and C-4. The X/L-band Fixture was designed to be assembled in the horizontal position with the array and L-band module radiating apertures facing upwards. Drawing 3499211 in Appendix A shows the fixture assembled.

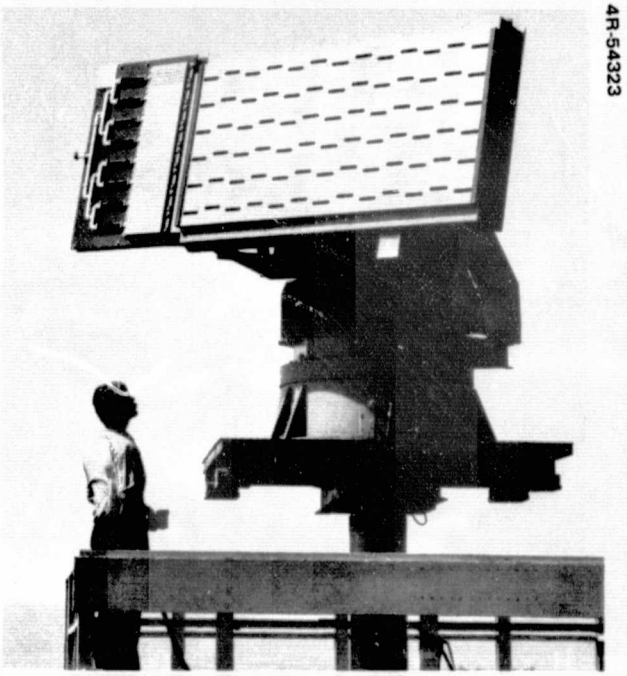

Figure C-2. X/L-band fixture mounted for H-plane patterns.

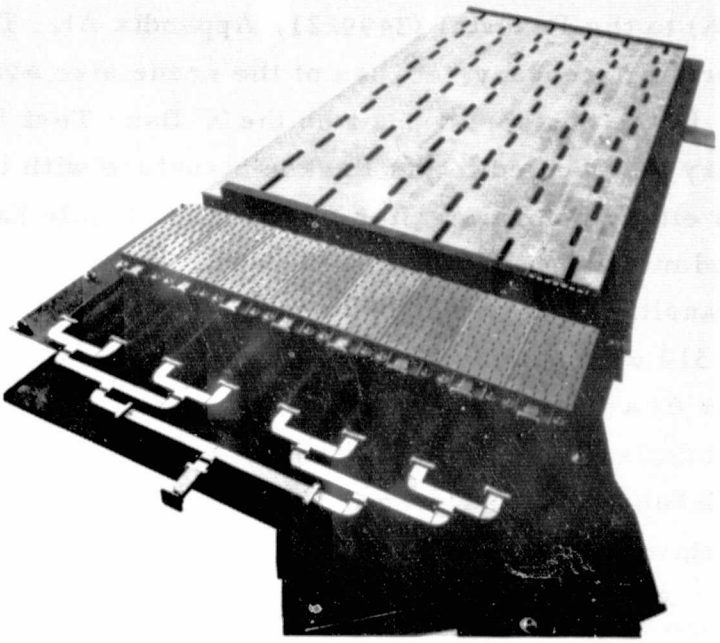

4R-54325

Figure C-3. X/L-band fixture showing mounting bolts for X-band mounting plate.

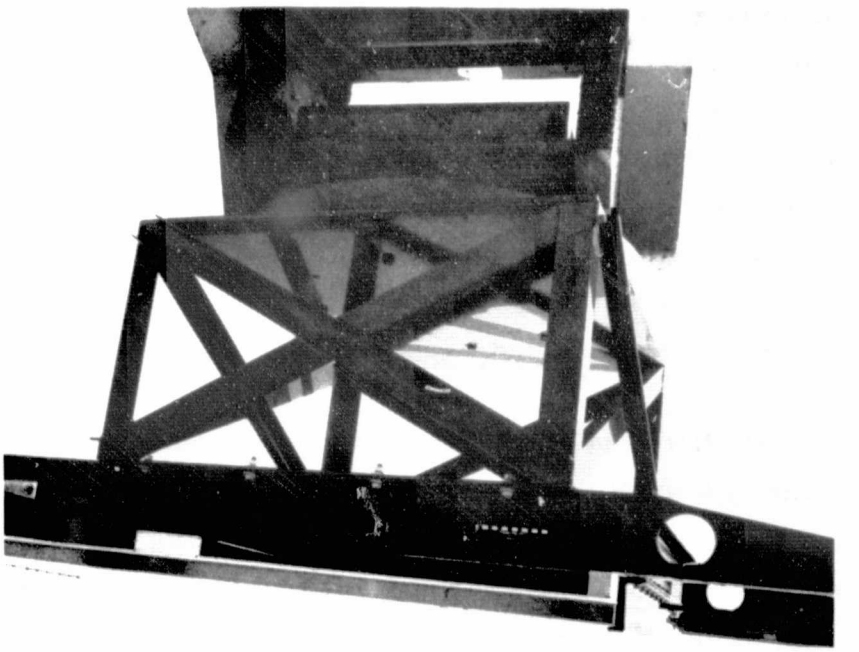

4R-54324

Figure C-4. X/L-band fixture side view of base mounting.

The assembly sequence should be to first mount the Backup Structure (3499220, Appendix A) to the Pedestal (3499221, Appendix A). This may be done on the ground or, if necessary because of the crane size available, done on the range mount. In the horizontal position the X-Band Test Panel assembly of Section C.1 may be mounted to the Backup Structure with the six bolts supplied and spacers either before or after the L-band Module has been secured. The L-band module is first assembled with a customer supplied waveguide to coax transition mate with the Hughes supplied step transition between regular WR 510 waveguide and the module waveguide. The end spacers (3499223-3, Appendix A) are then located where the ends of the L-band Module will seat and the module is placed on the spacers, with the input waveguide pointing toward the X-band Array as seen in Figure C-4. Note that for later bending, the middle shim/spacers (3499223-1-2, Appendix A) may be added with the end spacers. All shims and spacers are preliminarily aligned by the safety bolts on one side of the module which go through the module, shims, spacers, and backup structure to keep them from falling off the assembly should they be loosened.

Last, the Z-clamps (3499222, Appendix A) are attached and aligned to avoid interference with the drive screw heads on the module surface. The Z-clamps are relieved to clear the drive screw heads. Because the Z-clamps do not seat during the initial clamping, a secondary tool to hold the Z-clamps from slipping off the array is necessary. Large furniture clamps or bar stock with set-screw blocks can be used to hold the Z-clamps into the L-band module until the Z-clamps have been seated against the backup structure. The Z-clamps are tightened/torqued evenly to bend or secure the L-band module.

An Alignment Plate (3499224, Appendix A) is mounted on the side of the backup structure as seen in Figure C-2. This plate is used and adjusted on the range to provide a repeatable surface for mounting the boresight optics. The plate is mounted with two bolts through clearance holes which allow some adjustment in the antenna H-plane.

APPENDIX D
MECHANICAL ANALYSIS

APPENDIX D
MECHANICAL ANALYSIS

D.1 STRUCTURAL ANALYSIS OF THE L-BAND ARRAY TEST FIXTURE

D.1.1 Introduction

An analysis was performed to evaluate the structural performance of the L-BAND Array Test Fixture, shown in Figure D-1. The test fixture assembly includes two Z clamps, an I-beam backup structure, and an adapter (pedestal) framework. The Z-clamps and I-beam backup structure are fabricated from A-36 structural grade steel. The pedestal framework is a welded structure made of 6061-T6 aluminum alloy. The test fixture mounts on a pattern range pedestal. The fixture is designed to provide a means of displacing the center of the L-band array a maximum 0.25 inch, relative to the edges, as shown in Figure D-2. The analysis included the following:

- Determine the required thickness of the Z-clamp web to provide edge support to the L-band array. The Z-clamp should permit simple-support rotation of the edge.
- Determine the overall deflection and rotation of the test fixture assembly due to lateral gravity loading (zero degree elevation). A rotation of 0.004 radian was permissible (reference W. Feng).

D.1.2 Summary and Recommendations

- The recommended web thickness for the Z-clamp is 0.250 inch. This will provide adequate support of the edge of the L-band array without overly constraining edge rotation. Overall elastic deformation of the edge support is 0.05 inch. The required shim height to provide displacement of the array must allow for the elastic deformation of the edge supports.
- The calculated bolt load for the Z-clamp is 1206 lbs. per bolt. The recommended bolt size is 1/4 inch (F_{TU} = 125 ksi). Provide flat washers between the bolt heads and the Z-clamp to minimize gauling of the contact surfaces. Torque bolts to 61-75 in-lbs.

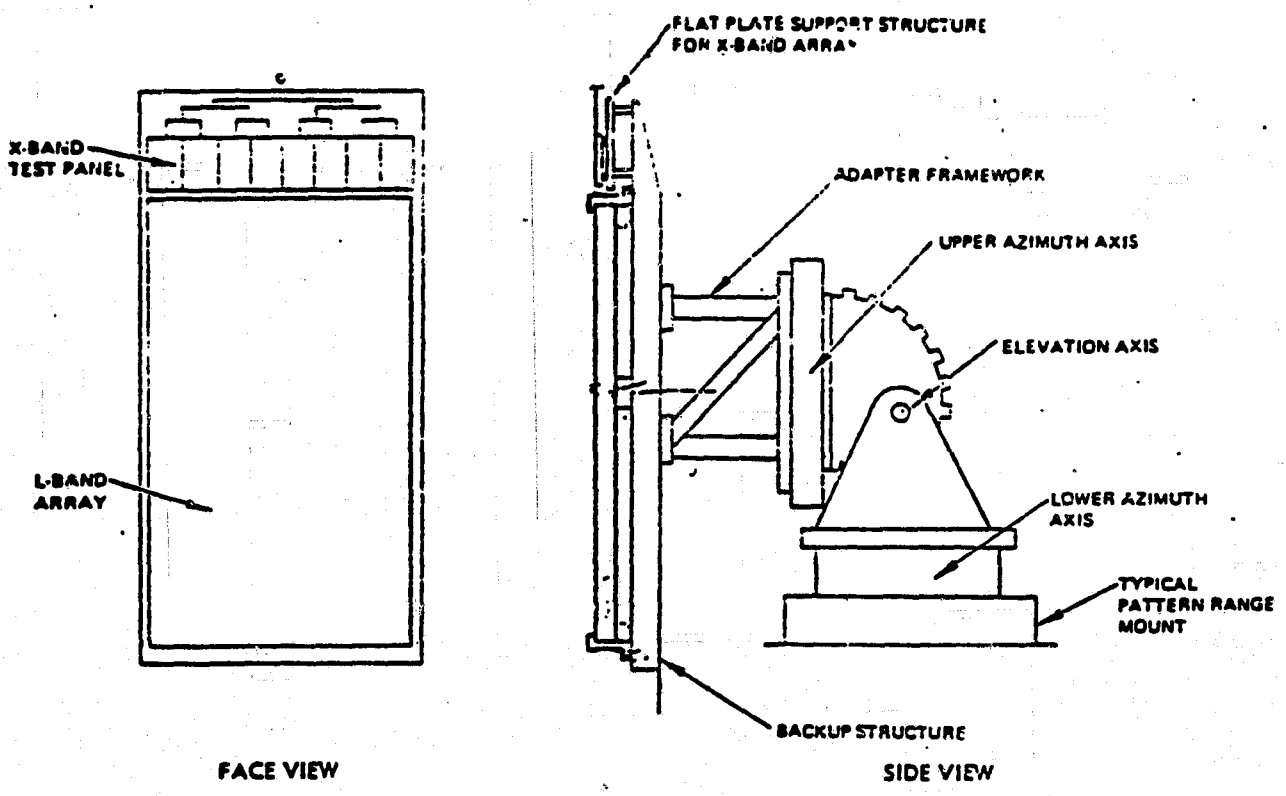

Figure D-1. Arrangement of arrays on antenna test fixture.

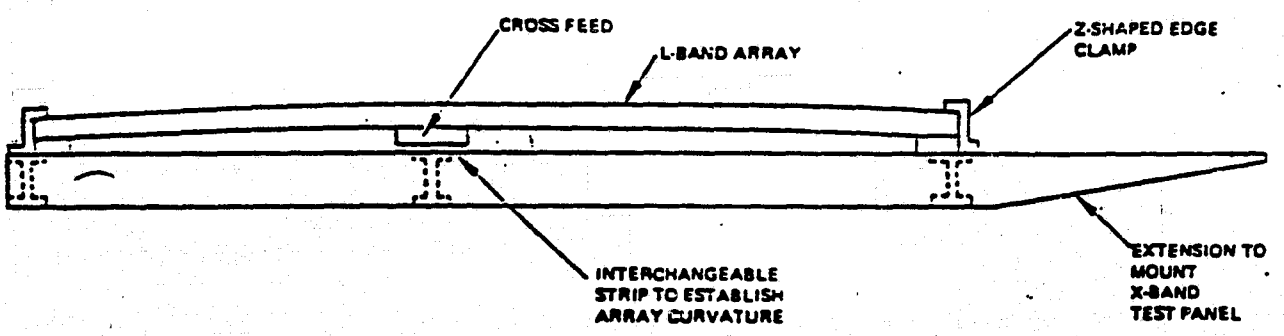

Figure D-2. Side view showing L-band array in position.

- Overall displacement (rotation) of the fixture assembly is primarily due to flexure of the pedestal base plate. The required thickness is 0.50 inch, which limits fixture rotation to 0.0036 radians.
- The recommended cross-section for the diagnonal members of the pedestal is as follows: channel section, web height = 3.00", web thickness = 0.13", flange height = 1.5", flange thickness = 0.20". This is a standard available shape. The channel section will provide adequate buckling resistance.
- The total weight, as determined by NASTRAN, is 799 lbs. The weight breakdown is given in Table D-1 below.

TABLE D-1. WEIGHT ESTIMATE

Member	Weight (pounds)
Backup Structure	360
Adapter (Pedestal)	164
L-band Array	240
Complete X-band Test Panel Assy	35
TOTAL WEIGHT	799

- The bending moment at the interface with the pattern range pedestal is 19730 in-lb.

D.1.3 Discussion

Detailed calculations are provided in Sections D.2 through D.4. Table D-2 gives material properties pertinent to the analysis.

D.1.3.1 Z-Clamp Analysis

The following assumptions were made.

1. 4000 lbs is required to displace to center of the L-band array relative to the edges (reference W. Feng).
2. The Z-clamp contacts the edge of the array at the tip of the flange.

TABLE D-2. MATERIAL PROPERTIES*

Property	Material	
	A36 Steel	6061-T6 Aluminum
Young's Modulus ($X10^6$ PSI)	30.0	10.0
Shear Modulus ($X10^6$ PSI)	11.0	3.8
F_{TU} (KSI)	55.0	42.0
F_{TY} (KSI)	36.0	34.0

*Reference: MIL Handbook 5-B, "Metallic Materials and Elements for Aerospace Vehicle Structures", 15 September 1976.

3. Out-of-plane bending of the backup structure is small relative to the distortion of the Z-clamp (reference W. Feng).

It was found that a web thickness of 0.25 inch is sufficient to provide adequate support of the array while allowing edge rotation. The flange tip deflection is 0.017 inch. The total edge deflection, including twisting of the supporting I-beams, is approximately 0.05 inch at the center of the span of the Z-clamp. Hence, in order to attain a relative deflection of 0.25 inch, the center shim should be approximately 0.03 inch. The web bending stress due to the clamping load is 7700 psi. The margin of safety for A36 structural carbon steel is +3.68. Maximum bolt load is 1206 lbs. The recommended fastener size is 1/4 inch (F_{tu} = 125 KSI).

D.1.3.2 Fixture Deflection

In order to facilitate a deflection analysis, a NASTRAN finite element model was developed for the pedestal framework. The model consisted of 16 plate elements and 30 beam elements. Plots of the grid point and element locations are given in Figures D-3 and D-4, respectively. The base plate was assumed pinned at the bolt circle represented by grid points 10 through 17.

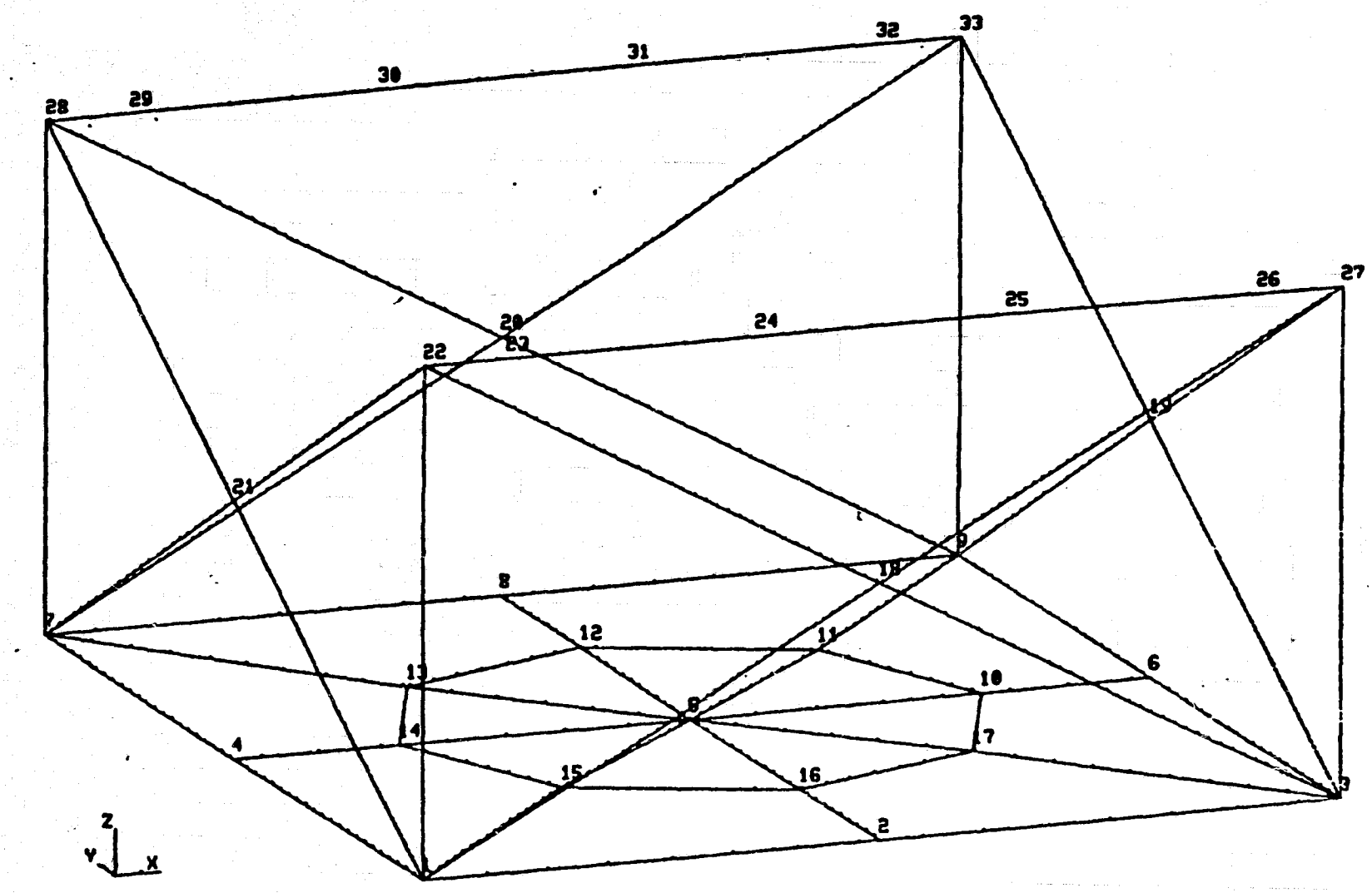

Figure D-3. NASTRAN grid point locations.

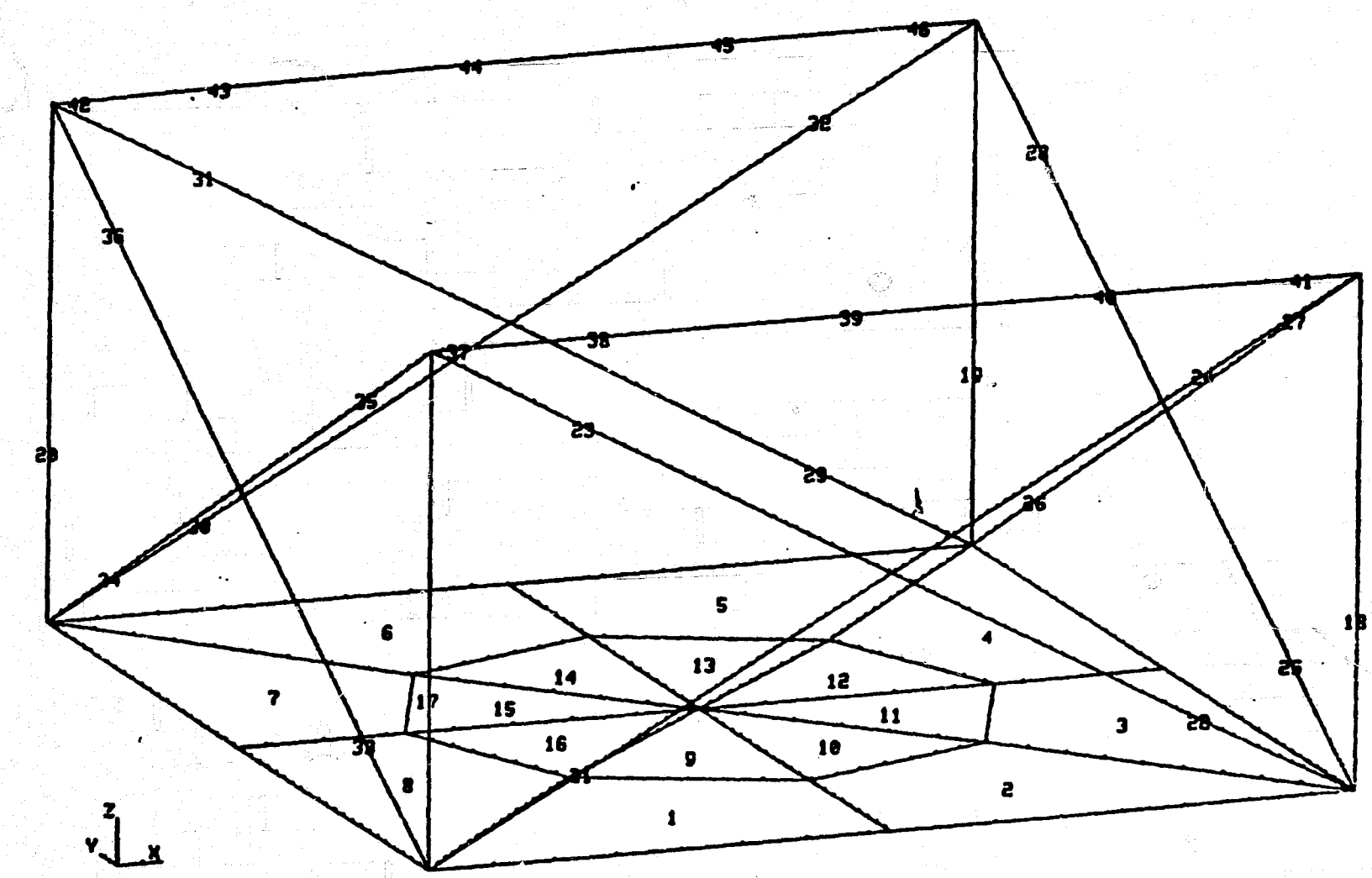

Figure D-4. NASTRAN element locations.

A total weight of 635 lbs. was located at the combined center-of-gravity of the L-band array and I-beam backup structure, which were assumed to be rigid. The center-of-gravity was located at a height of 30 inches above the base plate of the pedestal framework. A gravity load was applied in the lateral (X) direction. The results are summarized below.

Case 1 — 0.25 inch base plate
3.00 x 0.125 inch diagonal members

The lateral deflection due to gravity loading was 0.86 inch at the c.g. of the L-band and backup structure. This was deemed excessive. 97.1 percent of the strain energy was accounted for in out-of-plane bending of the base plate. In addition, the diagonal members carried a maximum compressive load of 234 lbs., which exceeded the allowable buckling load of 43.4 lbs. (see appendix).

Case 2 — 0.50 inch thick base plate
3.00 x 1.5 channel diagonal member

Since flexure of the base plate accounted for 97 percent of the strain energy, doubling the thickness reduced the overall deflection by nearly a factor of 8, as expected. The 0.12 inch deflection was judged acceptable. The maximum compressive load in the diagonal members was reduced to 226 lbs. The allowable buckling load is 19,550 lbs. The maximum stress in the base plate was 1600 psi.

Because of the gross mesh size of the finite element model, accurate resolution of the peak plate stresses is not possible. However, peak stresses in the plate will be small compared to the allowable of 35 ksi (reference Table D-2). The maximum stress in the bar elements was 2500 psi. The margin of safety is $\gg 1.0$.

D.2 Z-CLAMP ANALYSIS

D.2.1 L-Band Array, Z-Clamp

REFERENCE: HAC Drawing 3499222, Z-CLAMP, AWSOE ANTENNA

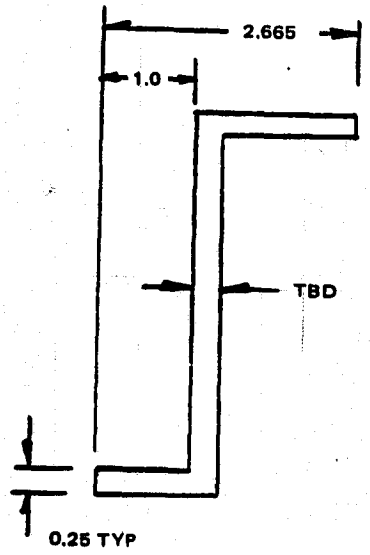

Z-CLAMP provides support to L-band Array along edge, as shown in Figure D-5 below. Determine required thickness of web to ensure adequate support without rotational constraint.

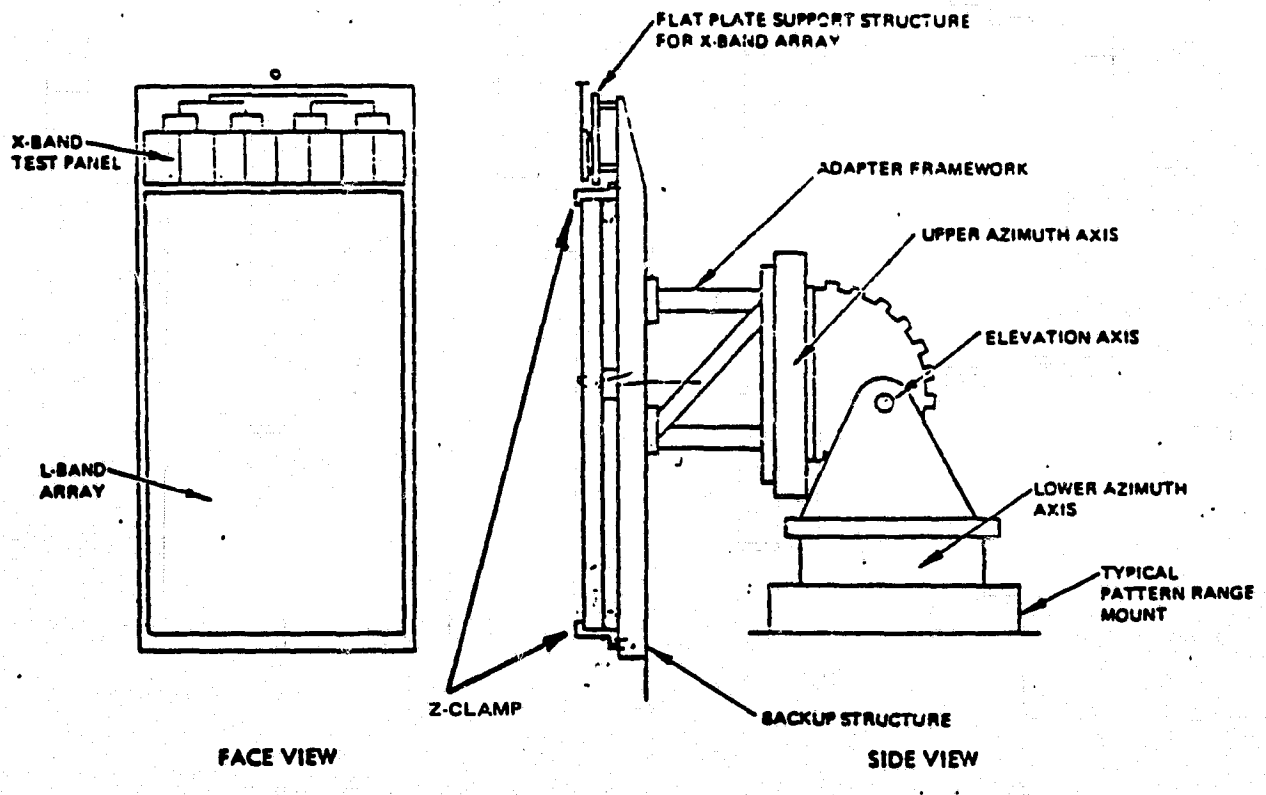

Figure D-5.

Assuming simply-supported edge conditions, determine edge rotation of L-band array due to 0.25 inch center deflection.

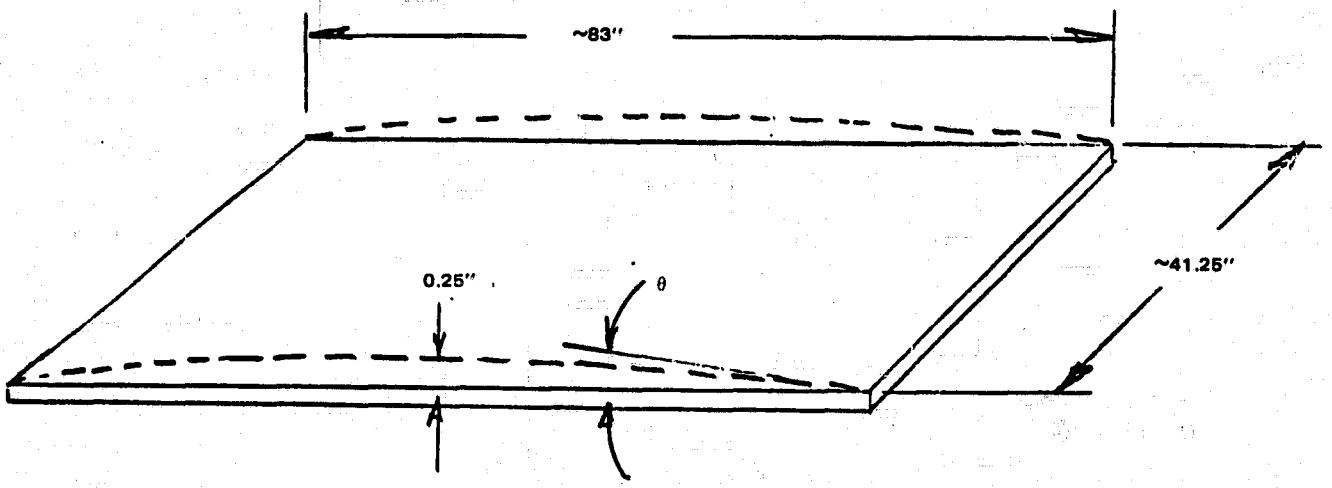

Given: 4000 lb. center load (conservative, W. Feng) to displace 0.25 inch

Calculate EI of array.

$$\Delta = \frac{PL^3}{48EI} \Rightarrow EI = \frac{PL^3}{48\Delta}$$

$$EI = \frac{(4000)(83)^3}{48(.25)} = 1.91 \times 10^8 \text{ lb-in}^2$$

Then

$$\theta = \frac{PL^2}{16EI} \text{ (Ref Roark, Formulas for Stress \& Strain)}$$

$$\therefore \theta = \frac{(4x10^3)(83)^2}{16\,(1.9x10^8)} = \underline{0.009 \text{ radian}}$$

Determine displacement of flage of Z-clamp due to edge restraint forces. Assume tip flange load

$$\frac{\text{Force}}{\text{Unit Length}} = \frac{2000\ \text{lb}}{41.25\ \text{inch}} = 48.25\ \#/\text{in}$$

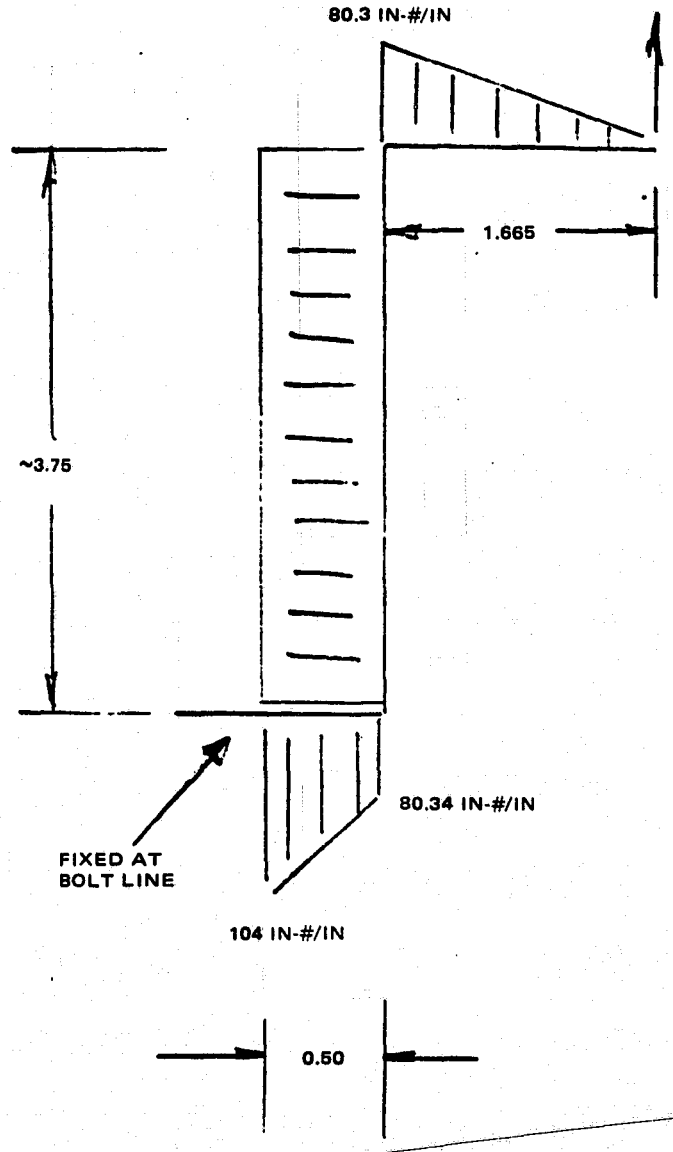

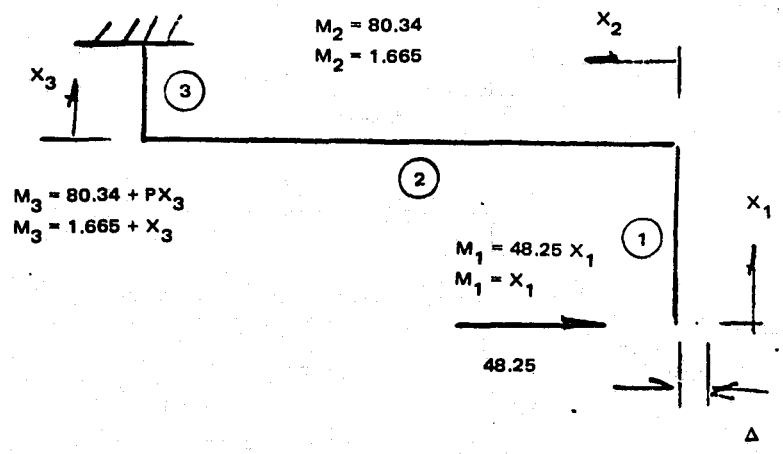

$$I_1 = I_3 = \frac{.25^3}{12} = 1.30 \times 10^{-3}\ \text{in}^4/\text{in}$$

$$I_2 = \text{TBD}$$

$$\Delta = \sum_{i=1}^{3} \int \frac{Mmdx_i}{EI_i} \quad \text{(Virtual Work)}$$

$$E\Delta = \sum^{3} \int \frac{Mmdx_i}{I_i}$$

$$E\Delta = \int^{1.665} \frac{PX_1(X_1)\,dX_1}{I_1} + \int^{3.75} \frac{80.34(1.665)\,dX_2}{I_2}$$

$$+ \int^{0.5} \frac{(80.3+PX_3)(1.665+X_3)dX_3}{I_3}$$

$$E\Delta = \frac{Px^3}{3I_1}\Bigg|^{1.665} + \frac{133.8x}{I_2}\Bigg|^{3.75} + \frac{1}{I_3}\left(133.8x + \frac{Px^3}{3} + \frac{1.665}{2}Px^2 + \frac{80.34x^2}{2}\right)\Bigg|^{.5}$$

$$E\Delta = \frac{48.25(1.665)^3}{3I_1} + \frac{133.8}{I_2}(3.75) + \frac{1}{I_3}\left(133.8(.5) + \frac{48.25}{3}(.5)^3\right.$$

$$\left. +1.665\,(48.25)(.5)^2 + \frac{80.34(.5)^2}{2}\right)$$

$$E\Delta = \frac{74.25}{I_1} + \frac{501.8}{I_2} + \frac{1}{I_3}(66.9 + 2.01 + 10.04 + 10.04)$$

$$E\Delta = \frac{74.25}{I_1} + \frac{501.8}{I_2} + \frac{89}{I_3}$$

$$E\Delta = 57120 + \frac{501.8}{I_2} + 68460$$

t_{WEB}	I_{WEB}	Δ (inch)	
		Alum	Steel
0.1	8.3-5	0.63	0.21
0.15	2.8-4	0.192	0.064
0.2	6.7-4	0.087	0.029
0.25	1.3-3	0.051	0.017

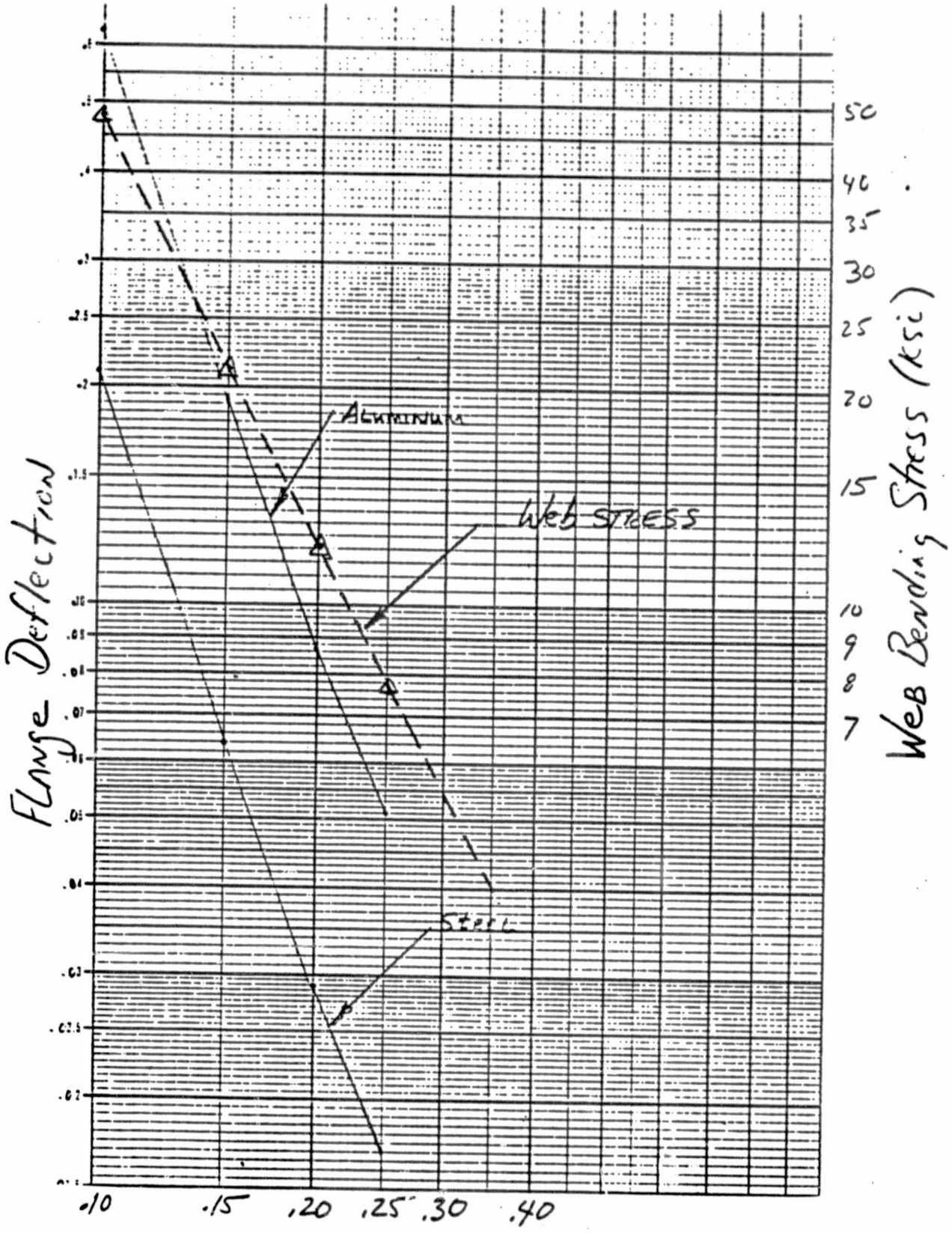
Flange Deflection
Web Bending Stress (ksi)
50
40
35
30
25
20
15
10
9
8
7
Aluminum
Web Stress
Steel
.10
.15
.20
.25
.30
.40
Web Thickness

D.2.2 Estimate Rotation of Flange

Use simple beam model, neglect flange flexibility

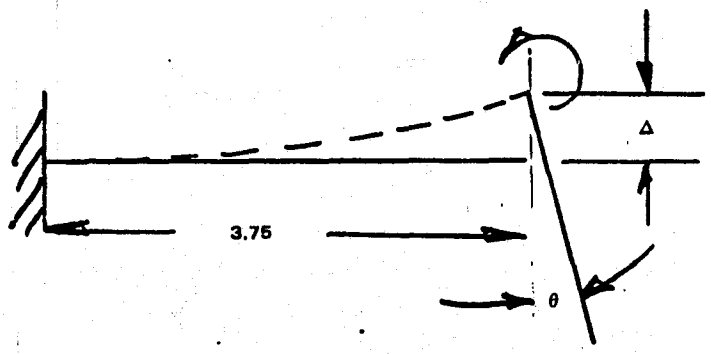

$$\theta = \frac{ML}{EI}$$

where $M = 80.34 \frac{\text{in-lb}}{\text{in}}$

$$\Delta = \frac{ML^2}{2EI}$$

$$\theta = \frac{80.34(3.75)}{EI} = \frac{301.3}{EI}$$

t_{WEB}	I_{WEB}	θ (RAD)		Δ (in)	
		Alum	Steel	Alum	Steel
0.1	8.3-5	0.36	0.12	0.68	0.23
0.15	2.8-4	0.108	0.036	0.2	0.07
0.2	6.7-4	0.045	0.015	0.084	0.028
0.25	1.3-3	0.024	0.008	0.043	0.014

CONCLUSION

To minimize edge deflection while maintaining sufficient rotational freedom, web thickness should be 0.25 inch.

MATERIAL → STEEL

D.2.3 Calculate Fastener Load

Worst case bolt load occurs for combination edge restraint loads and lateral gravity load of L-band array.

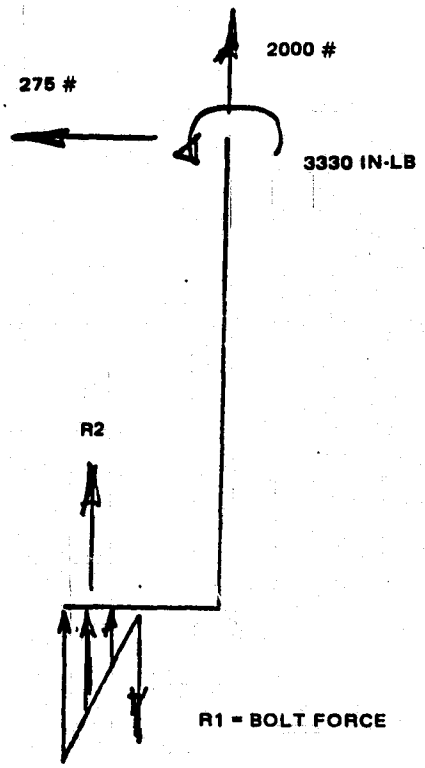

$M = 2000\ (0.5) + 3330 + 275\ (3.75)$

$M = 5361$ in-lb

Bolt Load

$M = 5361 = R2\ (.5)(2/3)$

$R2 = 3M = 16080\#$

$R2 + 2000 = R1$

$R1 = 18080\#$

Since there are 15 bolts, the load per bolt is

$$\frac{18080}{15} = \underline{\underline{1206\#}}$$

D.2.4 Calculate Lateral Deflection Due to Gravity

Assume complete fixity at bolt line

Matl' - Steel

t_{web} - 0.25"

$$I_W = I_F = (1.3 \times 10^{-3})\ (41.45) = 0.054$$

$$\Delta = \frac{PL_W^3}{3EI_{WEB}} + \frac{L_W\ (PL_W)\ (L_F)}{EI_F} \qquad \left(\theta = \frac{ML}{EI},\ \Delta = R\theta\right)$$

$$\Delta = \frac{275(3.75)^3}{3(30 \times 10^6)\ (.054)} + \frac{(3.75)\ (275)\ (3.75)\ (0.5)}{(30 \times 10^6)\ (0.054)}$$

$$\Delta = 0.003 + 0.0012 = \underline{0.0042}$$

Lateral deflection due to gravity load is small.

It has been assumed that the I-beam backup structure (see Figure 1 and HAC drawing 3499220) provides total moment fixity to the Z-clamp at the bolt line. Now, estimate maximum rotation of the I-beam (6I12.5). Assume uniform moment distribution along length of beam. Also assume beam fixed at ends.

(Reference: Restrained torsion of open sections, Design of Steel Structures, Bresler, Lin, Scalzi.)

D.2.5 I-BEAM (6I12.5)

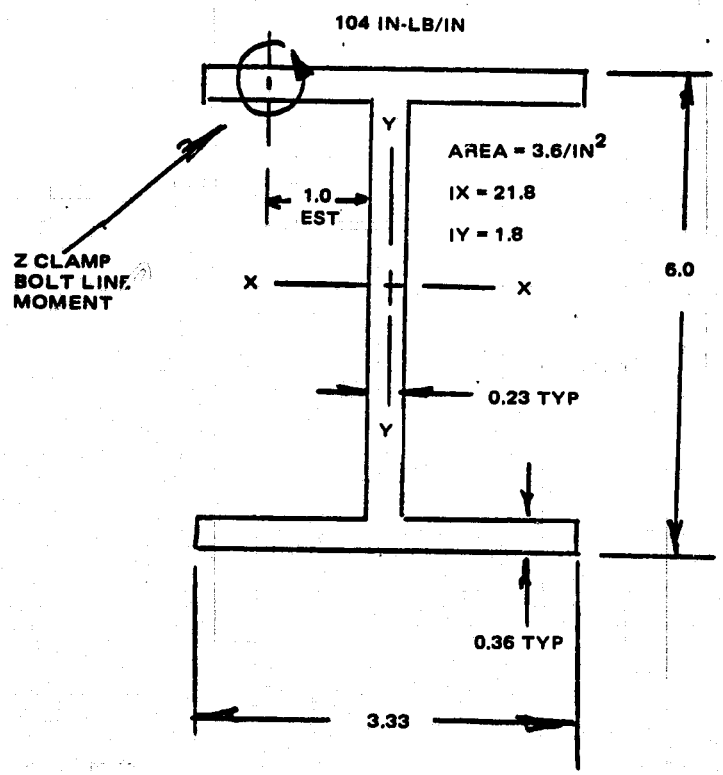

$$K_T = \frac{2bt_F^3 + ht_W^3}{3}$$

$$K_T = \frac{2(3.3)(0.36)^3 + 6(0.23)^3}{3}$$

$$K_T = 0.127 \text{ in}^4$$

$$K_B = \frac{b^3h^2t_F}{24} = \frac{(3.3)^3(6)^2(0.36)}{24}$$

$$K_B = 19.4$$

For a fixed-fixed beam with uniform twisting moment, the angle of twist is given by

$$\phi = \frac{mLa}{GK_T}\left[-\sinh\frac{z}{a} + \tanh\frac{L}{2a}\cosh\frac{Z}{a} + \frac{Z}{a} - \frac{Z^2}{aL} - \tanh\frac{L}{2a}\right]$$

The twist at each end is zero, maximum at center $\left(\frac{L}{2}\right)$

$$M = 104\ \frac{\text{in-lb}}{\text{in}} \qquad a = \sqrt{\frac{EK_B}{GK_T}} = \sqrt{\frac{(30\text{x}10^6)(19.4)}{(11.2\text{x}10^6)(.127)}} = 20.2$$

$$L = 44$$

$$\frac{L}{2a} = 1.09 \qquad \frac{L^2}{4aL} = 0.545$$

$$\phi_{MAX,\frac{L}{2}} = \frac{104(44)(20.2)}{(11.2\times10^{6})(.127)}\left[-\sinh 1.09 + \tanh 1.09 \cosh 1.09 + 1.09 - 0.545 - \tanh 1.09\right]$$

$$\phi_{MAX} = .065\left[-1.319 + 0.7969\,(1.6555) + 1.09 - 0.545 - 0.7969\right]$$

$$\phi_{MAX} = .065\,(-0.252) = -0.016 \text{ rad}$$

This calculation assumed that the moment was applied about the centroidal axis. Since the moment is introduced at the flange, estimate local distortion of flange.

Assume cantilever beam, L = 1.0, tip moment

$$\theta = \frac{ML}{EI} = \frac{104(1.0)}{(30\times10^{6})(0.36)^{3}/12} = 0.0009 \text{ rad}$$

SMALL

$$\phi_{TOTAL} = 0.016 + 0.0009 = 0.017 \text{ rad}$$

Estimate rigid body rotation of Z-clamp due to distortion of I-beam. This is conservative since it was assumed that I-beam does not rotate at end.

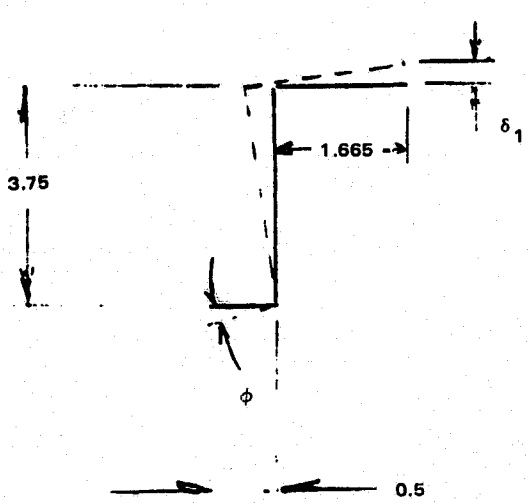

$\delta_1 = R\phi = (1.67)(0.017) = 0.03$ in

This displacement is additive with the elastic distortion of the Z-clamp.

D.2.6 Summary

To attain a 0.25" relative deflection (center to edge) of the L-band array, one must compensate for the elastic deformation of the edge supports (i.e., Z-clamp, I-beam). The elastic deformation (tip deflection) is approximately 0.05"* (0.017 + 0.03).

*NOTE: Due to additional flexibility of the backup structure not accounted for here, the deflection should be taken as an estimate only.

D. 3 SECTION PROPERTIES, NASTRAN MODEL

D. 3. 1 Diagonal

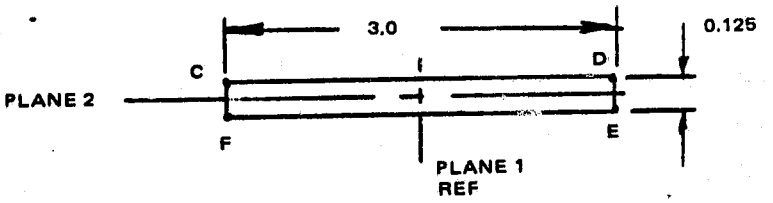

C1	C2	D1	D2
.063	-1.5	.063	1.5

E1	E2	F1	F2
-.063	1.5	-.063	-1.5

$$\text{Area} = 3(.125) = .375 \text{ in}^2 \qquad I1 = \frac{3(0.125)^3}{12} = 4.88\text{x}10^{-4} \text{ in}^4$$

$$I2 = \frac{(0.125)(3)^3}{12} = 0.281 \text{ in}^4$$

$$J = \frac{3(0.125)^3}{3} = 1.95\text{x}10^{-3} \text{ in}^4$$

D. 3. 2 Top Rail

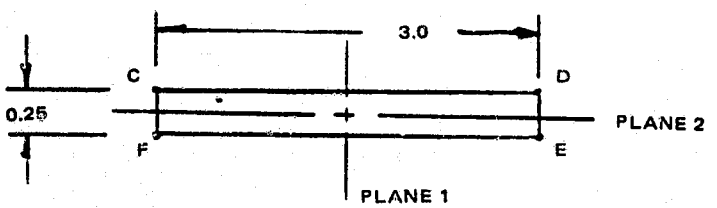

C1	C2	D1	D2
0.125	-1.5	0.125	1.5

E1	E2	F1	F2
-0.125	1.5	-0.125	-1.5

$$\text{Area} = 3(0.25) = 0.75 \text{ in}^2$$

$$I1 = \frac{3(0.25)^3}{12} = 3.91 \text{ x } 10^{-3} \text{ in}^4$$

$$I2 = \frac{0.25(3)^3}{12} = 0.563 \text{ in}^4$$

$$J = \frac{3(0.25)^3}{3} = 0.016$$

D.3.3 Upright

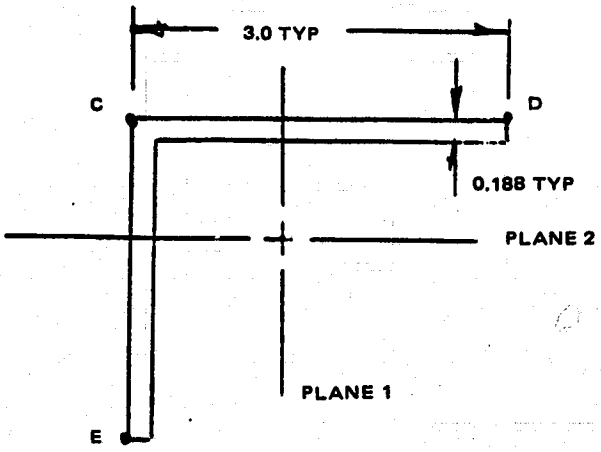

C1	C2	D1	D2	E1	E2
0.82	-0.82	0.82	2.18	-2.18	-0.82

F1	F2

$$\text{Area} = 0.188(2)(2.81) = 1.06 \text{ in}^2 \qquad \bar{X} = \bar{Y} = \frac{3^2 + 0.188(2.81)}{2(5.81)} = 0.82$$

$$IX = IY = \frac{1}{3}\left[0.188(3-0.82)^3 + 3(0.82)^3 - 2.81(0.82 - 0.188)^3\right]$$

$$IX = IY = \frac{1}{3}\left[1.95 + 1.65 - 0.709\right] = 0.963 \text{ in}^4$$

$$J = \frac{1}{3}\left[3 + 2.81\right](0.188)^3 = 0.013 \text{ in}^4$$

D.3.4 Diagonal Channel (Alternate)

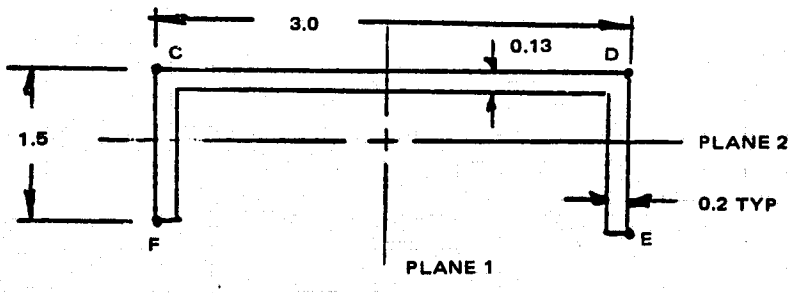

C1	C2	D1	D2	E1
0.5	-1.5	0.5	1.5	-1.0

E2	F1	F2
1.5	-1.0	-1.5

$$\text{Area} = 0.965 \text{ in}^2 \qquad I1 = 0.22 \text{ in}^4 \quad J = \frac{1}{3}\left[(1.5 + 1.5(0.2)^3 + 3(0.13)^3\right]$$

$$I2 = 1.41 \text{ in}^4 \quad J = 0.01 \text{ in}^4$$

These properties obtained from tables within Aluminum Standards & Data 1972-73, Martin-Marietta Aluminum.

C-2

D.4 CRITICAL BUCKLING LOAD (Pcr) FOR DIAGONAL MEMBERS

PEDESTAL BACKUP STRUCTURE

SIDE VIEW

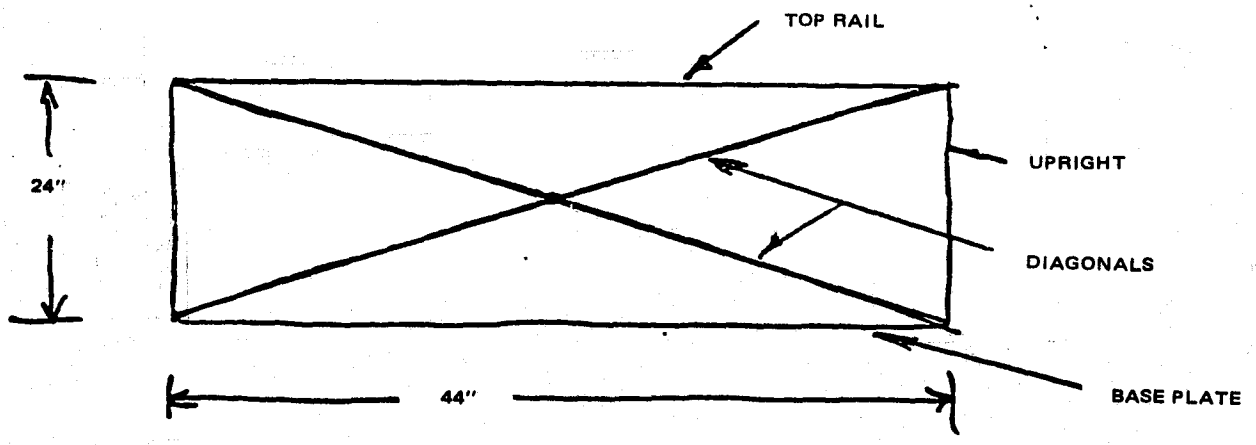

Assume following model

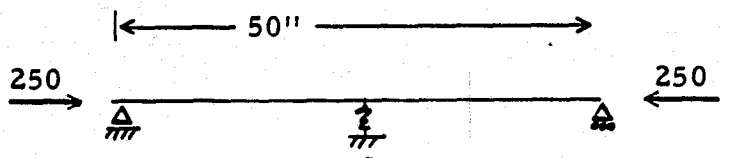

Let 2L = 50"

L = 25"

$$Por = \frac{\pi^2 EI}{L_e^2} \qquad L_e = \text{effective length of diagonal}$$

$$K = \frac{48EI}{(2L)^3} = \frac{8EI}{L^3} \Rightarrow \frac{KL^3}{EI} = \frac{8EI}{L^3}\left(\frac{L^3}{EI}\right) = 8$$

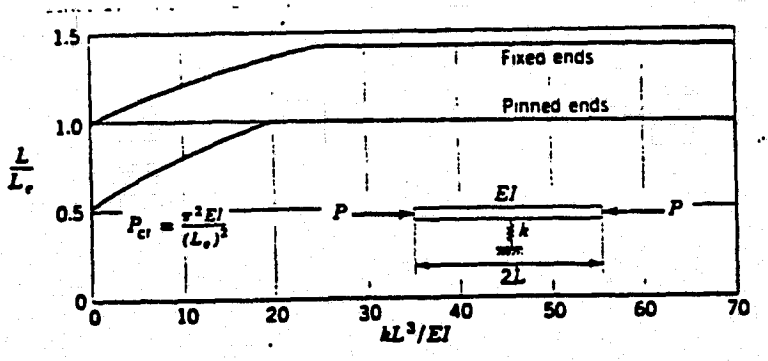

$$\frac{L}{L_e} = 0.75$$

$$L_e = \frac{L}{0.75} = \frac{25}{0.75} = 33.33 = 1.33L$$

For baseline cross-section

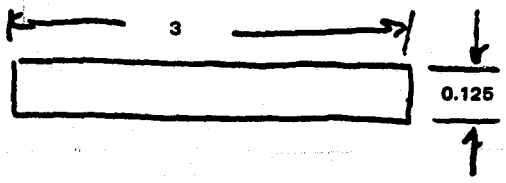

$I_{min} = 4.88 \times 10^{-4}$

$$Pcr = \frac{\pi^2 EI}{L_e^2} = \frac{\pi^2 (10^7)(4.88 \times 10^{-4})}{(33.33)^2} = 43.4\#$$

$Pcr = 43.4\#$

For new cross-section

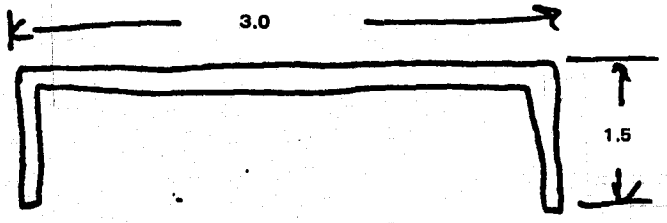

$I_{min} = 0.22$

$$Pcr = 43.4 \left(\frac{0.22}{4.88 \times 10^{-4}} \right) = 19550\#$$

if L = 50 Pcr = 8000

As an alternative try

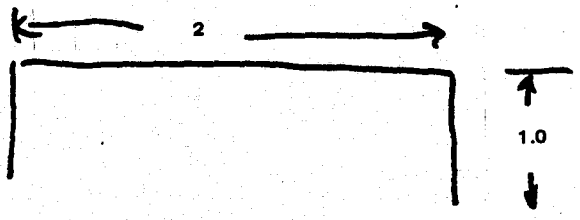

$I_{min} = 0.045$

$$Pcr = 43.4 \left(\frac{0.045}{4.88 \times 10^{-4}} \right) = 4003$$

if L = 50 Pcr = 1743

D.5 SAFETY DEVICES FOR THE L-BAND ARRAY TEST FIXTURES

Three bolts have been added to the X/L-band Assembly. These bolts serve the purpose of restraining the L-band Array Module, shims or spacers from sliding off the assembly if it is moved before the clamping hardware has been torqued. Figure D-6 shows the location of the three bolts. These bolts are not torqued but only serve as a safety device.

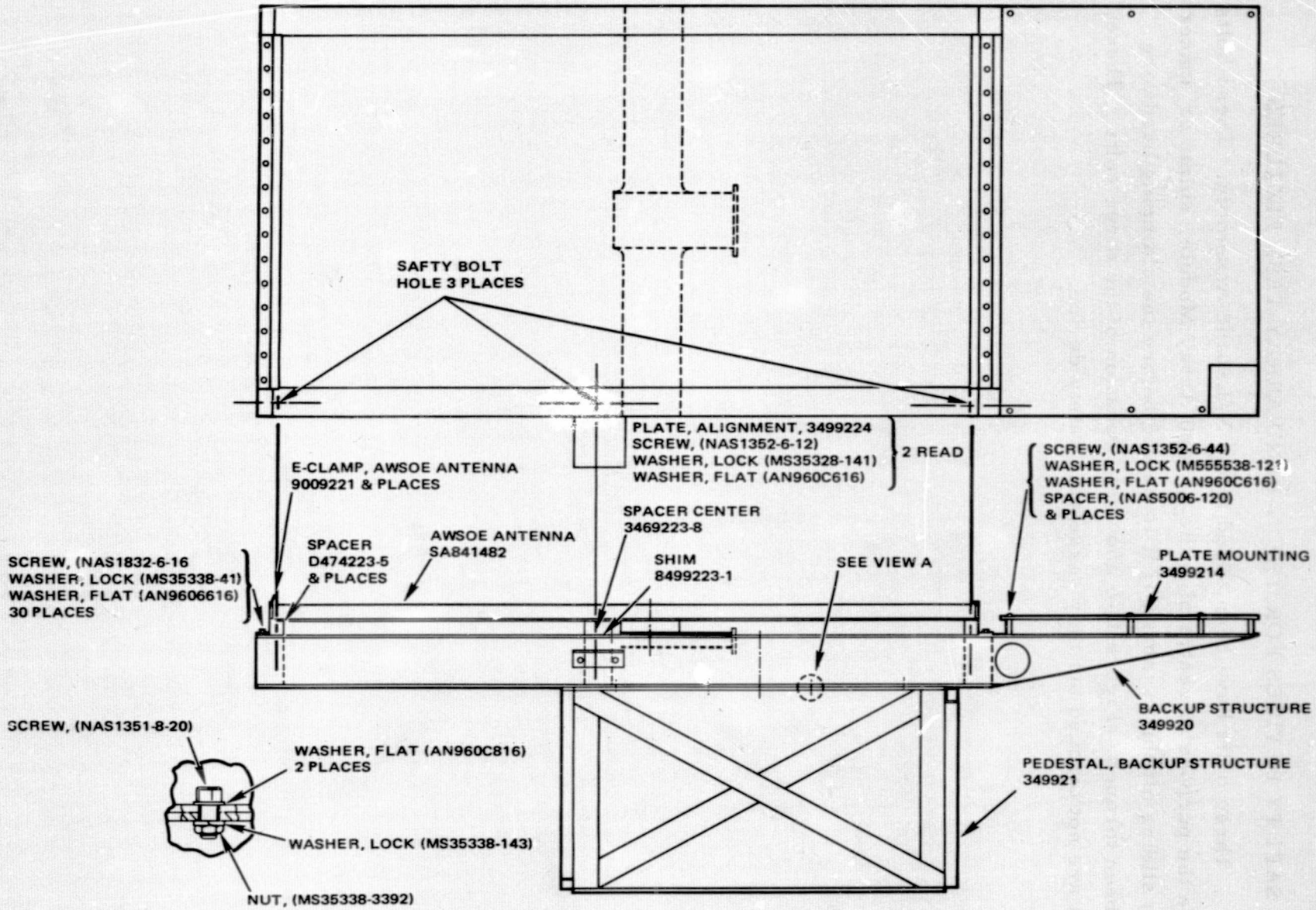

Figure D-6 Safty bolt hole locations

D.6 PREDICTION OF ULTIMATE STRUCTURAL FAILURE OF THE L-BAND MODULE

Structural analyses have indicated that ultimate structural failure of the L-band Array, Ref. 1, will occur at fastener failure. The detailed analysis showed that the drive screws, Ref. 2, had highest stress and lowest margin of safety for a bending deformation of the array. Based on a shear strength of 160 lbs., Ref. 3, or a shear stress of 45.4 ksi of the drive screw, the maximum deflection of the array is estimated to be 0.43 inch at the threshold of fastener failure. Based on the approximate yield stress of 30 ksi of carbon steel, the L-band array may be deformed as much as 0.28 inch before any permanent deformation occurs.

During mechanical loading of the array, visual inspection should be made for possible loosening of the fasteners.

APPENDIX E
L-BAND MODULE PERFORMANCE

APPENDIX E
L-BAND MODULE PERFORMANCE

E.1 BRASSBOARD MODEL OF AN L-BAND ARRAY MODULE

Figure E-1 presents a photograph of an array module that was fabricated to demonstrate the performance capabilities of a slotted waveguide array at L-band frequencies. This module contains six waveguide linear array elements; each waveguide element has 13 radiating slots. The cross feed runs across the back of the aperture between the sixth and seventh rows of radiating slots. The input guide couples into the center of the cross feed. Half-height waveguide (4.6 cm or 1.6 inch high) was used throughout to minimize the thickness of the structure. The module was designed for use in an array of eight such modules. The various components of the module are easily identified by a comparison of Figure E-1 and Figure 2-3.

The radiation patterns in both E- and H-planes, gain, and VSWR of the brassboard module were measured. Results are illustrated and discussed below.

E.2 RADIATION PATTERNS

The measured principal plane radiation patterns of the brassboard model are shown in Figure E-2. The aperture distribution along the long dimension of the module was designed to give a first sidelobe level of 16.5 dB. The small crosses on the corresponding H-plane pattern (Figure E-2(b)) indicate the design or predicted levels and positions of the sidelobe peaks. As can be seen, the agreement between theory and measurement is excellent. Intercardinal plane patterns, which were also recorded, showed no indications of spurious lobes.

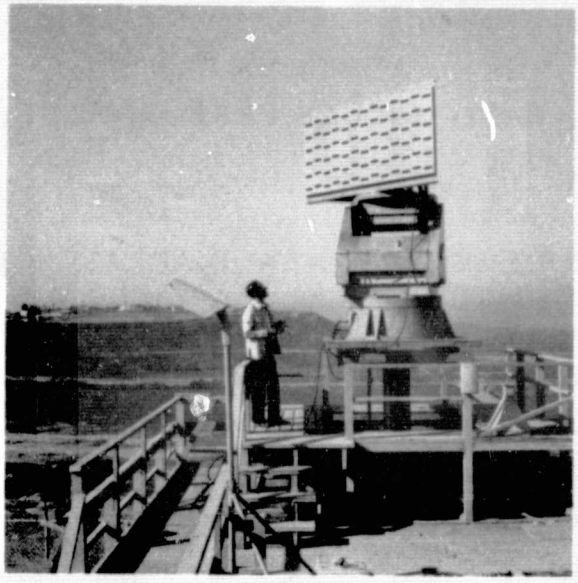

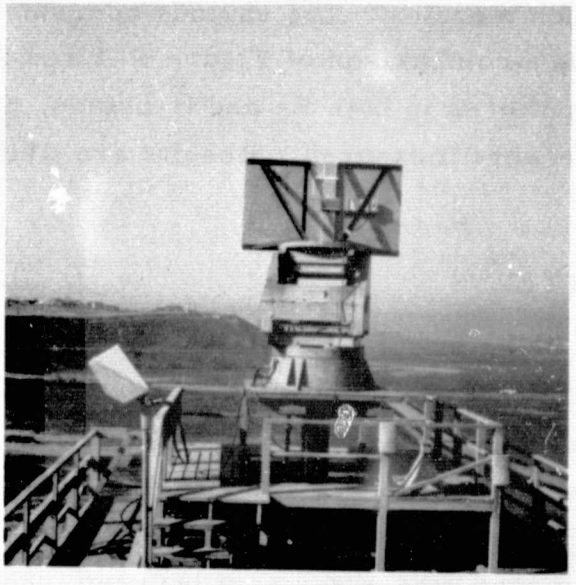

Figure E-1. Brassboard model of L-band module.

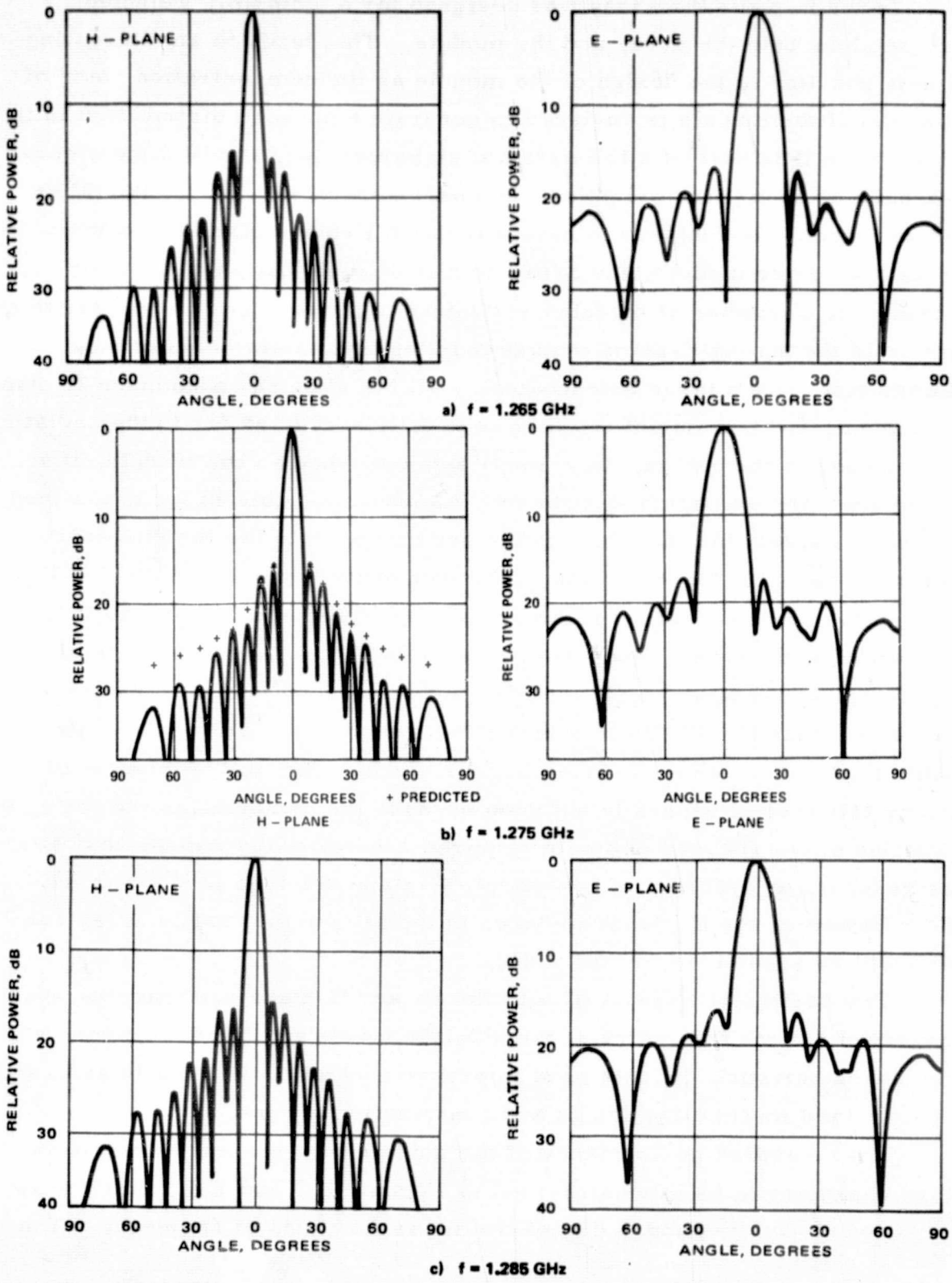

Figure E-2. Measured E- and H-plane patterns of brassboard module.

In the E-plane the array was designed for a uniformly weighted aperture along both the array and the module. This leads to an interesting dilemma peculiar to the design of the module as the demonstration piece of hardware: if the module is designed to generate a uniform distribution in the E-plane when it is part of a full array of eight modules, it will almost certainly have a nonuniform weighting when used separately. If, on the other hand, the module is designed to have a uniform E-plane distribution when used as a separate module, the array amplitude distribution will be nonuniform when a number of modules are joined together. The reason for this behavior is the strong E-plane mutual coupling that exists between the radiating slots. In a large antenna nearly all the slots see a common E-plane environment, and the mutual coupling is usually accounted for in the radiating slot data used in the design. In a small antenna, such as the module, if a uniform aperture excitation is required, the coupling slots in the cross feed are used to correct for the edge effects and compensate for the different behavior of the slots located close to the side of the array.

In the present design the module was designed and laid out as if it were part of a full array. As a result, the mutual coupling results in an effective amplitude taper in the module, and the sidelobe levels are considerably lower than the 13.3 dB normally to be expected. While it is quite feasible to calculate what the sidelobe levels should be, in the interest of economy this step is generally not done because the computation and the acquisition of the specific slot data required are relatively expensive. For these reasons, an estimate of the module E-plane sidelobe levels was not made. However, the E-plane sidelobes of the full, eight module array can confidently be predicted to be 13.3 dB.

Two particular aspects of both the E- and H-plane patterns that should be observed are the symmetry of the sidelobe levels and the deep clean nulls. These characteristics indicate good tolerance control of the module and small microwave and mechanical design and construction errors.

The measured performance of the module with respect to radiation pattern characteristics is summarized in Figures E-3 and E-4, which show the first sidelobe level and 3-dB beamwidth as functions of frequency. The

predicted curve for the 3-dB beamwidth of the H-plane pattern is also plotted in Figure E-4. The E-plane 3-dB beamwidth for the module was not predicted because the mutual coupling effects that lead to low sidelobes in this plane also produce a broader beamwidth than would otherwise be observed.

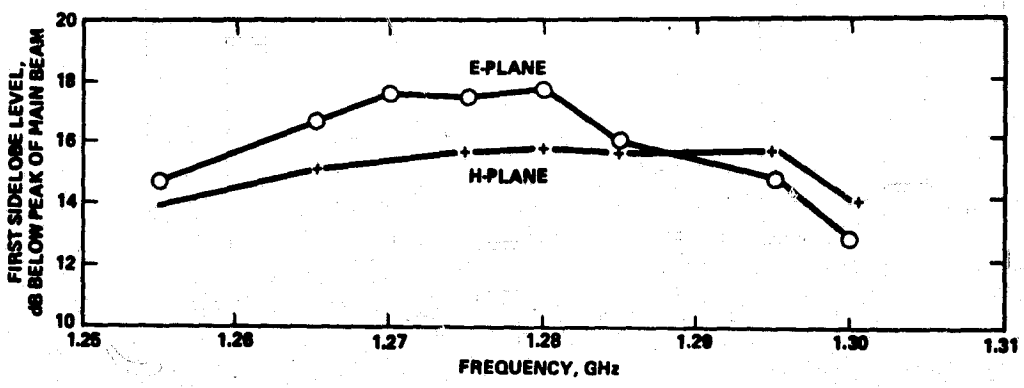

Figure E-3. Measured sidelobe levels.

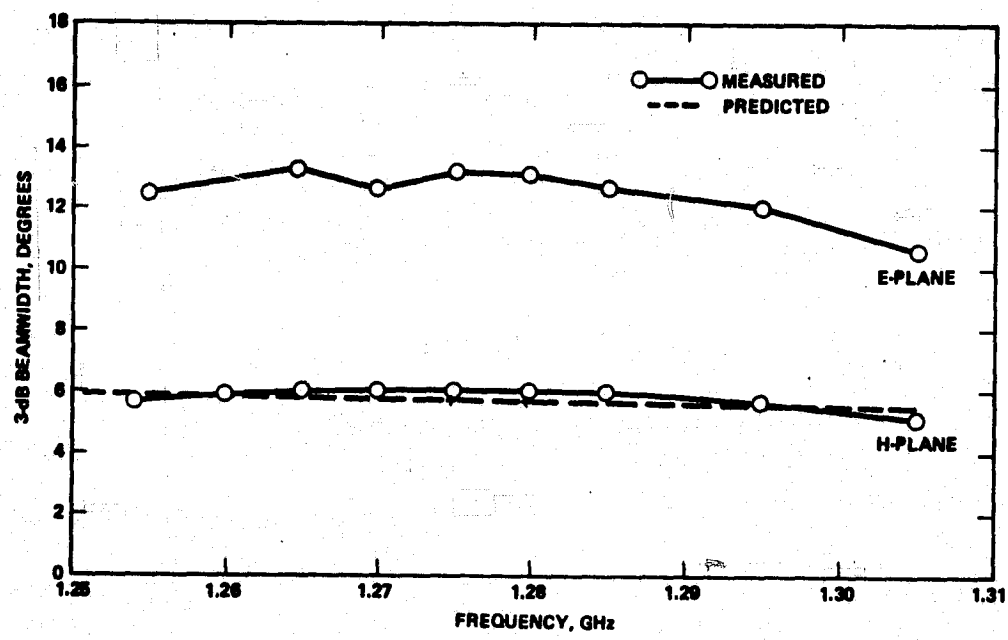

Figure E-4. Variation of 3-dB beamwidth with frequency.

E.3 GAIN

The maximum theoretical gain of a planar slot array is relatively simple to calculate with a high degree of precision. The procedure is to compute the so-called area gain from the well-known expression

$$G_0 = \frac{4\pi A}{\lambda^2}$$

where

A = aperture area

λ = wavelength

and then subtract the losses associated with the aperture weighting function used for sidelobe level control and beam shaping.

A gain of 26.9 dB was calculated for the brassboard module for the design frequency of 1.270 GHz. A loss allowance of 0.10 dB, which included the calculated value for the H-plane weighting and an estimated value, based on experience, for the E-plane weighting, was made for the aperture weighting. The measured gain of the module is plotted as a function of frequency in Figure E-5. For purposes of comparison, the maximum theoretical gain (G) achievable with an aperture of the module dimensions is also plotted on the same figure. The difference between the two curves at any frequency represents the losses due to random manufacturing errors, waveguide dissipative losses, design errors, and input mismatch.

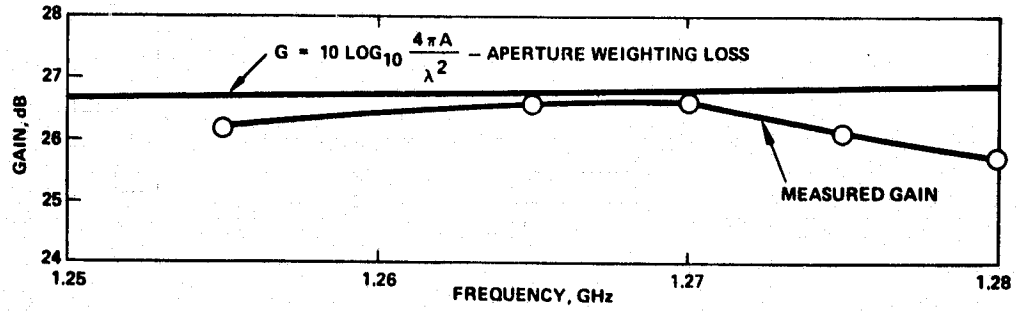

Figure E-5. Measured gain of brassboard module over design bandwidth.

The aperture efficiency is defined at Hughes as 100 times the ratio of the measured gain to the maximum theoretical gain of the aperture. When defined in this manner, the efficiency becomes a measure of the success of the antenna design in terms of achieving the theoretical pattern and gain characteristics. In the case of the L-band module, the aperture efficiency measured at 1.270 GHz is approximately 94 percent.

It should be noted that the gain data of Figure E-5 were measured through a stepped half-height to full-height transition and a coaxial-to-waveguide adapter. The gain was corrected for the gain reduction introduced by the waveguide transition and adapter dissipative losses. The input mismatch losses, however, were left in the data.

E.4 MODULE VSWR

The input voltage standing-wave ratio (VSWR) of the module, also measured through a stepped half-height to a full-height waveguide transition and a coaxial-to-waveguide adapter, is plotted in Figure E-6. As can be seen, the VSWR remained below 1.4:1 over most of the bandwidth. No matching or tuning devices were employed to obtain these results.

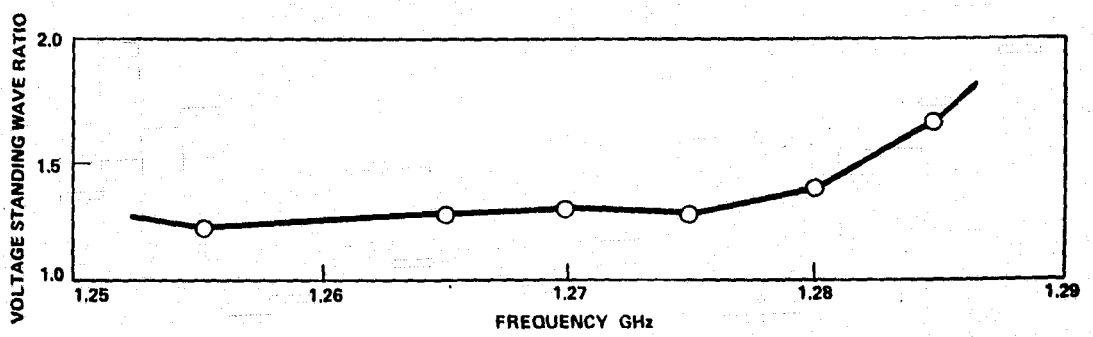

Figure E-6. Measured voltage standing-wave ratio of module.

E.5 SUMMARY OF MODULE PERFORMANCE CHARACTERISTICS

The performance of the module, as characterized by the microwave measurements, is summarized in Table E-1. The design objectives, which were based on theoretical values, are also tabulated for the purposes of comparison. Exact values of the cross polarization components of the radiation field are not given in the table because the measured values were so low

that they implied that the module cross polarization was significantly better than that of the transmitting source used for the pattern measurements.

TABLE E-1. PERFORMANCE OF L-BAND BRASSBOARD MODULE

Parameter	Design Objective	Measured (at 1.270 GHz)
Gain, dB	26.87	26.60
Beamwidth, degrees		
H-plane	5.9	6.0
E-plane	NA	13.2
First sidelobe, dB		
H-plane	16.5	-15.8
E-plane	NA	-17.4
Input VSWR	<1.5:1	<1.3:1
Bandwidth (GHz)	1.265 to 1.285	1.255 to 1.285
Cross polarization, dB	<30	<30
Efficiency (relative to weighted aperture), percent	>90	94
Aperture dimensions	1.04 x 2.12 x 0.04 meters (41.1 x 83.28 x 1.6 inches)	1.04 x 2.12 x 0.04 meters (41.1 x 83.28 x 1.6 inches)

E.6 FULL SCALE ARRAY PERFORMANCE

As a final step, the measured module data were utilized as the basis for a prediction of the performance characteristics of a full-scale array of eight modules. These results are given in Table E-2. It is believed that the numbers shown represent the full array performance with the same high degree of accuracy provided by the module data in Table E-1.

TABLE E-2. PROJECTED PERFORMANCE FOR ARRAY OF EIGHT MODULES

Parameter	Performance
Aperture	2.12 x 8.33 meters (83.28 x 328 inches)
Gain (eight times module gain less corporate feed losses), dB	35.3
Bandwidth	1.255 GHz to 1.285 GHz
Beamwidth, degrees	
H-plane	6.0
E-plane	1.31
First sidelobe levels, dB	
H-plane	-15.8
E-plane	-13.3
Input VSWR	<1.5:1
Cross polarization, dB	<30
Weight (array panels, structural support, thermal control systems), pounds	220

The estimate of the array weight was based on the use of thin wall (51 mm or 0.020 inch) aluminum waveguide for the module panels and corporate feed and an aluminum honeycomb support structure. The physical design of array and support was predicted on the assumption of a structural resonant frequency requirement of 25 Hz. The mechanical design did not provide for aperture folding. Techniques for forming and maintaining the necessary waveguide cross sections with the thin wall aluminum waveguide have been developed and demonstrated at Hughes under both funded and company-sponsored research efforts.

E.7 L-BAND PERFORMANCE WHEN BENDING

The bending plane of the L-band Module is the H-plane of the module and is the plane in which the distribution is tapered. Some pattern calculations were made to determine the pattern variations expected for the achievable mechanical deformation. The following array-factor computer plots, as shown in Figures E-7 through E-9, give an indication of the nature and degree of the effects on the pattern due to the forced mechanical deformation of the L-band module. For the planned test configuration the principal changes will be in the H-plane pattern. The mechanical perturbation was taken to be parabolic (and convex) along the length of the module with the peak displacement at the center.

Figure E-7 is the reference pattern (i.e., that of the unperturbed array). Figures E-8 and E-9 are for peak displacements of 0.4 and 1.2 inches. The expected working limit without permanent deformation is 0.3 inch. As evidenced by a comparison of these, the only detectable changes in the patterns may be the filled in first nulls. For the 0.4 inch deflection the calculated first sidelobe level rose less than 0.5 dB and the main beam power level dropped only 0.04 dB. The computed change in beamwidth for the same case was 0.01 degree.

To highlight these rather small changes in pattern, the more extreme deflection of 1.2 inches was considered.

E.8 CONCLUSIONS

The measured performance characteristics of the L-band module described in this paper demonstrate the feasibility of slotted waveguide planar arrays for L-band SAR systems. In every respect the module exhibits a superior level of microwave performance, and it was established that excellent agreement between predicted and measured performance can be obtained by the use of simple, straightforward design procedures.

The relatively low microwave frequencies for which this module was designed represent the lower end of the range for which waveguide slotted arrays are most attractive. Below L-band the dissipative loss characteristics of striplines and coaxial lines are sufficiently low as to warrant their

consideration for use as the feed elements. As the frequency is increased, however, the loss advantages of the slotted waveguide configuration become increasingly great. At the same time, the waveguide dimensions decrease rapidly to the point at which the volume savings that can be obtained through the use of TEM line configurations have no particular significance.

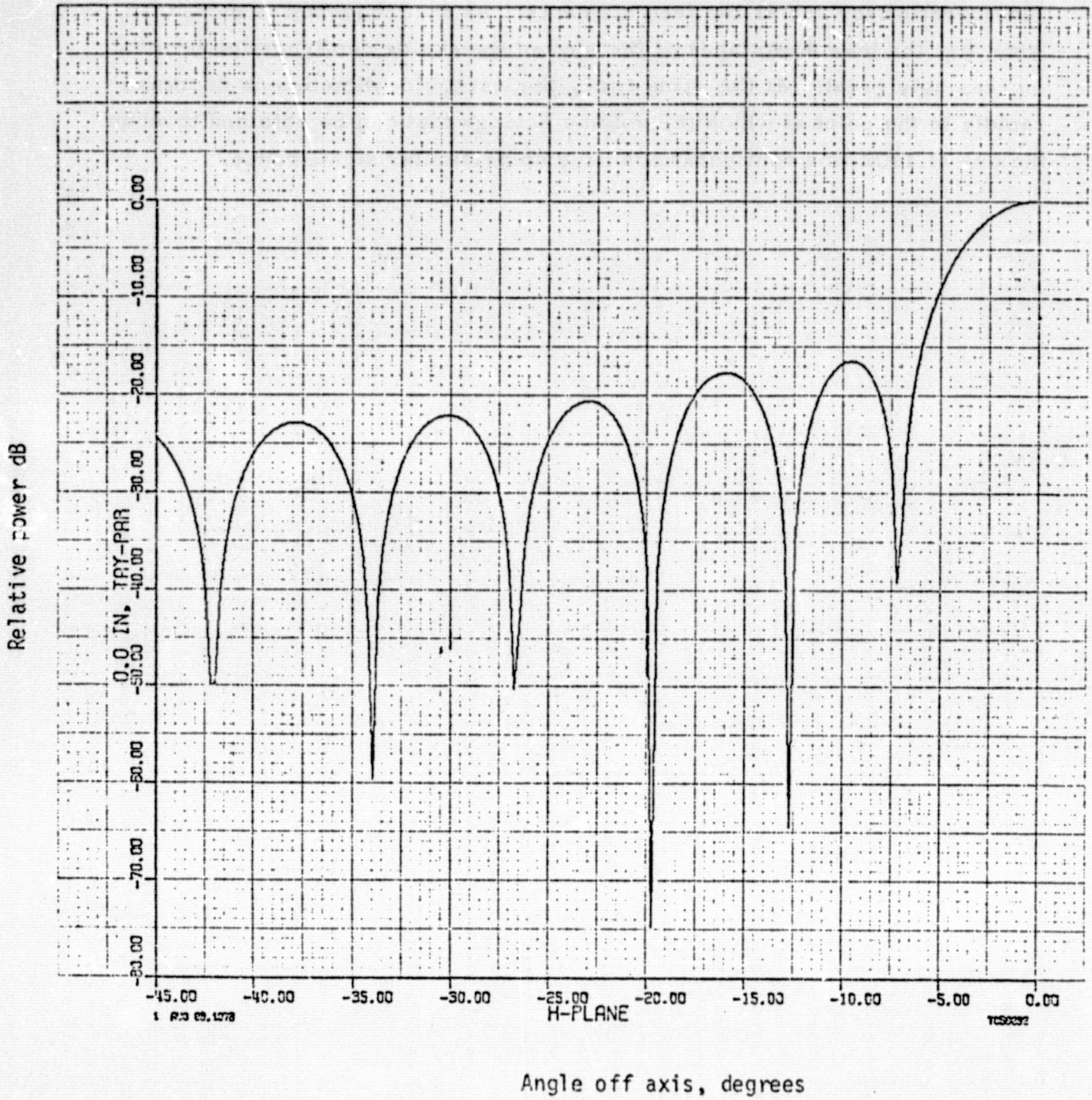

Figure E-7. Array factor pattern for the case of the unperturbed aperture plane.

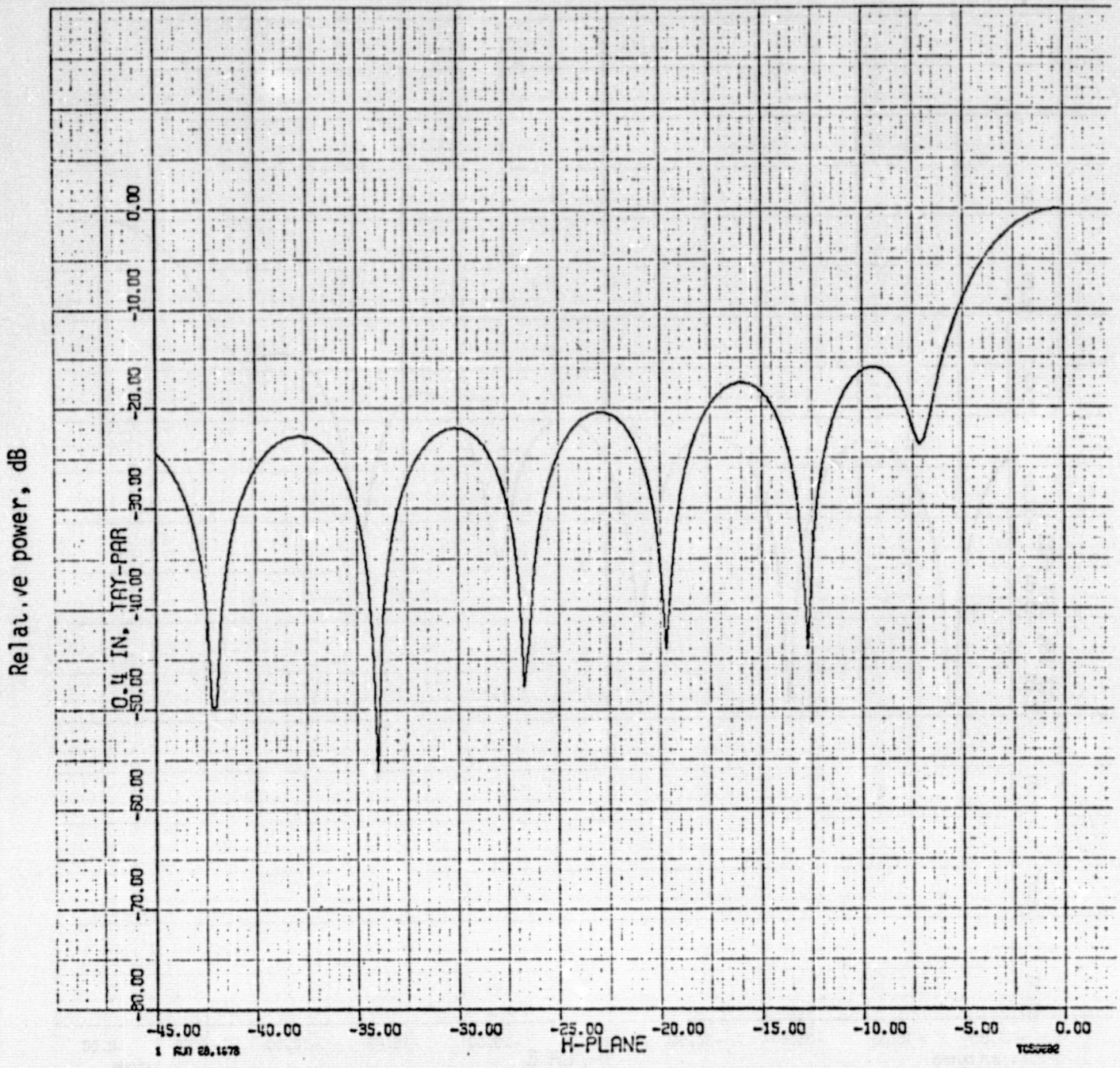

Figure E-8. Pattern for the case of a peak deflection of 0.40 inch.

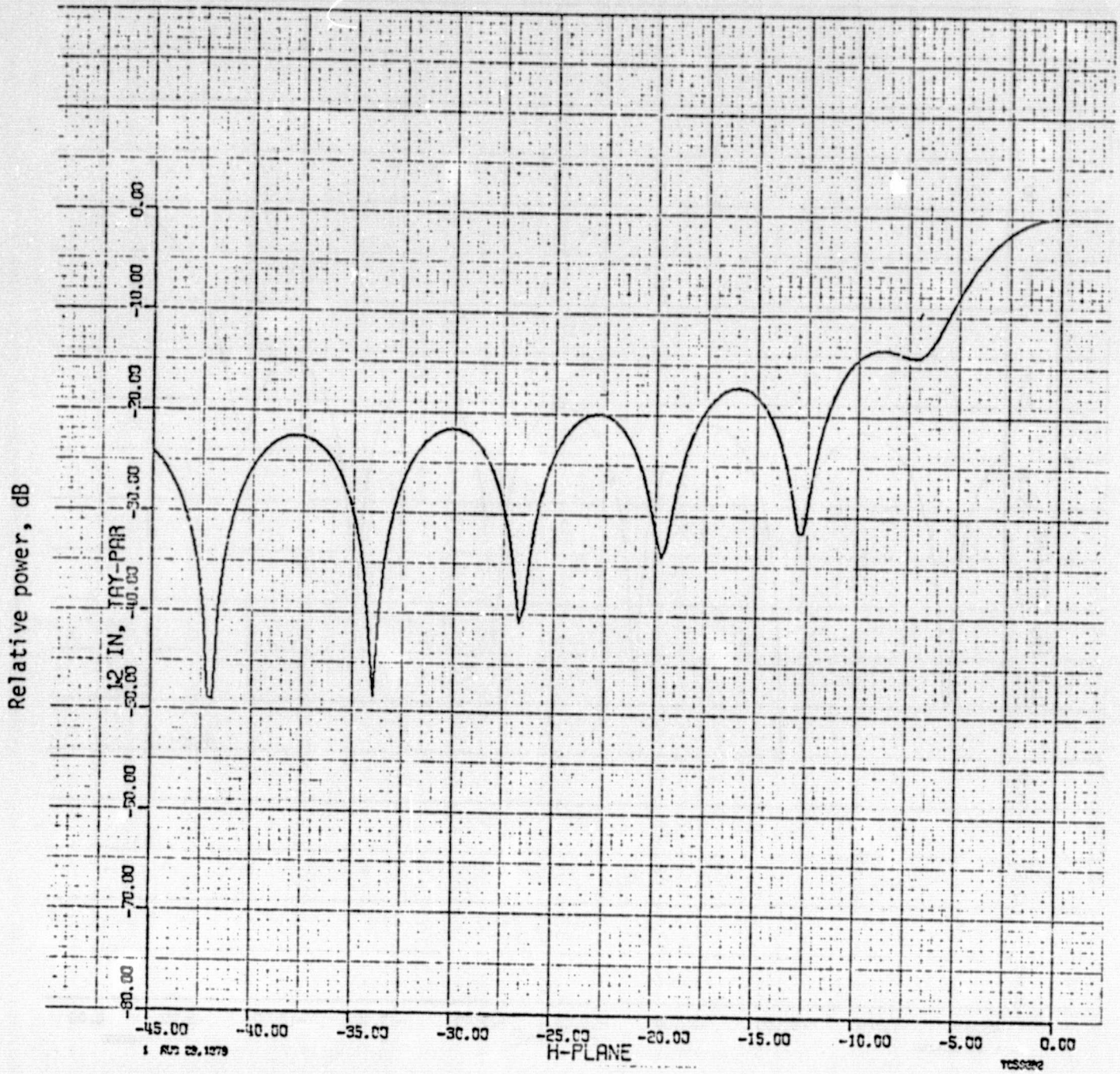

Figure E-9. Pattern for the case of a peak deflection of 1.20 inches.

E.9 COMPLETE SET OF MEASURED RADIATION PATTERNS

The following sequence of 36 radiation pattern plots describes the behavior of the L-band array over the frequency range from 1225 MHz to 1325 MHz in the two principle planes and in the ±45 degree intercardinal planes. The patterns marked by an asterisk have been previously shown in Figure E-2.

Pattern Number	Frequency	Plane	Page Number
1	1225	H	E-16
2	1255	H	E-17
3*	1265	H	E-18
4	1270	H	E-19
5*	1275	H	E-20
6	1280	H	E-21
7*	1285	H	E-22
8	1295	H	E-23
9	1325	H	E-24
10	1225	E	E-25
11	1255	E	E-26
12*	1265	E	E-27
13	1270	E	E-28
14*	1275	E	E-29
15	1280	E	E-30
16*	1285	E	E-31
17	1295	E	E-32
18	1325	E	E-33
19	1225	-45°	E-34
20	1255	-45°	E-35
21	1265	-45°	E-36
22	1270	-45°	E-37
23	1275	-45°	E-38
24	1280	-45°	E-39
25	1285	-45°	E-40
26	1295	-45°	E-41
27	1325	-45°	E-42
28	1225	+45°	E-43
29	1255	+45°	E-44
30	1265	+45°	E-45
31	1270	+45°	E-46
32	1275	+45°	E-47
33	1280	+45°	E-48
34	1285	+45°	E-49
35	1295	+45°	E-50
36	1325	+45°	E-51

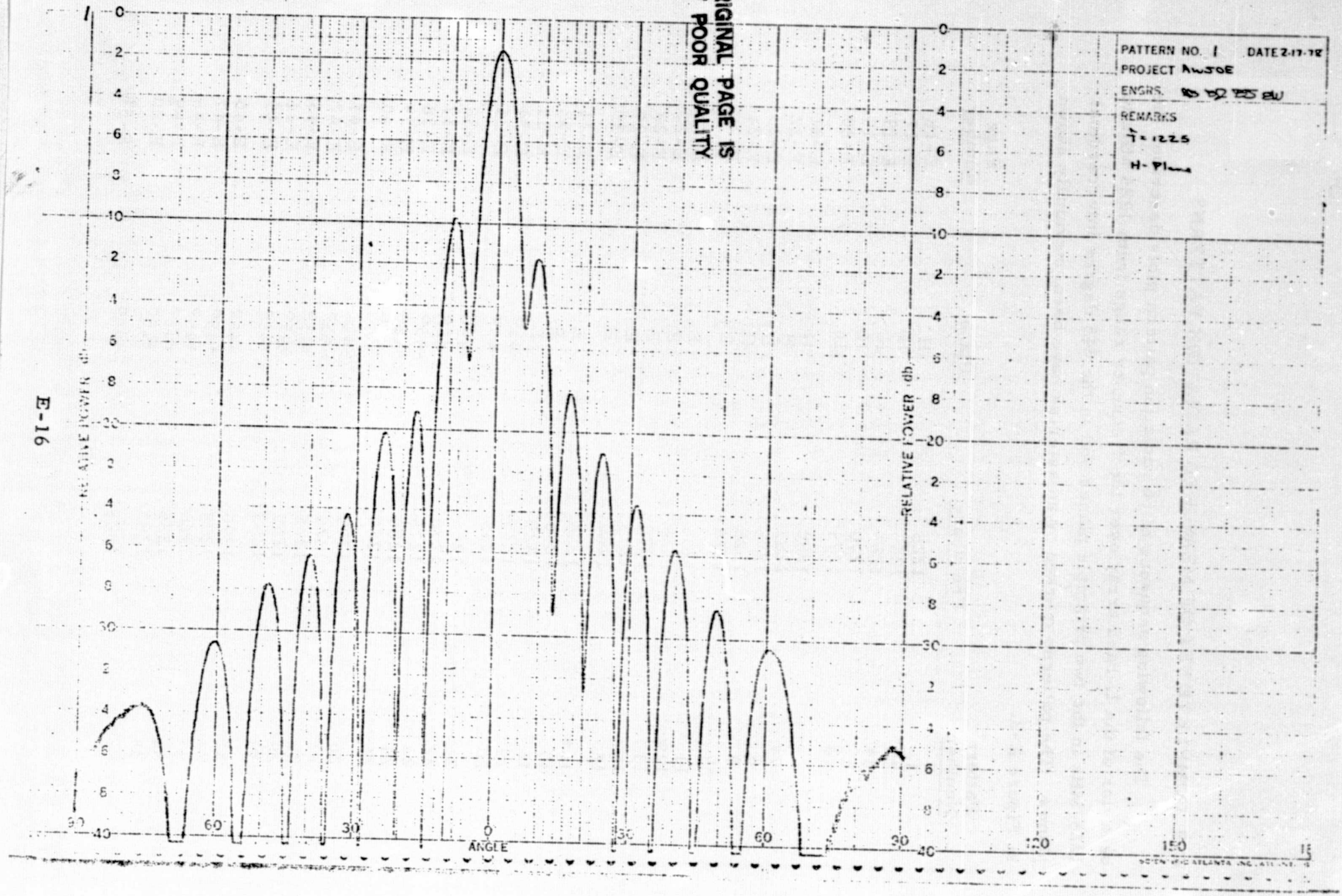

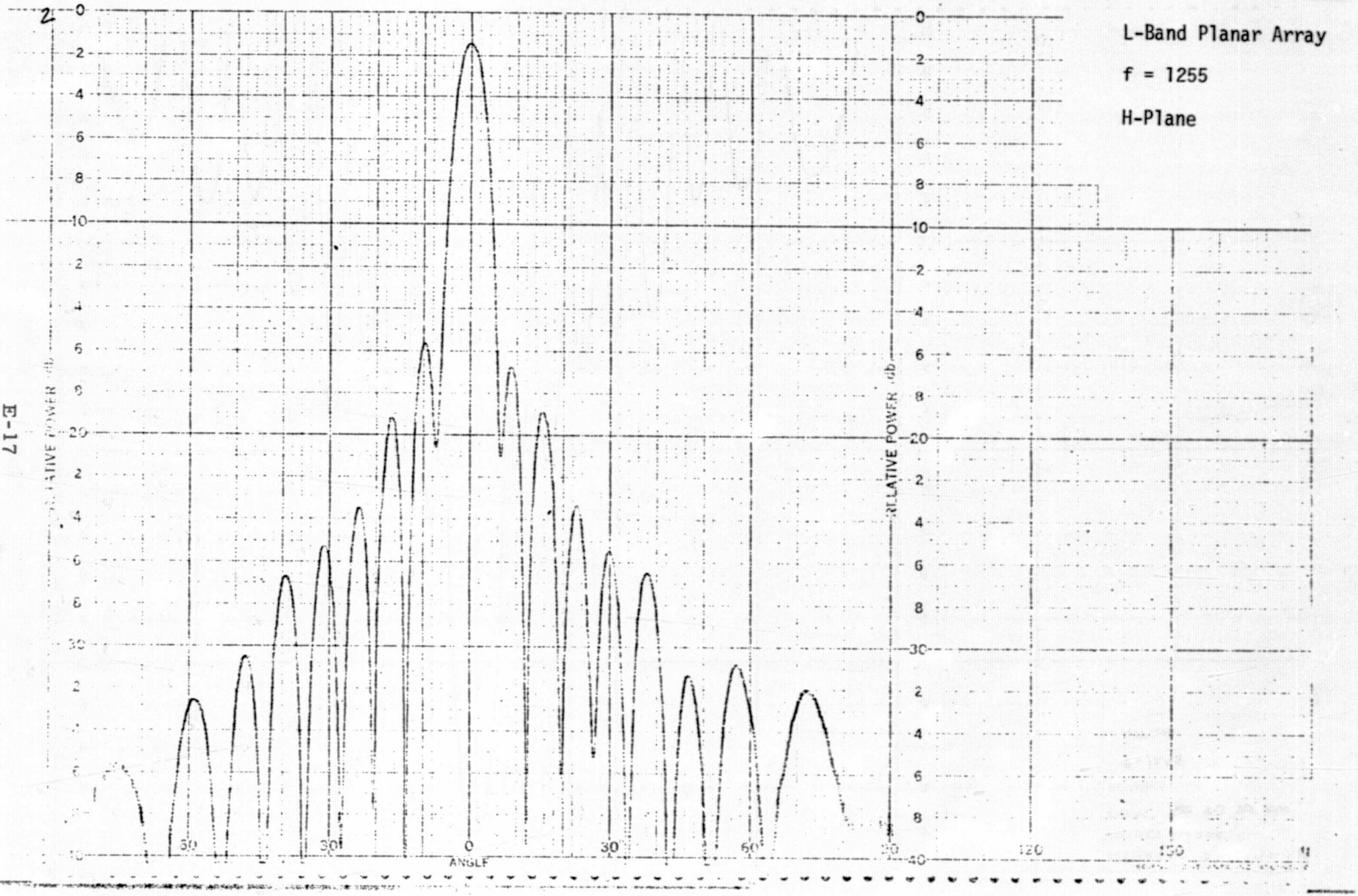
L-Band Planar Array
f = 1255
H-Plane
RELATIVE POWER db
ANGLE
0
2
4
6
8
10
20
30
40
50
60
90
120
150

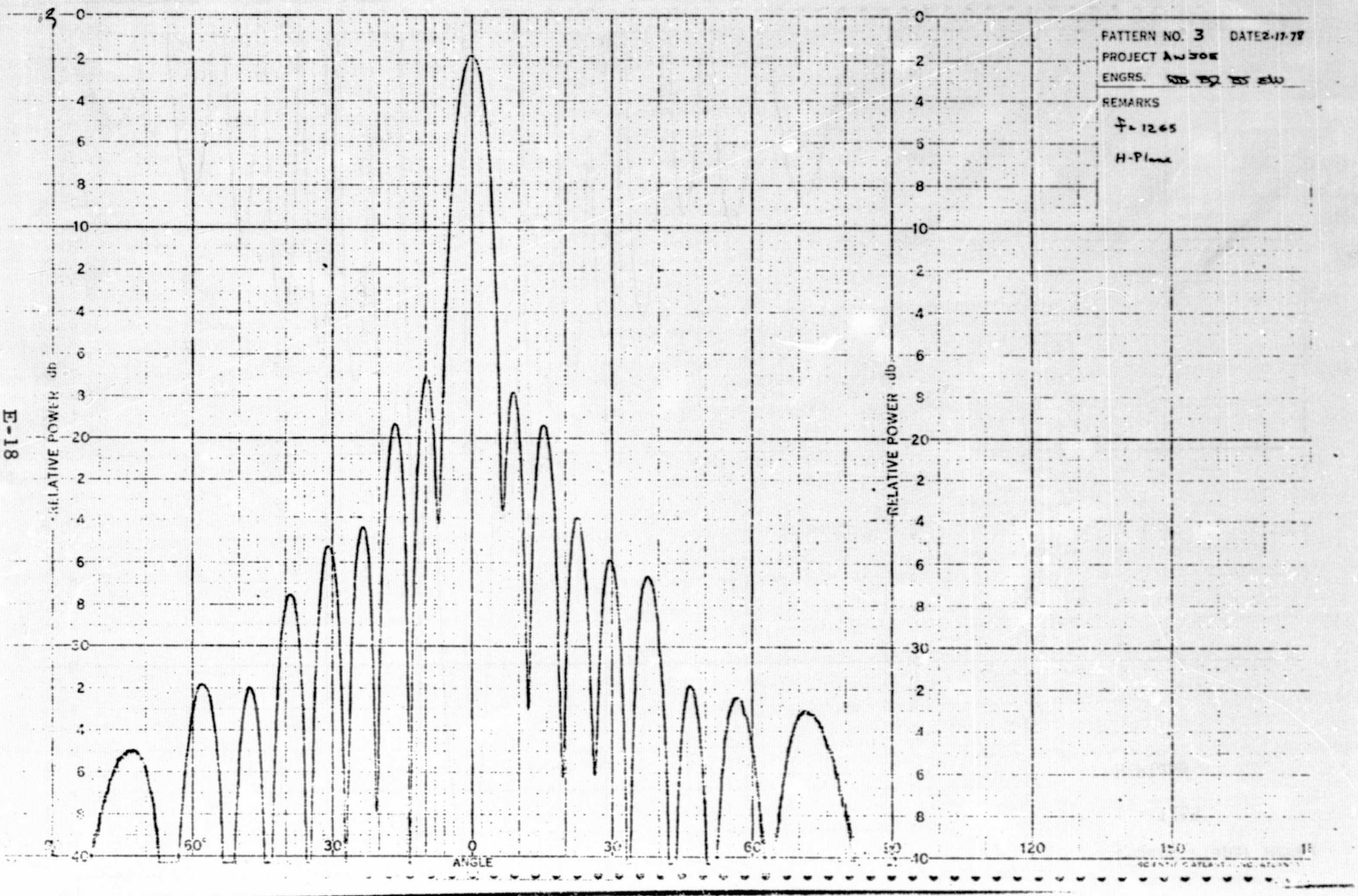
PATTERN NO. 3
DATE 2-17-78
PROJECT AWACS
ENGRS.
REMARKS
f = 1265
H-Plane
RELATIVE POWER db
ANGLE
60°
30°
0
30°
60°
120

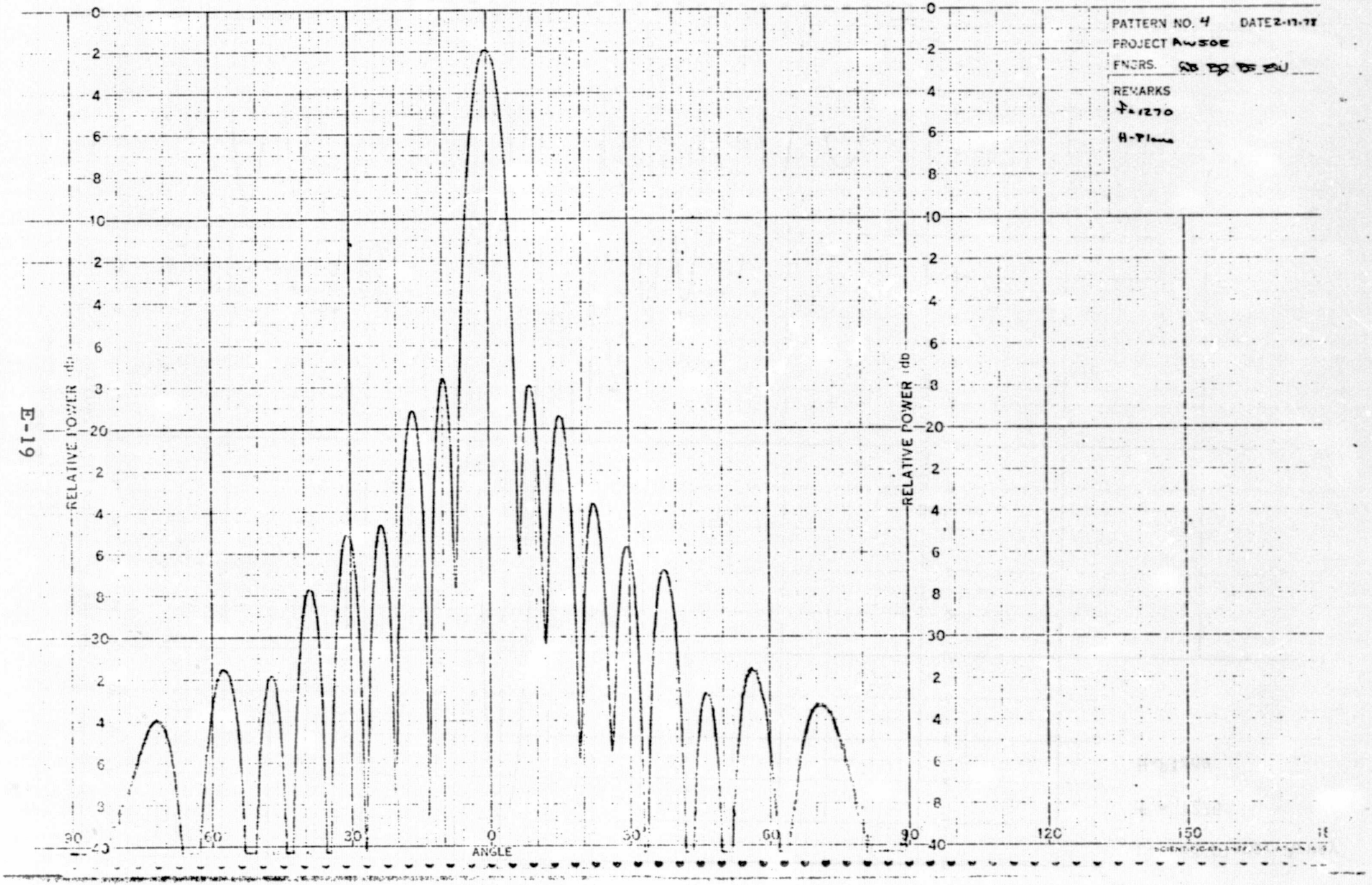
PATTERN NO. 4
DATE 2-17-72
PROJECT AWSOE
ENGRS.
REMARKS
f=1270
H-Plane
RELATIVE POWER db
ANGLE
0
2
4
6
8
10
20
30
40
90
60
30
0
30
60
90
120
150

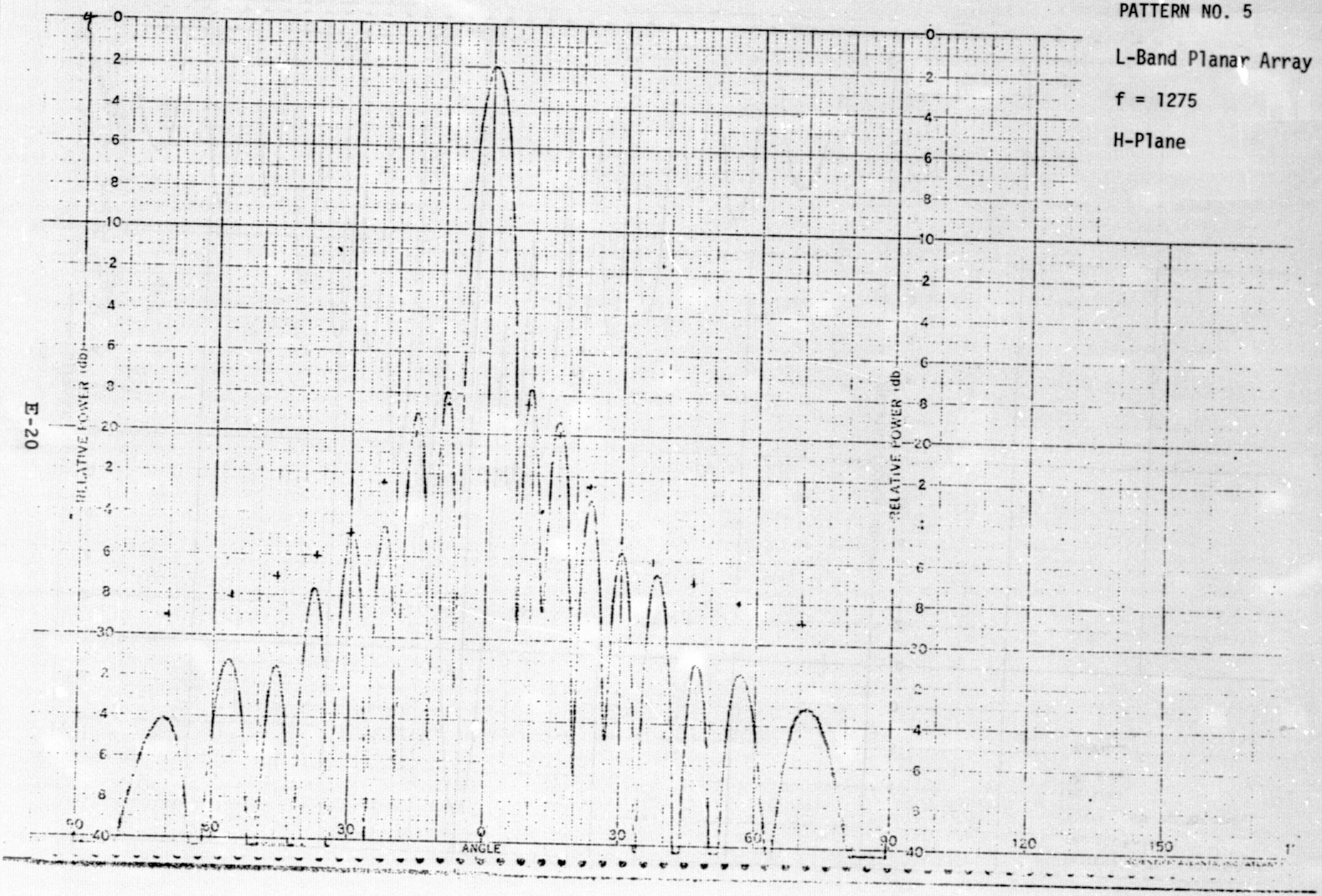
PATTERN NO. 5
L-Band Planar Array
f = 1275
H-Plane
RELATIVE POWER (db)
ANGLE
0
2
4
6
8
10
20
30
40
60
90
120
150

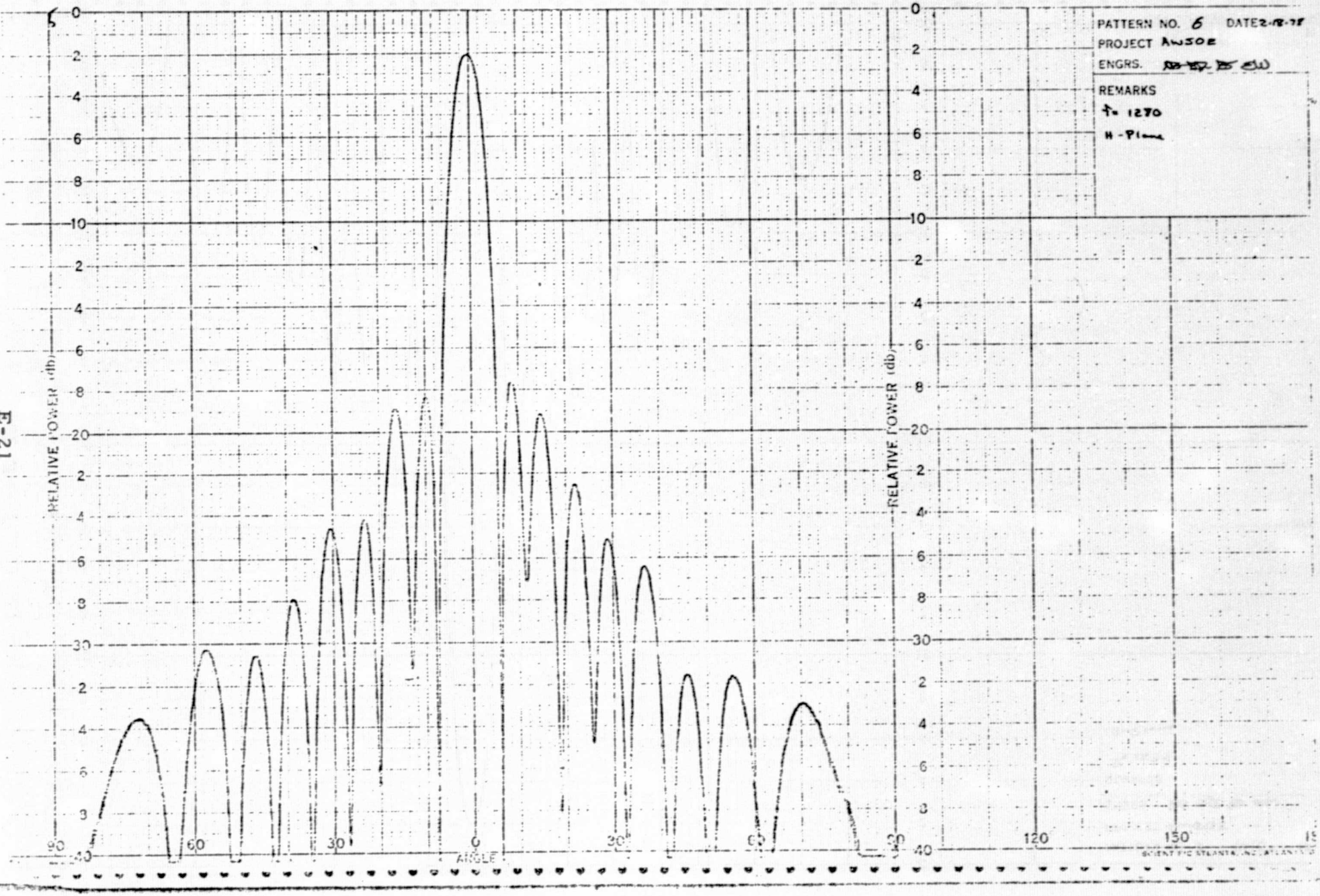
PATTERN NO. 6 DATE 2-18-75
PROJECT ANSOE
ENGRS.
REMARKS
f= 1270
H-Plane
RELATIVE POWER (db)
ANGLE
0
2
4
6
8
10
20
30
40
90
60
30
0
30
60
90
120
150

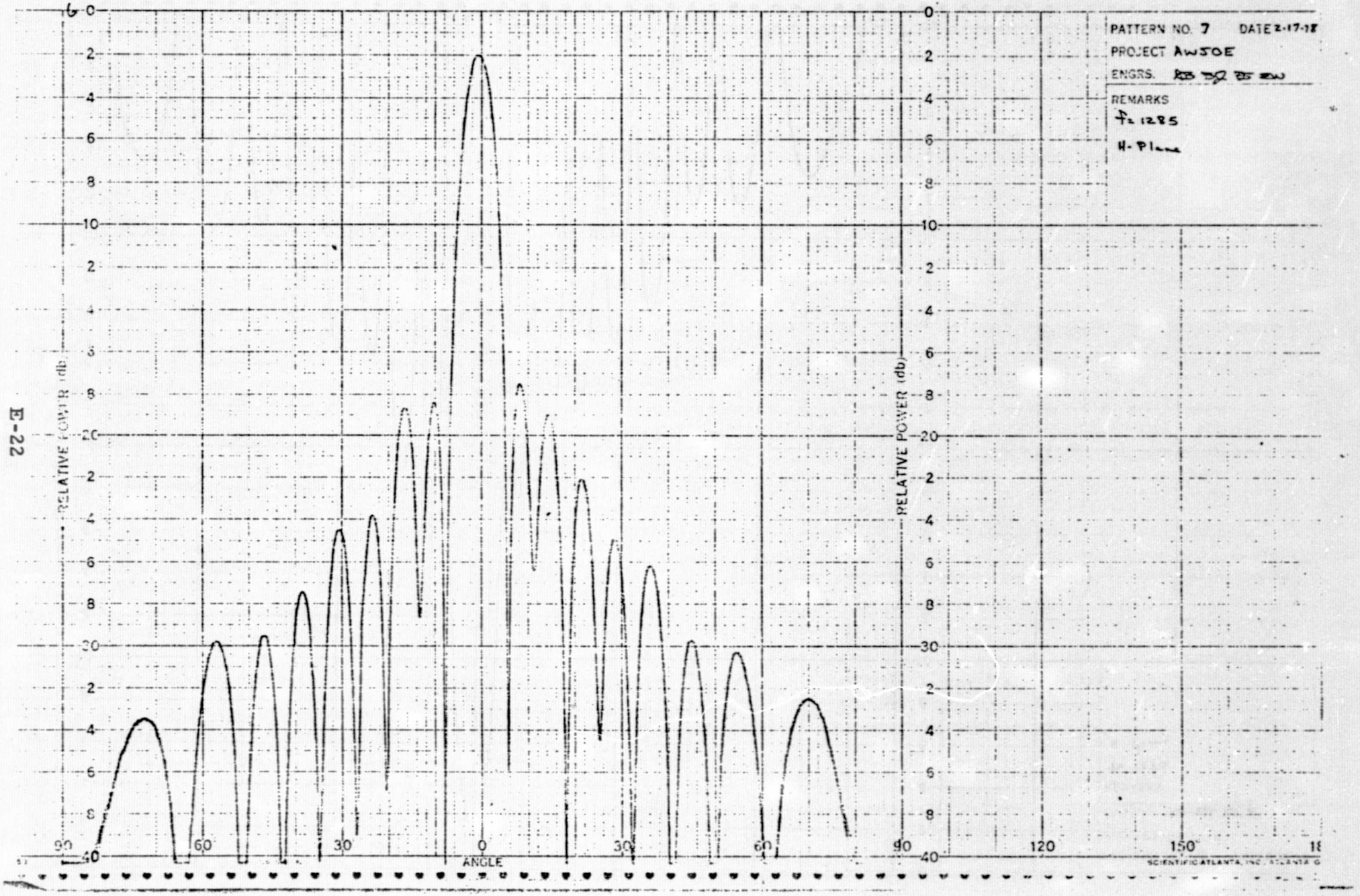
PATTERN NO. 7 DATE 2-17-78
PROJECT AWSOE
ENGRS. RB DR BS BW
REMARKS
f = 1285
H-Plane
RELATIVE POWER (db)
ANGLE
SCIENTIFIC-ATLANTA, INC., ATLANTA G

PATTERN NO. 8

L-Band Planar Array

f = 1295

H-Plane

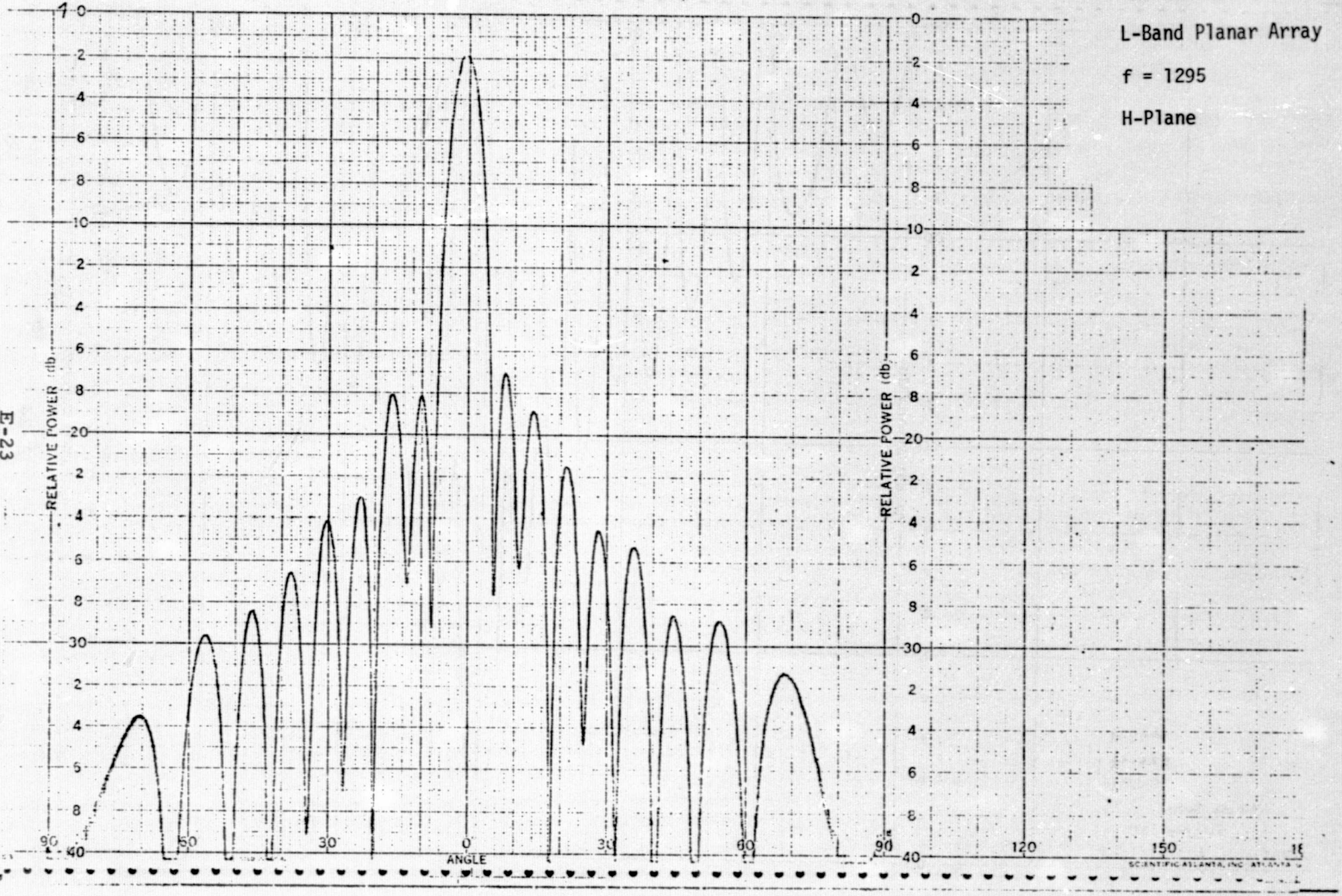

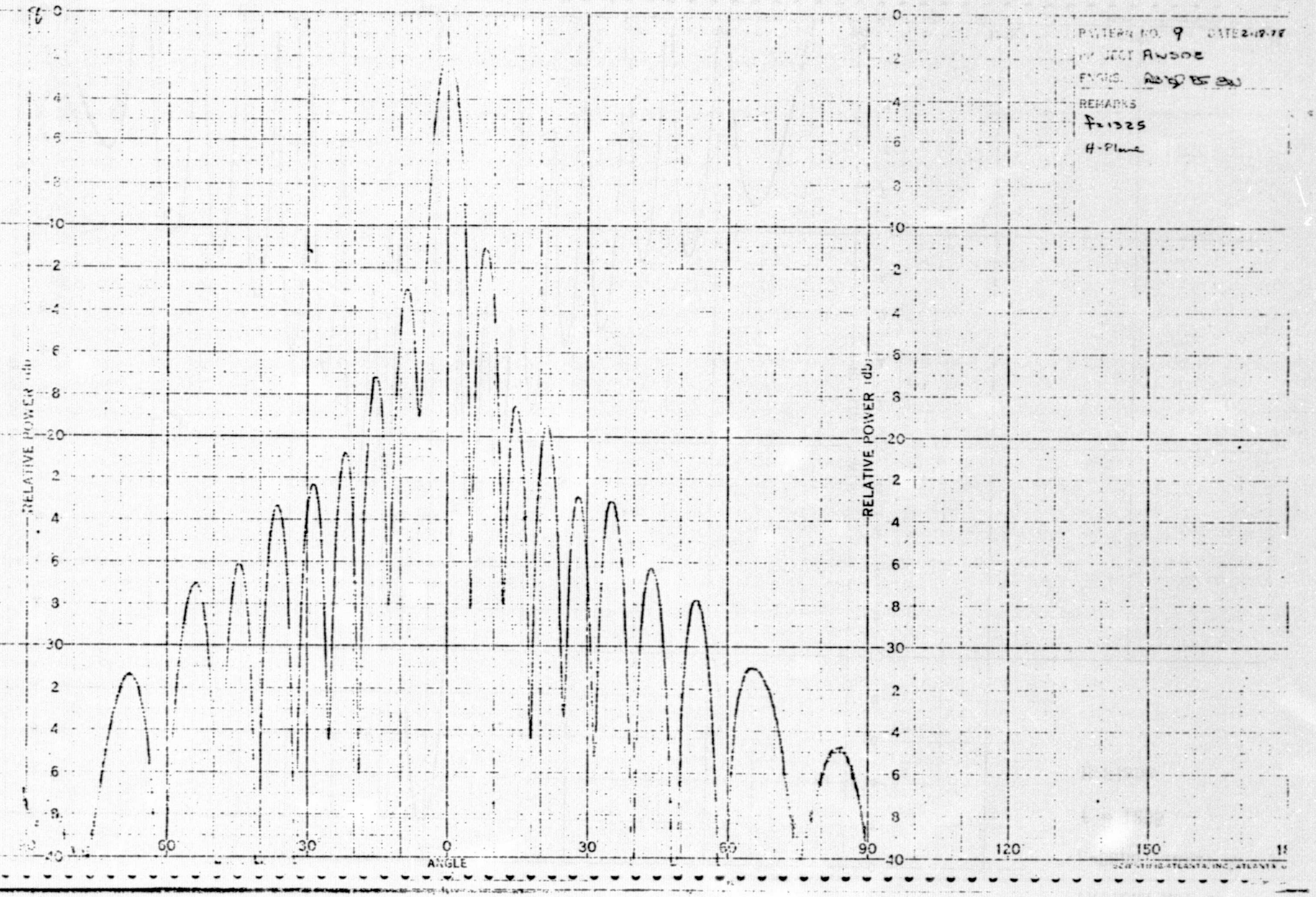

PATTERN NO. 9
REMARKS
f=1325
H-Plane
RELATIVE POWER (db)
ANGLE
0
-10
-20
-30
-40
60
30
0
30
60
90
120
150


PATTERN NO. 10 DATE 2-22-78
PROJECT AWSOE
ENGRS. SB EQ BS
REMARKS
f = 1225
E-Plane
RELATIVE POWER (db)
0
2
4
6
8
10
20
30
40
90°
60°
30°
0°
ANGLE
120°
150°

PATTERN NO. 11

L-Band Planar Array

f = 1255

E-Plane

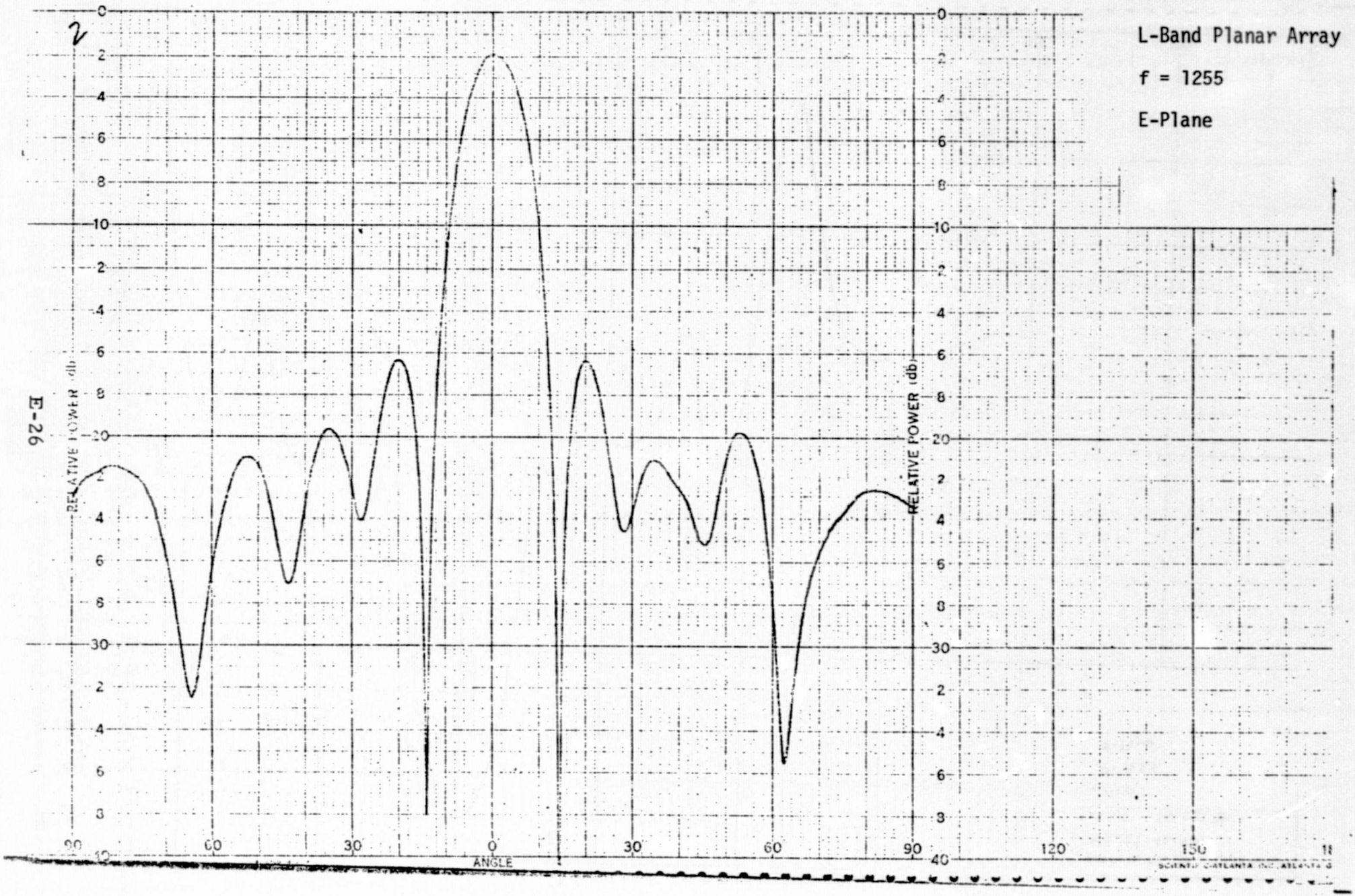

E-26

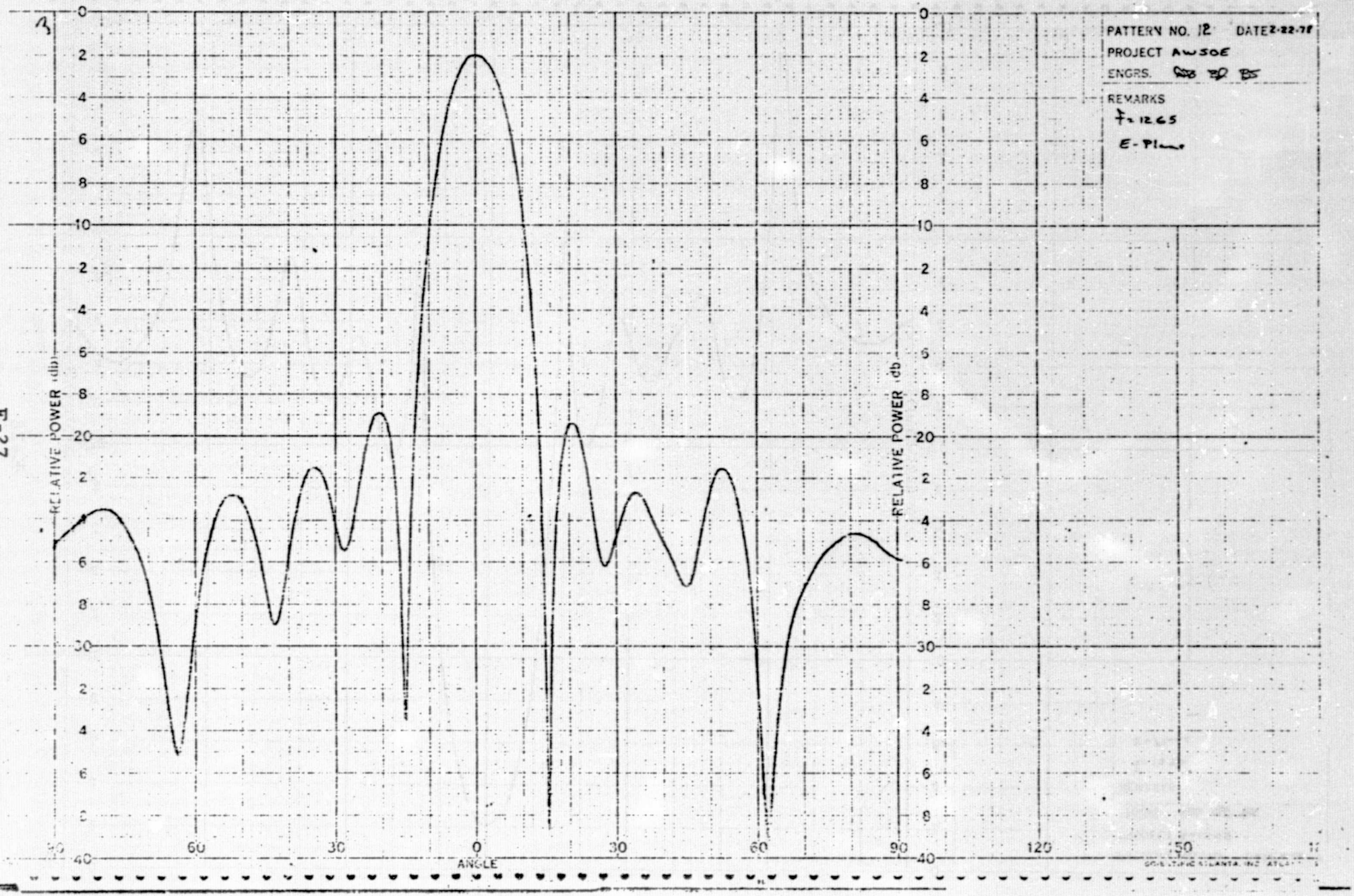
PATTERN NO. 12 DATE 2-22-78
PROJECT AW50E
ENGRS. BS BD BS
REMARKS
f = 1265
E-Plane
RELATIVE POWER (db)
RELATIVE POWER db
ANGLE
0
2
4
6
8
10
20
30
40
60
30
0
30
60
90
120
150

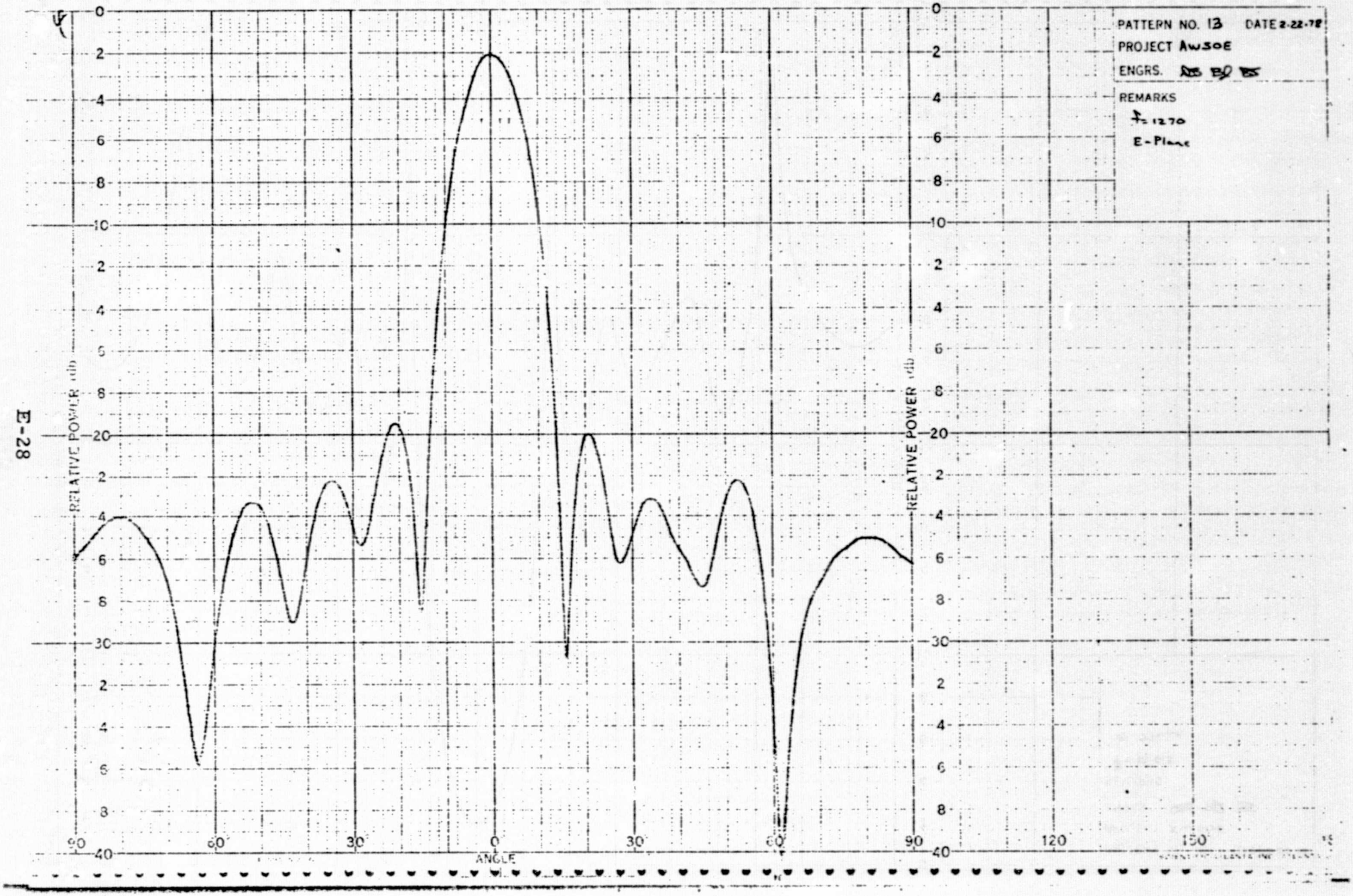
PATTERN NO. 13 DATE 2-22-78
PROJECT AWSOE
ENGRS.
REMARKS
f = 1270
E-Plane
RELATIVE POWER db
ANGLE
-90 -60 -30 0 30 60 90 120 150

PATTERN NO. 14

L-Band Planar Array

f = 1275

E-Plane

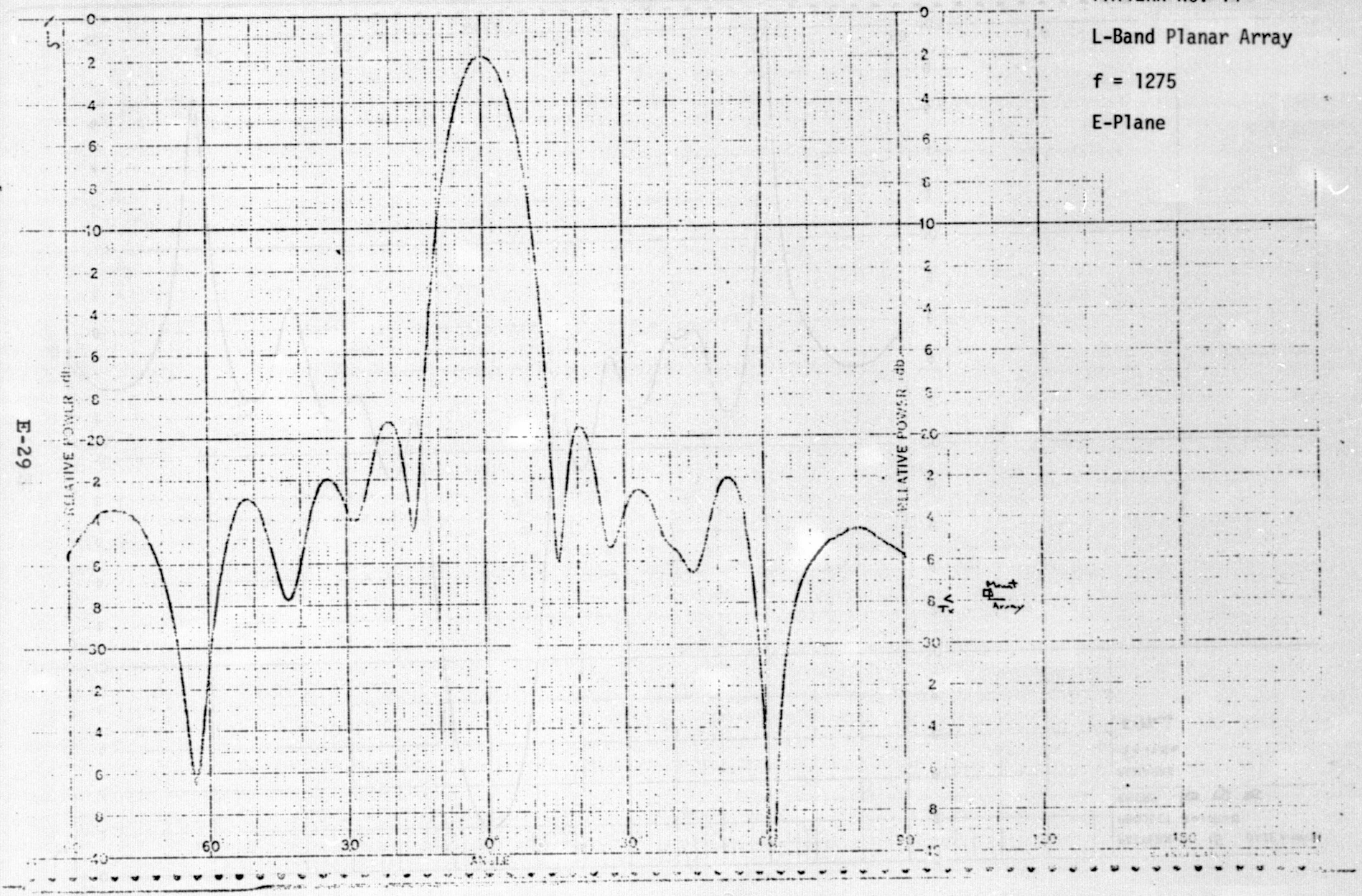


PATTERN NO. 15 DATE 2-28-79
PROJECT AWSOE
ENGRS. AS BJ BS
REMARKS
f = 1280
E-Plane
RELATIVE POWER (db)
ANGLE
0
2
4
6
8
10
20
30
40
60
30
0
30
60
90
120
150

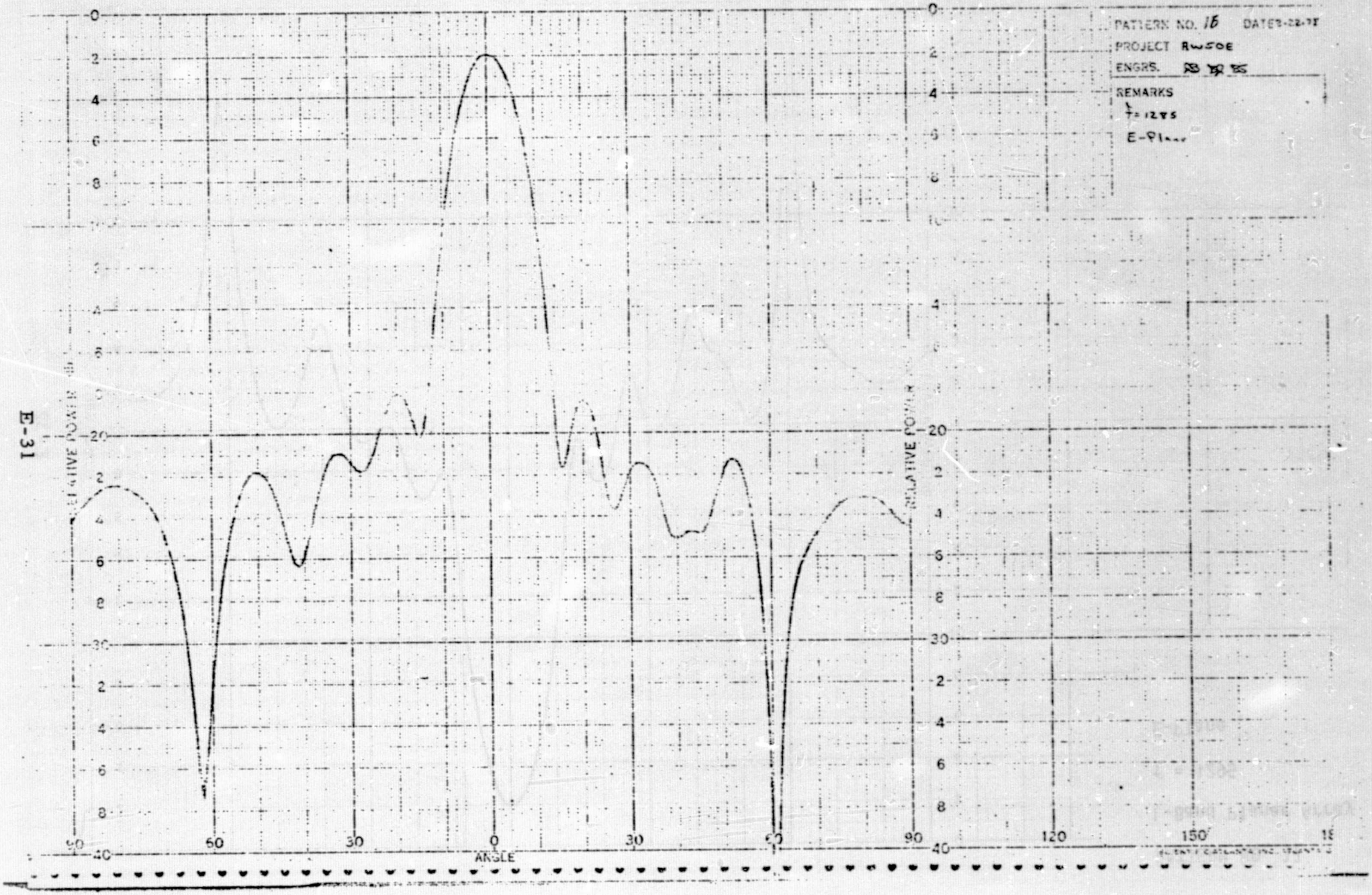
PATTERN NO. 16
PROJECT RW50E
REMARKS
f=1285
E-Plane
RELATIVE POWER
ANGLE
90
60
30
0
30
60
90
120
150

PATTERN NO. 17

L-Band Planar Array

f = 1295

E-Plane

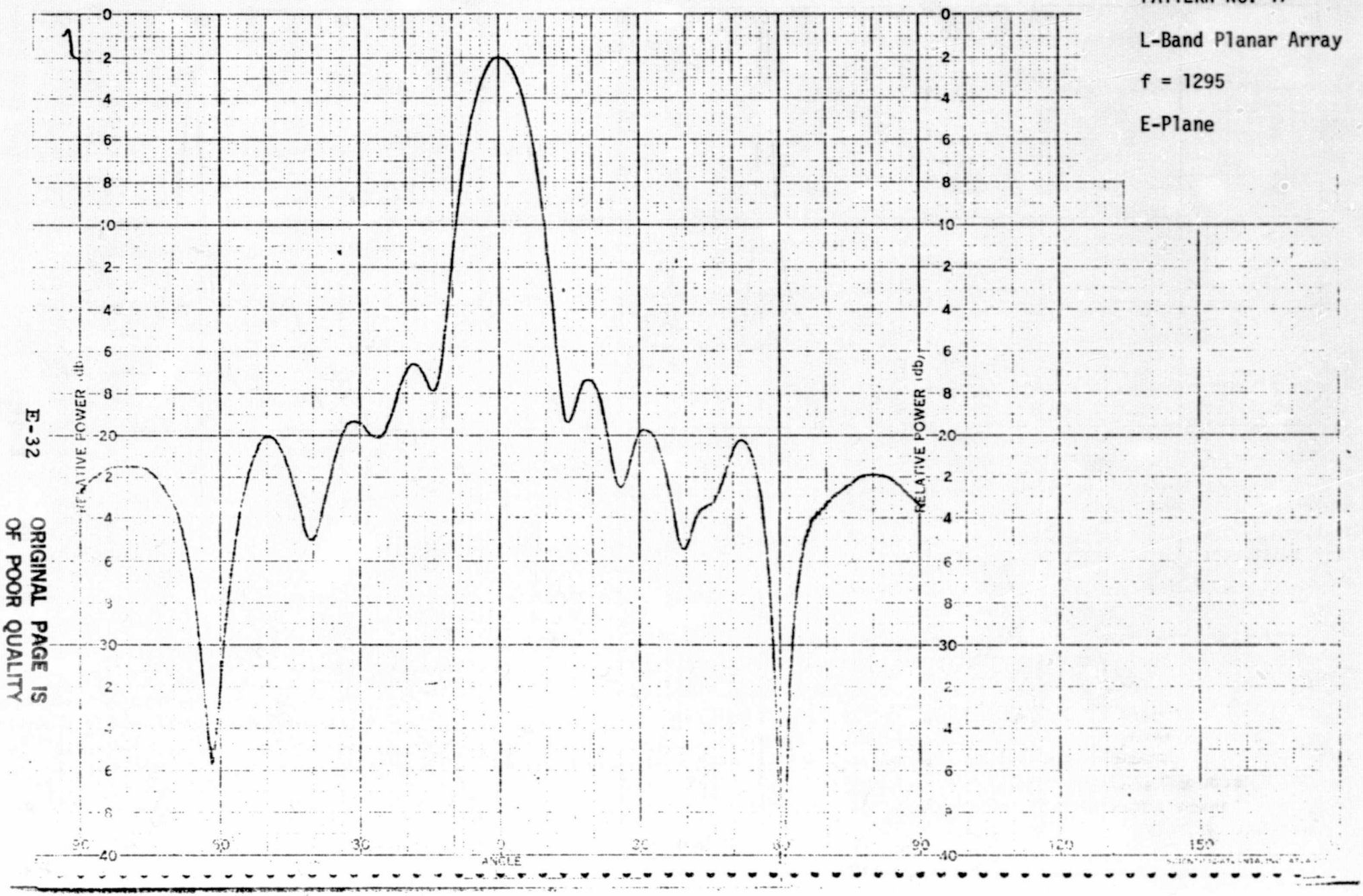

E-32

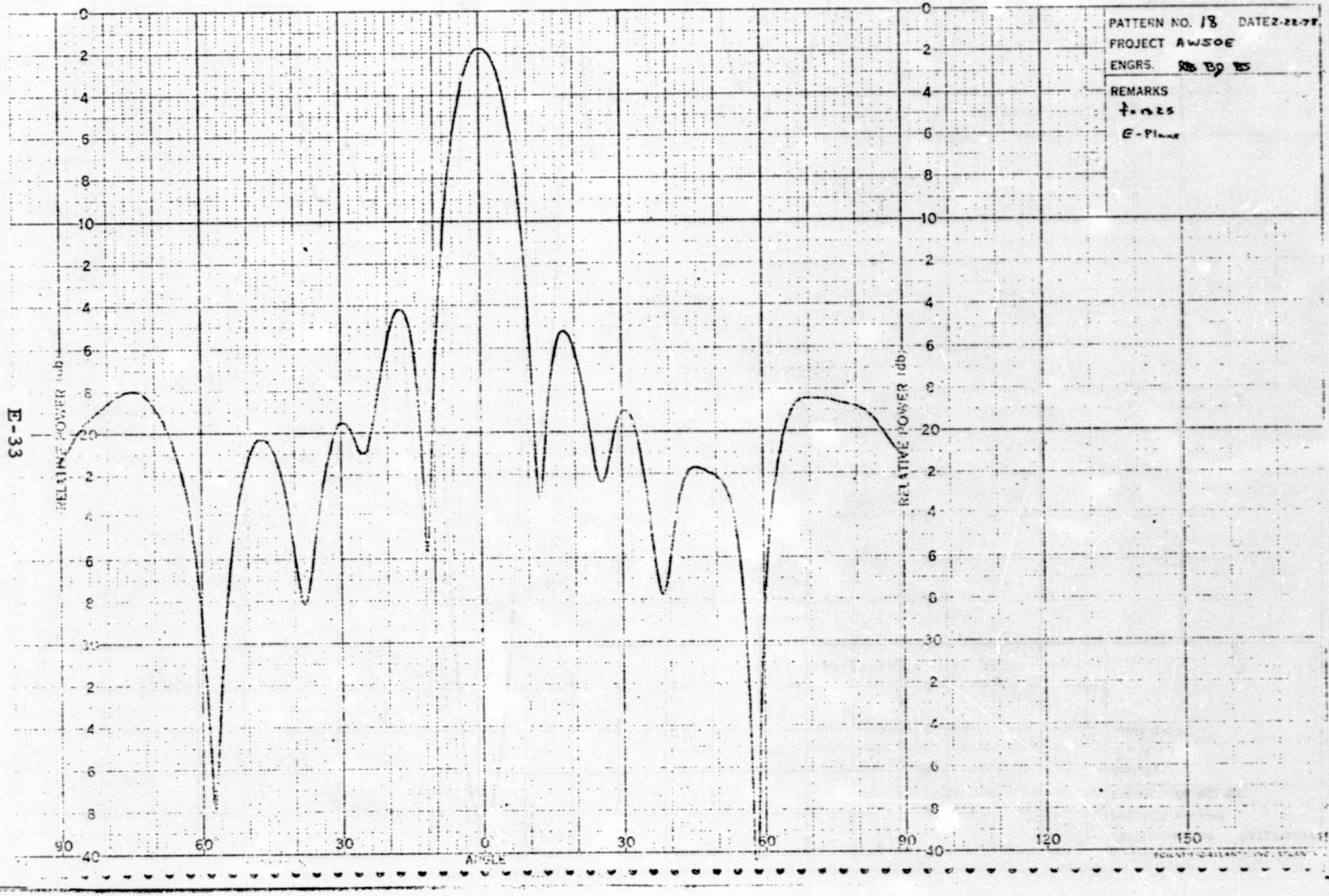
PATTERN NO. 18 DATE 2-22-78
PROJECT AWSOE
ENGRS. BB BJ BS
REMARKS
f=425
E-Plane
RELATIVE POWER (db)
0
2
4
5
8
10
20
30
40
90
60
30
0
30
60
90
120
150
ANGLE

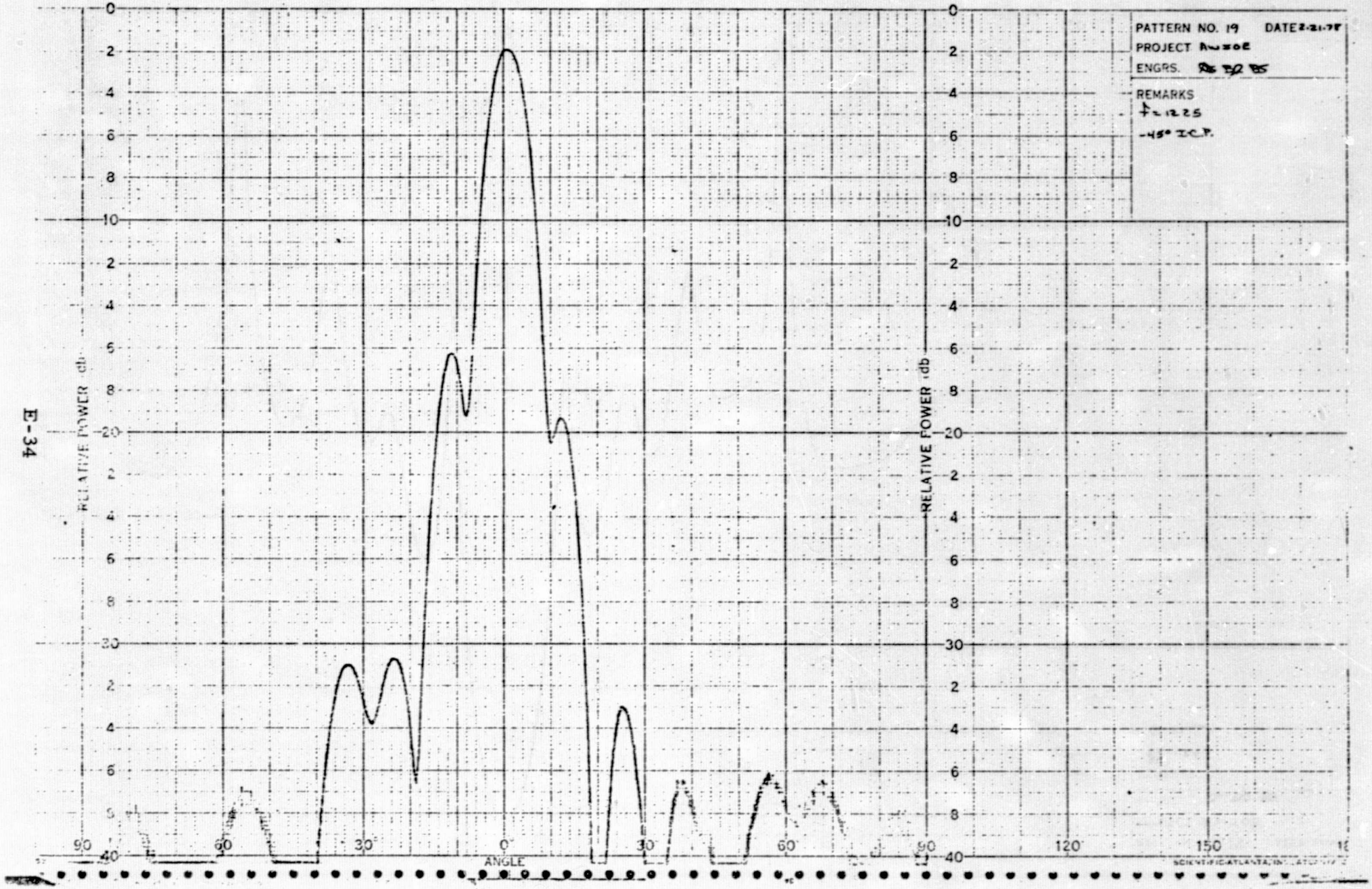
PATTERN NO. 19 DATE 2-21-75
PROJECT AWACS
ENGRS. RS BD BS
REMARKS
f = 1225
-45° ICP.
RELATIVE POWER db
ANGLE
0
2
4
6
8
10
20
30
40
90
60
30
0
30
60
90
120
150

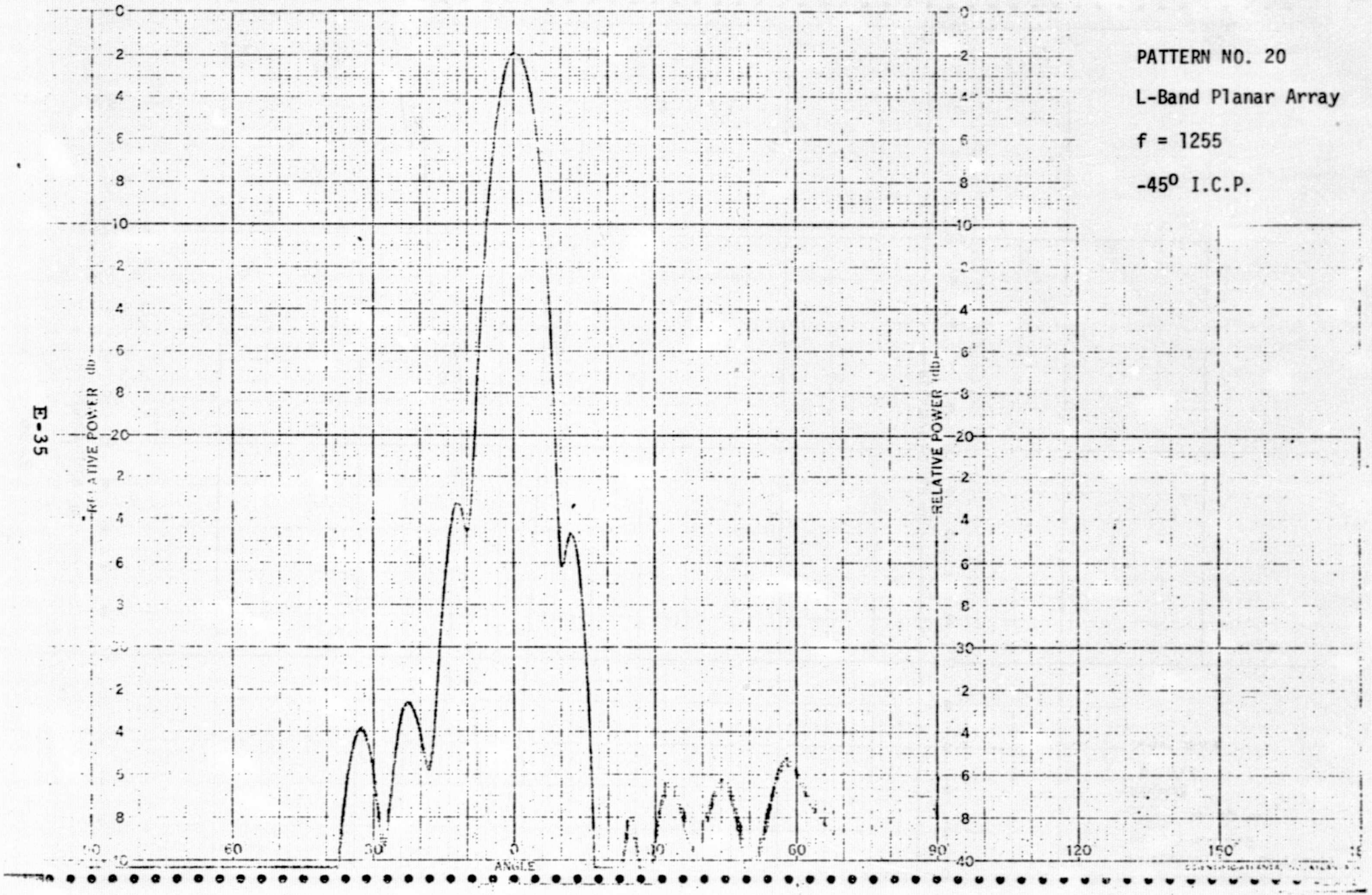
PATTERN NO. 20
L-Band Planar Array
f = 1255
-45° I.C.P.
RELATIVE POWER (db)
ANGLE

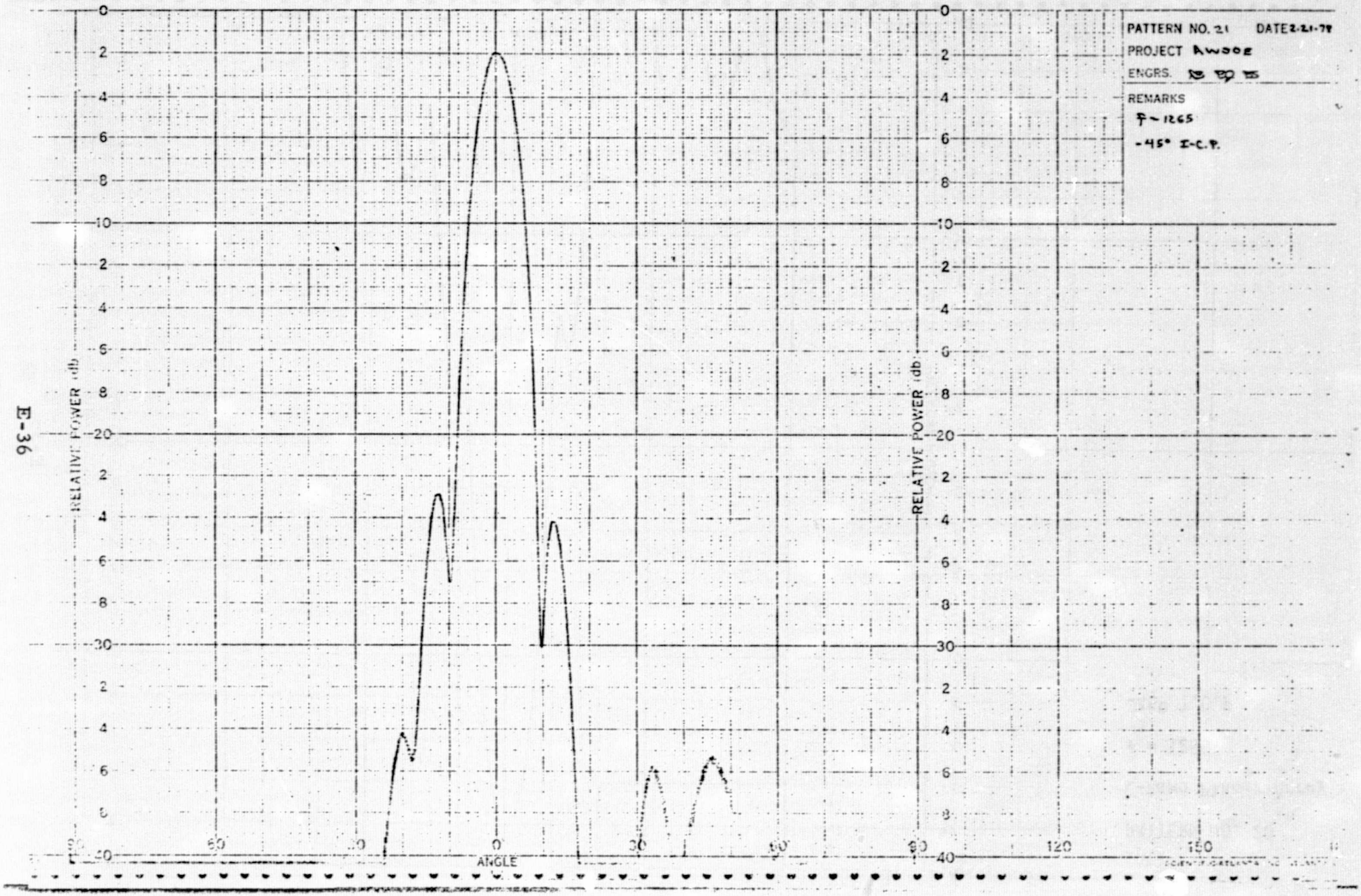
PATTERN NO. 21 DATE 2-21-79
PROJECT AWODE
ENGRS.
REMARKS
f ~ 1265
-45° I-C.P.
RELATIVE POWER (db)
ANGLE
0
2
4
6
8
10
20
30
40
60
90
120
150

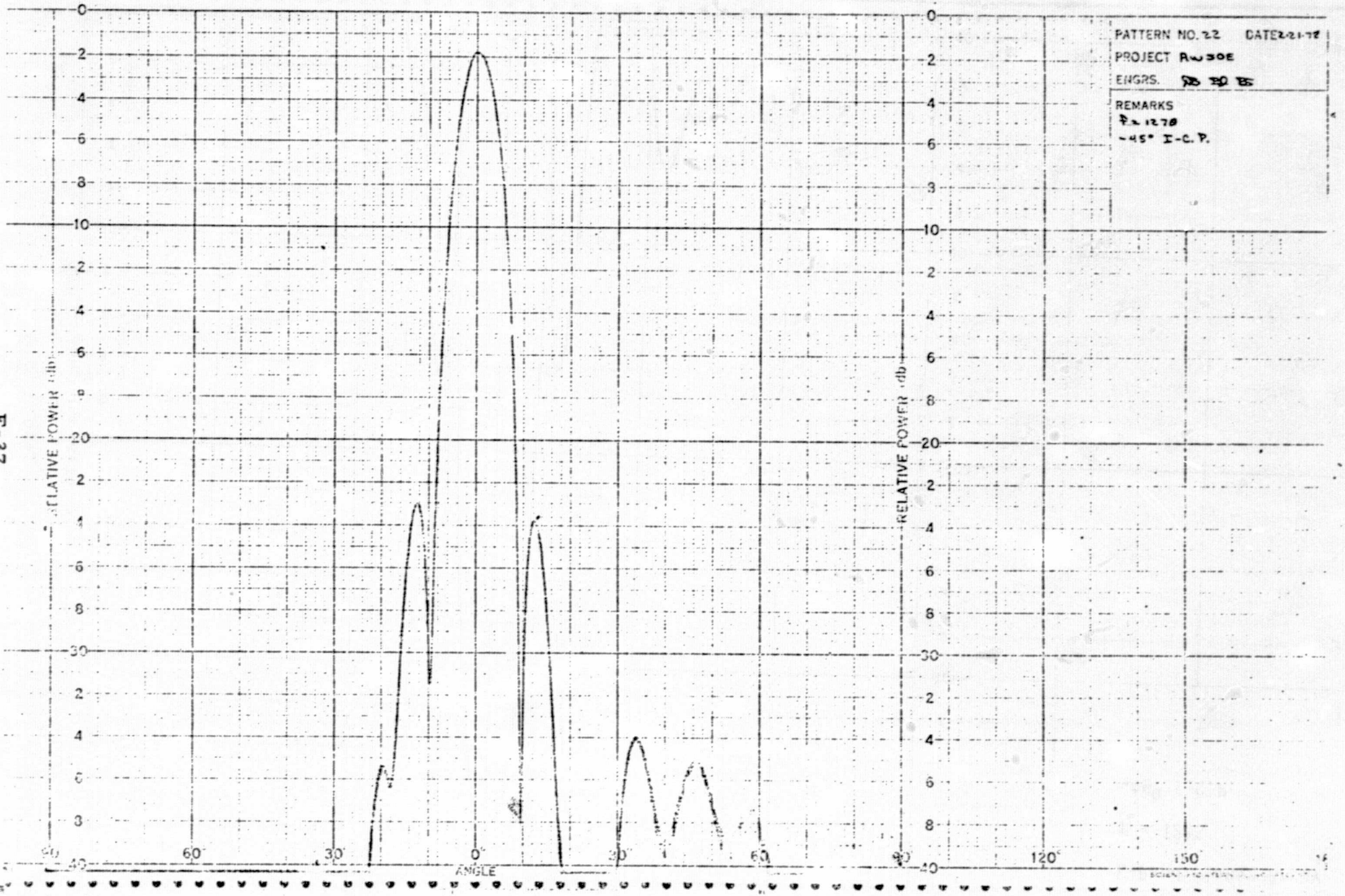
PATTERN NO. 22 DATE 2-21-78
PROJECT RW30E
ENGRS.
REMARKS
F = 1270
-45° I-C.P.
RELATIVE POWER db
ANGLE
0
2
4
6
8
10
20
30
40
60
30
0
30
60
90
120
150

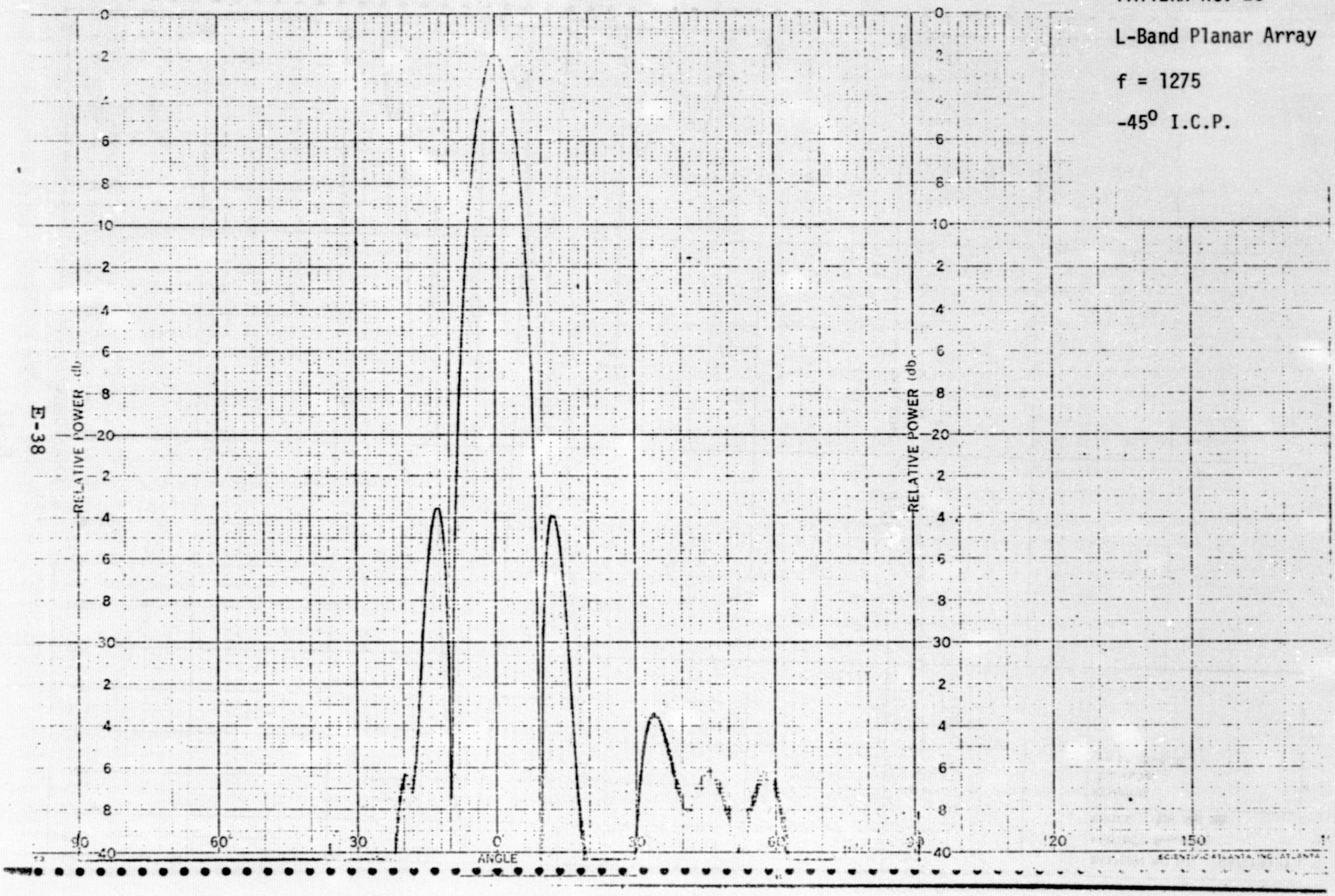
PATTERN NO. 23
L-Band Planar Array
f = 1275
-45° I.C.P.
RELATIVE POWER (db)
ANGLE
90
60
30
0
30
60
90
120
150
0
2
4
6
8
10
20
30
40

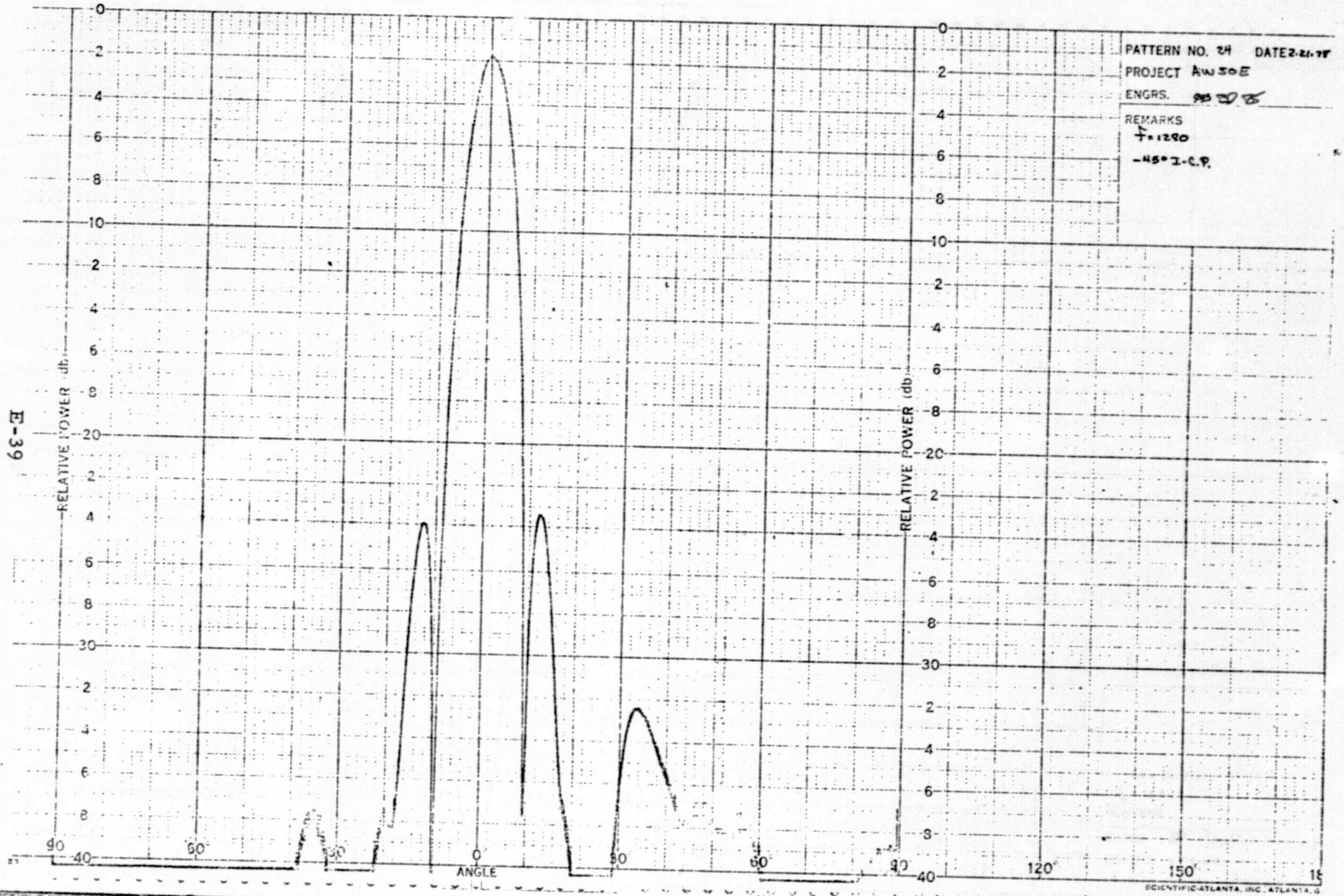
PATTERN NO. 24 DATE 2-21-78
PROJECT AWACS E
ENGRS.
REMARKS
f = 1290
-45° I-C.P.
RELATIVE POWER (db)
0
2
4
6
8
10
20
30
40
90°
60°
30°
0°
ANGLE
30°
60°
90°
120°
150°
SCIENTIFIC-ATLANTA, INC., ATLANTA, G

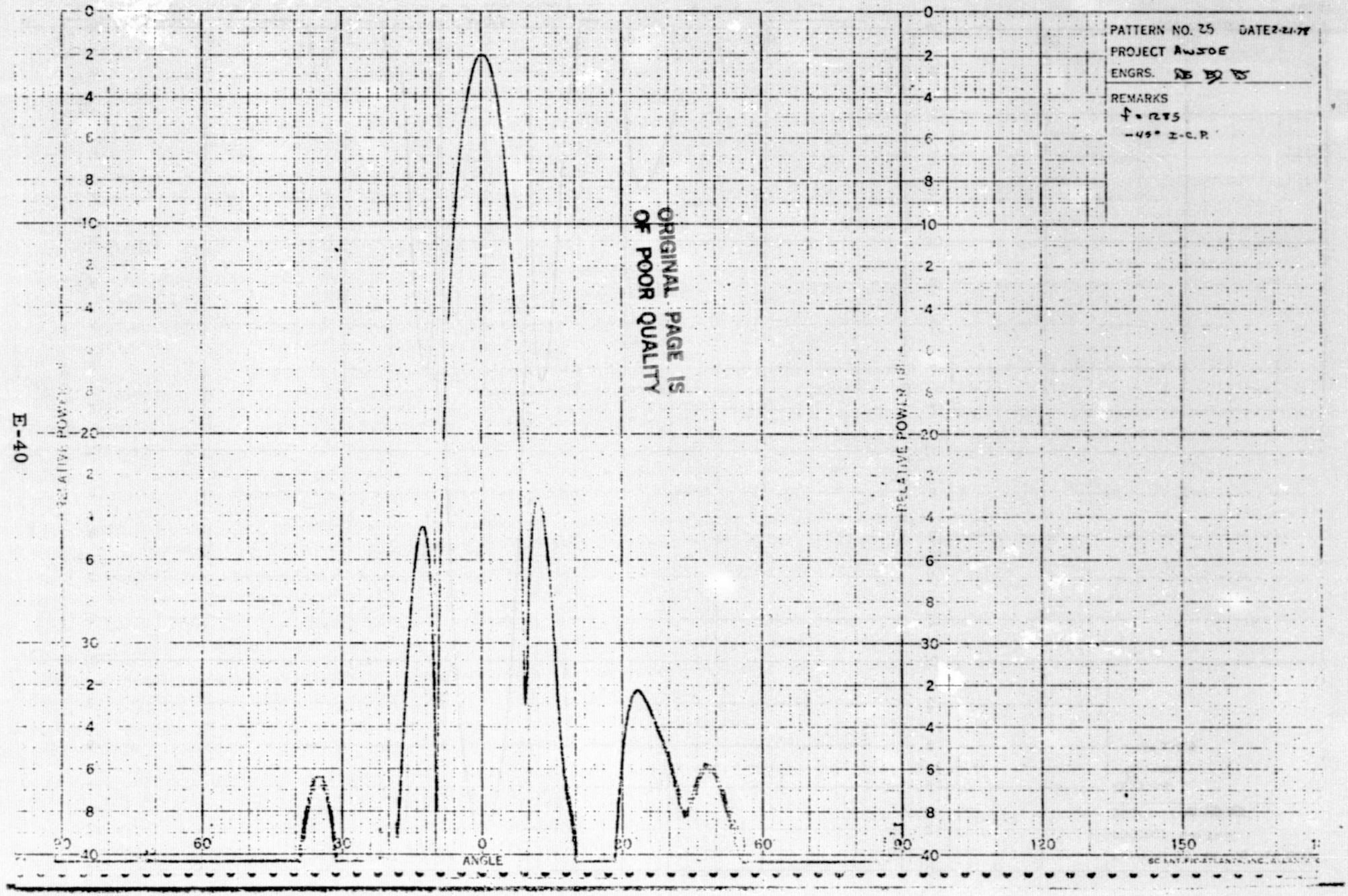

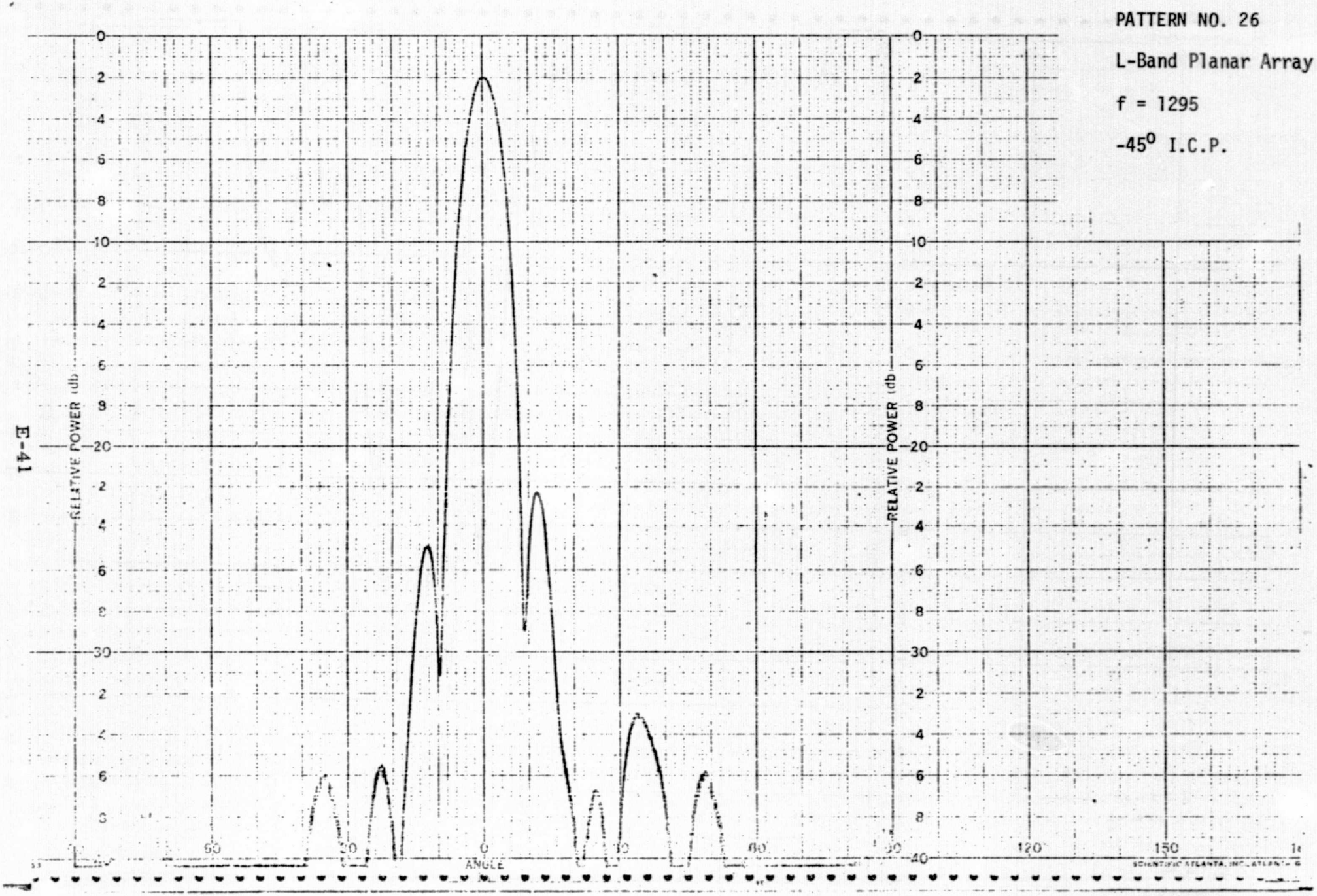
PATTERN NO. 26
L-Band Planar Array
f = 1295
-45° I.C.P.
RELATIVE POWER (db)
RELATIVE POWER (db)
ANGLE
SCIENTIFIC ATLANTA, INC., ATLANTA, G

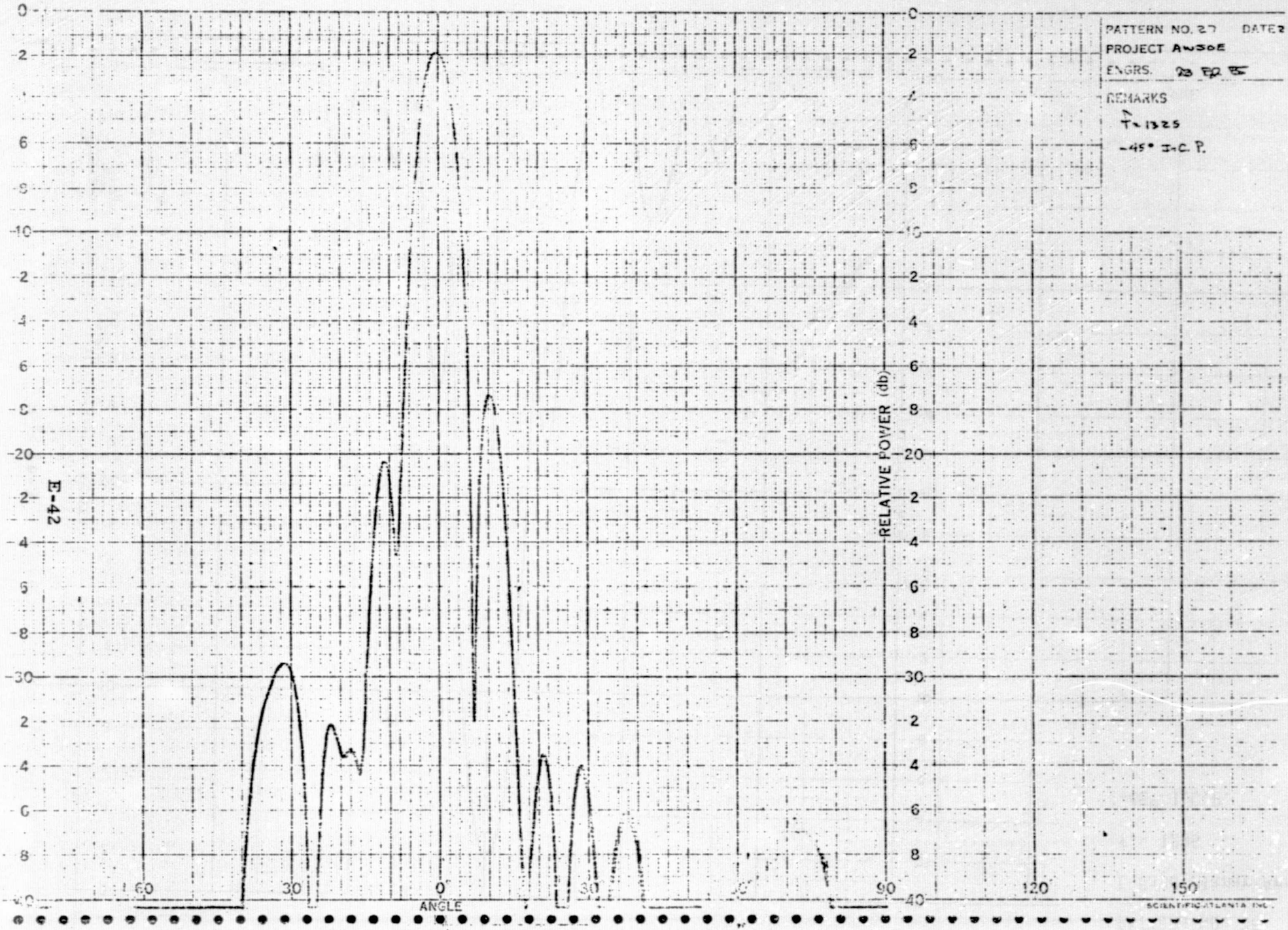
PATTERN NO. 27 DATE?
PROJECT AN/SOE
ENGRS. RB EP BS
REMARKS
F=1325
-45° I.C.P.
E-42
RELATIVE POWER (db)
ANGLE
60
30
0
30
90
120
150
SCIENTIFIC-ATLANTA INC.


PATTERN NO. 28 DATE 2-21
PROJECT AWSOE
ENGRS. RB BJ BS
REMARKS
f = 1225
+45° E.C.P.
RELATIVE POWER (db)
0
2
4
6
8
10
2
4
6
8
20
2
4
6
8
30
2
4
6
8
10
ANGLE
90°
60°
30°
0
30°
60°
90°
120°
150°
E-43
SCIENTIFIC-ATLANTA, INC., ATLA

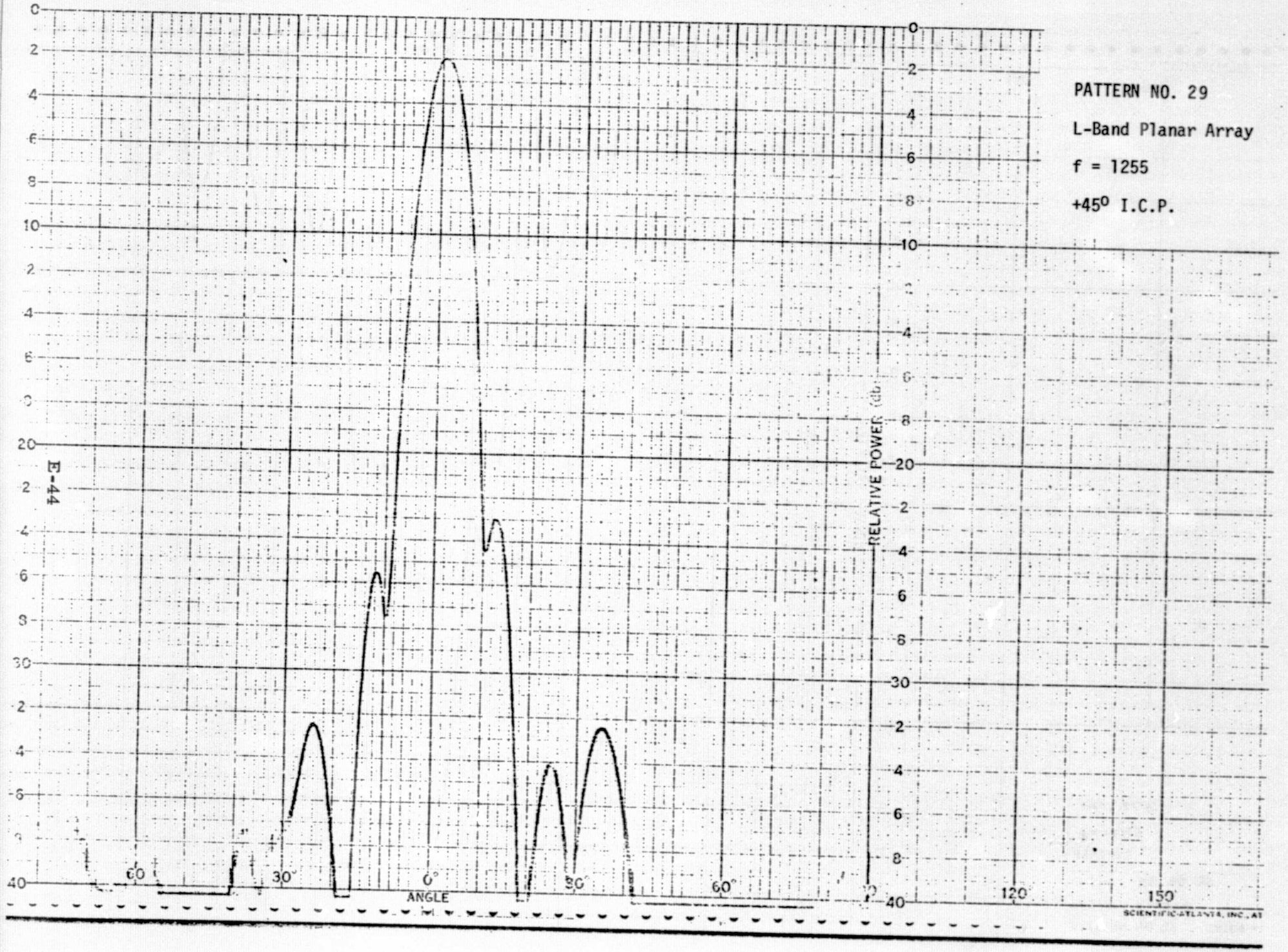
PATTERN NO. 29
L-Band Planar Array
f = 1255
+45° I.C.P.
E-44
RELATIVE POWER (db)
ANGLE
60°
30°
0°
30°
60°
120
150
SCIENTIFIC-ATLANTA, INC., AT

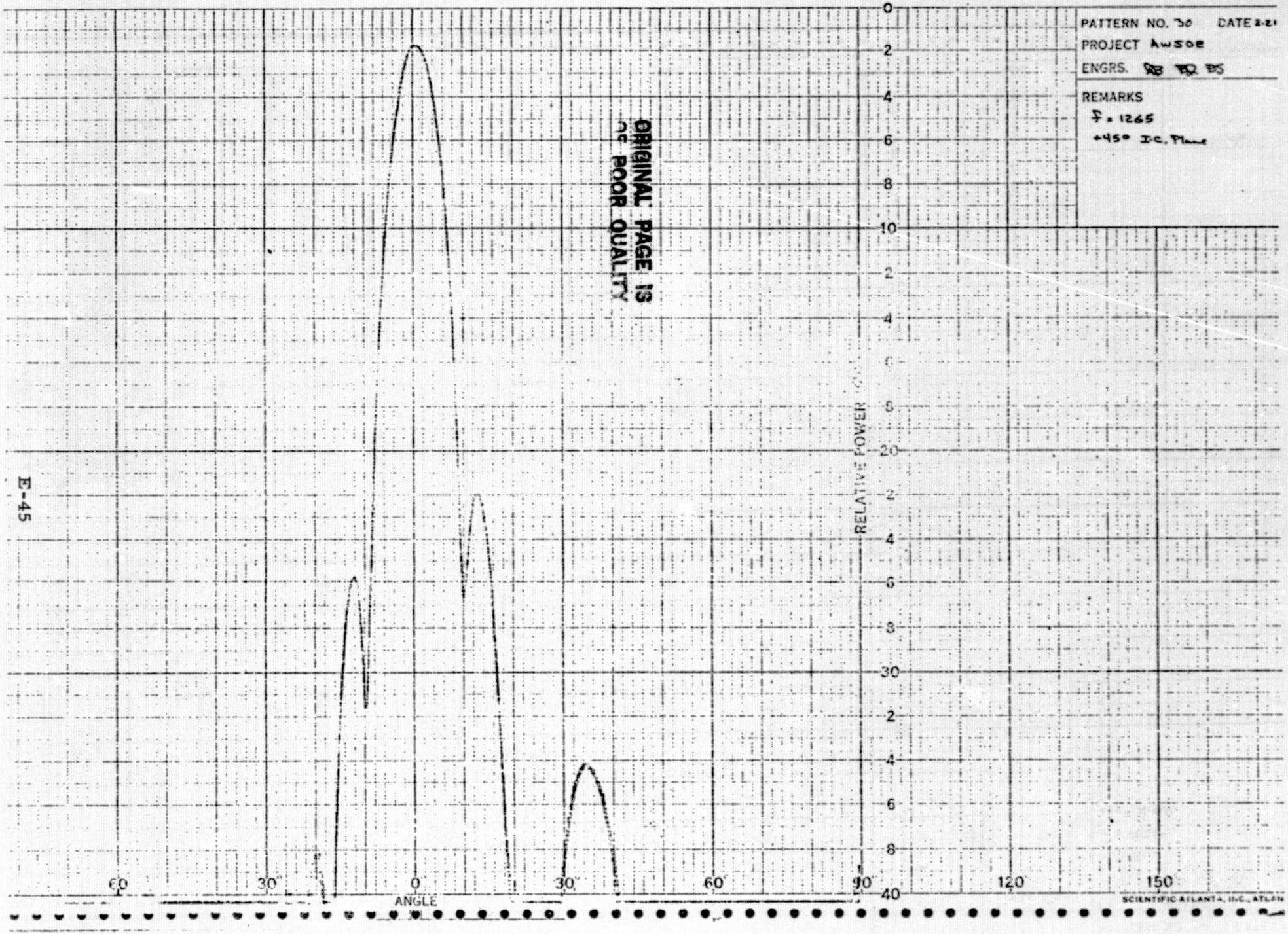
PATTERN NO. 30 DATE 2-21
PROJECT AWSOE
ENGRS.
REMARKS
f = 1265
+45° E-C. Plane
ORIGINAL PAGE IS
OF POOR QUALITY
RELATIVE POWER
0
2
4
6
8
10
2
4
6
8
20
2
4
6
8
30
2
4
6
8
40
60
30
0
30
60
90
120
150
ANGLE
SCIENTIFIC ATLANTA, INC., ATLAN

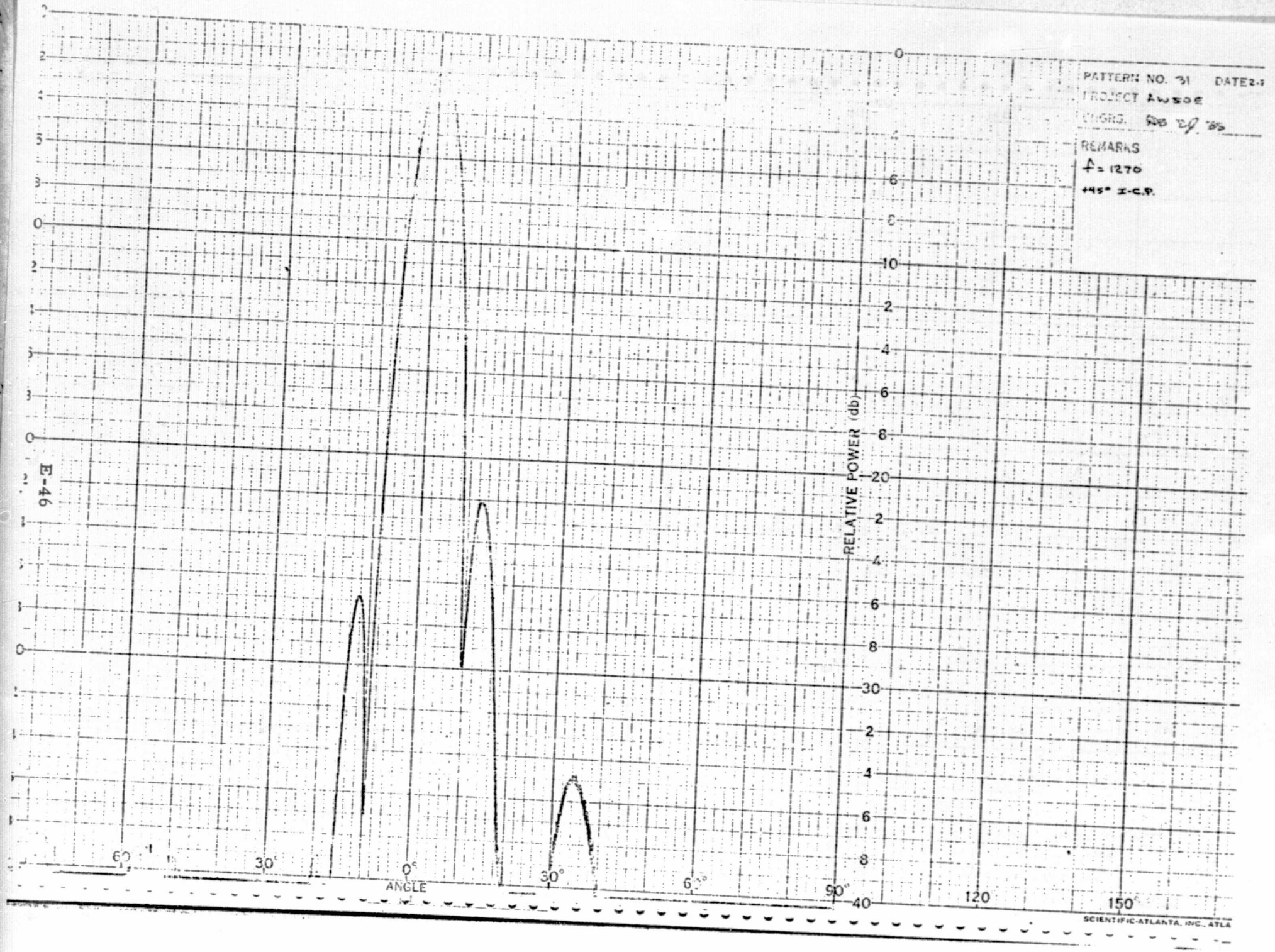
PATTERN NO. 31 DATE 2-1
PROJECT Ansoe
ENGRG. RB 29 '85
REMARKS
f = 1270
+45° I-C.P.
RELATIVE POWER (db)
0
6
10
2
4
6
8
20
2
4
6
8
30
2
4
6
8
40
60°
30°
0°
30°
60°
90°
120
150°
ANGLE
E-46
SCIENTIFIC-ATLANTA, INC., ATLA

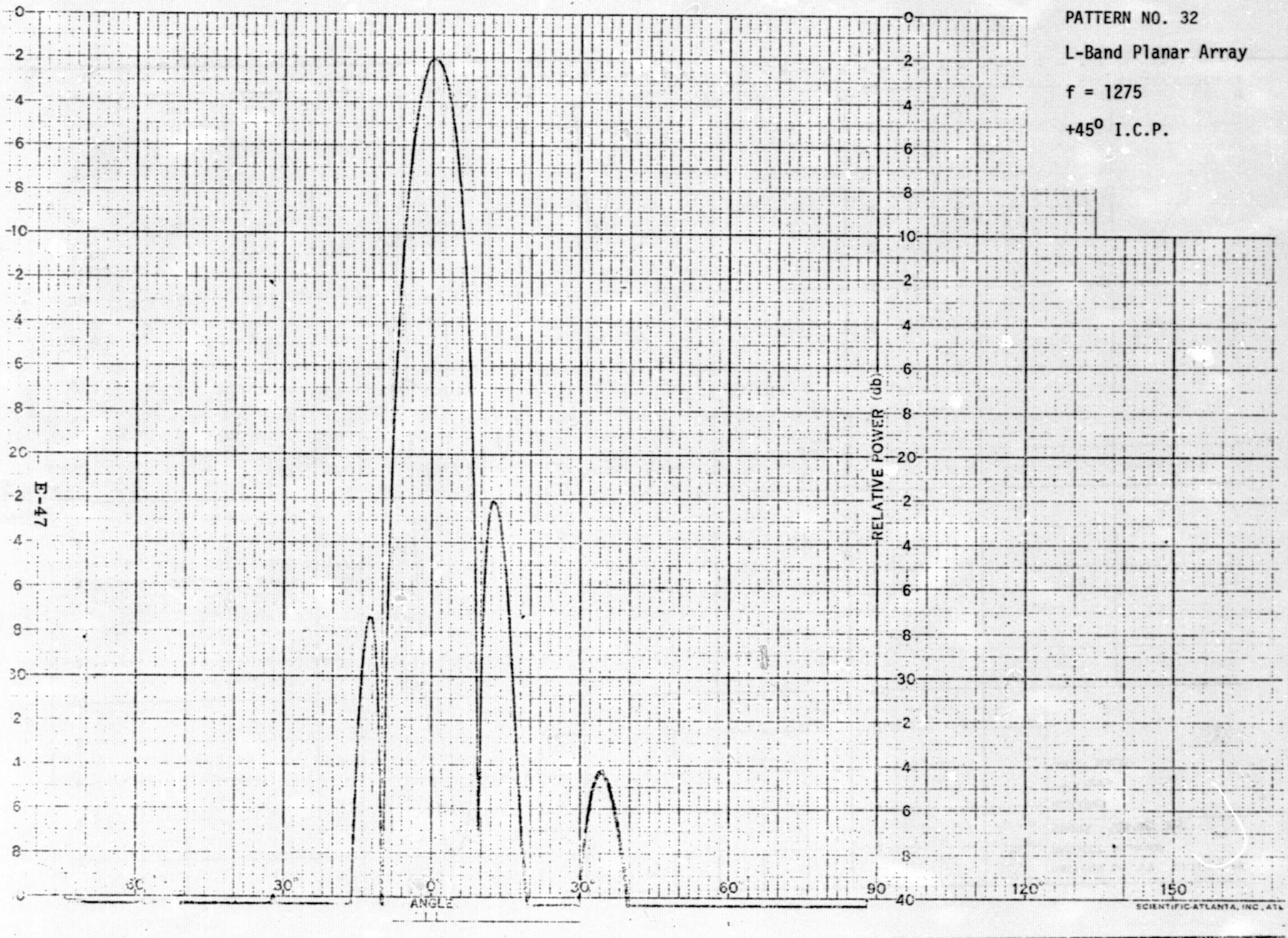
PATTERN NO. 32
L-Band Planar Array
f = 1275
+45° I.C.P.
RELATIVE POWER (db)
ANGLE
E-47
SCIENTIFIC-ATLANTA, INC., ATL

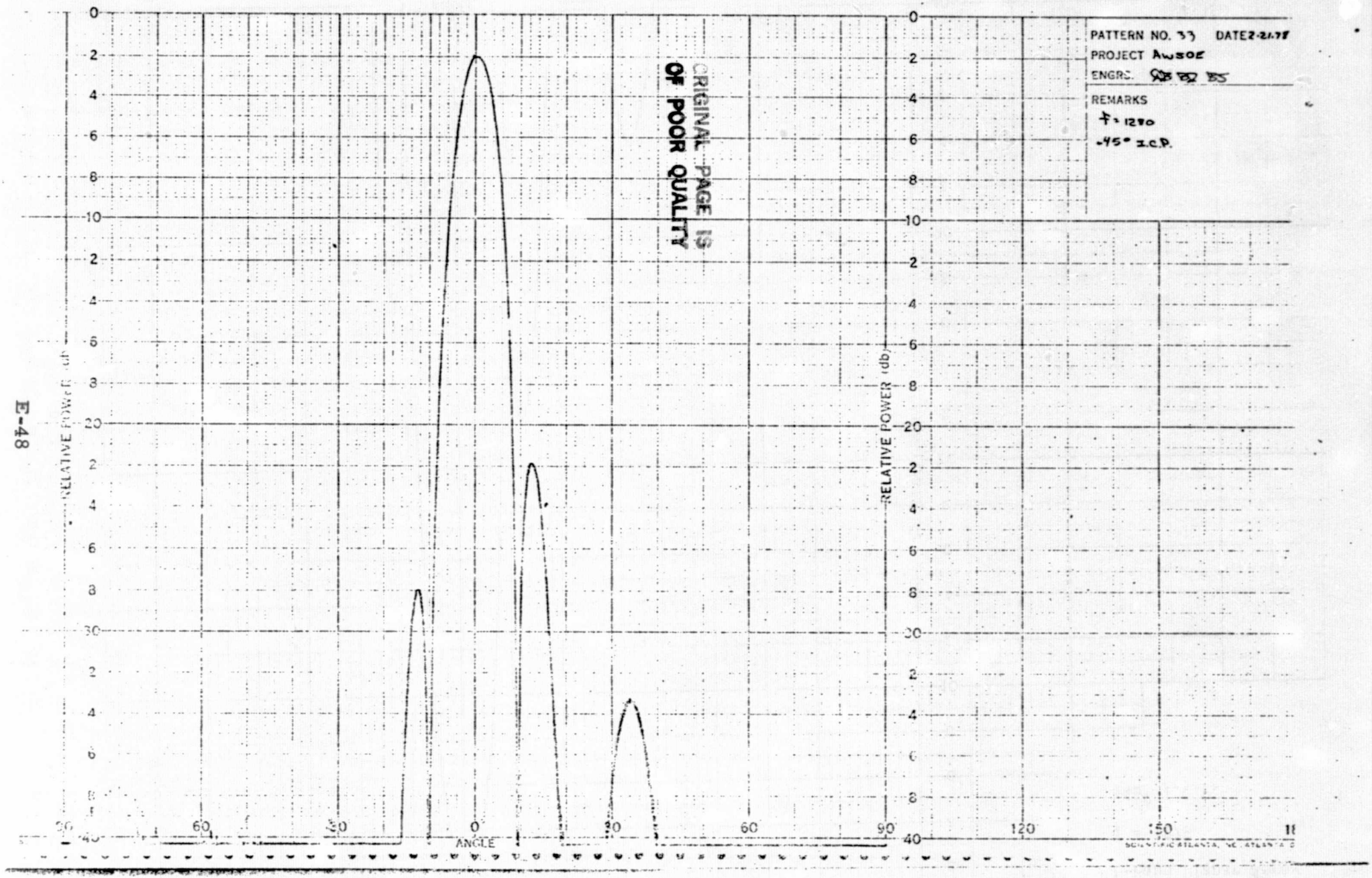

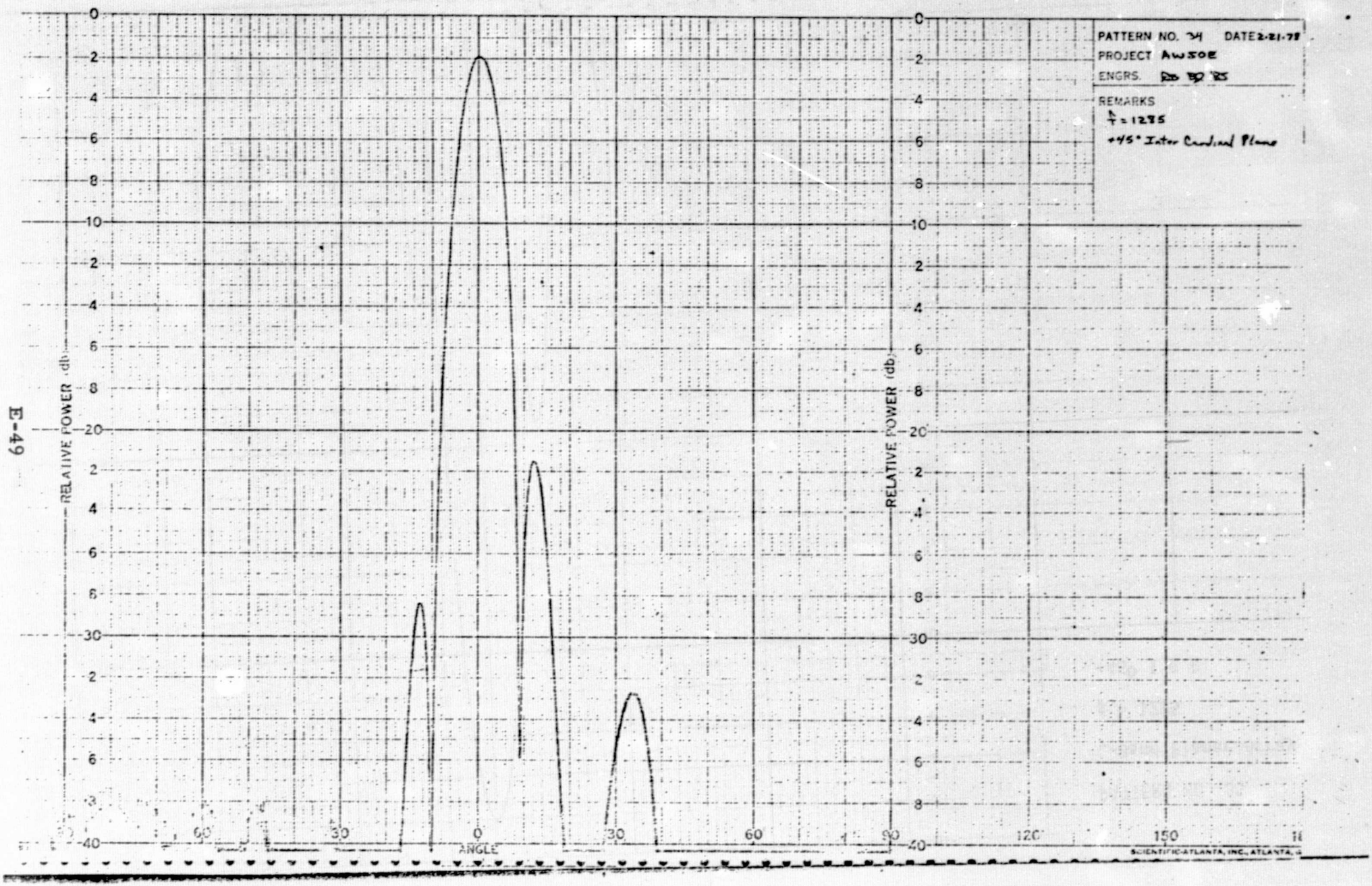
PATTERN NO. 34 DATE 2-21-78
PROJECT AWSOE
ENGRS. RD BD BS
REMARKS
f = 1285
+45° Inter Cardinal Plane
RELATIVE POWER (db)
0
2
4
6
8
10
20
30
40
60
30
0
30
60
90
120
150
ANGLE
SCIENTIFIC-ATLANTA, INC., ATLANTA, G

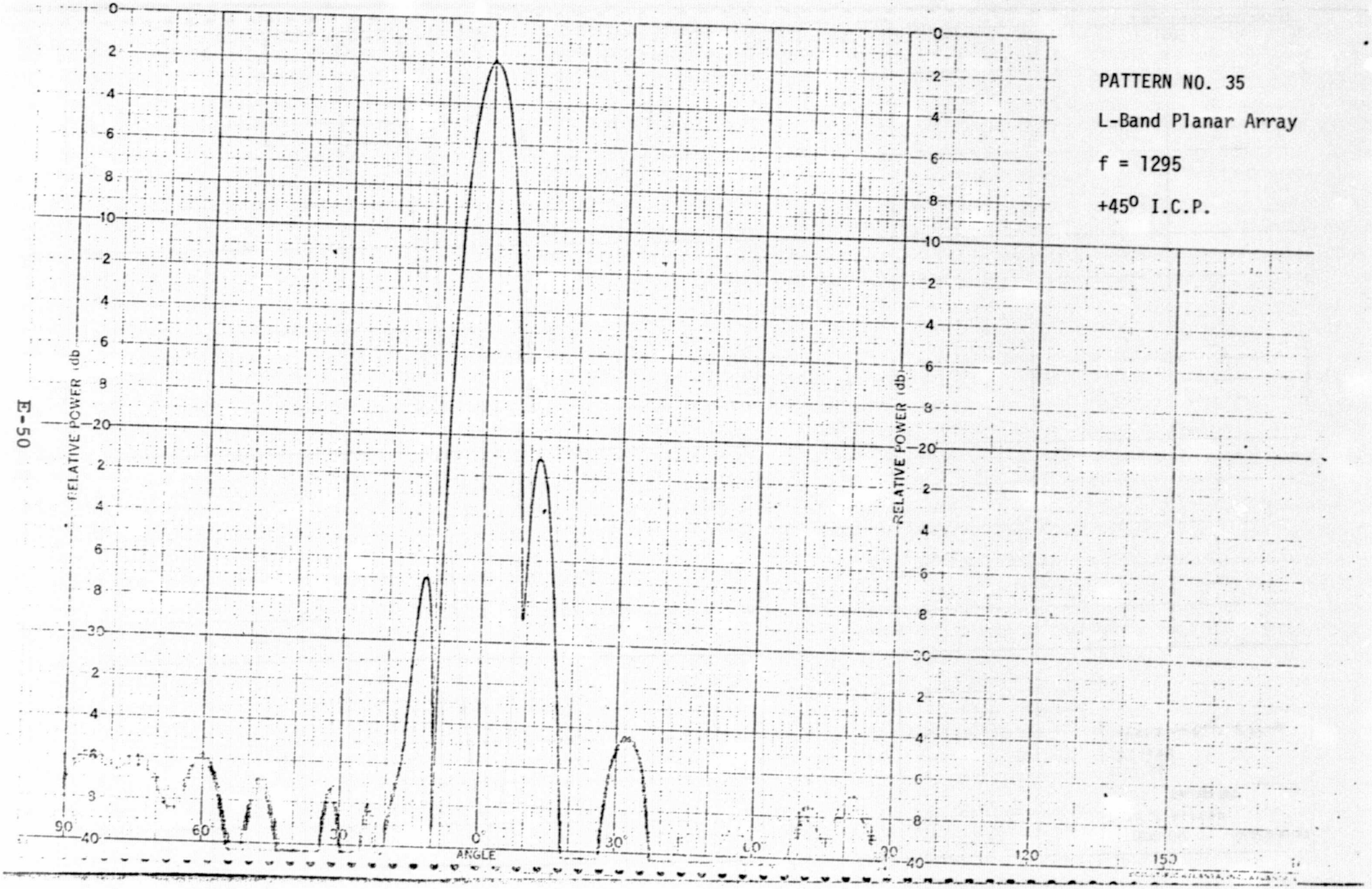
PATTERN NO. 35
L-Band Planar Array
f = 1295
+45° I.C.P.
RELATIVE POWER (db)
ANGLE
90
60
30
0°
30°
60
90
120
150

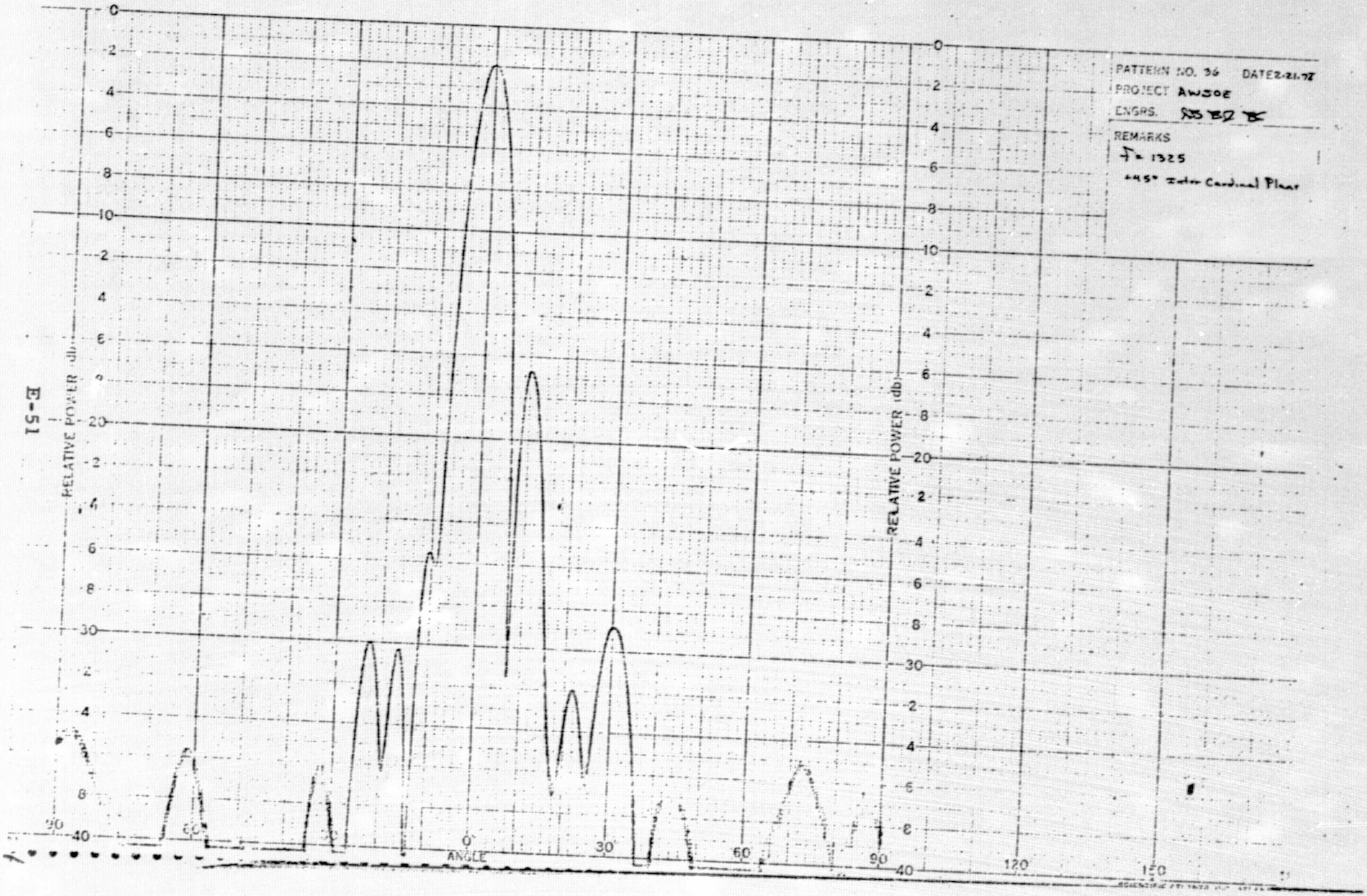
PATTERN NO. 36 DATE 2-21-72
PROJECT AWSOE
ENGRS.
REMARKS
f = 1325
+45° Inter Cardinal Plane
RELATIVE POWER (db)
ANGLE
0
30
60
90
120
150

APPENDIX F
MULTIPACTOR AND IONIZATION BREAKDOWN

APPENDIX F
MULTIPACTOR AND IONIZATION BREAKDOWN

F.1 MULTIPACTOR BREAKDOWN

In a space environment, or more specifically in an atmosphere where the mean free path is on the order of the electrode separation, multipactor breakdown is a possibility. Qualitatively, the necessary conditions for breakdown may be characterized as a resonance between the harmonic field and the electron transit time across the electrode separation. Multipacting will, for the general electrode configuration, occur within a bounded range of voltages for given frequency and separation. The electron transit time is related both to the field intensity (i. e. , the acceleration force) and the electrode separation. Because voltage distribution over the length of a radiating or coupling slot is sinusoidal there is no lower bound on the field intensity for multipacting. Our concern is then to determine the maximum allowable field intensity before breakdown.

Calculations show that, for the 6 kW maximum total power level anticipated, the associated voltages at the coupling slots correspond to a safe operating condition. The details of the computations follow.

The feed coupling slots will have the highest point-to-point field intensities. For a total power of 6 kW, each coupling slot will handle one eighth of this power; however, as a conservative worst case condition it was assumed that the power transmitted by each feed slot was 1 kW. The following expression given by Lewis[1] was then used to compute the peak slot voltage in the slot.

$$V_o = \frac{\pi \left[1-\left(\frac{\ell}{a}\right)^2\right]}{\ell \cos \frac{\pi \ell}{2a}} \cdot (a\, b\, Z_{TE10}\, p)^{1/2}$$

Evaluation for the case where

a = the waveguide width = 0.770 inch
b = the waveguide height = 0.200 inch
ℓ = the slot length = 0.834 inch
f = the frequency = 9.7 GHz

gives

$V_o = 49.2 \times p^{1/2}$ = 1550 volts (for p = 1 kW)

Figure F-1 from Reference 2 depicts the multipactor breakdown existence regions for the case of parallel plate electrodes. That reference indicates that for the case of a thin-walled slot, the breakdown voltage is substantially higher than that predicted for parallel plates of separation equal to the planned slot width.* At a frequency of 9.7 GHz and a corresponding plate separation or slot width of 0.236 cm (0.093 inch) the breakdown voltage is approximately 1500 volts. This operating point is plotted approximately on the graph of Figure F-1. It is evident that, at worst, an order of magnitude higher voltage will be required to cause multipacting. In the case of a slot of the same width in a thin walled waveguide, the breakdown voltage will be substantially increased. The conclusion is that the safety factor against multipactor breakdown is substantial at the prescribed total power of 6 kW. Thus, no breakdown problems are anticipated for a normal space environment.

*At 9.3 GHz and with a slot width of 0.0625 inch in a 0.020 inch thick wall, no breakdown was observed for voltages as high as 52 kV. The parallel plate theory predicted a threshold voltage of of 1 kV.

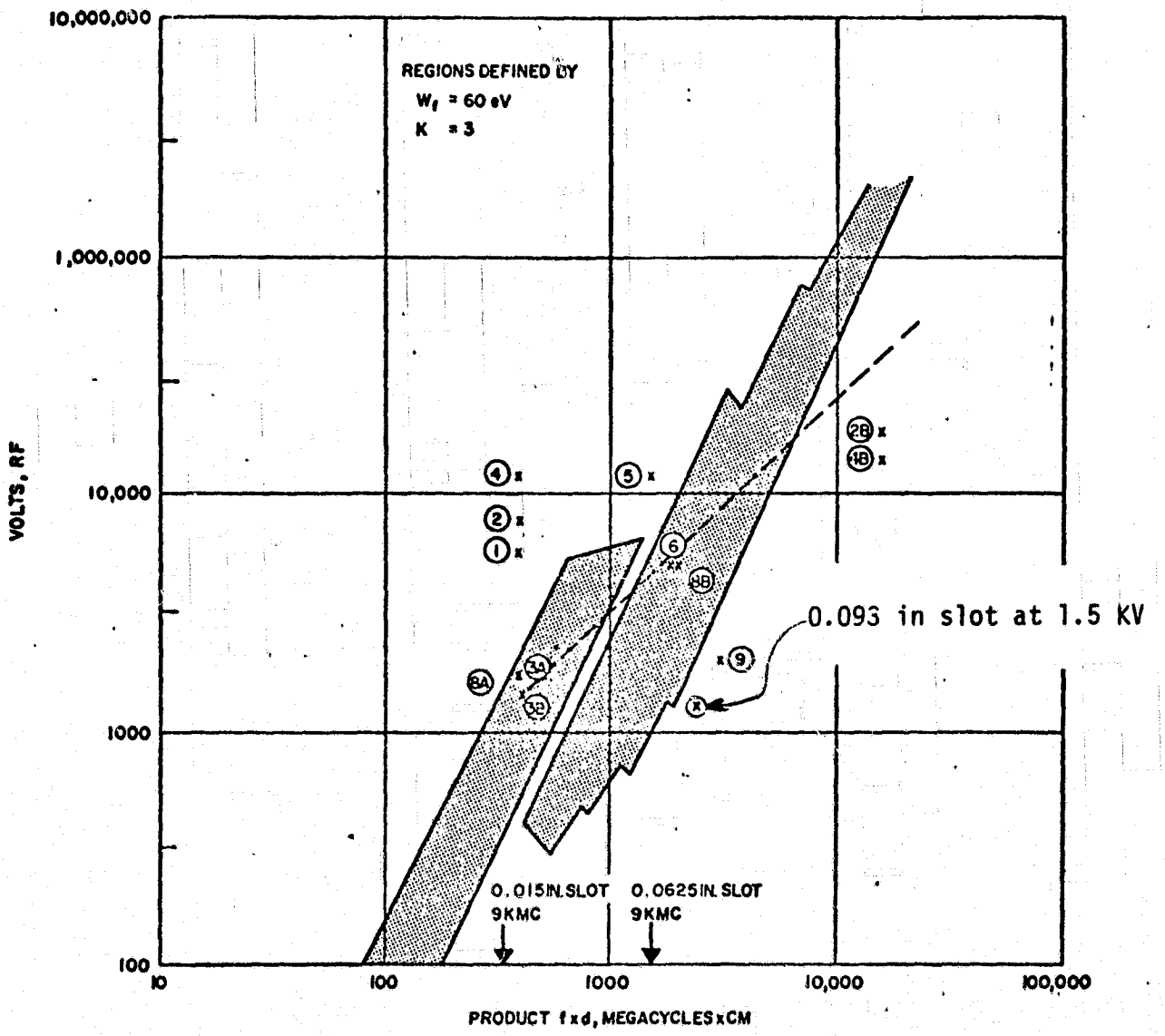

Figure F-1. Multipacting existence regions.

F.2 IONIZATION BREAKDOWN

During the design review, the potential problem of ionization RF breakdown in the X-Band array was discussed. It was speculated that breakdown due to ionization might occur due to the possible existence of a thin but discernible localized "atmosphere" in the shuttle bay. Such a local atmosphere conceivably could arise from outgassing of components in the

bay and also from gases trapped in the bay before launch. Because of the lack of data as to the pressure and nature of such an atmosphere, it is not possible to arrive at a definite conclusion about such breakdown. However, estimates were made of ionization breakdown power in the array at specified pressure levels.

For this breakdown mechanism the feed coupling slot is again the critical element in the system. The available data and techniques on ionization cannot be directly applied to the slot geometry, but as an approximation, the slot may be treated as a waveguide of height and width corresponding to the slot width and length. The slot field is approximated by the TE_{10} field in the equivalent waveguide. From the theory and results for ionization in rectangular waveguide operating in the dominant mode (Reference 3), we obtain the graphs of Figures F-2 and F-3. The plot is of threshold power in kilowatts versus pressure in millimeters of mercury, at a temperature of $20^{\circ}C$. The results indicate ionization breakdown levels within the slots of 3 kW at 58,000 feet and 1 kW at 72,000 feet. The worst case conditions correspond to a pressure of 10 mm Hg. Breakdown at this level is predicted at a power of 0.45 kW.

It should be emphasized that this data is obtained using the procedure developed for waveguides. In the case of the slot, the expected additional equivalent losses caused by diffusion of the ionized electron density suggests that the performance of the slot should be better than predicted by the waveguide approximation.

From the foregoing it is clear that an adequate margin of safety in ionization breakdown levels exists at pressure altitudes of up to 72,000 feet. As the pressure decreases beyond this point, the slots become vulnerable to breakdown at the assumed operating power level. However, it is anticipated that the actual pressure in the array in orbit will be very much less than the lowest pressures considered in this analysis. Because the breakdown power eventually increases rapidly as the pressure continues to lower, it is possible that breakdown will not occur. However, as stated previously, better shuttle pressure data will be required before a definite answer can be supplied.

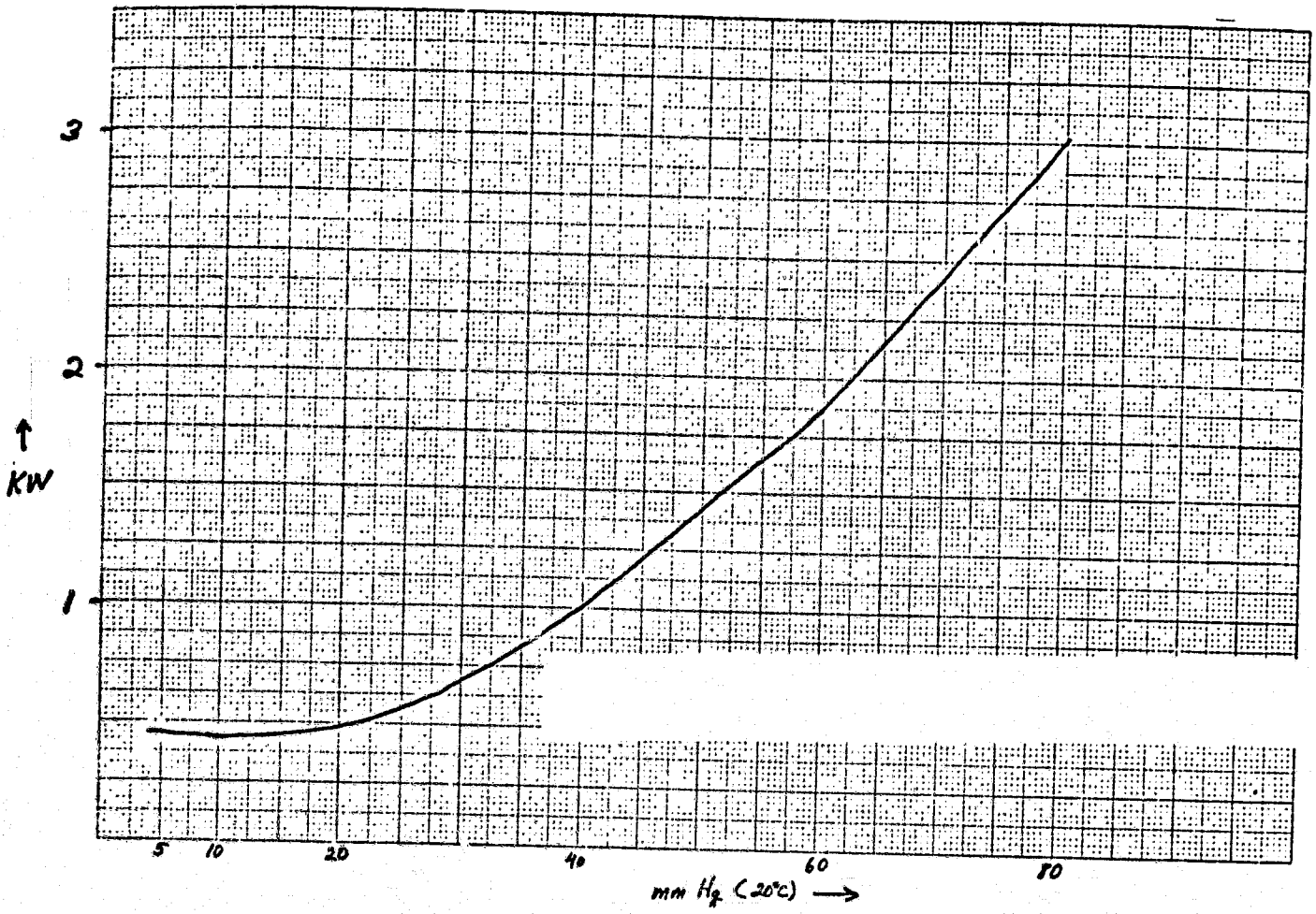

Figure F-2. Ionization breakdown power level.

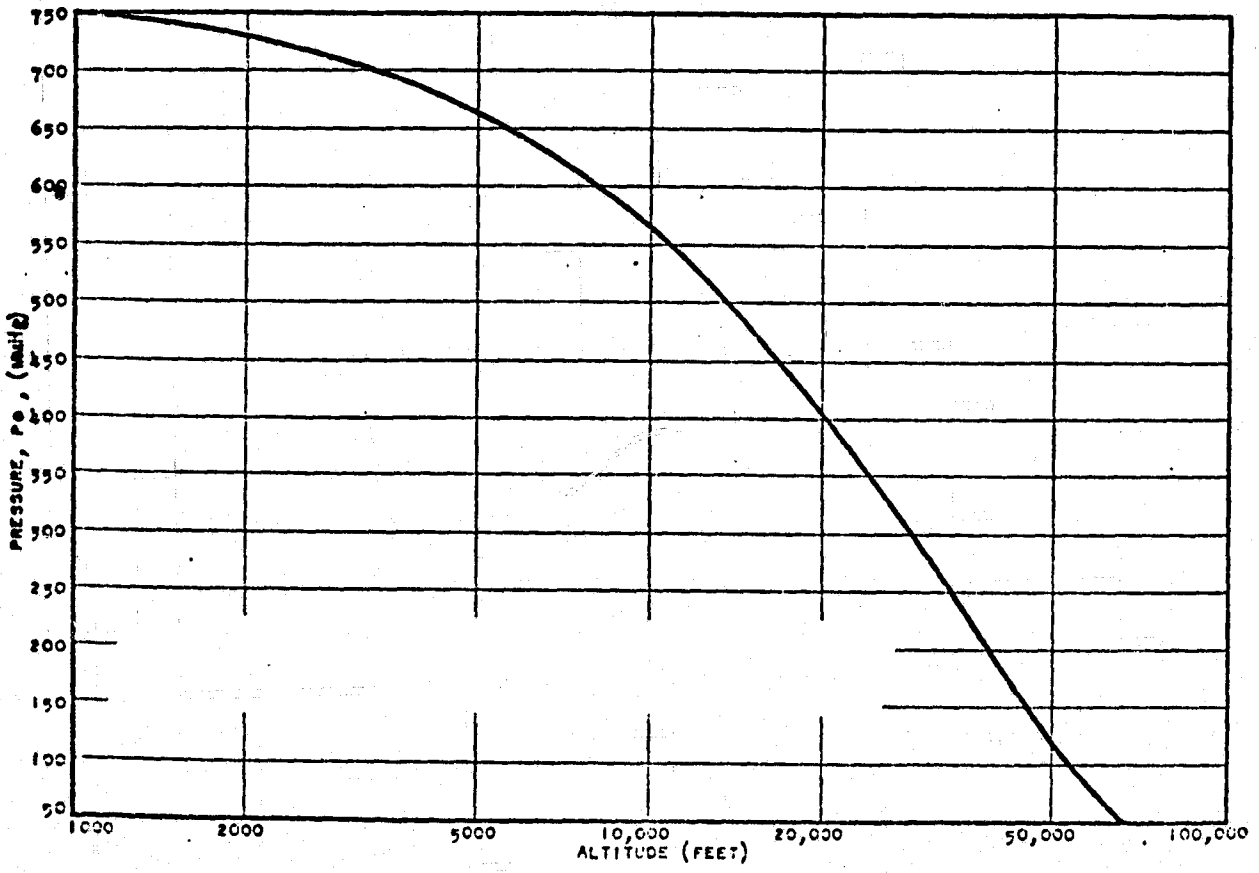

Figure F-3. Altitude pressure relationship.

F.3 REFERENCES

1. Lewis, D. J., "Waveguide Coupling Slots"
2. The Study of Multipactor Breakdown in Space Electronics Systems," Hughes Aircraft Company Report P65-49, April 1965.
3. Gould, L., "Breakdown of Air in Waveguide Systems," Microwave Associates, Incorporated, April 1956.